

Long Range Polymer Chain Dynamics Probed with Pyrene Excimer Fluorescence

by

Shiva Farhangi

A thesis
presented to the University of Waterloo
in fulfillment of the
thesis requirement for the degree of
Doctor of Philosophy
in
Chemistry

Waterloo, Ontario, Canada, 2016

© Shiva Farhangi 2016

Author's Declaration

This thesis consists of material all of which I authored or co-authored: see Statement of Contributions included in the thesis. This is a true copy of the thesis, including any required final revisions, as accepted by my examiners.

I understand that my thesis may be made electronically available to the public.

Statement of Contributions

Chapter 2: Effect of Side-Chain Length on the Polymer Chain Dynamics of Poly(alkyl methacrylate)s in Solution.

Contributor:	Contribution:
Farhangi, S.	In charge of the project, conducted the bulk of the experiments, analyzed the data, wrote the manuscript
Weiss, H.	Conducted some of the experiments and analyses
Duhamel, J.	Designed and supervised the project, edited the manuscript

Chapter 5: Characterization of the Long Range Internal Dynamics of Pyrene-Labeled Macromolecules by Pyrene Excimer.

Contributor:	Contribution:
Farhangi, S.	In charge of the project, conducted the bulk of the experiments, analyzed the data, wrote the manuscript
Casier, R.	Conducted some of the experiments and analyses
Li, L.	Conducted some of the experiments and analyses
Duhamel, J.	Designed and supervised the project, edited the manuscript

Abstract

A series of fluorescently labeled vinyl polymers bearing a C1-C18 side-chain (namely poly(methyl methacrylate), poly(butyl methacrylate), poly(octyl methacrylate), poly(lauryl methacrylate), and poly(stearyl methacrylate)) were synthesized and their polymer chain dynamics (PCD) were characterized by applying the Fluorescence Blob Model (FBM). This report is the first example in the literature where the PCD of actual polymers are being compared as a function of the polymer chemical composition. The study of these polymers having large M_n values in the 170,000-810,000 $\text{g}\cdot\text{mol}^{-1}$ range was accomplished by labeling these samples randomly with pyrene. The FBM takes advantage of the ability of the dye pyrene to form an excimer. Global FBM analysis of the pyrene monomer and excimer fluorescence decays yielded the blob size N_{blob} and the rate of pyrene excimer formation inside a blob from the product $k_{\text{blob}} \times N_{\text{blob}}$. In the future, the body of results found in this study is expected to become a reference for other polymer dynamics studies, including protein chain dynamics, influenced by the bulkiness of different side-chains.

Secondly, we designed a functionalized pyrene derivative, namely 1-pyrenemethoxyethanol (PyMeOEtOH), that remains sensitive to solvent polarity. The 0-0 pyrene vibronic transition is symmetry-forbidden for pyrene, and in non-polar solvents the fluorescence intensity corresponding to this transition is low. Typically, the modification of pyrene with a reactive substituent destroys its symmetry, therefore functionalized pyrene derivatives lose their sensitivity to solvent polarity. In this work, the I_1/I_3 ratio of PyMeOEtOH was determined in 20 different solvents and the I_1/I_3 ratios were similar to those of the unmodified pyrene molecule. The product $k_{\text{blob}} \times N_{\text{blob}}$ retrieved from the FBM analysis remained the same

regardless of the pyrene-labeled polymer. Therefore, PyMeOEtOH has the ability to probe the polarity of its local environment, and its use to probe polymer chain dynamics yields similar results as those obtained with PyButOH.

In the third part of the study, four different pyrene-labeled polymers were prepared by radical copolymerization of *n*-butylmethacrylate (BMA) and 1-pyrenemethyl methacrylate, 1-pyrenemethoxyethyl methacrylate, 1-pyrenemethoxyethoxyethyl methacrylate, and 1-pyrenemethoxydiethoxyethyl methacrylate to yield PyEG₀-PBMA, PyEG₁-PBMA, PyEG₂-PBMA, and PyEG₃-PBMA, respectively. The number of atoms in the side chain of the pyrene-labeled copolymers increased from 3 in PyEG₀-PBMA to 12 in PyEG₃-PBMA. Steady-state fluorescence was used to monitor the efficiency of excimer formation while time-resolved fluorescence was applied to investigate and describe the kinetics of diffusive encounters between excited and ground-state pyrenes as a function of spacer length.

In turn, FBM analysis of the fluorescence decays provided a means to represent how the volume probed by an excited pyrene and the kinetics of pyrene excimer formation were affected by the length of the spacer connecting pyrene to the main chain.

The strong effect that the side chain length had on pyrene excimer formation in the PyEG_X-PBMA samples suggests that pyrene excimer fluorescence could be an excellent technique to probe the conformation of highly branched macromolecules such as dendrimers or polymeric bottle brushes in solution.

Fourthly, different pyrene-labeled constructs were studied in four different organic solvents using steady-state and time-resolved fluorescence. The Model Free Analysis (MFA) was used as a

mathematical model to determine the diffusional rate constant of excimer formation for the end- and randomly labeled pyrene constructs with different architecture from linear to branched. This study established a universal calibration curve from the absolute value of I_E/I_M plotted as a function of $\langle k \rangle$, the average rate constant of excimer formation.

Acknowledgements

I would like to thank my supervisor Prof. Jean Duhamel for his support, patience, guidance, and the contribution he has made to this dissertation.

I would also like to thank my committee members: Mario Gauthier, Neil McManus, Alexander Penlidis, and Xiaosong Wang for their guidance throughout my PhD.

I would like to thank my current and former colleagues in the Duhamel and Gauthier lab groups for all of the help and good memories over the years.

I would like to thank my sister, and most importantly my parents for their encouragement.

Table of Contents

Author's Declaration	ii
Statement of Contributions	iii
Abstract	iv
Acknowledgements.....	vii
Table of Contents	viii
List of Figures	xii
List of Tables	xvii
List of Schemes	xviii
List of Abbreviations	xix
List of Symbols	xxi
Chapter 1	1
Literature Review.....	1
1.1 Overview	2
1.2 Introduction	2
1.3 Polymer End-To-End Cyclization Probed By Fluorescence.....	4
1.4 Birks' Scheme	8
1.5 End-to-End Cyclization of Pyrene End-Labeled Polymers.....	10
1.6 Loop Formation During Protein Folding	12
1.7 Dynamic Fluorescence Quenching.....	14

1.8 Triplet-Triplet Energy Transfer (TTET)	15
1.9 Fluorescence Resonance Energy Transfer (FRET).....	16
1.10 Suitability of Fluorescence EEC Experiments to Probe LRPCD.....	17
1.11 Fluorescence Quenching Experiments to Probe the LRPCD of Stiff Polymers	26
1.12 A Universal Parameter to Describe LRPCD in Solution Based on Randomly Labeled Polymers.....	29
1.13 Relevance of Fluorescence Quenching Experiments to Study Protein Folding	32
1.14 Project Objective.....	34
1.15 Thesis Summary.....	36
1.16 Thesis Outline	38
Chapter 2.....	40
2.1 Overview	41
2.2 Introduction.....	42
2.3 Experimental	45
2.4 Results and Discussion.....	56
2.5 Conclusions.....	70
Chapter 3.....	73

3.1 Overview	74
3.2 Introduction	75
3.3 Experimental	76
3.4 Results and Discussion.....	83
3.5 Conclusions	98
Chapter 4.....	99
4.1 Overview	100
4.2 Introduction	101
4.3 Experimental	103
4.4 Results	110
4.5 Discussion	122
4.6 Conclusions	126
Chapter 5.....	128
5.1 Overview	129
5.2 Introduction	130
5.3 Experimental	136
5.4 Results and Discussion.....	142

5.5 Conclusions	155
Chapter 6.....	157
6.1 Summary of Accomplished Work.....	158
6.2 Future Work	164
Letters of Copyright Permission	166
References.....	175
Appendices.....	208
Appendix SI2- Supporting Information for Chapter 2: Effect of Side-Chain Length on the Polymer Chain Dynamics of Poly(alkyl methacrylate)s in Solution.....	208
Appendix SI3- Supporting Information for Chapter 3: Pyrenyl Derivative with a Four Atom-Linker That Can Probe the Local Polarity of Pyrene-Labeled Macromolecules	234
Appendix SI4-Supporting Information for Chapter 4: Probing Side Chain Dynamics of Branched Macromolecules by Pyrene Excimer Fluorescence.....	261
Appendix SI5-Supporting Information for Chapter 5: Characterization of the Long Range Internal Dynamics of Pyrene-Labeled Macromolecules by Pyrene Excimer.....	277

List of Figures

- Figure 1.1:** Log-log plots of the rate constant $\langle k_1 \rangle$ of pyrene excimer formation vs. mean chain length N of Py₂-PS constructs in (○) cyclohexane at 34.5 °C; (△) toluene at 22 °C; (▲) $\langle k_1 \rangle$ values in toluene adjusted to the viscosity of toluene at 34.5 °C.²² 11
- Figure 1.2:** Dependence of the intramolecular quenching rate constant on peptide length.⁴⁵ 16
- Figure 1.3:** Dependency of f_{free} as a function of $r_{\text{EE}}/R_{\text{blob}}$. Left: $r_{\text{EE}}/R_{\text{blob}} \ll 1$ and $f_{\text{free}} = 0$. Right: $r_{\text{EE}}/R_{\text{blob}} > 1$ and $f_{\text{free}} > 0$.³⁷ 20
- Figure 1.4:** Plot of $\langle k_1 \rangle$ vs. N in toluene for (□, Winnik) Py₂-PS at 22°C,²² (■, Ingratta et al.) Py₂-PS,³⁶ (○, Ghiggino et al.) Py₂-PEO,³⁴ (●, Chen et al.) Py₂-PEO,³⁷ (▲, Svirskaya et al.) Py₂-PDMS,³³ and (△, Boileau et al.) Py₂-PC.³⁵ 24
- Figure 1.5:** Steady-state fluorescence spectra of polystyrene A) Py₂-PS(8K) with a 2.6 mol% pyrene content³⁶ and B) PyBA-PS with a 2.1 mol% pyrene content.⁶² Solvents from top to bottom: methyl ethyl ketone, dichloromethane, tetrahydrofuran, toluene, dimethyl formamide, dioxane, and dimethyl acetamide. 27
- Figure 1.6:** Plots of the products $\langle k_{\text{blob}} \times N_{\text{blob}} \rangle$ and $k_{\text{cy}} \times N$ after normalization as a function of the inverse of solvent viscosity for A) Py₂-PS (▲), PyAN-PS (□), PyBA-PS (○), PyMe-PS (◇) and B) PyBAN-PNIPAM (◇), Py₂-PNIPAM (◆). 32
- Figure 2.1:** Chemical structure of Py-PC1MA, Py-PC4MA, Py-PC6MA, Py-PC8MMA, Py-PC12MA, Py-PC18MA, Py-C1A, Py-PC4TMA, and Py-PC6CyMA. 48

Figure 2.2: Steady-state fluorescence spectra of Py-PC4MA in THF; Pyrene content decreases from 7 mol% (top) to 1 mol% (bottom). $[Py] = 2.5 \times 10^{-6} \text{ M}$, $\lambda_{ex} = 344 \text{ nm}$ 57

Figure 2.3: A) I_E/I_M ratios for all polymers with increasing pyrene contents. B) $m(I_E/I_M)$ for the polymers. Left axis: (●) Py-PC1MA, (■) Py-PC4MA, (□) Py-PC4TMA, (◆) Py-PC6MA, (◇) Py-PC6CyMA, (▲) Py-PC8MMA, (×) Py-PC12MA, (+) Py-PC18MA. Right axis: (○) Py-PC1A; $[Py] = 2.5 \times 10^{-6} \text{ M}$, $\lambda_{ex} = 344 \text{ nm}$ 59

Figure 2.4: Monomer (left, $\lambda_{em}=375 \text{ nm}$) and excimer (right, $\lambda_{em}=510 \text{ nm}$) fluorescence decays of PC1MA labeled with ~ 5 mol% pyrene in THF. Acquired decays were analyzed globally using Eqs. 2 and 3; $[Py] = 2.5 \times 10^{-6} \text{ M}$, $\lambda_{ex} = 344 \text{ nm}$, $\chi^2 = 1.1$ 63

Figure 2.5: $f_{M_{free}}$ as a function of pyrene content; (●) Py-PC1MA, (■) Py-PC4MA, (◆) Py-PC6MA, (▲) Py-PC8MMA, (×) Py-PC12MA, (+) Py-PC18MA..... 65

Figure 2.6: A) Plot of N_{blob} as a function of pyrene content for all poly(alkyl methacrylate)s. B) Plot of $\langle N_{blob} \rangle$ versus the number of carbon atoms per side-chain. (●) Py-PC1MA, (■) Py-PC4MA, (□) Py-PC4TMA, (◆) Py-PC6MA, (◇) Py-PC6CyMA, (▲) Py-PC8MMA, (×) Py-PC12MA, (+) Py-PC18MA, (○) Py-PC1A..... 67

Figure 2.7: A) Plot of $k_{blob} \times N_{blob}$ as a function of pyrene content for all poly(alkyl methacrylate)s. B) Plot of $\langle k_{blob} \times N_{blob} \rangle$ versus the number of carbon atoms per side-chain.

(●) Py-PC1MA, (■)Py-PC4MA, (□) Py-PC4TMA, (◆) Py-PC6MA, (◇) Py-PC6CyMA, (▲) Py-PC8MMA, (×) Py-PC12MA, (+) Py-PC18MA, (○) Py-PC1A. 69

Figure 3.1: Steady-state fluorescence spectra of A) PyMeEGOH and B) PyButOH in the 21 solvents listed in Table 3.2. The solvent polarity increases from top to bottom in Figure 3.1A). $[Py] = 2.5 \times 10^{-6}$ M, $\lambda_{ex} = 344$ nm. 83

Figure 3.2: Comparison of the I_1/I_3 ratios of molecular pyrene reported by Thomas (+,×)¹⁷ and Winnik (○,□)¹⁹ as a function of the I_1/I_3 ratio of (+,○) PyMeEGOH and (×,□) PyButOH..... 85

Figure 3.3: Steady-state fluorescence spectra of PyBut-PBMA labeled with 2.2, 3.0, 3.6, 5.3, and 7.2 mol% pyrene (from bottom to top) in A) DMF, B) DCM, C) THF, D) toluene, and E) cyclohexane and PyMeEG-PBMA labeled with 1.8, 2.7, 3.8, 4.6, and 5.4 mol% pyrene (from bottom to top) in F) DMF, G) DCM, H) THF, I) toluene, and J) cyclohexane. $[Py] = 2.5 \times 10^{-6}$ M, $\lambda_{ex} = 344$ nm. Traces with a dashed line in Figures A-E are for PyButOH and in Figures F-J are for PyMeEGOH. 88

Figure 3.4: Plot of A) $\langle N_{blob} \rangle$ and B) $\langle k_{blob} \times N_{blob} \rangle$ as a function of η^{-1} for the Py-PBMA samples in different solvents. (◆)PyBut-PBMA, (◇)PyMeEG-PBMA..... 92

Figure 3.5: Plots of A) $\langle N_{blob} \rangle$ and B) $\langle k_{blob} \times N_{blob} \rangle$ as a function of pyrene lifetime for the Py-PBMA samples in THF. (◆)PyBut-PBMA, (◇)PyMeEG-PBMA. The lifetime of the PyMeEG-PBMA samples was adjusted by addition of nitromethane..... 94

Figure 4.1: Normalized steady-state fluorescence spectra of (....., $\phi_F = 0.38$) Py(4.0)EG₀-PBMA, (—, $\phi_F = 0.27$) Py(3.8)EG₁-PBMA, (-.-, $\phi_F = 0.32$) Py(3.9)EG₂-PBMA, and (----, $\phi_F = 0.28$) Py(4.2)EG₃-PBMA in THF. $[Py] = 2.5 \times 10^{-6}$ M, $\lambda_{ex} = 344$ nm. 111

Figure 4.2: A) Comparison of the I_E/I_M ratios of (■)PyEG₀-PBMA labeled with 4.0, 5.3, 6.3, 7.1, and 8.1 mol% pyrene, (◇)PyEG₁-PBMA labeled with 1.8, 2.7, 3.8, 4.6, and 5.4 mol% pyrene, (■)PyEG₂-PBMA with 1.8, 2.3, 3.2, 3.9, and 5.3 mol% pyrene, and (×)PyEG₃-PBMA labeled with 1.0, 1.8, 2.1, 2.7, and 4.3 mol% pyrene. B) $m(I_E/I_M)$ for the same polymers in THF. $[Py] = 2.5 \times 10^{-6}$ M, $\lambda_{ex} = 344$ nm. 114

Figure 4.3: Plot of A) N_{blob} , B) k_{blob} , and C) $k_{blob} \times N_{blob}$ as a function of pyrene content and D) $\langle N_{blob} \rangle$, E) $\langle k_{blob} \rangle$, and F) $\langle k_{blob} \times N_{blob} \rangle$ as a function of the number of spacer atoms for (■)PyEG₀PBMA labeled with 4.0, 5.3, 6.3, 7.1, and 8.1 mol% pyrene, (◇)PyEG₁PBMA labeled with 1.8, 2.7, 3.8, 4.6 and 5.4 mol% pyrene, (■)PyEG₂PBMA with 1.8, 2.3, 3.2, 3.9, and 5.3 mol% pyrene, and (×)PyEG₃PBMA labeled with 1.0, 1.8, 2.1, 2.7, and 4.3 mol% pyrene in THF. $[Py] = 2.5 \times 10^{-6}$ M, $\lambda_{ex} = 344$ nm. 117

Figure 4.4: Comparison of R_{blob} (□) and the spacer length d (■) for the PyEG_x-PBMA series. 121

Figure 4.5: Comparison of the chemical structure of the Py-PC_xMA and PyEG_x-PBMA samples that were studied in ref #3 and the present report, respectively. 124

Figure 4.6: Plot of $m(I_E/I_M)$, $\langle N_{blob} \rangle$, and $\langle k_{blob} \times N_{blob} \rangle$ as a function of side chain atoms for the (□)Py-PC_xMA and (■)PyEG_x-PBMA series. 126

Figure 5.1: MFA of the monomer (left, $\lambda_{\text{ex}} = 344 \text{ nm}$, $\lambda_{\text{em}} = 375 \text{ nm}$) and excimer (right, $\lambda_{\text{ex}} = 344 \text{ nm}$, $\lambda_{\text{em}} = 510 \text{ nm}$) fluorescence decays of Py(5.0)-PC1A in DMF. $\chi^2 = 1.1$ 146

Figure 5.2: Plots of $(I_E/I_M)^{\text{TRF}}(f_{\text{free}}=0)$ as a function of $\langle k \rangle$ in A) degassed toluene, B) degassed THF, C) degassed DMF, and D) aerated DMSO. (◆) Py-PC1A in B-D, (◇) Py-PC1MA in A-C, (◈) Py-PC4MA in A-C, (■) Py-PC4TMA in B), (□) Py-PC6MA in B), (▣) Py-PC6CyMA in B), (▲) Py-PC8MA in B) or Py-Amylose in C-D, (△) Py-PC12MA in B) or Py-Amylopectin in C-D, (▲) Py-PC18MA in B, (●) Py-CoE-PS in A-C, (○) Py₂-PEO in A-D, (●) Py_n-GX-PP in A-D, (×) PPyBuMA in A-D, (+) PPyEG₃MA in A-D, and (✱) DiPyMe in A-D. 147

Figure 5.3: Plot of $\langle k^{\text{MF}} \rangle^{\text{blob}}$ versus A) pyrene content and B) the number of side chain atoms for a series of poly(alkyl methacrylate)s randomly labeled with pyrene in THF. (◇) Py-PC1MA, (◈) Py-PC4MA, (□) Py-PC6MA in B), (▲) Py-PC8MA, (△) Py-PC12MA, (▲) Py-PC18MA. 154

List of Tables

Table 1.1: Chemical structure of the pyrene end-labeled polymers discussed in this Chapter.	7
Table 2.2: Chemical structure of polystyrene and poly(<i>N</i> -isopropylacrylamide) randomly labeled with pyrene.	30
Table 2.1: Pyrene content, absolute molecular weight, and PDI of the pyrene-labeled polymers whose chemical structure was shown in Figure 2.1.	50
Table 3.1: Chemical structure, pyrene content, absolute M_n , and PDI values of the PyBut-PBMA and PyMeEG-PBMA samples.	79
Table 3.2: Natural lifetime τ_M and I_1/I_3 ratios of PyButOH and PyMeEGOH in 21 solvents.	86
Table 4.1: Chemical structure, pyrene content, absolute M_n , and PDI values of the PyEG _{<i>x</i>} -PBMA samples with $x = 0 - 3$	107
Table 5.1: Chemical structure, pyrene content in mol%, λ_{Py} in $\mu\text{mol/g}$, number-average molecular weights, and PDIs of the pyrene-labeled constructs used in this study.	137
Table 5.2: Diagrams of the four excited pyrene species often encountered in PyLMs.	143
Table 5.3: Parameters τ_E and α used to fit $(I_E/I_M)^{\text{TRF}}(f_{\text{free}}=0)$ as $\tau_E \times \langle k \rangle^\alpha$	151

List of Schemes

Scheme 1.1: Application of Birks' scheme to excimer formation for a pyrene end-labeled monodisperse polymer. ²²	10
Scheme 3.1: Synthetic procedure applied to prepare PyMeEG-MA.	78
Scheme 4.1: Synthetic procedure applied to prepare a) PyEG ₂ -OH and PyEG ₃ -OH, and b) the monomer series PyEG _x -MA with $x = 0 - 3$	105
Scheme 5.1: Excimer formation between pyrenyl groups covalently attached onto a PyLM.	131

List of Abbreviations

AIBN: Azobisisobutyronitrile

CoEs-PS-BuPy: Polystyrene randomly labeled with pyrenebutanol via an ester linkage

DEG: Diethylene glycol

DMF: *N,N*-Dimethylformamide

DMSO: Dimethylsulfoxide

EEC: End-to-End Cyclization

FBM: Fluorescence Blob Model

FRET: Fluorescence Resonance Energy Transfer

FQ-EEC: Fluorescence Quenching End-to-End Cyclization

GPC: Gel Permeation Chromatography

HBM: Highly Branched Macromolecules

LED: Light-Emitting Diode

LRPCD: Long Range Polymer Chain Dynamics

MHS: Mark-Houwink-Sakurada

MF: Model-Free

NMR: Nuclear Magnetic Resonance

PDI: Polydispersity Index

PDMA: Poly(*N,N*-dimethylacrylamide)

PEO: Poly(ethylene oxide)

PNIPAM: Poly(*N*-isopropylacrylamide)

PS: Polystyrene

PyEG_x-PBMA: Randomly pyrene labeled oligo(ethylene glycol)

PyBuOH: 1-Pyrenebutanol

Py₂-PEO: Pyrene End-Labeled PEO

Py₂-PS: Pyrene End-Labeled PS

PP-G1-4-BuPy4-16: Generation 1–4 dendrons end-labeled with 1-pyrenebutyric acid

SEC: Size Exclusion Chromatography

SPC: Single Photon Counting

SS: Steady-State

TC-SPC: Time-Correlated Single Photon Counting

TEG: Tri(ethylene glycol)

TTET: Triplet-Triplet Energy Transfer

THF: Tetrahydrofuran

UV: Ultraviolet

List of Symbols

a_i	Pre-exponential factor obtained from fitting a fluorescence decay with a sum of exponentials.
EO^*	Properly stacked pyrene dimer that generates upon direct excitation an excimer that emits with a lifetime τ_{EO} .
EL^*	Improperly stacked pyrene dimer that generates upon direct excitation an excimer that emits with a lifetime τ_D .
ϵ	Molar extinction coefficient.
f_{Mdiff}	Fraction of pyrene species in a monomer decay which form excimer by diffusion.
f_{Mk_2}	Fraction of pyrene species in a monomer decay which form excimer with a rapid rate constant k_2 .
f_{Mfree}	Fraction of pyrene species in a monomer decay which do not form excimer.
f_{Ediff}	Fraction of pyrene species in an excimer decay which form excimer by diffusion.
f_{Ek_2}	Fraction of pyrene species in an excimer decay which form excimer with a rapid rate constant k_2 .
f_{EE0}	Fraction of pyrene species in an excimer decay which are properly stacked and form an excimer EO^* quasi-instantaneously upon direct excitation.
f_{EEL}	Fraction of pyrene species in an excimer decay which are improperly stacked and form an excimer D^* quasi-instantaneously upon direct excitation.
f_{diff}	Fraction of pyrene species in the solution which form excimer by diffusion.
f_{k_2}	Fraction of pyrene species in the solution which form excimer with a rapid rate constant k_2 .

f_{free}	Fraction of pyrene species in the solution which are isolated and do not form excimer.
f_{E0}	Fraction of pyrene species in the solution which form an excimer $E0^*$ quasi-instantaneously and are properly stacked.
f_{EL}	Fraction of pyrene species in the solution which form an excimer D^* quasi-instantaneously and are improperly stacked.
$f(t)$	Rate of pyrene excimer formation.
$h\nu$	Energy of a photon.
η	Solvent viscosity.
$[\eta]$	Intrinsic viscosity of a polymer in a given solvent.
I_1	Intensity of the first peak of the fluorescence spectrum of pyrene.
I_3	Intensity of the third peak of the fluorescence spectrum of pyrene.
I_1 / I_3	Ratio of the intensities of the first to the third peak of the fluorescence spectrum of pyrene.
I_E	Steady-state excimer fluorescence emission intensity.
I_M	Steady-state monomer fluorescence emission intensity.
I_E / I_M	Ratio of the excimer to monomer fluorescence emission intensities calculated from the steady-state fluorescence spectra.
$(I_E / I_M)^{SPC}$	Ratio of the excimer to monomer fluorescence emission intensities calculated from the time-resolved fluorescence decay.
k_1	Bimolecular diffusional rate constant of pyrene excimer formation between an excited and a ground-state pyrene.
k_2	Rapid excimer formation rate constant.
k_{-1}	Rate constant of excimer dissociation.

k_{blob}	Excimer formation rate constant inside a blob containing one excited and one ground-state pyrene.
k_{cy}	Cyclization rate constant.
k_{-cy}	Ring opening rate constant.
k_q	Pyrene quenching rate constant.
$\langle k \rangle, \langle k_{MF} \rangle$	Average rate constant of excimer formation, model free.
λ_{em}	Wavelength of light emitted by fluorescence.
λ_{ex}	Wavelength of excitation light.
λ_{py}	Pyrene content of a pyrene-labeled polymer, measured in $\mu\text{mol/g}$.
\overline{M}_n	Number-average molecular weight of a polymer sample.
N	Degree of polymerization of a polymer sample.
n	The number of exponentials used in a sum of exponentials analysis.
N_{blob}	The size of a blob measured in number of structural units.
$\langle n \rangle$	The average number of ground-state pyrenes per blob.
Py_{diff}^*	The pyrene species which form excimer by diffusion.
$Py_{k_2}^*$	The pyrene species which form excimer with a rapid rate constant k_2 .
Py_{free}^*	The pyrene species which are isolated and do not form excimer.
Py_S^*	A short-lived pyrene species.
$[Py]_{loc}$	Local concentration of ground-state pyrenes within a pyrene-labeled polymer.

R_{blob}	Hydrodynamic radius of a <i>blob</i> .
S_0	Ground-state electronic level of an electron.
S_1	First excited-state electronic level of an electron.
T	Temperature in Kelvin.
τ_i	Lifetime of the i 'th exponential obtained from a sum of exponentials analysis of a fluorescence decay.
τ_E	Excimer lifetime.
τ_{E0}	Lifetime of a properly stacked excimer.
τ_{EL}	Lifetime of an improperly stacked excimer.
τ_M	Lifetime of the pyrene monomer.
τ_S	Short pyrene lifetime.
$\langle \tau \rangle$	Number-average lifetime of a monomer fluorescence decay
V	Volume.

Chapter 1

Literature Review

Reproduced with permission from Farhangi, S.; Duhamel, J. Long Range Polymer Chain Dynamics Studied by Fluorescence Quenching. *Macromolecules* **2016**, *49*, 6149-6162.
Copyright 2016, American Chemical Society.

1.1 Overview

Over the years, fluorescence quenching experiments have proven to be a robust analytical tool to retrieve information about the internal dynamics of macromolecules in general, and about the Long Range Polymer Chain Dynamics (LRPCD) of linear chains in particular. This chapter reviews the results obtained to date with the two main types of fluorescence quenching experiments that have been used over the years to describe LRPCD. These experiments involve the labeling of a chain with dyes and quenchers, either at the end of a monodisperse chain for fluorescence quenching end-to-end cyclization (FQ-EEC) experiments, or randomly along a polydisperse chain for fluorescence decay analysis with the Fluorescence Blob Model (FBM). The advantages and disadvantages of these two types of experiments are discussed as well as their range of applications and applicability to the field of protein folding.

1.2 Introduction

Dynamics and energetics continually oppose each other as a macromolecule folds towards its equilibrium conformation. In the case of an isolated linear chain having some structural units bearing associative pendants that can interact with each other, interactions between the pendants will induce association of the structural units only if the dynamics of the main chain are sufficiently slow to allow enough contact time between the associative pendants to establish an interaction. In effect, if the kinetic energy of the structural units of a highly mobile chain is too large as compared to the interaction energy between the associative pendants, this imbalance will prevent association. At the other extreme, despite the low kinetic energy of the structural units of a rigid polymer chain, these units will be unable to

interact with each other due to the stiff backbone that prevents the macromolecule from changing its conformation and bringing the associative pendants into contact regardless of the strength of their interactions. Consequently, the fast and slow dynamics of highly flexible or rigid macromolecules bearing associative pendants are expected to prevent their interactions and thus their association. In summary, interactions between the side chains of a polymer subject to its own internal dynamics will lead to a specific macromolecular conformation, and thus a specific macromolecular behavior in solution, only if dynamics and energetics within the macromolecule are finely balanced.

One example where these considerations apply is with associative thickeners and polymeric dispersants¹⁻⁶ such as alkali swellable emulsion copolymers (HASEs),² hydrophobically modified ethoxylated urethanes (HEURs),^{7,8} or hydroxypropyl cellulose⁹ in aqueous solutions, whose different solution properties are rooted in their different backbone flexibility, HEUR and HASE with their poly(ethylene oxide) components showing much greater flexibility than the rigid backbone of cellulose made of anhydroglucose units. While the solution properties of these macromolecules rely in part on their hydrophilic-lipophilic balance (HLB),^{5,8} the behavior of biological macromolecules such as proteins is usually much more difficult to predict due to the infinite variations in protein sequences that lead to an infinite number of combinations of backbone dynamics and associative energies. For polypeptides, backbone dynamics and associative energies depend on the nature of the amino acid substituents, the bulkiness of the substituents and their level of aggregation affecting the latter, while the former depends on whether the substituents can interact via H-bonds, electrostatic repulsion or attraction, disulfur bridge formation, and hydrophobic association.

Due to this inherent complexity, the characterization of the internal dynamics of biological macromolecules is a very active research area, in particular to determine the folding pathway of proteins.¹⁰⁻¹⁴ The overarching goal in these studies is to determine the time taken for the folding of structural intermediates or *foldons* toward the ultimate 3-dimensional structure of the protein, a process that would benefit from the characterization of the internal dynamics of individual polypeptide chains in solution. As a result, techniques capable of probing polymer chain dynamics in solution have attracted strong scientific interest. These include dynamic light scattering (DLS),¹⁵ Nuclear Magnetic Resonance (NMR),¹⁶ Electron Spin Resonance (ESR),¹⁷ rheology,¹⁸ optical tweezers,¹⁹ and various fluorescence-based techniques such as fluorescence microscopy,²⁰ fluorescence anisotropy,²¹ fluorescence dynamic quenching end-to-end cyclization (FQ-EEC) with end-labeled polymers,²² and more recently Fluorescence Blob Model experiments with randomly labeled polymers.^{23,24} Among these techniques, the two former ones based on fluorescence quenching experiments are the only ones capable of providing information about the translational diffusion coefficient of individual units on isolated polymer chains in solution, and thus report on the long range polymer chain dynamics (LRPCD) in solution, whereby two segments of the chain separated by long polymer stretches diffuse through the solution and encounter. For these reasons, they have garnered strong scientific interest and have been employed to characterize the LRPCD of numerous synthetic and biological polymers. Their features are discussed hereafter.

1.3 Polymer End-To-End Cyclization Probed By Fluorescence

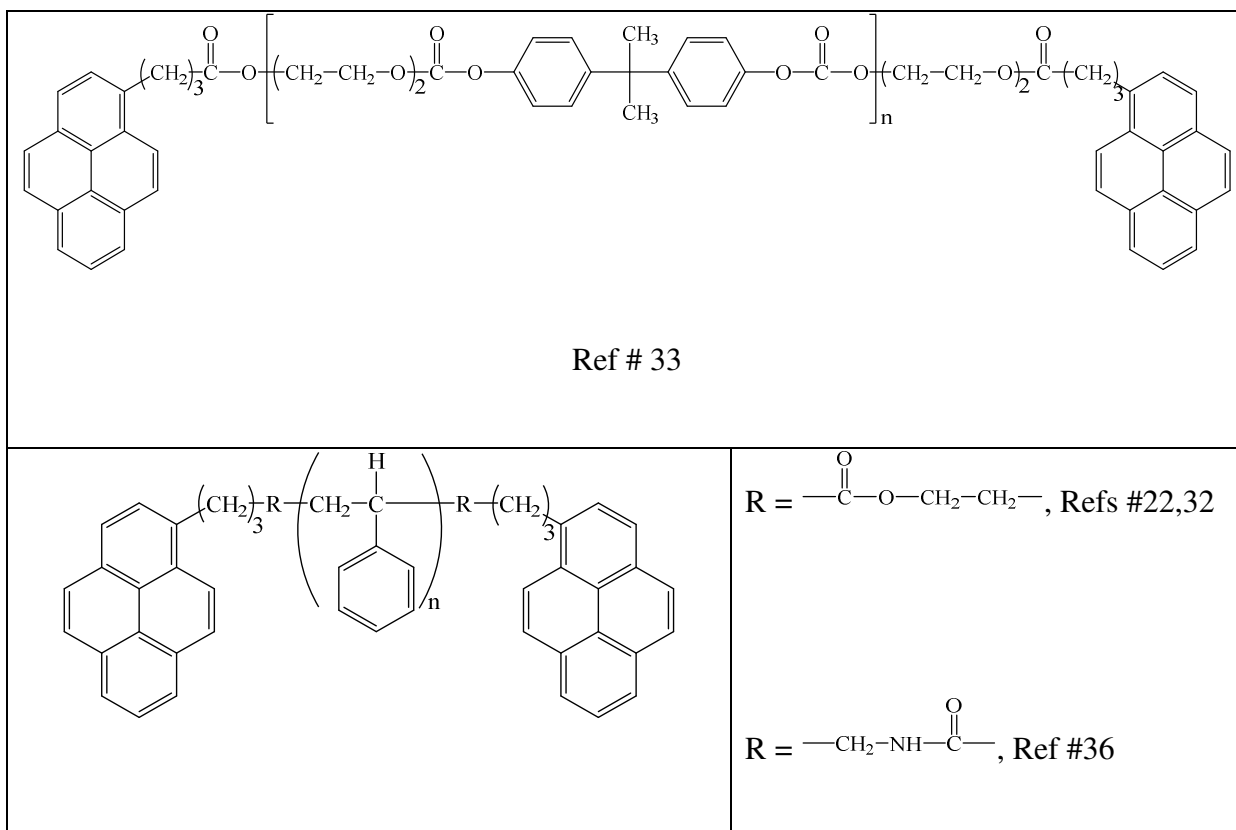
To date, the procedure most applied and trusted to characterize LRPCD in solution consists in labeling the two ends of a monodisperse linear chain with a dye and its quencher, and

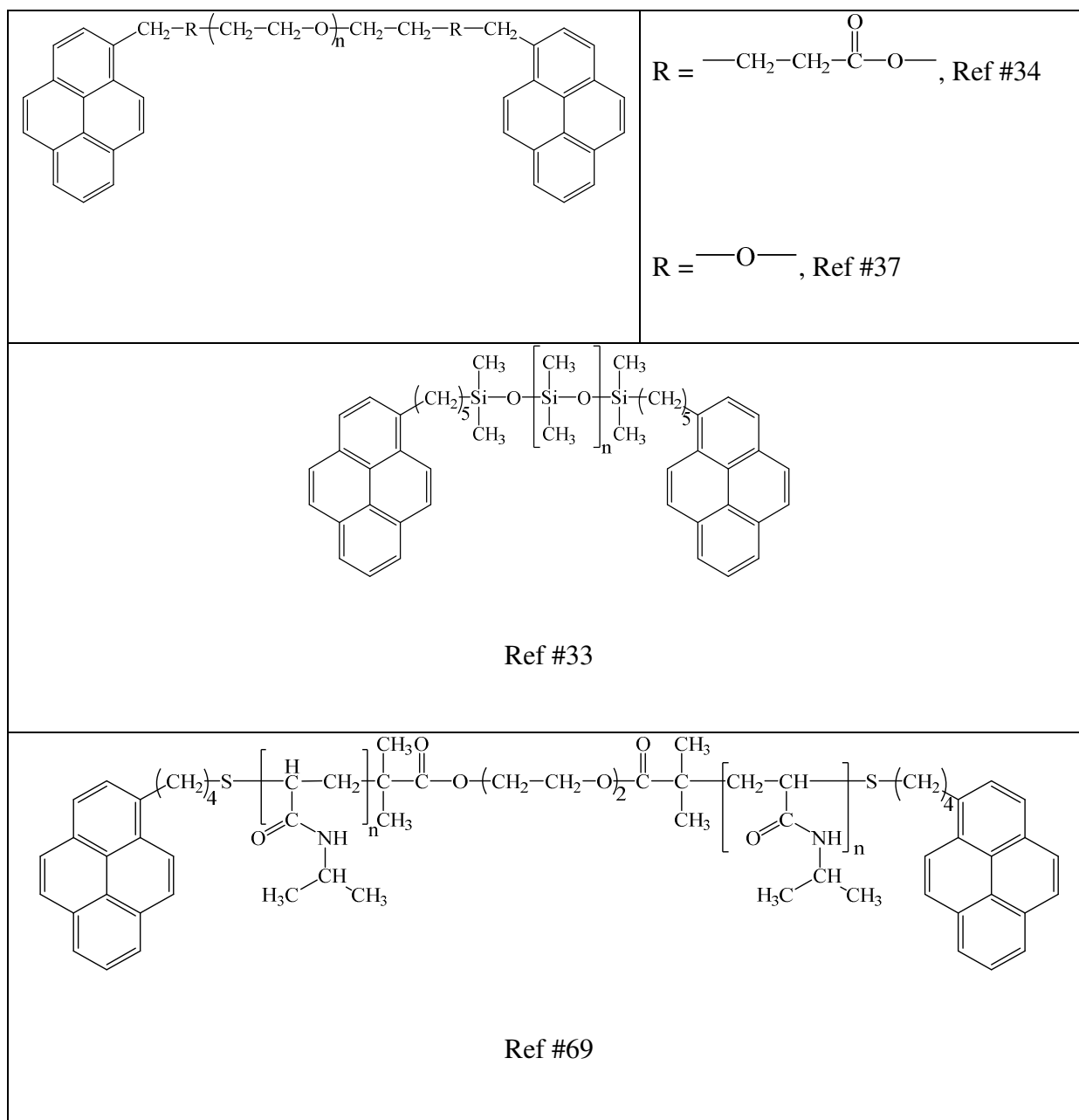
monitoring how the rate constant of end-to-end cyclization (k_{cy}) changes with the nature of the polymer backbone.²² Fluorescence being extremely sensitive, fluorescently labeled macromolecules can be studied at concentrations that are so low that only individual macromolecules are being probed. Consequently, a single fluorescence experiment conducted at low concentration of a fluorescently labeled polymer reports on the entire population of isolated polymer chains in solution. Fluorescence dynamic quenching experiments on linear monodisperse polymer chains end-labeled with a dye and quencher provide a quantitative measure of the translational diffusion coefficient of a given polymeric backbone through the measure of k_{cy} . Since k_{cy} describes the translational diffusion of the two ends of a linear chain made of many structural units, k_{cy} is a measure of the LRPCD for linear polymers in solution. The interest for studying the end-to-end cyclization (EEC) of fluorescently end-labeled monodisperse linear polymers was triggered by a theoretical report by Wilemski and Fixman that demonstrated that EEC was well described by a single rate constant k_{cy} .^{25,26} This theoretical conclusion reached by Wilemski and Fixman opened the path for using fluorescence to probe EEC of linear chains end-labeled with a dye and its quencher, by monitoring the quenching of the excited dye by the quencher through diffusive encounter by fluorescence. For reasons that have been already presented earlier,^{23,24} the most common EEC experiment for synthetic polymers consists in end-labeling a linear polymer chain with pyrene and monitoring the rate constant of excimer formation (k_{cy}) between an excited and a ground-state pyrene.²² This type of experiment was introduced 40 years ago by Zachariasse and Kuhnle for a series of α,ω -dipyrenylalkanes ($\text{Py}(\text{CH}_2)_n\text{Py}$) with $n=2-16$.²⁷ A smaller n value meant that the pyrenes were close to each other and the $\text{Py}(\text{CH}_2)_n\text{Py}$ constructs formed a larger amount of excimer unless the conformational space became so

restricted at very low n values that no excimer could be produced. When the pyrenes were held far from each other for alkyl chains having a large n value, much less excimer was formed. Consequently the ratio of the fluorescence intensity of the excimer over that of the monomer, namely the I_E/I_M ratio, showed a strong dependency with the number of methylene units in the alkyl chain, the I_E/I_M ratio decreasing with increasing alkyl chain length.^{27,28} This work was quickly extended to pyrene end-labeled poly(ethylene oxide) samples by Cuniberti and Perico,²⁹ who observed a decrease in I_E/I_M with increasing PEO molecular weight akin to the decrease in I_E/I_M with alkyl chain length reported by Zachariasse and Kuhnle.^{27,28} As it turns out, the decrease in EEC events reflected by the decrease in the I_E/I_M ratio with increasing chain length observed with these pyrene end-labeled linear chains is quite general and constitutes a cornerstone of any EEC study regardless of the selected type of quenching mechanism. While informative, the I_E/I_M ratio used in these earlier studies only provided qualitative information about the dynamics of EEC. A truly representative measure of EEC dynamics should be expressed in s^{-1} , while the unitless I_E/I_M ratio is not. One important development in the characterization of the LRPCD probed by EEC experiments was pioneered by Winnik in 1980, by demonstrating that Birks' scheme analysis^{30,31} of the pyrene monomer and excimer fluorescence decays acquired with pyrene end-labeled monodisperse linear polymers yielded k_{cy} .³² Thanks to the high efficiency of pyrene excimer formation, which results from an EEC event between two pyrene end-groups, the rate constant $\langle k_1 \rangle$ of excimer formation between two pyrenyl end groups retrieved from Birks' scheme analysis of the monomer and excimer fluorescence decays could be equated with k_{cy} . The brackets used to represent the rate constant of pyrene excimer formation $\langle k_1 \rangle$ for pyrene end-capped polymers prepared with narrow molecular weight distributions (MWDs) indicate that this

rate constant is averaged over all chain lengths of the MWD of the polymer. The first study carried out with a series of pyrene end-capped polystyrene (Py₂-PS)^{22,32} was rapidly expanded to pyrene end-labeled polydimethylsiloxane (Py₂-PDMS),³³ poly(ethylene oxide) (Py₂-PEO),³⁴ and poly(bisphenol A-diethylene glycol carbonate) (Py₂-PC)³⁵ whose chemical structures are depicted in Table 1.1. The studies on Py₂-PS³⁶ and Py₂-PEO³⁷ were later repeated in this laboratory.

Table 1.1: Chemical structure of the pyrene end-labeled polymers discussed in this Chapter.





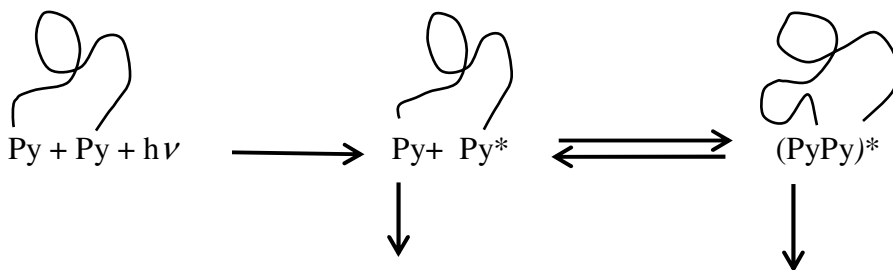
1.4 Birks' Scheme

In 1963, J. B. Birks proposed a model to describe the kinetics of excimer formation between an excited and a ground-state (GS) chromophore like pyrene in solution.³⁰ Birks' scheme assumes that the diffusive encounters between an excited and ground-state chromophore

produce an excimer with a bimolecular rate constant k_1 , but that this process is reversible and that the reversibility can be accounted for with the rate constant k_{-1} (see Scheme 1.1).^{30,31} There are several advantages associated with the use of pyrene to monitor excimer formation. First, pyrene forms excimer very effectively, due to its four fused benzene rings that display a large binding energy, and on contact. Second, the excimer fluorescence emission is well-separated from that of the pyrene monomer emission, which allows for easy detection of the reactants and products of this reaction. Third, pyrene is endowed with an unusually long lifetime τ_M between 200 and 400 ns depending on the solvent, which provides a broad temporal window to probe the slow dynamics of macromolecules. Fourth, k_{-1} is negligible at temperatures lower than 35 °C, which simplifies greatly the kinetics of excimer formation. According to this kinetic scheme, the monomer and excimer fluorescence decays could be well-accounted for by sums of two exponentials that share the same decay times but have different pre-exponential factors. The biexponential fit of the monomer and excimer decays was shown to yield the rate constants k_1 and k_{-1} , as well as τ_E , the excimer lifetime.^{30,31}

In 1980, Winnik expanded the applicability of Birks' scheme that was originally introduced to probe the diffusive encounters between chromophores forming excimers in solution, by demonstrating that Birks' scheme also applied to probe excimer formation between two pyrenes covalently attached to the ends of a monodisperse PS chain.³² That the complex dynamics experienced by the two ends of a linear chain in solution could be accounted for by a single rate constant $\langle k_1 \rangle$ where the meaning of the brackets have been already discussed, as correctly predicted six years earlier by Wilemski and Fixman,^{25,26} was quite remarkable. Most importantly, this study demonstrated that fluorescence EEC

experiments provided a unique experimental means to probe quantitatively the LRPCD of a population of isolated polymer chains in solution.



Scheme 1.1: Application of Birks' scheme to excimer formation for a pyrene end-labeled monodisperse polymer.²²

1.5 End-to-End Cyclization of Pyrene End-Labeled Polymers

In successive studies on different types of pyrene end-capped polymers having narrow molecular weight distributions, the Winnik group established that k_{cy} scaled as $\langle N \rangle$, where $\langle N \rangle$ is the polymer chain length expressed in terms of number of chain atoms. For instance, the log-log plot of $\langle k_1 \rangle$ -vs- N shown in Figure 1.1 demonstrated that $\langle k_1 \rangle$ for polystyrene in cyclohexane at 34.5 °C, a θ -solvent for PS, scaled as $N^{-1.6}$.^{22,32} Considering that $\langle k_1 \rangle$ is a pseudo-unimolecular rate constant equal to the product $k_{diff} \times [Py]_{loc}$, where k_{diff} is the bimolecular rate constant of excimer formation and $[Py]_{loc}$ is the concentration equivalent to one pyrene inside the polymer coil ($[Py]_{loc} = 1/V_{coil}$), the exponent γ of 1.62 found for the relationship $\langle k_1 \rangle \propto N^{-1.62}$ suggested that R_{coil} scaled as $N^{0.54}$, a γ value close to the Flory exponent of 0.50 expected for a polymer in a θ -solvent.

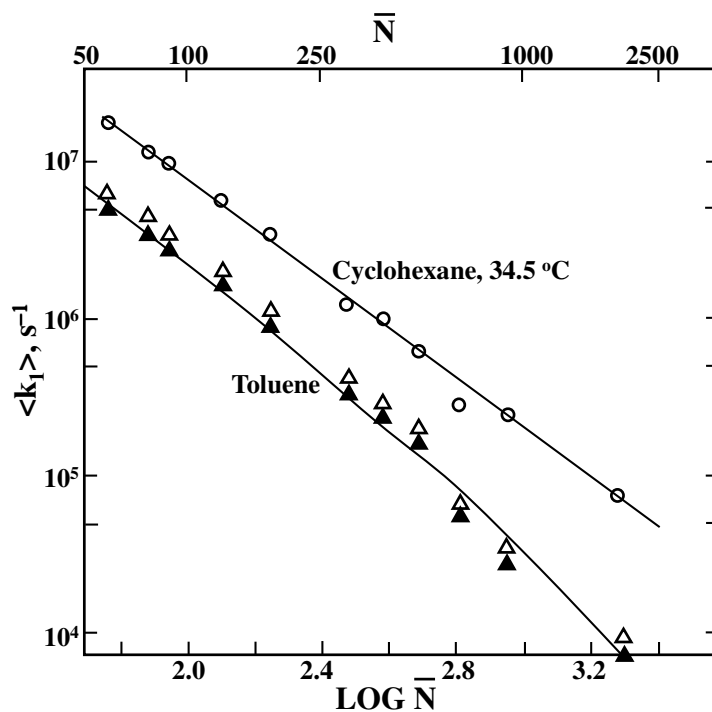


Figure 1.1: Log-log plots of the rate constant $\langle k_1 \rangle$ of pyrene excimer formation vs. mean chain length N of Py₂-PS constructs in (○) cyclohexane at 34.5 °C; (△) toluene at 22 °C; (▲) $\langle k_1 \rangle$ values in toluene adjusted to the viscosity of toluene at 34.5 °C.²²

While interesting from a *Polymer Science* point of view, the strong dependency of k_{cy} with chain length represented a major limitation to the application of EEC to probe polymer chain dynamics. As a matter of fact, this relationship implied that a 10-fold increase in N resulted in a 40 fold decrease in $\langle k_1 \rangle$ for PS under θ -conditions, with a more pronounced decrease expected in good solvents where the Flory exponent takes a larger value. Since excimer formation between pyrenes covalently attached to the ends of a linear chain is limited due to the large polymer end-to-end distance separating them, a 40-fold decrease in

$\langle k_1 \rangle$ reduces excimer fluorescence to levels that are too low for excimer fluorescence decay acquisition. Furthermore, the fluorescence decay of the pyrene monomer for the doubly end-labeled polymers approached monoexponential behavior with a decay time τ for large N values and became indistinguishable from that of the singly pyrene end-labeled polymer which decays with its natural lifetime τ_M . Consequently, τ tends to τ_M for large N values. Since $\langle k_1 \rangle = 1/\tau - 1/\tau_M$ under such conditions, $\langle k_1 \rangle$ became vanishingly small and harder to measure accurately. One solution proposed by the Winnik group to this problem was to use the proportionality that is observed between I_E/I_M and $\langle k_1 \rangle$ for short polymers where $\langle k_1 \rangle$ could be measured accurately, and to apply it to predict the $\langle k_1 \rangle$ value of longer chains based on their I_E/I_M ratio.^{22,32} This approximation was used to build the plot shown in Figure 1.1 for N values larger than about 600 in cyclohexane at 34.5 °C, or about 250 in toluene at 22 °C, corresponding to a $\langle k_1 \rangle$ value of $\sim 5 \times 10^5 \text{ s}^{-1}$. As discussed earlier, toluene being a good solvent for PS makes it more challenging to probe the longer PS chains studied in cyclohexane at 34.5 °C, since Py₂-PS is less extended in this θ -solvent and thus forms more excimer. As it turned out, the experiments carried out on pyrene end-labeled synthetic polymers to gain information about their LRPCD could also be readily applied to peptides as described hereafter.

1.6 Loop Formation During Protein Folding

The complete sequencing of the human genome has led to the identification of the sequence of all the proteins found in humans. Unfortunately, the 1-dimensional sequence of proteins did not enable the prediction of their 3-dimensional structure that would ultimately determine

their function such as their enzymatic activity. To facilitate the 3D-structure characterization of proteins, which can be arduous by X-ray crystallography or NMR, computer modeling has been instrumental to predict how strings of amino acids fold into a well-defined 3-D arrangement.¹²⁻¹⁴ As alluded to earlier, the quasi infinite number of peptide sequences that can be generated from the 23 amino acids makes it particularly challenging to predict the LRPCD of proteins that depends on the size of the substituent on each amino acid. In this context, the dynamic information retrieved from fluorescence quenching EEC (FQ-EEC) experiments about the relative flexibility of a given peptide sequence could be employed to impose additional constraints in computer models, to save precious computational time by reducing the conformational space being probed when trying to determine the folding pathway of a peptide sequence *in silico*. In particular, FQ-EEC experiments provide information about the folding pathway of the most elementary structural element found in a protein, namely loop formation.^{38,39}

Fluorescence quenching EEC experiments conducted on oligopeptides are based on the same principles that were first introduced for pyrene end-labeled linear polymers,²² namely attaching a luminophore at one end of the chain and an appropriate quencher at the other end, and measuring the rate constant for FQ-EEC. The luminophore can be quenched on contact either by a simple fluorescence⁴⁰⁻⁴⁴ or phosphorescence^{45,46} dynamic quenching experiment, by triplet-triplet energy transfer⁴⁷⁻⁵⁵ through space by fluorescence resonance energy transfer (FRET),^{55,56-59} or by electron transfer through a Dexter mechanism.^{60,61} As compared to synthetic polymers prepared by anionic polymerization and initiated typically by an electron transfer process to generate two ends with a similar reacting group (hydroxyl,

carboxylic acid, or amine), proteins and oligopeptides present a major difference in that the two chain ends are chemically distinct, one being an amine at the N-terminal and the other a carboxylic acid at the C-terminal. Consequently, the labeling scheme of oligopeptides differs from that of synthetic polymers, which favor attachment of a same dye derivative to both ends of the chain. In the case of oligopeptides, two different dye derivatives are usually selected to react with the N- and C-terminals. Whereas pyrene derivatives are commonly used to probe synthetic polymers in organic solvents where pyrene is soluble, pyrene being insoluble in water is less relevant to study oligopeptides in aqueous solution. Yet as for pyrene end-labeled synthetic polymers, FQ-EEC experiments conducted with oligopeptides take advantage of long-lived dyes that enable the retrieval of the rate constant $\langle k_1 \rangle$ from the difference $\langle k_1 \rangle = \tau^{-1} - \tau_M^{-1}$, where τ and τ_M are the decay times of the quenched and unquenched dyes, respectively. The advantage in dealing with a very long-lived dye comes from the fact that, when τ is much shorter than τ_M , $\langle k_1 \rangle$ can be retrieved with high accuracy, sometimes by simply neglecting the τ_M^{-1} term. As for synthetic polymers, some FQ-EEC experiments conducted on short end-labeled peptides were applied to establish the $k_{cy} \propto N^{-\gamma}$ scaling law.

1.7 Dynamic Fluorescence Quenching

In FQ-EEC experiments, k_{cy} for oligopeptides is influenced by the amino acid sequence and the length of the chain since a more rigid or longer peptide results in a smaller k_{cy} value. The effect of the chain length on k_{cy} was investigated for the oligopeptide Trp-(Gly-Ser)_n-DBO-NH₂ ($n=0,1,2,4,6$, and 10).⁴¹ In these experiments, the fluorophore was 2,3-diazobicyclo [(2.2.2)]oct-2-ene (DBO) and tryptophane (Trp) was the quencher. The quenching of DBO by

Trp in water at 23 °C was monitored by time-resolved fluorescence and the collision rate $\langle k_1 \rangle$ was determined by fitting the fluorescence decays with a monoexponential function. k_{cy} was found to decrease continuously from 4.1 to $1.1 \times 10^7 \text{ s}^{-1}$ when the oligopeptide length was increased from $n = 0$ to 10, approaching the expected trend $k_{cy} \propto N^{-1.5}$ for the longest peptides. Similar experiments were carried out with a series of Oxa-(Gly-Ser) $_n$ -Trp ($n = 2-15$) where the oxazine(Oxa) dye was quenched by Trp.⁵³ For the longer peptides, the scaling relationship $k_{cy} \propto N^{-1.4}$ was obtained in quite good agreement with the previous study.

1.8 Triplet-Triplet Energy Transfer (TTET)

TTET involves the transfer of two electrons from a triplet donor to a triplet acceptor upon van der Waals contact. This technique has been employed to measure the loop formation rate constant of peptides. In these experiments, xanthane (Xan) is often used as a triplet donor and naphthalene (N) as acceptor.⁴⁷⁻⁵² The intrachain diffusion contact in Xan-(Gly-Ser) $_n$ -Ala-Gly-Ser samples with $n = 1 - 28$ was characterized by monitoring the decay of the xanthane triplet absorbance band at 590 nm. The single exponential kinetics of the absorbance decays facilitated the determination of the decay time. As usual, the decay time increased with increasing peptide length and the rate constant k_{cy} was found to decrease as $N^{-1.7}$.⁴⁹

The dependency of k_{cy} on the peptide length has also been reported in other studies, in particular for a series of peptides that were prepared with Trp at one end and Cys at the other, for the peptidic constructs Cys-(Ala-Gly-Gln) $_n$ -Trp with n taking values between 1 and 6.⁴⁵ Upon excitation of Trp into the triplet state, the excited Trp could transfer its excess energy to Cys upon contact by TTET. Due to the long lifetime of the excited triplet state of Trp (τ_M

= 40 μ s), the approximation $k_{cy} = \tau^{-1} - \tau_M^{-1} \approx \tau^{-1}$ was used to determine k_{cy} in Figure 1.2. As can be seen in Figure 1.2, the expected scaling relationship $\langle k_1 \rangle \propto N^{-1.5}$ in a θ -solvent was only observed for the longest peptides with 19 peptide bonds.⁴⁵ The fact that a sufficiently long chain must be reached before the $\langle k_1 \rangle \propto N^g$ relationship is being obeyed is a general observation.

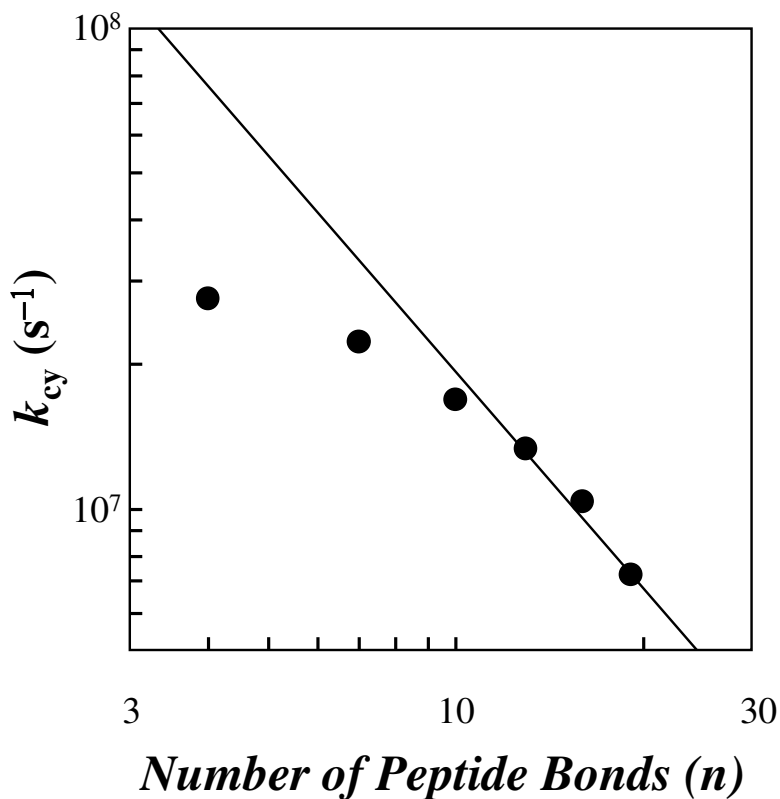


Figure 1.2: Dependence of the intramolecular quenching rate constant on peptide length.⁴⁵

1.9 Fluorescence Resonance Energy Transfer (FRET)

FRET has been applied to probe peptide chain dynamics by labeling the chain ends with a fluorescence donor and acceptor. The efficiency of FRET depends strongly on the distance

between the donor and the acceptor molecule and this effect can be employed to probe diffusive encounters between the two ends. At the initial time, the donor-acceptor pairs separated by a short distance undergo much more efficient FRET than those separated by a long distance. The depletion of donor-acceptor pairs separated by a short distance at early times creates a diffusion sink whereby D-A pairs separated by a large distance will use diffusion to reduce their average distance. Since the entire process takes place over a period of time that is measurable by time-resolved fluorescence, the fluorescence decay can be analyzed to yield the rate constant for quenching by FRET (k_{ET}), which depends on the flexibility of the chain, a more flexible chain resulting in a larger k_{ET} .⁴⁷

The FRET efficiency between the excited Trp and the ground-state DBO was investigated for a series of oligopeptides Trp-(Pro)_n-DBO-NH₂ ($n=1, 2, 4, \text{ and } 6$) by steady-state and time-resolved fluorescence.⁵⁷ The fluorescence intensity and average decay time of Trp were found to increase with increasing chain length, a clear indication of reduced FRET with increasing chain length, but the small number of samples investigated did not allow the author to provide a scaling relationship.

1.10 Suitability of Fluorescence EEC Experiments to Probe LRPCD

To date, FQ-EEC experiments have been used intensively to probe the LRPCD of numerous synthetic and biological polymers in solution. But despite the claim made since their inception in the late 1970s that they can provide quantitative information on the magnitude of LRPCD in solution, it is fair to state that to date, these experiments have failed to deliver a unique parameter like T_g , the glass transition temperature for polymers in the bulk, that would allow experimentalists to gauge the magnitude of the LRPCD of a polymer of interest

in solution. Furthermore, as this survey of the current literature on FQ-EEC experiments has highlighted, FQ-EEC experiments are never applied to “real” polymers in solution, i.e. with a degree of polymerization greater than 200. The main reason for this state of affair was rationalized for polymers such as PS⁶² or poly(butyl methacrylate)⁶³ (PBMA) in tetrahydrofuran where the pyrene labels were randomly incorporated into the chain via copolymerization with 1-pyrenebutyl acrylate and methacrylate, respectively. For these samples whose fluorescence decays were analyzed according to the Fluorescence Blob Model (FBM), pyrene excimer formation was found to occur locally within a subvolume of the polymer coil referred to as a *blob* made of about 50 monomers. This insight led to the unavoidable conclusion that LRPCD does not enable diffusive encounters between a dye and a quencher that are covalently attached to the ends of a PS or PBMA chain made of many more than two *blobs* or 100 monomers. This is the reason why hardly any excimer could be detected in cyclohexane at 34.5 °C and in toluene at 22 °C for Py₂-PS constructs that had a degree of polymerization (X) greater than 100.^{22,32} Past a critical degree of polymerization (X_{crit}), a fraction of the end-labeled chains have an end-to-end distance that it is too large for an excited and a ground-state pyrene to encounter and form an excimer while one of the two pyrenes remains excited.

Of course, X_{crit} where diffusive encounters between the two ends of a linear chain are no longer possible depends on several factors. The parameter X_{crit} increases for lower solvent viscosity, poorer solvent quality toward the polymer, greater backbone flexibility, and longer lifetime of the dye. The effect of solvent viscosity on the likelihood of diffusive EEC was illustrated with a series of Py₂-PEO samples.³⁷ The fraction of pyrene monomers that did not

form any excimer and emitted as if they were free in solution (f_{free}) was found to increase linearly with increasing solvent viscosity for a given Py₂-PEO sample, as well as increasing polymer molecular weight in a given solvent, both effects contributing to hindering the encounters between an excited and a ground-state pyrene. In dioxane, an organic solvent with a viscosity (η) of 1.37 mPa.s, an f_{free} value of 0.85 was obtained for Py₂-PEO(10K), a 10K monodisperse PEO end-capped with pyrene, indicating that hardly any excimer was produced under these conditions. This result supported the conclusion reached earlier that FQ-EEC experiments apply solely for oligomers rather than polymers. For longer chains, FQ-EEC experiments probe the distribution of chains whose degree of polymerization is larger or smaller than X_{crit} , the longer chains emitting fluorescence as if no quencher was attached at the other chain end and the shorter chains were undergoing diffusive EEC encounters. As the degree of polymerization becomes much larger than X_{crit} , little EEC takes place, the fluorescence signal of the doubly labeled chains is dominated by the chains whose end-to-end distance is too large for pyrene-pyrene encounters to occur and becomes identical to that of the monolabeled chains, and no information on EEC can be retrieved.

Figure 1.3 illustrates these considerations. As long as the volume probed by the excited pyrene (i.e. a *blob*) is larger than the polymer coil volume, the excited pyrene at one end of the chain will encounter the ground-state pyrene at the other end and form an excimer, resulting in a zero f_{free} value. Under these conditions, Birks' scheme applies. But as the chain length increases, X_{crit} is reached where the *blob* becomes smaller than the polymer coil and a fraction of the chains have their ground-state pyrene located outside the *blob*, preventing excimer formation and yielding non-zero f_{free} values. Birks' scheme no longer applies. The

kinetics of excimer formation must reflect that excimer formation occurs inside the *blob* and that the ground-state pyrene can move in and out of the *blob*. A model was developed to account for these facts and was applied to fit globally the monomer and excimer decays acquired with a series of Py₂-PEO constructs. The fits were excellent and yielded sets of parameters that were consistent with the *blob* concept presented in Figure 1.3.³⁷

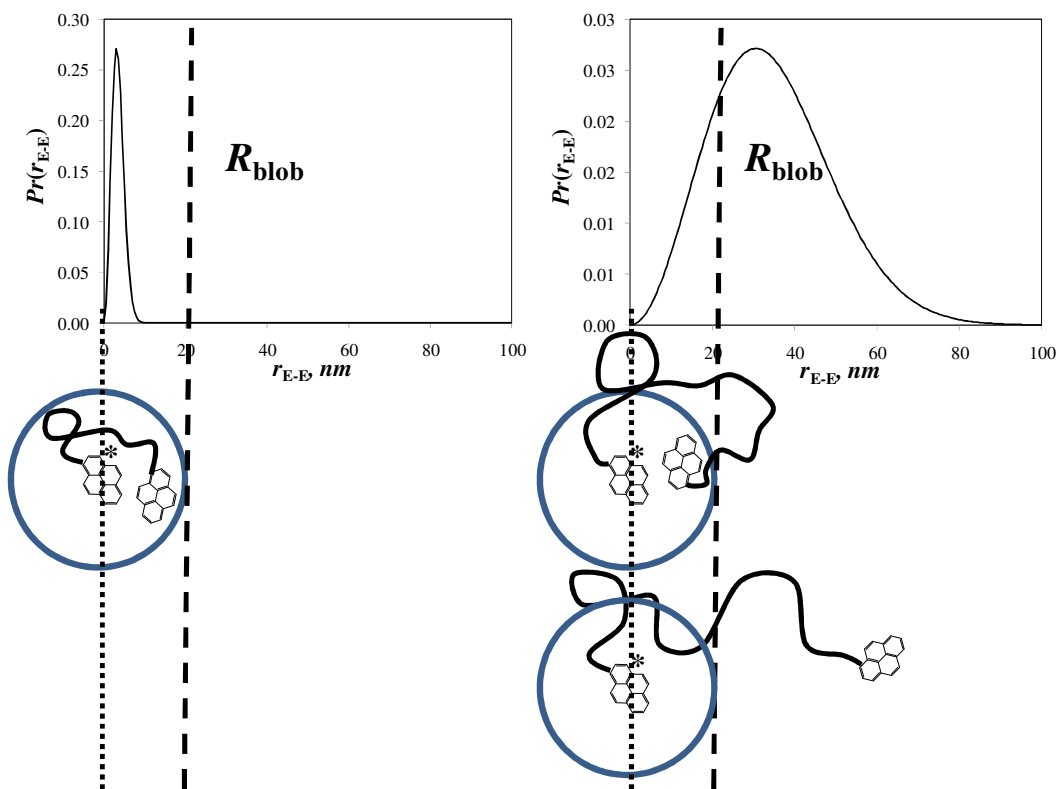


Figure 1.3: Dependency of f_{free} as a function of r_{EE}/R_{blob} . Left: $r_{EE}/R_{blob} \ll 1$ and $f_{free} = 0$. Right: $r_{EE}/R_{blob} > 1$ and $f_{free} > 0$.³⁷

Since the information retrieved on LRPCD is questionable for chains with a degree of polymerization greater than X_{crit} , FQ-EEC experiments should focus on shorter chains where

a strong fluorescence quenching reflects efficient EEC, as is usually being done in the literature. One problem that arises from such a requirement however is that the oligomers must be long enough for the kinetics of FQ-EEC to generate a scaling behaviour between $\langle k_1 \rangle$ and the chain length, as was observed in Figure 1.2 for a series of $-(\text{Ala-Gly-Gln})_n-$ oligopeptides⁴⁵ and another report.⁴¹ The implication of this requirement is that any FQ-EEC experiment involves the preparation of several oligomeric constructs with increasing chain length, whose EEC kinetics need to be characterized to establish the $k_{cy} \propto N^{-\gamma}$ relationship. The necessity of establishing the scaling relationship makes comparison of the LRPCD of one backbone with another somewhat challenging, since a series of fluorescently end-labeled polymers must be prepared whose chain length N must be long enough to obey the scaling relationship, while remaining shorter than X_{crit} .

The difficulty in using $\langle k_1 \rangle$ data to compare the LRPCD of different polymeric backbones is made evident in Figure 1.4, where the $\langle k_1 \rangle$ values obtained for different series of Py_2 -PS,^{22,32,36} Py_2 -PEO,^{34,37} Py_2 -PDMS,³³ and Py_2 -PC³⁵ samples in toluene are compared as a function of the polymer chain length. Using a similar solvent eliminates differences in solvent viscosity, although solvent quality toward the polymer might play a role. Assuming that toluene is a good solvent for all the polymers included in Figure 1.4, all the data series yielded a scaling relationship of the type $\langle k_1 \rangle \propto N^{-\gamma}$. Similar trends were obtained for the Py_2 -PS samples in toluene by Winnik²² and by Ingratta et al.³⁶ Larger differences in $\langle k_1 \rangle$ were observed for longer chains due to differences in the analysis of the fluorescence decays, the analysis being based either on the fit of the monomer fluorescence decays or the equivalence between the I_E/I_M ratio and $\langle k_1 \rangle$ in the Winnik²² study, while Ingratta et al.³⁶ applied solely

global analysis of the monomer and excimer decays to retrieve $\langle k_1 \rangle$. For similar chain lengths N expressed in number of chain atoms, similar $\langle k_1 \rangle$ -vs- N trends were obtained for the Py₂-PEO series studied by Ghiggino et al.³⁴ and by Chen et al.,³⁷ despite similar differences in decay analysis as between the Winnik²² and Ingratta et al.³⁶ studies, whereby single and global analyses of the decays were applied, respectively. Based on the trends shown in Figure 1.4, the Py₂-PS series yielded the slowest LRPCD, whereas the Py₂-PEO series yielded the fastest. For a similar chain length, the $\langle k_1 \rangle$ values obtained for the Py₂-PEO series were only slightly higher than those of Py₂-PDMS. These trends are somewhat reasonable based on the T_g values, which reflect the flexibility of a polymer based on free volume. Indeed, T_g has been reported to equal 100 °C, 67 °C, between –115 and –50 °C, and –123 °C for PS, PC, PEO, and PDMS, respectively.⁶⁴ The unexpected result in Figure 1.4 was the trend obtained for Py₂-PC,³⁵ which yielded $\langle k_1 \rangle$ values that were similar to those obtained for Py₂-PDMS.³³ The rigid bisphenol A spacer, which is a structural unit of the PC backbone, makes it highly unlikely that Py₂-PC and Py₂-PDMS would yield similar EEC kinetics. Most probably, as inferred by the authors,³⁵ Py₂-PC must adopt a conformation in toluene that is more compact than expected, possibly that of a helix. The more compact conformation would result in a larger $[Py]_{loc}$, which would enhance $\langle k_1 \rangle$ for Py₂-PC to values similar to those obtained for Py₂-PDMS.

One other feature made evident from the rapid visual inspection of Figure 1.4 is that, except for the study by Winnik for the Py₂-PS series in toluene that reports $\langle k_1 \rangle$ values as low as 10^4 s^{-1} and extends up to N values as large as 2,000,²² all other trends report $\langle k_1 \rangle$ values that are never lower than 10^6 s^{-1} , which corresponds to the threshold below which

excimer fluorescence becomes barely detectable in a steady-state fluorescence spectrum, when the degree of polymerization becomes larger than X_{crit} . It is clear from Figure 1.4 that if X_{crit} corresponds to the degree of polymerization where $\langle k_1 \rangle$ equals 10^6 s^{-1} , X_{crit} increases with greater flexibility of the polymeric backbone. The reason for the unusual range in N values covered by the Winnik study has been discussed earlier and is due to the use of the I_E/I_M ratio to predict the small $\langle k_1 \rangle$ values obtained for the longer chains. Yet the validity of this procedure has been questioned,³⁷ as it is an indirect measure of $\langle k_1 \rangle$ that does not account for the balance between the chain ends that are inside or outside the *blob*, namely the volume described by the chain-end bearing the excited pyrene label. Consequently, the $\langle k_1 \rangle$ -vs- N trends shown in Figure 1.4 suggest that for pyrene end-labeled synthetic polymers, FQ-EEC experiments provide reliable $\langle k_1 \rangle$ values as long as $\langle k_1 \rangle$ is greater than 10^6 s^{-1} , corresponding to X_{crit} values of $\langle N \rangle = 91$ (Winnik²² or 172 (Duhamel)³⁶ for $\text{Py}_2\text{-PS}$, $\langle N \rangle = 431$ (Duhamel)³⁷ for $\text{Py}_2\text{-PEO}$, and $\langle N \rangle = 468$ (Winnik)³³ for $\text{Py}_2\text{-PDMS}$. After accounting for the number of chain atoms found in each structural unit of the different polymers, the X_{crit} values retrieved from the trends shown in Figure 1.4 follow the sequence $\text{PS} < \text{PEO} < \text{PDMS}$, a sequence that reflects their expected chain flexibility.

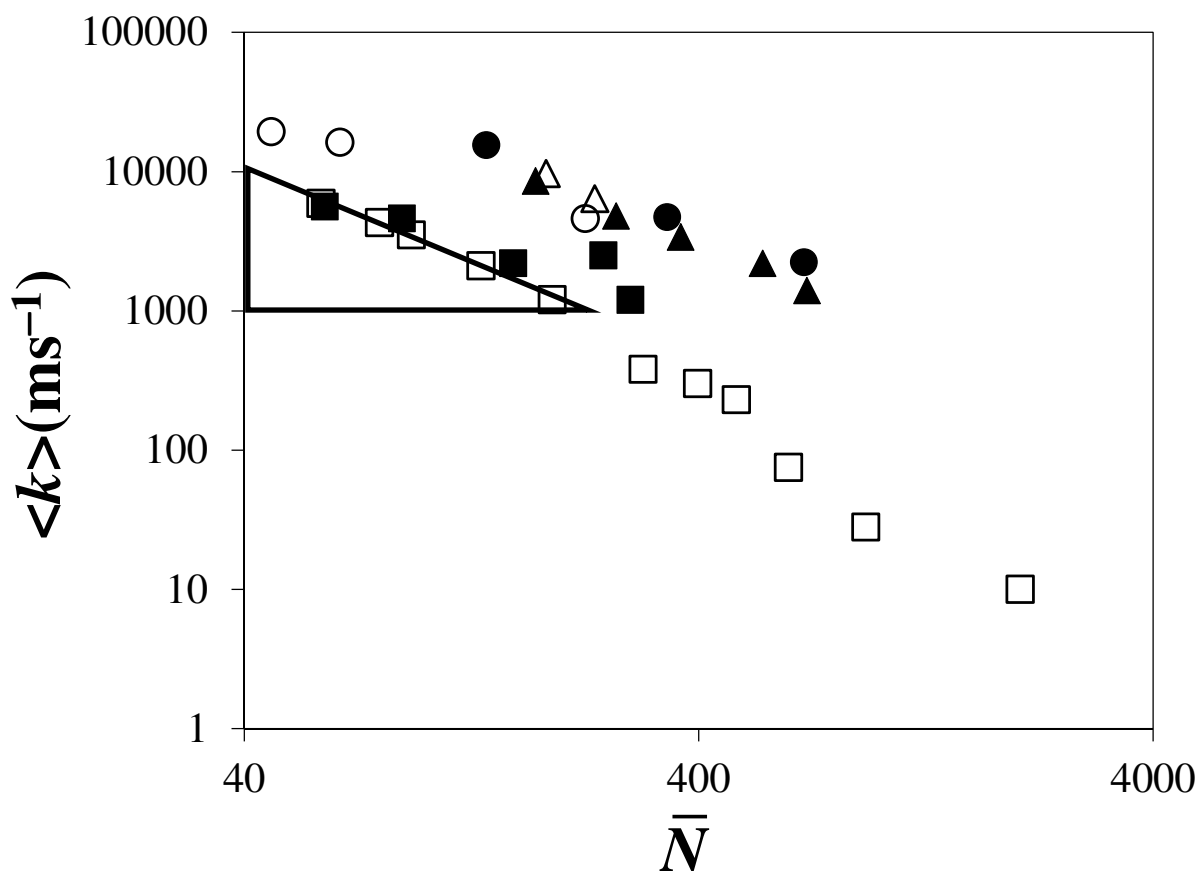


Figure 1.4: Plot of $\langle k_1 \rangle$ vs. N in toluene for (\square , Winnik) $\text{Py}_2\text{-PS}$ at 22°C ,²² (\blacksquare , Ingratta et al.) $\text{Py}_2\text{-PS}$,³⁶ (\circ , Ghiggino et al.) $\text{Py}_2\text{-PEO}$,³⁴ (\bullet , Chen et al.) $\text{Py}_2\text{-PEO}$,³⁷ (\blacktriangle , Svirskaya et al.) $\text{Py}_2\text{-PDMS}$,³³ and (\triangle , Boileau et al.) $\text{Py}_2\text{-PC}$.³⁵

The $\langle k_1 \rangle$ -vs- N trend obtained with the $\text{Py}_2\text{-PS}$ series in Figure 1.4 represents an interesting case as polystyrene exhibits the slowest LRPCD among the $\text{Py}_2\text{-PS}$, Py_2PEO , $\text{Py}_2\text{-PDMS}$, and $\text{Py}_2\text{-PC}$ series. For the $\text{Py}_2\text{-PS}$ in toluene, X_{crit} values of 91 and 172 were retrieved representing M_n values of 9 and 17K. In the Ingratta et al. study where the monomer and excimer fluorescence decays of a $\text{Py}_2\text{-PS}$ sample with an M_n value as large as 13K were

investigated, this analysis was complicated by the similarity that exists between the lifetimes of Py₂-PS(13K) and the singly labeled Py₁-PS.³⁶ The analysis of the monomer and excimer fluorescence decays acquired with a Py₂-PS(19K) sample could not be carried out, as the monomer decays of the singly and doubly labeled chains overlapped within experimental error. The implication of this discussion is that FQ-EEC experiments conducted with pyrene end-labeled polymers will be challenging to implement for polymeric backbones that are stiffer than polystyrene, such as polypeptides. Indeed if the LRPCD of such polymers were investigated by excimer formation between two pyrene end groups, the range of N and $\langle k_1 \rangle$ values available for FQ-EEC would correspond to a rather small triangle in Figure 1.4. The N values would be ranging between 40 and 340, an N value of 40 at the lower end corresponding to a degree of polymerization of 20 for vinyl polymers, or 13 for peptides, which would hardly qualify such samples as polymers. Based on the triangle drawn in Figure 1.4, the range of $\langle k_1 \rangle$ values would have lower and upper boundaries of 10^6 and 10^7 s⁻¹, respectively, which represents a rather short range to build a scaling law. We note with interest that an upper k_{cy} value of close to 10^7 s⁻¹ was obtained for the (Ala-Gly-Gln)₄ oligopeptide in Figure 1.2 when the $k_{cy} \propto N^{-\gamma}$ relationship was approached. The upper boundary of 10^7 s⁻¹ of this short range of $\langle k_1 \rangle$ values will be further reduced, since stiffer backbones with an N value of 40 will yield a lower $\langle k_1 \rangle$ value. This $\langle k_1 \rangle$ value is too small to build the $\langle k_1 \rangle \propto N^{-\gamma}$ trend in Figure 1.4 needed to compare polymers having different backbone stiffnesses. Of course, the use of a longer-lived dye would extend the range of N and $\langle k_1 \rangle$ values accessible to FQ-EEC experiments, but the procedure would still remain limited to oligomers and could not apply to polymers, particularly so if they have a stiff

backbone. The procedure based on FQ-EEC experiments is very well-suited for polymers with a backbone that is more flexible than polystyrene such as poly(ethylene oxide) or polydimethylsiloxane, as illustrated in Figure 1.4. For stiffer polymers such as polypeptides with high degrees of polymerization comparable to those of proteins, whose LRPCD would be most valuable to characterize in order to facilitate the prediction of the 3-dimensional structure they fold into, the above discussion leads to the conclusion that FQ-EEC experiments in their current form will struggle to deliver relevant information on their LRPCD, since they will be limited to short oligopeptides making it difficult to generate the $k_{cy} \propto N^{-\gamma}$ relationship.

1.11 Fluorescence Quenching Experiments to Probe the LRPCD of Stiff Polymers

Despite the limitations of FQ-EEC experiments for the characterization of the LRPCD of stiff polymers in solution, quenching experiments conducted on fluorescently labeled macromolecules are still endowed with a number of worthwhile features, particularly their ability to probe isolated macromolecules in solution. The two main drawbacks of FQ-EEC experiments are first, the small amount of EEC events being generated between a dye and its quencher covalently attached to the opposite ends of a chain and second, the strong $\langle k_1 \rangle$ dependency on N which imposes that a series of end-labeled polymers with narrow MWD be prepared to establish the $\langle k_1 \rangle \propto N^{-\gamma}$ trend. These drawbacks could be circumvented by studying polymers randomly labeled with a dye and quencher. As shown in Figure 1.5 for different pyrene-labeled polystyrenes, pyrene excimer formation is greatly enhanced at the same pyrene content when polystyrene is randomly labeled with pyrene rather than end-labeled.³⁶ This massive enhancement in pyrene excimer formation can be explained as

follows. Whereas two pyrene labels attached to the ends of a polymer have a 100% probability to be held far apart from each other, thus reducing dramatically the chance of EEC encounter for longer chains, the same two pyrene labels always have a non-zero probability to be attached next to each other along a chain of any length, and thus form excimer efficiently, as long as the polymer is randomly labeled with pyrene. Consequently, if the purpose of a fluorescence quenching experiment is to probe the diffusive encounters between a dye and a quencher, Figure 1.5 indicates that randomly labeled chains are much better suited for this purpose than end-labeled chains, contrary to common belief.

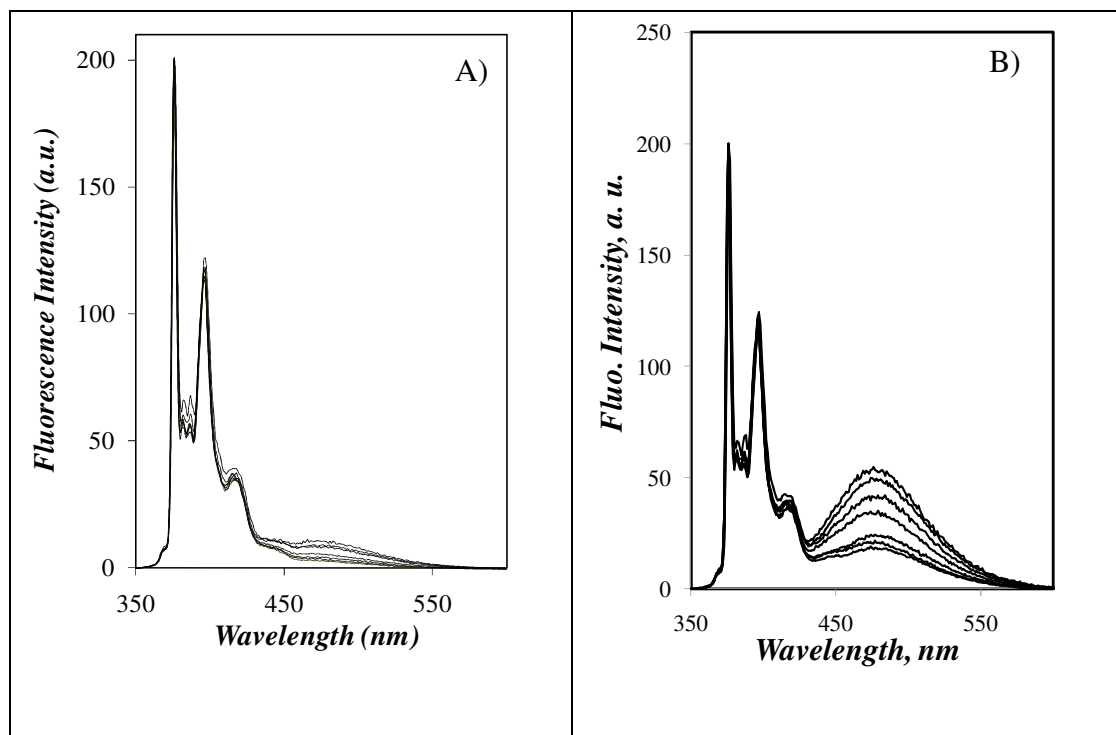


Figure 1.5: Steady-state fluorescence spectra of polystyrene A) $\text{Py}_2\text{-PS}(8\text{K})$ with a 2.6 mol% pyrene content³⁶ and B) PyBA-PS with a 2.1 mol% pyrene content.⁶² Solvents from top to bottom: methyl ethyl ketone, dichloromethane, tetrahydrofuran, toluene, dimethyl formamide, dioxane, and dimethyl acetamide.

While the study of randomly labeled polymers appeared to be best suited to characterize their LRPCD in solution, it was complicated early on by the absence of a model such as Birks' scheme for pyrene end-labeled monodisperse polymers²² that would enable the analysis of the complex quenching kinetics of an excited dye by quenchers randomly distributed along the chain. In order to fill this theoretical gap, a first version of the fluorescence blob model (FBM) was introduced in 1999.⁶⁵ The 1999 version of the FBM defined the *blob* as the volume within the polymer coil probed by an excited dye. The *blob* could then be viewed as a unit volume that could be used to compartmentalise the polymer coil into a cluster of *blobs*, among which the quenchers would be randomly distributed according to a Poisson distribution. The equations that were derived by Tachiya⁶⁶ to describe the quenching of dyes by quenchers randomly distributed among surfactant micelles could then be applied to the fluorescence decays of randomly labeled polymers, by considering that dyes and quenchers randomly distributed among *blobs* would display the same quenching kinetics as if they were randomly distributed among surfactant micelles. To date, the FBM has been applied to the analysis of the monomer and excimer decays acquired with several polymers randomly labeled with pyrene.^{36,62-70} Through FBM analysis of the fluorescence decays, the size of a *blob* N_{blob} , expressed in terms of the number of monomers encompassed inside a *blob*, and the rate constant k_{blob} of excimer formation between one excited and one ground-state pyrene located inside a same *blob* could be determined. The pair of parameters N_{blob} and k_{blob} obtained with the fluorescence decays of randomly labeled polydisperse polymers analyzed according to the FBM were equivalent to the pair of parameters N and $\langle k_1 \rangle$ obtained from FQ-EEC experiments carried out on end-labeled monodisperse polymers analyzed with Birks' scheme.

After noting that the global analysis of the monomer and excimer fluorescence decays with the FBM yielded poor fits at early times when the decays were acquired with a time-resolved fluorometer with improved time resolution, the FBM was further expanded in 2010⁶² to account for the rapid rearrangement of the dyes that takes place with a larger rate constant k_2 after slow diffusive motions have brought the pyrene-labeled monomers in the chains in close contact with each other. The excellent fits obtained through FBM global analysis of the monomer and excimer fluorescence decays of several polymers randomly labeled with pyrene, combined with the relevance of the parameters k_{blob} and N_{blob} retrieved from this type of analysis, led to the establishment of the product $k_{\text{blob}} \times N_{\text{blob}}$ as a reliable measure of the LRPCD in solution. How this conclusion was reached is presented in the following section.

1.12 A Universal Parameter to Describe LRPCD in Solution Based on Randomly Labeled Polymers

Many experiments have been conducted over the past 15 years to assess the validity of the FBM and have been summarized in a number of reviews.^{23,24} Among these experiments, one important step toward the establishment of a parameter that would describe LRPCD in solution was the study of the effect that the mode of incorporation of the pyrene label into polystyrene might have on the kinetics of excimer formation.^{36,62} Three series of pyrene-labeled polystyrene were prepared by copolymerizing styrene with 1-pyrenemethylacrylamide, 1-pyrenebutyl acrylate, or 4-(1-pyrene)methoxymethylstyrene yielding PyAN-PS, PyBA-PS, and PyMe-PS, respectively; their chemical structure is presented in Table 1.2. In the case of PyAN-PS, the pyrene label was held close to the main

chain via a rigid methylamide bond. By comparison, the butyl ester linker connecting pyrene to the main chain of PyBA-PS was more flexible and held pyrene further away from the PS backbone. The reach of pyrene away from the main chain was further enhanced in the PyMe-PS series.

Table 2.2: Chemical structure of polystyrene and poly(*N*-isopropylacrylamide) randomly labeled with pyrene.

PyMe-PS	PyBA-PS	PyAN-PS	PyBAN-PNIPAM

The fluorescence decays of the Py-PS constructs in a wide range of solvents were analyzed according to the FBM and each Py-PS construct was found to yield a different set of parameters k_{blob} , N_{blob} , and product $k_{\text{blob}} \times N_{\text{blob}}$. This result underlined the importance of using a similar pyrene derivative for comparison purposes. Yet despite the different trends obtained for k_{blob} , N_{blob} , and $k_{\text{blob}} \times N_{\text{blob}}$, these parameters could be normalized so that all N_{blob} or $k_{\text{blob}} \times N_{\text{blob}}$ values fell on a master curve when plotted as a function of the inverse of solvent viscosity (η^{-1}), an indication that these trends reported on the LRPCD of polystyrene in

solution (Figure 1.6) regardless of the chemical composition of the monomer bearing the pyrene label.⁶² Furthermore, the product $k_{cy} \times N$ obtained for several pyrene end-labeled monodisperse polystyrenes yielded trends as a function of η^{-1} that, after normalization, overlapped those obtained with $k_{blob} \times N_{blob}$ for PyAN-PS, PyBA-PS, and PyMe-PS.²³ The overlapping trends demonstrated that these pyrene-labeled polystyrenes reported in the same manner on the LRPCD of polystyrene, regardless of the mode of pyrene labeling selected to prepare the Py-PS constructs. Similar conclusions were reached after comparing the products $k_{blob} \times N_{blob}$ and $k_{cy} \times N$ for a series of poly(*N*-isopropylacrylamide) randomly and end-labeled with pyrene, respectively, where overlapping trends were obtained for both types of constructs.⁶⁹ These trends are shown in Figure 1.6. Together these studies demonstrated the equivalence that exists between the information on the LRPCD retrieved from monodisperse end-labeled polymers or polydisperse polymers randomly labeled with pyrene and, consequently, that the FBM analysis of polymers randomly labeled with pyrene provided the same information on the LRPCD of polymers as the FQ-EEC experiments did. But instead of being limited to the study of oligomers as typically done with FQ-EEC experiments, FBM analysis could be applied to actual polymers with any degree of polymerization, as long as it was larger than that of a *blob*. In practice, that is meant that contrary to FQ-EEC experiments on end-labeled monodisperse oligomers, polymers with degrees of polymerization much greater than 100 could be employed.

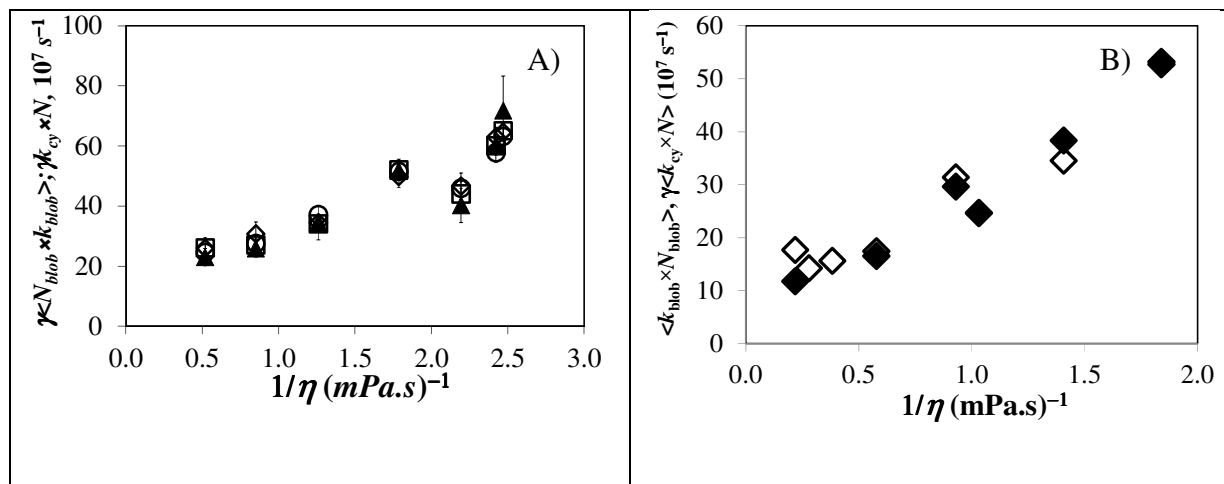


Figure 1.6: Plots of the products $\langle k_{blob} \times N_{blob} \rangle$ and $k_{cy} \times N$ after normalization as a function of the inverse of solvent viscosity for A) Py₂-PS (▲), PyAN-PS (□), PyBA-PS (○), PyMe-PS (◇) and B) PyBAN-PNIPAM (◇), Py₂-PNIPAM (◆).

1.13 Relevance of Fluorescence Quenching Experiments to Study Protein Folding

Fluorescence quenching experiments on linear chains have been instrumental in providing robust experimental tools to probe the LRPCD in synthetic polymers, and more importantly biological polymers such as polypeptides. Fluorescence quenching EEC experiments carried out on end-labeled oligopeptides provide a direct measure of the time scale over which the most elementary step in protein folding takes place, namely loop formation. These experiments, together with FBM studies on randomly labeled polymers, have enabled the comparison of the LRPCD of different polymeric backbones. But another possibly important impact of fluorescence quenching experiments might be the demonstration through the FBM analysis of fluorescence decays of randomly labeled polymers that the mobility of a monomer in a chain is limited to a subvolume of the polymer coil. As pointed out in a 2006 article,⁷² this insight could help resolve Levinthal's famous paradox.⁷³

In 1969, Levinthal pointed out that a protein made of a large number of amino acids would take an infinitely long time to sample its entire conformational space before folding into its final 3-dimensional structure.⁷³ Indeed, if the protein was made of 300 amino acids (aa), each taking 1 ps to probe three possible conformations, it would take $3^{300} \times 1 \text{ ps} = 4.3 \times 10^{121}$ centuries for the 300 aa-long protein to fold. Since proteins are capable of folding within the much shorter lifetime span of living organisms, Levinthal's paradox demonstrated that proteins could not probe the entire conformational space. This conclusion led scientists to postulate theories that would enable a protein to fold without having to probe its entire conformational space. Such theories include the framework model,⁷⁴ the nucleation model,^{75,76} the hydrophobic collapse model,⁷⁷ or a folding pathway along an energy funnel.^{78,79} Yet, if the theoretical framework of the FBM is correct and the monomers of a chain can only probe a subvolume of a polymer coil called a *blob*, then the folding time of a protein would be that required for a *blob* to fold times the number of *blobs* constituting the protein. If one uses the N_{blob} value of ~ 20 aa found for poly(L-glutamic acid) labeled with 1-pyrenemethylamine and studied with the FBM,^{80,81} the same 300 aa protein discussed earlier would be made of 15 *blobs* and its folding time would decrease from 4.3×10^{121} centuries down to $15 \times 3^{20} \times 1 \text{ ps} = 52 \text{ ms}$, a much more reasonable folding time. As a matter of fact, the *blobs* determined by the FBM might be equivalent to the recently introduced *foldons*, a *foldon* being a ~ 20 aa segment of a protein where folding is initially believed to occur.⁸² The *foldons* might very well be equivalent to the *blobs* introduced as early as 1993 in an early version of the FBM as the loci where folding of a much longer chain is believed to take place.⁸³

1.14 Project Objective

As demonstrated in the literature review, the research conducted in the Duhamel Laboratory has established that Fluorescence Blob Model (FBM) analysis of the process of excimer formation between pyrene labels randomly attached onto a linear chain provides the same information about the chain dynamics of a given polymer as the more traditional experiments conducted with monodisperse oligomers end-labeled with two pyrenyl moieties. Main advantages associated with the use of a randomly labeled polymer include the ease of synthesis and the ability to study actual long chain polymers instead of oligomers. Among the many questions that remain to be answered is the extent to which the kinetics of pyrene excimer formation reflects the long range polymer chain dynamics (LRPCD) of a given backbone. It is noteworthy that despite three decades devoted to the study of LRPCD with end-labeled linear polymers, there exists only a single report in the scientific literature that compares the LRPCD of only two different backbones (ref #33). The other direct comparison of the results obtained with different backbones was shown in Figure 1.4 of this thesis, that describes the $\langle k \rangle$ value for EEC of polystyrene (PS), poly(ethylene oxide) (PEO), poly(dimethyl siloxane) (PDMS), and a polycarbonate (PC). The results showed that PEO and PDMS were more flexible than PS as expected, but rigid PC yielded surprisingly large $\langle k \rangle$ values that would infer that its backbone was more flexible than that of PS, an implausible conclusion.

The main objective of this thesis was thus to gauge how reliable the kinetics of pyrene excimer formation were to probe the internal dynamics in solution of macromolecules randomly labeled with pyrene. This was achieved by studying the process of pyrene excimer formation in a series of poly(alkyl methacrylate)s where the pyrene label was linked to the

main chain via the same linker and the size of the alkyl side chain was varied, or where the alkyl side chain was maintained constant and the length of the linker connecting the pyrene label to the main chain was varied. In each case, relevant information about the LRPCD experienced by the pyrene labels could be retrieved that properly reflected the architecture of the macromolecule being investigated. These studies were expanded to include the characterization of the internal dynamics of 72 pyrene-labeled constructs that included linear poly(alkyl methacrylate)s, but also macromolecules having highly branched architectures (dendrimers, amylopectin). In this case, Model Free Analysis (MFA) was applied to investigate how general the process of pyrene excimer formation is to probe the internal dynamics of virtually any type of macromolecule.

A second, but no less important objective, was to investigate how the chemical composition of the linker connecting the pyrene label to the main chain affects its ability to probe the polarity of its local environment. Since this property of pyrene is associated with the fact that its 0-0 transition is symmetry-forbidden, modification of pyrene with a linker for the purpose of covalent attachment onto a macromolecule breaks the symmetry and restores the 0-0 transition, so that the pyrene label becomes much less sensitive to the polarity of its local environment. Based on comments made in a few articles,⁸⁴⁻⁸⁶ this thesis investigated whether the introduction of an oxygen atom in the β -position to pyrene would re-symmetrise the electronic wavefunction of the pyrene label and re-establish its ability to probe the polarity of its local environment.

The experiments described in this thesis are expected to enrich our understanding on how the fluorescence of pyrene can be applied to yield information about the internal

dynamics and local polarity within a macromolecule, by monitoring the pyrene excimer and monomer fluorescence, respectively.

1.15 Thesis Summary

The results presented in this thesis demonstrate that FBM analysis of fluorescence decays acquired with polymers randomly labeled with pyrene yields reliable information about their LRPCD from the product $\langle k_{\text{blob}} \times N_{\text{blob}} \rangle$, where k_{blob} is the rate constant of pyrene excimer formation inside a *blob* containing one excited and one ground-state pyrene and N_{blob} is the number of structural units found within a *blob*. In particular, when a series of poly(alkyl methacrylate)s with different side chain lengths was randomly labeled with pyrene, $\langle k_{\text{blob}} \times N_{\text{blob}} \rangle$ was found to decrease with increasing side chain length until it reached a plateau for a dodecyl side chain indicating that the LRPCD were no longer affected by an increase in side chain length. Additional controls showed that removing the methyl substituent of poly(methyl methacrylate) to yield poly(methyl acrylate) resulted in a two-fold increase in $\langle k_{\text{blob}} \times N_{\text{blob}} \rangle$. Substituting an *n*-butyl or *n*-hexyl side chain by a *tert*-butyl or cyclohexyl side chain resulted in a marked decrease in $\langle k_{\text{blob}} \times N_{\text{blob}} \rangle$, reflecting the slower LRPCD associated with a stiffer side chain. The combination of these results justifies the claim that the product $\langle k_{\text{blob}} \times N_{\text{blob}} \rangle$ provides a reliable measure of the LRPCD of linear chains, akin to the glass transition temperature which characterizes the flexibility of polymers in the bulk.

This first series of experiments dealt with polymers where pyrene was linked to the main chain with a same linker while the side chain of the methacrylate monomer was varied. Since branched macromolecules that have been under increased scientific scrutiny, the effect

of the linker length connecting pyrene to a poly(butyl methacrylate) chain was investigated by introducing 0, 1, 2, and 3 ethylene glycol units between the 1-pyrenemethoxy moiety and the methacrylate monomer. Application of the FBM analysis to the fluorescence decays showed that N_{blob} increased quasi linearly with the number of ethylene glycol units used in the pyrene linker. In fact, the increase in N_{blob} was found to match the expected increase in linker length associated with the addition of one ethylene glycol unit. The excellent agreement found between the molecular changes applied to the pyrene-labeled methacrylate monomer and the results obtained by fluorescence suggests that pyrene excimer fluorescence could be used effectively to probe the behaviour of highly branched macromolecules such as dendrimers or polymeric bottle brushes by covalently attaching pyrene at the branch extremities.

The experiments conducted with different oligo(ethylene glycol) linkers led to a surprising experimental observation. While the modification of pyrene with a reactive substituent introduced for labeling purposes at the end of a 4-carbon atom butyl spacer reduced its ability to probe the polarity of its local environment, the presence of an oxygen atom in the β -position to pyrene was found to restore the sensitivity of pyrene to the solvent polarity. This led to a complete investigation of this effect where the fluorescence behaviour of 1-pyrenemethoxyethanol was compared to that of 1-pyrenebutanol, either as free molecules in solution or bound to a poly(butyl methacrylate) backbone. The study confirmed that 1-pyrenemethoxyethanol displayed the same response to solvent polarity as unsubstituted pyrene does, but that the response of 1-pyrenebutanol was strongly reduced. An additional benefit of using a pyrene derivative with an oxygen atom in the β -position was the lengthening of its natural lifetime by more than 60 ns, an important advantage to probe the

slow internal dynamics of macromolecules. The combined improvements of better probing the polarity of the environment and working with a longer-lived dye should result in the more widespread use of such pyrene derivatives to study macromolecules in solution.

Finally, the demonstrated ability of pyrene excimer fluorescence to yield quantitative information on the internal dynamics of different series of pyrene-labeled poly(alkyl methacrylate)s, polystyrene, poly(*N,N*-dimethylacrylamide), or polybutadiene led to the investigation of whether the process of excimer formation could be harnessed to determine the internal dynamics of macromolecules having different architectures (linear-versus-branched) and prepared with different pyrene-labeling strategies (randomly-versus-end-labeled). To this end, the average rate constant $\langle k \rangle$ of pyrene excimer formation by diffusion was investigated with 72 pyrene-labeled macromolecules (PyLMs) in toluene, tetrahydrofuran, dimethyl formamide, and dimethyl sulfoxide. Master curves were obtained for $\langle k \rangle$ in all solvents and the range of applicability of these master curves was found to cover three orders of magnitude. This impressive dynamic range suggests that pyrene excimer formation can be used to describe quantitatively the internal dynamics of most macromolecules in solution.

1.16 Thesis Outline

Chapter 1 reviewed the work that has been done with pyrene-labeled polymers to gain quantitative information on the internal dynamics of linear chains. Chapter 2 presents the results describing the efficiency of pyrene excimer formation through, in part, the product $\langle k_{\text{blob}} \times N_{\text{blob}} \rangle$ for nine series of poly(alkyl methacrylate) that bore alkyl side chains of different length and were randomly labeled with pyrene. Chapter 3 introduces 1-

pyrenemethoxyethanol (PyMeEGOH) as an alternate fluorescent probe to study the internal dynamics and the polarity of macromolecules. In Chapter 4, the number of atoms in the linker connecting pyrene to a series of poly(butyl methacrylate)s is varied from 3 to 12 and the diffusive motions of the main chains were probed by the pyrene labels attached to the tip of the extended linkers using pyrene excimer fluorescence. This chapter reports the effect of the linker length on the polymer backbone dynamics perceived by the pyrene label as it is placed further away from the main chain. In Chapter 5, the applicability of the Model Free Analysis (MFA) to probe the internal dynamics of a variety of pyrene-labeled macromolecular constructs is investigated in four different solvents. Chapter 6 summarizes the entire thesis and suggested potential future work.

Chapter 2

Effect of Side-Chain Length on the Polymer Chain Dynamics of Poly(alkyl methacrylate)s in Solution

Reproduced with permission from Farhangi, S.; Weiss, H.; and Duhamel, J. Effect of Side-Chain Length on the Polymer Chain Dynamics of Poly(alkyl methacrylate)s in Solution. *Macromolecules* **2013**, *46*, 9738-9747. Copyright 2013, American Chemical Society.

2.1 Overview

Eight series of poly(alkyl methacrylate)s bearing different side-chains and one series of poly(methyl acrylate) were randomly labeled with pyrene and their ability to form pyrene excimer was characterized quantitatively by steady-state and time-resolved fluorescence to demonstrate that such measurements provide a quantitative measure of polymer chain dynamics (PCD) in solution. Each series of pyrene-labeled polymer showed increased excimer formation with increasing pyrene content, but the increase was more pronounced for the polymers known to be more flexible based on their reported glass transition temperature (T_g). In the case of the poly(alkyl methacrylate)s with a linear side-chain, a shorter side-chain resulted in increased excimer formation. Replacing a linear side-chain with a more rigid one containing the same number of carbon atoms resulted in decreased mobility of the polymer. Fluorescence Blob Model (FBM) analysis of the fluorescence decays provided a more accurate representation of those pyrenes that formed excimer by diffusion, and thus reflected PCD more precisely. Global FBM analysis of the pyrene monomer and excimer fluorescence decays yielded the blob size N_{blob} and the product $k_{\text{blob}} \times N_{\text{blob}}$ which reflects PCD. For each series, both N_{blob} and $k_{\text{blob}} \times N_{\text{blob}}$ remained constant with pyrene content. Their average value $\langle N_{\text{blob}} \rangle$ and $\langle k_{\text{blob}} \times N_{\text{blob}} \rangle$ decreased substantially with increasing side-chain length, addition of the α -methyl substituent to poly(methyl acrylate) to yield poly(methyl methacrylate), or increased rigidity of the side chain, demonstrating that an increase in bulkiness or stiffening of the side- or main chain is associated with a pronounced decrease in chain mobility. These experiments are the first to demonstrate that pyrene excimer formation can be used to characterize quantitatively PCD in solution in the same manner that T_g is being used to characterize PCD in the bulk.

2.2 Introduction

The parameter most commonly used to characterize polymer chain dynamics (PCD) in the bulk is certainly the glass transition temperature (T_g).¹ Depending on the polymer chemical composition, T_g increases substantially with increasing backbone stiffness, as crankshaft motions involving a stretch of ~50 – 60 backbone atoms within a much larger polymer chain require additional thermal energy to occur.² Rheology, calorimetry, and dielectric spectroscopy have been extremely successful at determining T_g for a wide variety of polymeric backbones.^{1,2} By contrast, the only other technique capable of characterizing PCD in solution by probing a similar stretch of tens of backbone atoms within a much larger polymer chain isolated in solution is time-resolved fluorescence (TRF), that is being used to determine the rate constant of quenching between an excited dye and its quencher both covalently attached to a same macromolecule.³ For reasons which have been reviewed in a number of publications,^{4,5} the experiment most commonly encountered to probe PCD in solution by TRF consists in labeling a linear chain with the chromophore pyrene and monitoring the rate constant of pyrene excimer formation between an excited and a ground-state pyrene. This type of experiments introduced close to 40 years ago by Zachariasse and Kühnle with pyrene end-labeled alkyl chains⁶ were quickly extended to series of first, monodisperse poly(ethylene oxide) end-labeled with pyrene by Cuniberti and Perico⁷ and second, pyrene end-capped monodisperse polystyrene by Winnik et al.⁸ Advertised since their inception as a means to probe PCD in solution, it is fair to acknowledge that to this day, TRF experiments based on the study of monodisperse short polymers end-labeled with pyrene have failed to establish a single parameter as widely accepted as T_g that could be used to characterize the PCD of different polymeric backbones in solution. This is unfortunate, as

a better characterization of PCD in solution could lead to a better understanding of how polypeptides fold into the three dimensional structure of a catalytically active protein⁹⁻¹³ or how solutions of associative thickeners shear-thin as the polymers undergo conformational rearrangement that favors intra- over intermolecular associations.¹⁴

Reasons for this state-of-affair include the relatively challenging preparation of monodisperse linear chains labeled at each end with a single pyrenyl moiety, the massive reduction in the efficiency of pyrene excimer formation for stiff polymeric backbones, and the strong dependency of the rate constant of end-to-end cyclization with chain length which complicates the direct comparison of the PCD of different polymeric backbones having different flexibility. Due to these complications, some of the most basic experiments aiming to demonstrate the ability of TRF to probe the PCD of polymers in solution have not been reported in the scientific literature. One of these experiments would consist in monitoring how varying a single molecular parameter such as the side chain length of a series of poly(alkyl methacrylate)s affects their PCD in solution. In the bulk, it is common knowledge that the extra free volume introduced by long, flexible side-chains leads to a decrease in the T_g of poly(alkyl methacrylate)s as it enables easier motion of their backbone.¹ Since such a basic experiment remains to be conducted by applying TRF to pyrene end-labeled monodisperse polymers, it suggests that its implementation is challenging, in part due to the issues raised earlier. It follows from this discussion that a redesign of the experiment might be in order.

To conduct this experiment, the ideal TRF-based procedure must be easy to implement and yield a single parameter that could be used to characterize the PCD of a wide

variety of polymers in solution in a manner similar to how T_g is being used to characterize PCD in the solid state. Work conducted by this laboratory over the past 15 years has established that quantitative information about PCD can be retrieved through the Fluorescence Blob Model (FBM) analysis of the fluorescence decays acquired with polymers randomly labeled with pyrene. The FBM assumes that the motion of a pyrene label covalently attached onto a polymer is restricted to a small volume within the much larger polymer coil.^{15,16} This small volume is referred to as a *blob*, which is then used to divide the polymer coil into a cluster of *blobs* among which the pyrenyl groups, themselves covalently attached onto the polymer in a random fashion, distribute themselves randomly according to a Poisson distribution. FBM analysis of the fluorescence decays yields N_{blob} , the number of monomers encompassed inside a *blob*, and k_{blob} , the rate constant of excimer formation between an excited and a ground-state pyrene both located inside a same *blob*. So far, two studies have shown that the product $k_{\text{blob}} \times N_{\text{blob}}$ provides a quantitative measure of the rate constant of pyrene excimer formation similar to that of pyrene end-labeled monodisperse polymers.¹⁷⁻¹⁹ Contrary to the latter polymers, whose synthesis requires the implementation of controlled living polymerizations, the randomly labeled polymers used in a FBM study do not need to be monodisperse and can be prepared in a much easier manner.

The present study takes advantage of the synthetic ease afforded by the random copolymerization of 1-pyrenebutyl methacrylate and eight alkyl methacrylates to prepare eight poly(alkyl methacrylate)s randomly labeled with pyrene, whose fluorescence decays were analyzed according to the FBM. The $k_{\text{blob}} \times N_{\text{blob}}$ products retrieved from the FBM study of all polymer series show a clear correlation between the chemical composition of a side-

chain and its effect on the PCD of the resulting polymer. To this date, any other study using fluorescently end-labeled monodisperse linear chains to probe their PCD has never involved more than 3 polymeric backbones. By comparison, the present study characterizes no less than 9 different polymers. These experiments demonstrate the relative ease of characterizing PCD in solution by applying the FBM to the analysis of the fluorescence decays acquired with solutions of polymers randomly labeled with pyrene. These experiments also confirm that FBM analysis can characterize PCD in solution directly and quantitatively. Considering the importance of PCD in solution to rationalize a variety of macromolecular phenomena ranging from protein folding to the complex rheological behavior of associative polymer solutions, the methodology presented herein offers a robust means to characterize quantitatively PCD in solution, which should find a broad range of applications.

Materials: Chemicals were purchased from Sigma-Aldrich and used as received unless otherwise stated. Distilled in glass tetrahydrofuran (THF) was purchased from Caledon Laboratories and used as received. n-Octyl methacrylate was purchased from Scientific Polymer Products, Inc.

Synthesis of 1-pyrenebutyl acrylate: The synthesis and purification of 1-pyrenebutyl acrylate has been described elsewhere.¹⁸

Synthesis of 1-pyrenebutyl methacrylate (PyBuMA): 1-Pyrenebutanol (1.00 g, 3.64 mmol) and dry triethylamine (1.2 g, 12 mmol) were dissolved in 20 mL of dichloromethane (DCM) and transferred to a 50 mL round bottom flask. The solution was cooled to 5 °C and purged

with N₂ for 20 minutes. Methacryloyl chloride (0.55, 6 mmol) was dissolved in 6 mL DCM and added drop-wise. The solution was stirred under N₂ at room temperature for 24 hours. After the reaction, the solution was washed with 0.5 M HCl, saturated sodium carbonate solution, saturated NaCl solution, and water in that sequence. The organic phase was dried over anhydrous sodium sulfate overnight. The solvent was removed under a gentle flow of nitrogen under the fumehood, and the yellow remaining crude product was dissolved in a minimum amount of DCM and purified on a silica gel column using a 60:40 DCM to hexane mixture. The solid was then re-crystallized in methanol to obtain a pale-yellow solid in a 60% yield.

300 MHz ¹H NMR (CDCl₃) PyBuMA: δ 1.81-1.99 (m, 7H, -CH₂-CH₂-, CH₃-), δ 3.39 (t, 2H, Py-CH₂-), δ 4.2 (t, 2H, -CH₂-O), δ 5.5 (s, 1H, =CH₂), δ 6.08 (s, 1H, =CH₂), δ 7.9-8.4 (m, 9H, Py H's).

Random copolymerization: The pyrene-labeled poly(alkyl methacrylate)s were prepared by copolymerization of 1-pyrenebutyl methacrylate with methyl methacrylate (C1MA), butyl methacrylate (C4MA), tert-butyl methacrylate (C4TMA), hexyl methacrylate (C6MA), cyclohexyl methacrylate (C6CyMA), octyl methacrylate (C8MA), lauryl methacrylate (C12MA), and stearyl methacrylate (C18MA) to yield Py-PC1MA, Py-PC4MA, Py-PC4TMA, Py-PC4TMA, Py-PC4MA, Py-PC6CyMA, Py-PC8MA, Py-PC12MA, and Py-PC18MA, respectively. Pyrene-labeled poly(methyl acrylate) (Py-PC1A) was prepared by copolymerizing 1-pyrenebutyl acrylate with methyl acrylate (C1A). The chemical structure of all the polymers is shown in Figure 2.1. The synthesis of all the polymers was conducted in a similar manner. The preparation of Py-PC1MA is described in more detail hereafter.

The monomethyl ether hydroquinone (MEHQ) stabilizer in methyl methacrylate was removed by filtration through a column filled with MEHQ inhibitor-remover beads. A Schlenk tube was flamed under vacuum to remove residual traces of water before being filled with dry N₂. To the Schlenk tube were added C1MA (0.88 g, 8.79 mmol), 1 mL toluene solution of 1-pyrenebutyl methacrylate (0.026 g, 0.076 mmol), and 1 mL toluene solution of azobisisobutyronitrile (AIBN, 1.45 mg, 9 μmol). The molar amount of monomers was kept constant for all copolymerizations and the ratio of pyrene-labeled to unlabeled monomer was varied to achieve different pyrene contents. The initiator concentration was kept the same in all the copolymerizations.

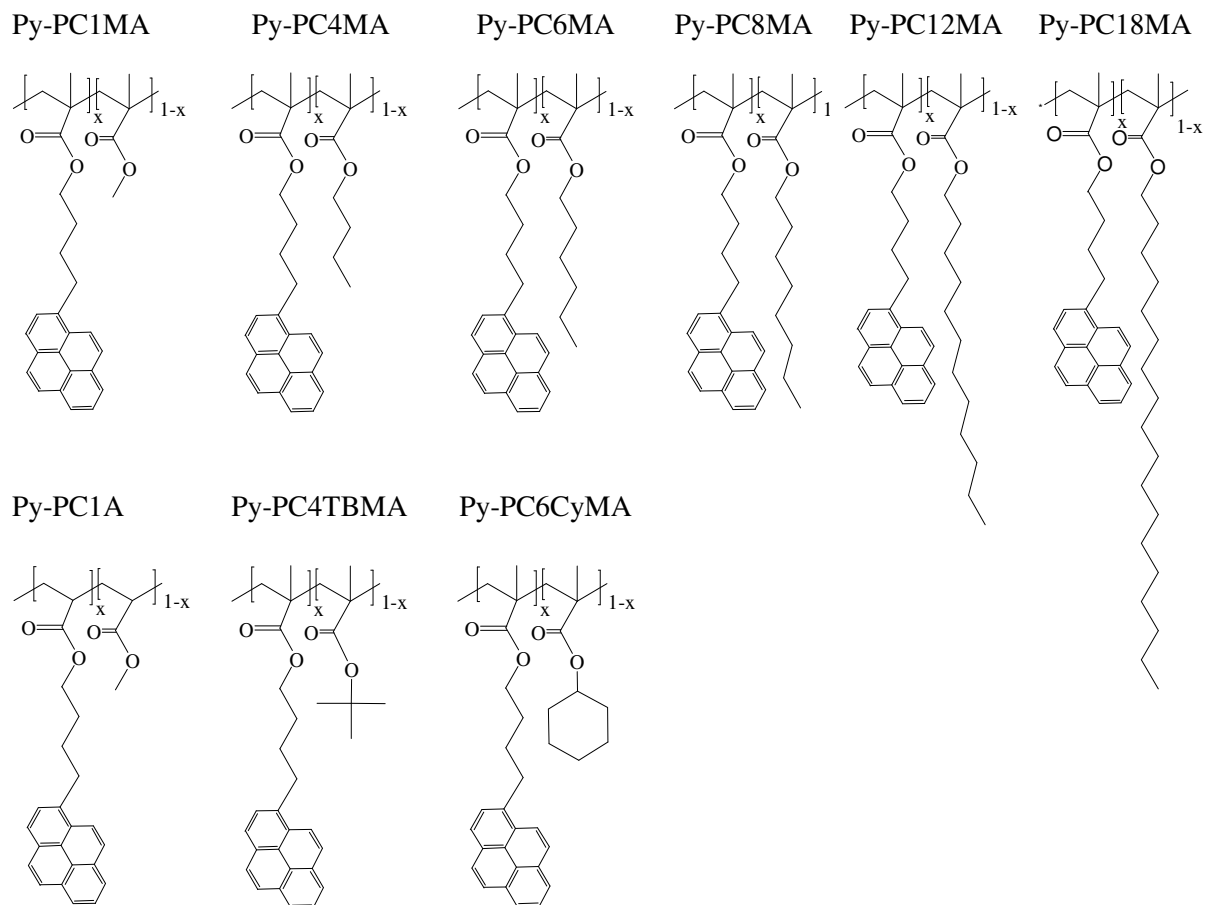


Figure 2.1: Chemical structure of Py-PC1MA, Py-PC4MA, Py-PC6MA, Py-PC8MMA, Py-PC12MA, Py-PC18MA, Py-C1A, Py-PC4TMA, and Py-PC6CyMA.

The copolymerizations were carried out in an oil bath at 65 °C and the composition drift was minimized by stopping the copolymerization at a conversion of 0.2 or less. The conversion at the end of the copolymerization was determined by ^1H NMR as described in the Appendices (Supporting Information for Chapter 2 (SI2)). Once the desired conversion was reached, the reaction vessel was cooled on ice and the polymer in the reaction mixture was precipitated in methanol. The recovered polymer was re-dissolved in THF and re-precipitated in methanol. The precipitation cycle was repeated 5-7 times to remove any unreacted 1-pyrenebutyl

methacrylate monomer. The final yield was approximately 10% in each copolymerization. Typical ^1H NMR spectra of all the polymers prepared in this study and the method used to determine the conversion after termination of the copolymerization are given in Figures SI2.3-SI2.11 and Table SI2.1, respectively.

Molecular weight determination: The characterization of the molecular weight distribution (MWD) of the polymers was done by Gel Permeation Chromatography (GPC) on a Viscotek GPC device equipped with a 305 Triple Detector Array that includes the differential refractive index (DRI), viscosity, and light scattering. A Viscotek UV-Vis absorption detector 2600 was added for characterization of the fluorescently labeled polymers. Before injection, the polymer samples with a concentration of about 0.5 mg/mL in THF were filtered through 0.2 μm pore size PTFE filters from Waters. The GPC instrument was operated at a constant flow rate of 1 mL/min. Representative GPC traces for all the polymer series prepared in this study are shown in SI2 (Figure SI2.2). In all the GPC analyses, the DRI signal was used to locate where the polymer eluted, while the UV signal was used to confirm that first, the polymer was actually labeled with pyrene, and second, a minimal amount of pyrene-labeled monomer eluted at the solvent peak, indicating its successful removal thanks to the successive precipitations. The DRI, viscosity, and light scattering signals were used to determine the absolute molecular weight of the polymers. The absolute molecular weights and polydispersity indices (PDIs) of all the samples are listed in Table 2.1.

Table 2.1: Pyrene content, absolute molecular weight, and PDI of the pyrene-labeled polymers whose chemical structure was shown in Figure 2.1.

Py-PC1MA			Py-PC4MA			Py-PC6MA		
Pyrene Content	Mn	PDI	Pyrene Content	Mn	PDI	Pyrene Content	Mn	PDI
[mol %]	[g/mol]	[-]	[mol %]	[g/mol]	[-]	[mol %]	[g/mol]	[-]
0.3	134,000	1.70	0.3	174,000	1.93	0.3	249,000	1.86
1.3	130,000	1.42	1.1	272,000	1.99	2.0	139,000	1.93
2.7	200,000	1.33	2.2	296,000	1.44	3.3	125,000	1.95
4.0	135,000	1.60	3.0	197,000	1.39	4.7	151,000	1.97
5.3	206,000	1.70	3.6	264,000	1.68	5.8	183,000	1.84
5.6	170,000	1.55	5.3	275,000	1.97	6.6	116,000	1.76
7.3	176,000	1.80	7.2	416,000	1.76	8.1	179,000	1.97
Py-PC8MA			Py-PC12MA			Py-PC18MA		
Pyrene Content	Mn	PDI	Pyrene Content	Mn	PDI	Pyrene Content	Mn	PDI
[mol %]	[g/mol]	[-]	[mol %]	[g/mol]	[-]	[mol %]	[g/mol]	1.45
0.4	244,000	1.87	0.5	530,000	1.72	0.7	563,000	1.54
1.8	305,000	1.88	1.4	265,000	1.70	1.4	810,000	1.52
2.7	312,000	1.75	3.5	244,000	2.43	4.5	480,000	1.44
4.3	146,000	2.04	5.6	507,000	1.70	5.9	663,000	1.42
5.1	371,000	1.83	6.0	174,000	2.17	6.8	705,000	1.41
6.1	234,000	1.88	7.7	662,000	2.10	6.7	719,000	1.49
7.3	271,000	2.07	10.2	265,000	1.68	14.2	770,000	1.45
Py-PC1A			Py-PC4TMA			Py-PC6CyMA		
Pyrene Content	Mn	PDI	Pyrene Content	Mn	PDI	Pyrene Content	Mn	PDI
[mol %]	[g/mol]	[-]	[mol %]	[g/mol]	[-]	[mol %]	[g/mol]	1.67
1.7	148,000	2.00	0.2	112,000	1.58	0.2	296,000	1.93
2.6	236,000	1.40	2.0	150,000	1.80	2.0	187,000	1.61
2.6	313,000	1.40	3.6	127,000	1.72	3.0	206,000	2.00
3.0	173,000	1.42	3.8	183,000	1.56	3.8	244,000	2.14
5.0	138,000	2.08	4.7	233,000	1.25	5.1	263,000	2.19
6.2	145,000	1.38	5.6	147,000	1.65	6.2	192,000	2.04
6.7	870,000	2.40	7.6	141,000	2.19	7.0	268,000	1.67

Pyrene content of the pyrene-labeled polymers: The pyrene content (λ_{Py} expressed in μmol of pyrene per gram of polymer) was determined by acquiring the absorption spectrum of solutions of a carefully weighed mass (m) of the polymer samples dissolved in THF on a Varian Cary 100 Bio spectrophotometer. Knowing the molar absorbance coefficient of 1-pyrenebutanol at 344 nm ($41,000 \text{ M}^{-1} \cdot \text{cm}^{-1}$), the absorbance yielded the concentration of 1-pyrenebutanol [Py] in the solution by applying Beer-Lambert law at 344 nm and λ_{Py} was obtained from the ratio $[\text{Py}]/m$. The molar fraction (x) of pyrene-labeled monomers in the copolymer was determined by applying Eq. 2.1 where M and M_{Py} represent the molar mass of the unlabeled and pyrene-labeled monomer, respectively.

$$x = \frac{M}{M - M_{\text{Py}} + 1/\lambda_{\text{Py}}} \quad (2.1)$$

Steady-state fluorescence measurements: Steady-state fluorescence spectra were acquired on a Photon Technology International LS-100 steady-state fluorometer with an Ushio UXL-75 Xenon lamp and a PTI 814 photomultiplier detection system. The spectra were obtained using the usual right angle geometry. The samples were dissolved in THF and diluted to an optical density of ~ 0.1 , equivalent to a pyrene concentration of $\sim 2.5 \times 10^{-6} \text{ M}$, low enough to prevent intermolecular excimer formation. The solutions were degassed for 30 minutes by bubbling nitrogen. This step expels oxygen out of the solution, which otherwise would act as a quencher of pyrene. The polymer solutions were excited at 344 nm and the fluorescence

spectra were acquired from 350 to 600 nm. The fluorescence intensity of the excimer (I_E) and that of the monomer (I_M) were obtained by integrating the signal in the fluorescence spectra from 500 to 530 nm and from 372 to 378 nm, respectively. The I_E and I_M values were used to calculate the I_E/I_M ratio, that provides a qualitative measure of the efficiency of pyrene excimer formation for a given pyrene-labeled polymer.

Time-resolved fluorescence measurements: The monomer and excimer fluorescence decays were acquired with an IBH Ltd. time-resolved fluorometer using an IBH 340 nm NanoLED as the excitation source. Samples were prepared in the same manner as for steady-state fluorescence. Samples were excited at a wavelength of 344 nm, and the monomer and excimer emission were detected at 375 nm and 510 nm, respectively. The fluorescence decays were acquired over 1,024 channels using a time-per-channel of 1.02 or 2.04 ns/ch.

Fluorescence Decay Analysis – The Fluorescence Blob Model. The FBM was applied to fit the fluorescence decays of the pyrene monomer and excimer globally. Within the FBM framework,^{18,19} five pyrene species are being considered. The pyrene population Py_{diff}^* represents the structural units of the polymer bearing a pyrene label that diffuse slowly inside the polymer coil. These diffusive motions are well-described by the three FBM parameters that are $\langle n \rangle$, the average number of ground-state pyrenes per *blob*, k_{blob} , the rate constant of excimer formation in a *blob* that contains one excited pyrene and a single ground-state pyrene, and the product $k_e \times [blob]$, where k_e is the rate constant describing the exchange of ground-state pyrenes between blobs and $[blob]$ is the local *blob* concentration inside the polymer coil. When two structural units bearing a pyrene pendant encounter, the excited

pyrene monomer Py_{diff}^* turns into the pyrene species $Py_{k_2}^*$ which undergoes a rapid rearrangement with the nearby ground-state pyrene to form an excimer EO^* with a rate constant k_2 . The excimer EO^* fluoresces with a lifetime τ_{EO} . The random labeling of the polymer results in a population Py_{free}^* of pyrenes that are isolated along the backbone and cannot form excimer. They emit as if they were free in solution with the lifetime τ_M of the pyrene monomer. The random labeling of the polymer generates some pyrene clusters where direct excitation of poorly stacked pyrenes results in long-lived pyrene dimers EL^* that emit with a lifetime τ_{EL} . Eqs. 2 and 3 were derived to account for the five different pyrene species present in solution, and they have been found to fit satisfactorily the fluorescence decays of the pyrene monomer and excimer for a number of polymers randomly labeled with pyrene.^{18,19}

$$\begin{aligned}
[Py^*]_{(t)} = & [Py_{diff}^*]_{(t)} + [Py_{k_2}^*]_{(t)} + [Py_{free}^*]_{(t)} = [Py_{diff}^*]_o \exp\left(-\left(A_2 + \frac{1}{\tau_M}\right)t - A_3(1 - \exp(-A_4 t))\right) \\
& + \left([Py_{k_2}^*]_o + [Py_{diff}^*]_o e^{-A_3} \sum_{i=0}^{\infty} \frac{A_3^i}{i!} \frac{A_2 + iA_4}{A_2 + iA_4 - k_2} \right) \exp\left(-\left(k_2 + \frac{1}{\tau_M}\right)t\right) \\
& - [Py_{diff}^*]_o e^{-A_3} \sum_{i=0}^{\infty} \frac{A_3^i}{i!} \frac{A_2 + iA_4}{A_2 + iA_4 - k_2} \exp\left(-\left(A_2 + iA_4 + \frac{1}{\tau_M}\right)t\right)
\end{aligned}$$

$$+[Py_{free}^*]_o \exp\left(-\frac{t}{\tau_M}\right) \quad (2.2)$$

$$\begin{aligned}
[E^*]_{(t)} = [E0^*]_{(t)} + [EL^*]_{(t)} = k_2 & \left(\left([Py_{k_2}^*]_o + [Py_{diff}^*]_o e^{-A_3} \sum_{i=0}^{\infty} \frac{A_3^i}{i!} \frac{A_2 + iA_4}{A_2 + iA_4 - k_2} \right) \right. \\
& \times \frac{\exp\left(-\frac{t}{\tau_{E0}}\right) - \exp\left(-\left(k_2 + \frac{1}{\tau_M}\right)t\right)}{k_2 + \frac{1}{\tau_M} - \frac{1}{\tau_{E0}}} \\
& \left. + [Py_{diff}^*]_o e^{-A_3} \sum_{i=0}^{\infty} \frac{A_3^i}{i!} \frac{A_2 + iA_4}{A_2 + iA_4 - k_2} \frac{\exp\left(-\left(A_2 + iA_4 + \frac{1}{\tau_M}\right)t\right) - \exp\left(-\frac{t}{\tau_{E0}}\right)}{A_2 + iA_4 + \frac{1}{\tau_M} - \frac{1}{\tau_{E0}}} \right) \\
& + [E0^*]_o \times \exp\left(-\frac{t}{\tau_{E0}}\right) + [EL^*]_o \times \exp\left(-\frac{t}{\tau_{EL}}\right) \quad (2.3)
\end{aligned}$$

The expressions of the parameters A_2 , A_3 , and A_4 used in Eqs. 2.2 and 2.3 are given in Eq. 2.4 as a function of $\langle n \rangle$, k_{blob} , and $k_e \times [blob]$.

$$A_2 = \langle n \rangle \frac{k_{blob} k_e [blob]}{k_{blob} + k_e [blob]} \quad A_3 = \langle n \rangle \left(\frac{k_{blob}}{k_{blob} + k_e [blob]} \right)^2 \quad A_4 = k_{blob} + k_e [blob] \quad (2.4)$$

The fluorescence decays of the pyrene monomer and excimer were fitted globally according to Eqs. 2 and 3, and the parameters used in these equations were optimized with the Marquardt-Levenberg algorithm.²⁰ The fit yielded the parameters $\langle n \rangle$, k_{blob} , and $k_e [blob]$. The monomer decay analysis yielded the molar fractions f_{Mdiff} , f_{Mk2} , and f_{Mfree} representing the pyrene species Py_{diff}^* , Py_{k2}^* , and Py_{free}^* contributing to the monomer decays, respectively. In a similar manner, the excimer decay analysis with Eq. 3 yielded the fractions f_{Ediff} , f_{Ek2} , f_{EE0} , and f_{EEL} which represent the molar fractions of the pyrene species Py_{diff}^* , Py_{k2}^* , $E0^*$, and EL^* contributing to the excimer decays, respectively. The fractions f_{Mdiff} , f_{Mk2} , f_{Mfree} , f_{Ediff} , f_{Ek2} , f_{EE0} , and f_{EEL} can then be combined to determine the overall molar fractions of each pyrene species present in solution f_{diff} , f_{k2} , f_{free} , f_{E0} , and f_{EL} . The molar fraction f_{Mfree} together with $\langle n \rangle$ and the pyrene content λ_{Py} can be used to determine N_{blob} , the average number of structural units per *blob* whose expression is given in Eq. 2.5.

$$N_{blob} = \frac{1 - f_{Mfree}}{\lambda_{Py}} \frac{\langle n \rangle}{[M_{Py}(x) + M_{MA}(1-x)]} \quad (2.5)$$

The fits of the monomer and excimer decays were considered good if the χ^2 was smaller than 1.2 and the residuals and the autocorrelation function of the residuals were randomly distributed around zero.

Error determination of the parameters retrieved from the FBM analysis: For each pyrene-labeled sample, the monomer and excimer fluorescence decays were acquired and analyzed globally according to the FBM to yield the parameters listed in Tables SI2.2 and SI2.3. An estimate of the error generated by this analysis was obtained by taking the set of parameters retrieved from each analysis for a given pyrene-labeled sample and using these parameters to simulate 20 monomer fluorescence decays and 20 excimer fluorescence decays with different Poisson noise patterns. These 20 sets of monomer and excimer decays with different noise patterns were analyzed according to the FBM and the 20 sets of parameters retrieved from these analyses were averaged and their standard deviation was reported in Tables SI2.2 and SI2.3. Except for the samples with lower pyrene contents, that formed little excimer and for which the parameters were retrieved with larger error bars, the error retrieved on each parameter was relatively small, i.e. less than 5%, except for these parameters such as the fractions f_{Mfree} or f_{EE0} that took a value close to zero and which were retrieved with larger error bars.

2.4 Results and Discussion

The steady-state fluorescence spectra acquired for the series of Py-PC4MA samples in THF with pyrene content ranging from 1 – 7 mol% are shown in Figure 2.2. The intensity is

normalized at 375 nm and set to an arbitrary value of 100. The fluorescence spectra were acquired for samples with a pyrene concentration of 2.5×10^{-6} M, dilute enough to avoid intermolecular excimer formation. The fluorescence spectra show the sharp peaks at 375 and 410 nm, characteristic of the pyrene monomer, as well as the broad structureless emission of the pyrene excimer centered at 480 nm. As the pyrene content of the polymer increased from 1 to 7 mol%, more pyrene excimer was formed as a result of increased encounters between the pyrene labels inside polymer coils that are isolated in solution.

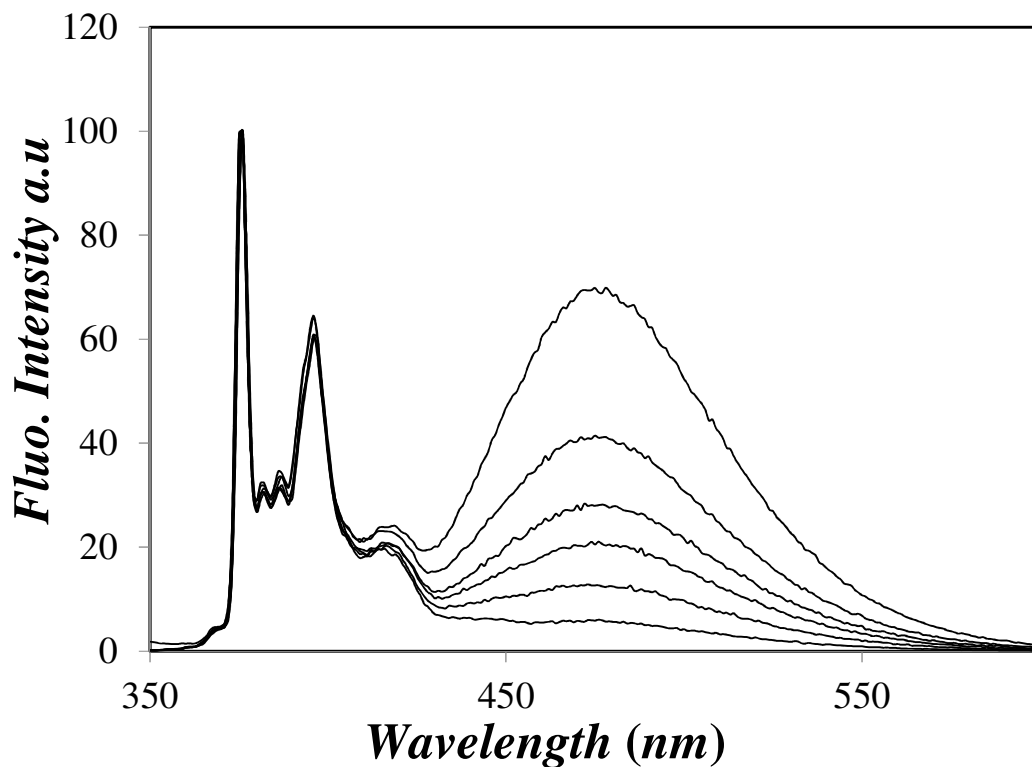


Figure 2.2: Steady-state fluorescence spectra for Py-PC4MA in THF; the pyrene content decreases from 7 mol% (top) to 1 mol% (bottom). $[\text{Py}] = 2.5 \times 10^{-6}$ M, $\lambda_{\text{ex}} = 344$ nm.

The I_E/I_M ratios were calculated from the fluorescence spectra for the eight series of poly(alkyl methacrylate)s and the series of poly(methyl acrylate) and they were plotted as a function of pyrene content in Figure 2.3A. For all polymer series, the I_E/I_M ratio increased with increasing pyrene content as a result of the increased local pyrene concentration $[Py]_{loc}$, which leads to more pyrene-pyrene encounters and consequently increased excimer formation. None of the lines representing the I_E/I_M ratio as a function of pyrene content in Figure 2.3A passed through the origin. Excimer formation was delayed in Figure 2.3A, as enough pyrene needed to be covalently attached to the polymer to bring the pyrene labels within striking range from each other to form an excimer. Indeed, pyrene excimer formation is a local phenomenon that occurs between an excited and a ground-state pyrene labels that are separated by less than a few tens of monomers, as will be found later in Figure 2.6. Consequently, the pyrene content must be large enough to allow at least two pyrene units within a polymer stretch constituted of a few tens of monomers. No pyrene excimer can be formed until this threshold pyrene content, i.e. ~ 1.5 mol% in Figure 2.3A, is reached. After the pyrene content corresponding to this threshold was reached, all the trends in Figure 2.3A showed a somewhat linear increase of the I_E/I_M ratio with increasing pyrene content. The slopes of the lines, $m(I_E/I_M)$, shown in Figure 2.3A were determined and plotted as a function of the number of carbon atoms in the side-chain of the poly(alkyl methacrylate)s in Figure 2.3B. Since the slope $m(I_E/I_M)$ is a measure of the efficiency of pyrene excimer formation, the trend shown in Figure 2.3B illustrates clearly the decrease in the efficiency of pyrene excimer formation with increasing side-chain length. For linear side-chains made of 8 carbon atoms or more, the slope $m(I_E/I_M)$ reaches a plateau indicating that the PCD of the poly(alkyl methacrylate)s are no longer affected by side-chain length.

The decrease in $m(I_E/I_M)$ with increasing side-chain length observed in Figure 2.3B is the result of a number of effects that all combine to slow down PCD. The first effect is a dampening of the backbone dynamics as a result of the larger side-chain that the backbone needs to drag in the solution. The second effect is due to steric hindrance, whereby the larger side-chains trying to pass past each other hinder backbone motion. The third effect is excluded volume as the larger side-chains occupy a larger volume, which leads to a stiffening of the main chain as is being observed with polymer bottlebrushes.²¹ Together, these three effects contribute to slowing the PCD of the poly(alkyl methacrylate)s.

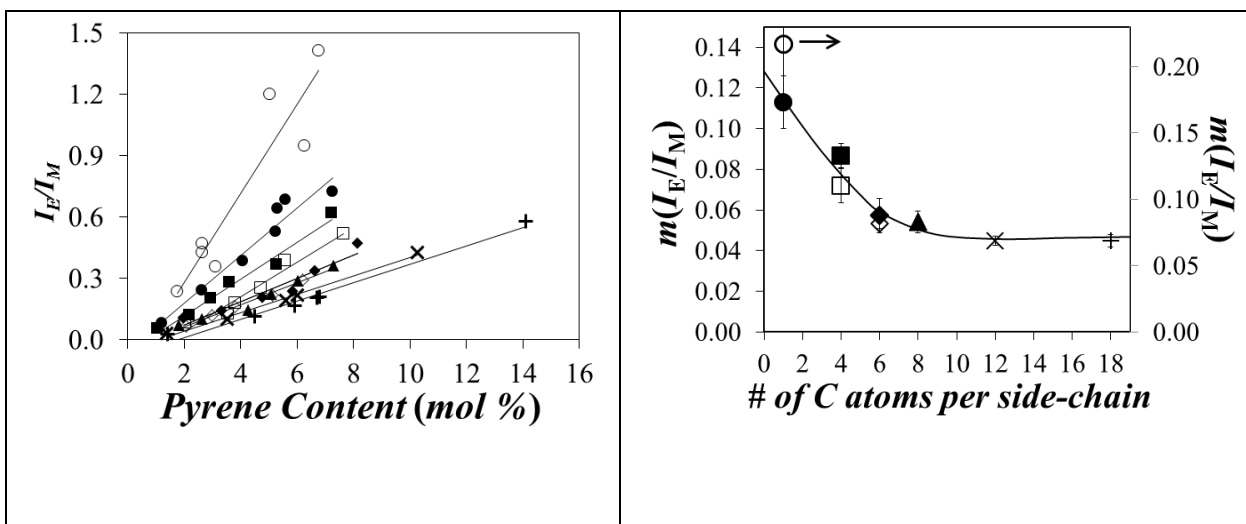


Figure 2.3: A) I_E/I_M ratios for all polymers with increasing pyrene contents. B) $m(I_E/I_M)$ for the polymers. Left axis: (●) Py-PC1MA, (■) Py-PC4MA, (□) Py-PC4TMA, (◆) Py-PC6MA, (◇) Py-PC6CyMA, (▲) Py-PC8MMA, (×) Py-PC12MA, (+) Py-PC18MA. Right axis: (○) Py-PC1A; $[Py] = 2.5 \times 10^{-6}$ M, $\lambda_{ex} = 344$ nm.

The trend in Figure 2.3B obtained for $m(I_E/I_M)$ with the poly(alkyl methacrylate)s having a linear side-chain can be used as a reference against which the slope $m(I_E/I_M)$ obtained with other polymers can be compared. In the case of Py-PC1A where the α -methyl substituent has been removed for each monomer along the backbone, $m(I_E/I_M)$ was found to be very large and equal to 0.22 ± 0.04 . This increase in $m(I_E/I_M)$ reflects the increase in PCD when comparing Py-PC1A and Py-PC1MA. The α -methyl substituent is known to slow PCD in the bulk substantially as T_g equals 10 and 105 °C for PC1A and PC1MA, respectively. Changing the side-chain from *n*-butyl to *tert*-butyl is also known to decrease PCD as T_g in the solid-state increases from 27 °C for PC4MA to 118 °C for PC4TMA. Similarly $m(I_E/I_M)$ decreases from 0.09 ± 0.01 to 0.07 ± 0.01 in Figure 2.3B. However, the magnitude of the change is not as pronounced as for T_g , mostly because the range of side-chain length for which a difference in $m(I_E/I_M)$ can be observed is smaller for the poly(alkyl methacrylate)s in solution. Indeed, when the *n*-hexyl side-chain of Py-PC6MA is replaced by a cyclohexyl side-chain, the $m(I_E/I_M)$ values obtained for Py-PC6MA and Py-PC6CyMA are equal within experimental error.

The relatively small range of side-chain length over which a change in PCD can be observed for the poly(alkyl methacrylate)s in THF appears to be a mere consequence of the limited effect that an increase in side-chain length has on PCD in solution for linear side-chains containing more than 8 carbon atoms. Nevertheless, the trend shown in Figure 2.3B demonstrates that the PCD in solution can be characterized quantitatively using pyrene excimer formation. However, the I_E/I_M ratio obtained from the analysis of the fluorescence spectra suffers from a number of drawbacks. As mentioned in the Experimental section

where Eqs. 2 and 3 were introduced for the fluorescence decays, several pyrene species are present in solution whose combined contributions result in the fluorescence spectrum. Only time-resolved fluorescence measurements can distinguish between the different pyrene species such as Py_{free}^* and EL^* , whose contribution becomes more important at low and high pyrene content, respectively. In terms of pyrene excimer formation by diffusion, the species Py_{free}^* that do not form excimer, and EL^* that form excimer instantaneously upon excitation, act as fluorescent impurities whose contributions should be accounted for if the fluorescence spectra of pyrene-labeled polymers are used to characterize PCD in solution. Fortunately, FBM analysis of the fluorescence decays is capable of isolating the species Py_{diff}^* in the fluorescence decays which is actually responsible for pyrene excimer formation by diffusion, and whose contribution to the fluorescence signal yields N_{blob} and the product $k_{blob} \times N_{blob}$, which provides a quantitative measure of PCD that is more accurate than that obtained from the parameter $m(I_E/I_M)$, derived from the analysis of steady-state fluorescence spectra.

Consequently, the fluorescence decays of the pyrene monomer and excimer of all the samples were acquired and fitted according to Eqs. 2.2 and 2.3, respectively. To minimize the number of floating parameters in the analysis program, the monomer lifetime τ_M was determined independently by preparing for each polymer series a copolymer with a low pyrene content of less than 0.7 mol%. With these polymers sparingly labeled with pyrene, most pyrene labels are incapable of forming excimer and they emit as if they were free in solution. Their decays were fitted with a sum of exponentials. The exponential with the longest decay time had the strongest contribution and the corresponding decay time was

attributed to τ_M . The τ_M values ranged from 195 ns for the Py-PC1MA series up to a maximum value of 207 ns for the Py-PC4TMA series. A shorter lifetime of 190 ns was obtained for Py-PC1A, possibly because the more flexible polyacrylate backbone might enhance deactivation of the excited pyrene by collisional encounters with solvent molecules and the polymer backbone. The value of τ_M found for each polymer series was then fixed in Eqs. 2.2 and 2.3 to fit the fluorescence decays.

Global analysis of the monomer and excimer decays was first carried out with Eqs. 2.2 and 2.3 by letting all parameters beside τ_M float. The rate constant k_2 obtained for all the polymer samples in a given polymer series was then averaged, and its averaged value was fixed in the decay analysis which was repeated. This procedure has been found to yield a much tighter set of values for the parameters $\langle n \rangle$, k_{blob} , and $k_e[\text{blob}]$ which represent the PCD.^{18,19} The fits were good with χ^2 values less than 1.20, and the residuals and autocorrelation of residuals were randomly distributed around zero. A sample of the fits is shown in Figure 2.4.

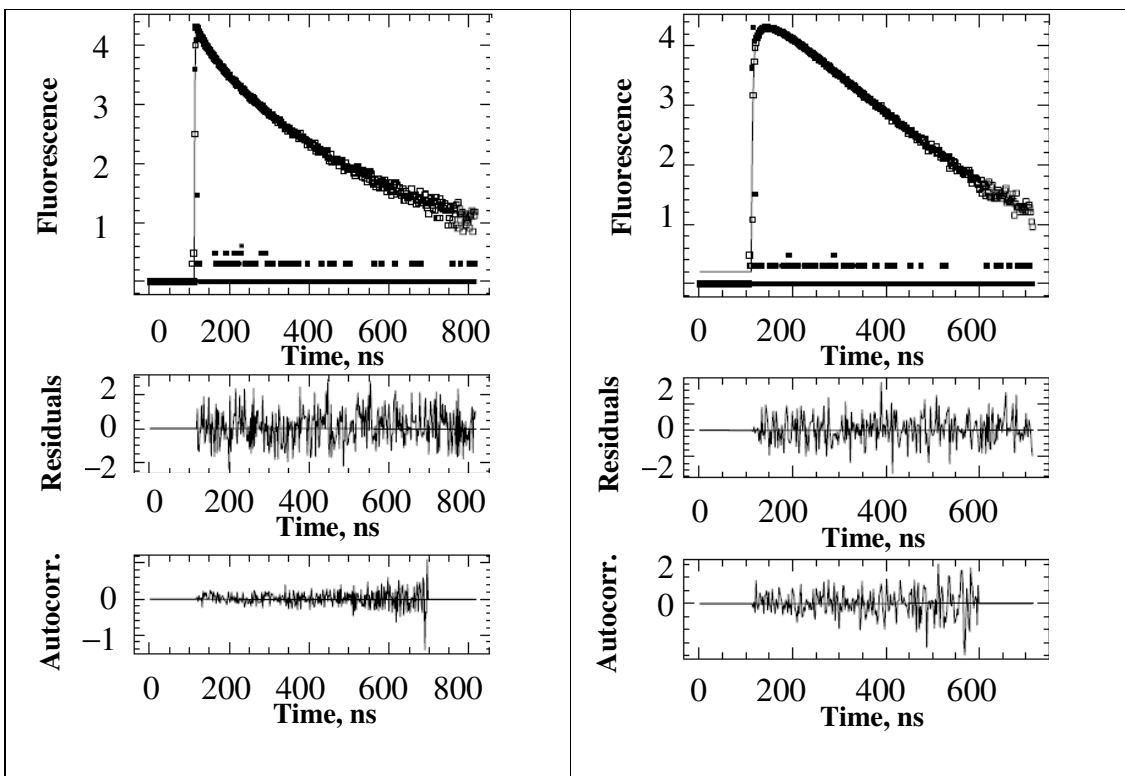


Figure 2.4: Monomer (left, $\lambda_{em}=375$ nm) and excimer (right, $\lambda_{em}=510$ nm) fluorescence decays of PC1MA labeled with ~ 5 mol% pyrene in THF. Acquired decays were analyzed globally using Eqs. 2 and 3; $[Py] = 2.5 \times 10^{-6}$ M, $\lambda_{ex} = 344$ nm, $\chi^2 = 1.1$.

One of the strengths of time-resolved fluorescence is on display in Figure 2.5, that shows a plot of f_{Mfree} versus pyrene content for the poly(alkyl methacrylate)s having a linear alkyl side-chain. The fraction f_{Mfree} represents the molar fraction of pyrene monomers that contribute as Py_{free}^* to the monomer decays. For each polymer series, f_{Mfree} takes a large value at low pyrene content, before decreasing to zero for higher pyrene contents. This trend parallels very nicely the observation made in Figure 2.3A that a minimum pyrene content

needs to be reached before excimer formation takes place. According to Figure 2.5, f_{Mfree} can reach up to 0.60 at low pyrene contents for the poly(alkyl methacrylate) samples having a large side-chain (Py-PC12MA and Py-PC18MA). Under such conditions, very little excimer formation takes place at low pyrene content. Another interesting finding from Figure 2.5 is that f_{Mfree} reaches zero at a higher pyrene content for poly(alkyl methacrylate) samples having a longer side-chain. This result is reasonable because a longer side-chain is expected to hinder the encounter between two pyrene labels more strongly, and thus result in a larger f_{Mfree} value.

The values of $\langle n \rangle$ and f_{Mfree} obtained from the decay analyses were then used in Eq. 2.5 to calculate N_{blob} which was plotted as a function of the pyrene content in Figure 2.6A for all the poly(alkyl methacrylate)s. Within experimental error, N_{blob} was found to remain constant with the pyrene content and to decrease with increasing side-chain length. The N_{blob} values were averaged for each polymer and the standard deviation was calculated. The averaged N_{blob} value, $\langle N_{blob} \rangle$, was plotted as a function of the number of carbon atoms in the side-chain of the poly(alkyl methacrylate)s in Figure 2.6B. $\langle N_{blob} \rangle$ decreased continuously with increasing side-chain length from 59 ± 5 for Py-PC1MA to 16 ± 1 for Py-PC18MA. The decrease in $\langle N_{blob} \rangle$ indicates that an excited pyrene probes a smaller volume inside the polymer coil when the side-chain length increases. The fact that the volume probed by an excited pyrene is reduced reflects a decrease in backbone mobility which can be attributed to the combination of a number of effects which have been described earlier. They include steric hindrance, excluded volume, and molecular friction.

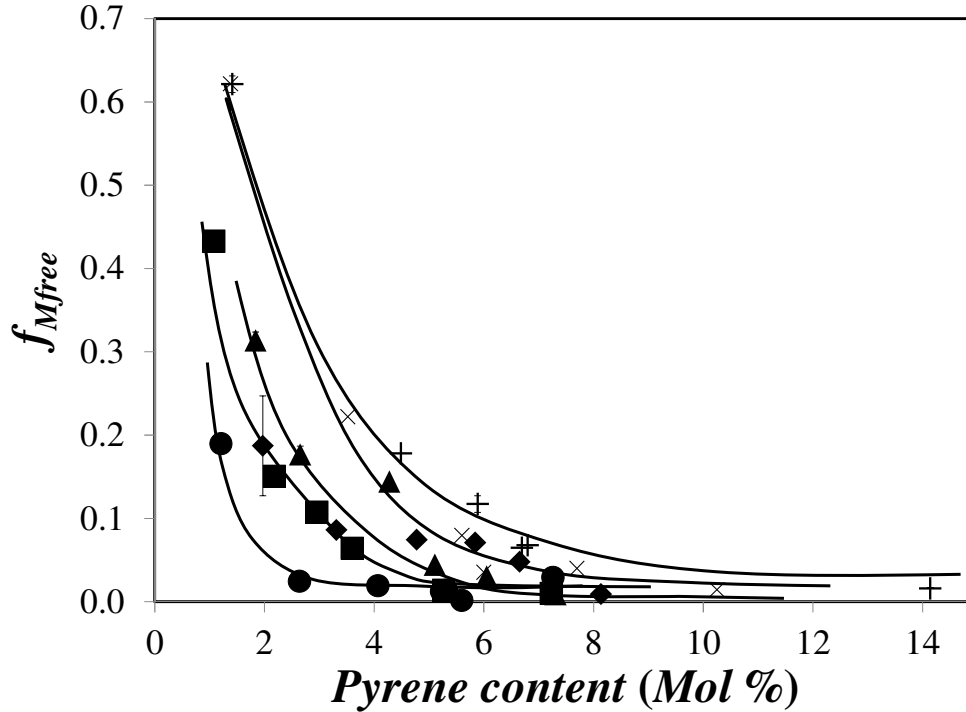


Figure 2.5: f_{Mfree} as a function of pyrene content; (●) Py-PC1MA, (■) Py-PC4MA, (◆) Py-PC6MA, (▲) Py-PC8MMA, (×) Py-PC12MA, (+) Py-PC18MA.

Beside chain length, there are other effects that are known to affect PCD in the bulk. One of them is the rigidity of the alkyl side-chain. For instance, T_g increases, respectively, from 27 to 118 °C between PC4MA and PC4TMA and from -5 to 83 °C between PC6MA and PC6CyMA. Similarly, $\langle N_{blob} \rangle$ was found to decrease from 44 ± 5 to 27 ± 4 between Py-PC4MA and Py-PC4TMA, and from 30 ± 4 to 24 ± 2 between Py-PC6MA and Py-PC6CyMA, respectively. The decrease in $\langle N_{blob} \rangle$ indicates a decrease in mobility, in agreement with what would be expected from T_g measurements in the bulk. Another effect

known to affect PCD is the presence of a methyl group in the α -position of the methacrylate monomer which reduces backbone flexibility as compared to polyacrylates. This is illustrated with the T_g of PC1MA and PC1A which equals 105 and 10 °C, respectively. The large decrease in T_g reflects the increase in backbone flexibility experienced by PC1A due to the absence of a methyl substituent in the α -position. Surprisingly, $\langle N_{\text{blob}} \rangle$ for Py-PC1A was found to equal 59 ± 10 , taking a value comparable to the value of 59 ± 5 found for Py-PC1MA. This result suggests that $\langle N_{\text{blob}} \rangle$ might not be able to describe PCD properly in all cases. One reason for this is that $\langle N_{\text{blob}} \rangle$ describes the *blob* size, but not how quickly the *blob* volume is being probed by the excited pyrene. As demonstrated in two earlier examples,^{18,19} a more accurate measure of the mobility of the excited pyrene inside a *blob* is provided by the product $k_{\text{blob}} \times N_{\text{blob}}$ which is being investigated hereafter.

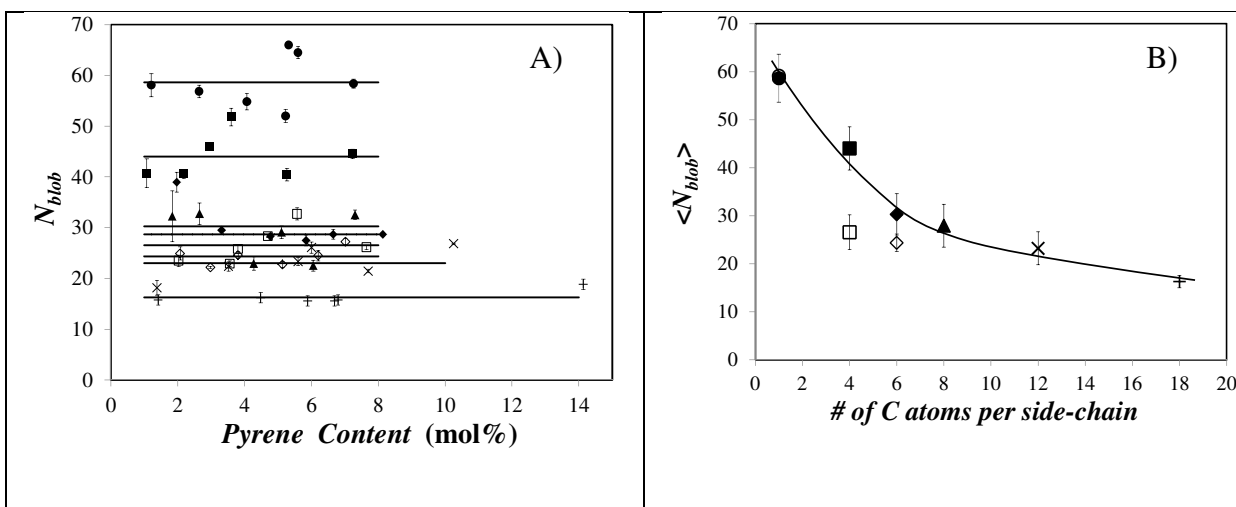


Figure 2.6: A) Plot of N_{blob} as a function of pyrene content for all poly(alkyl methacrylate)s.

B) Plot of $\langle N_{blob} \rangle$ versus the number of carbon atoms per side-chain. (●) Py-PC1MA, (■) Py-PC4MA, (□) Py-PC4TMA, (◆) Py-PC6MA, (◇) Py-PC6CyMA, (▲) Py-PC8MMA, (×) Py-PC12MA, (+) Py-PC18MA, (○) Py-PC1A.

When plotted against pyrene content in Figure 2.7A, $k_{blob} \times N_{blob}$ was found to remain more or less constant with pyrene content. For each polymer series, the data were averaged and $\langle k_{blob} \times N_{blob} \rangle$ was plotted as a function of side-chain length in Figure 2.7B. As for N_{blob} , $\langle k_{blob} \times N_{blob} \rangle$ decreased continuously with increasing side-chain length from $0.41 \pm 0.02 \text{ ns}^{-1}$ for Py-PC1MA to $0.14 \pm 0.01 \text{ ns}^{-1}$ for Py-PC18MA. No difference in $\langle k_{blob} \times N_{blob} \rangle$ was observed for Py-PC12MA and Py-PC18MA, suggesting that the length of a linear alkyl side-chain does not affect PCD when the side-chain is composed of more than 12 carbon atoms, a

conclusion that parallels nicely what was observed in Figure 2.3B with the parameter $m(I_E/I_M)$ obtained by analysis of the fluorescence spectra. Replacing an *n*-butyl by a *tert*-butyl side-chain reduces $\langle k_{\text{blob}} \times N_{\text{blob}} \rangle$ from $0.29 \pm 0.03 \text{ ns}^{-1}$ to $0.20 \pm 0.03 \text{ ns}^{-1}$, while replacing an *n*-hexyl by a cyclohexyl side-chain decreases $\langle k_{\text{blob}} \times N_{\text{blob}} \rangle$ from $0.22 \pm 0.01 \text{ ns}^{-1}$ to $0.18 \pm 0.02 \text{ ns}^{-1}$. The decrease in $\langle k_{\text{blob}} \times N_{\text{blob}} \rangle$ reflects the slower PCD expected for the polymethacrylate backbone when an *n*-alkyl side-chain is replaced by a more rigid one, and is in agreement with the trends reported with T_g for the same polymers in the bulk.

Most interestingly, $\langle k_{\text{blob}} \times N_{\text{blob}} \rangle$ equals $0.80 \pm 0.09 \text{ ns}^{-1}$ for Py-PC1A, which is double the value of $0.41 \pm 0.02 \text{ ns}^{-1}$ obtained for Py-PC1MA. Although Py-PC1MA and Py-PC1A have a similar N_{blob} values of 59, k_{blob} equals $14 \pm 1 \mu\text{s}^{-1}$ and $7.0 \pm 0.7 \mu\text{s}^{-1}$ for Py-PC1A and Py-PC1MA respectively. It appears that the less sterically hindered polyacrylate backbone allows an excited pyrene to probe a *blob* with a rate constant k_{blob} that is twice larger than for the polymethacrylate backbone. In turn, the product $\langle k_{\text{blob}} \times N_{\text{blob}} \rangle$ reflects what is expected about the PCD of the different polymers based on the trends which have been obtained with T_g for the same polymers in the bulk. The main difference between the results obtained in the bulk with T_g and in solution with $\langle k_{\text{blob}} \times N_{\text{blob}} \rangle$ is that the side-chain length of poly(alkyl methacrylate)s affects PCD in the bulk and in solution in an opposite manner. An increase in the length of a linear side-chain generates more free volume in the polymer matrix, which allows increased mobility of the main chain. Consequently, T_g is found to decrease continuously with increasing side-chain length. By comparison, a longer linear side-chain slows down PCD in solution to the point where it becomes so large that it no longer has

an effect on PCD. Based on the trend shown in Figure 2.7B, this limit is reached for side-chains containing 12 carbon atoms.

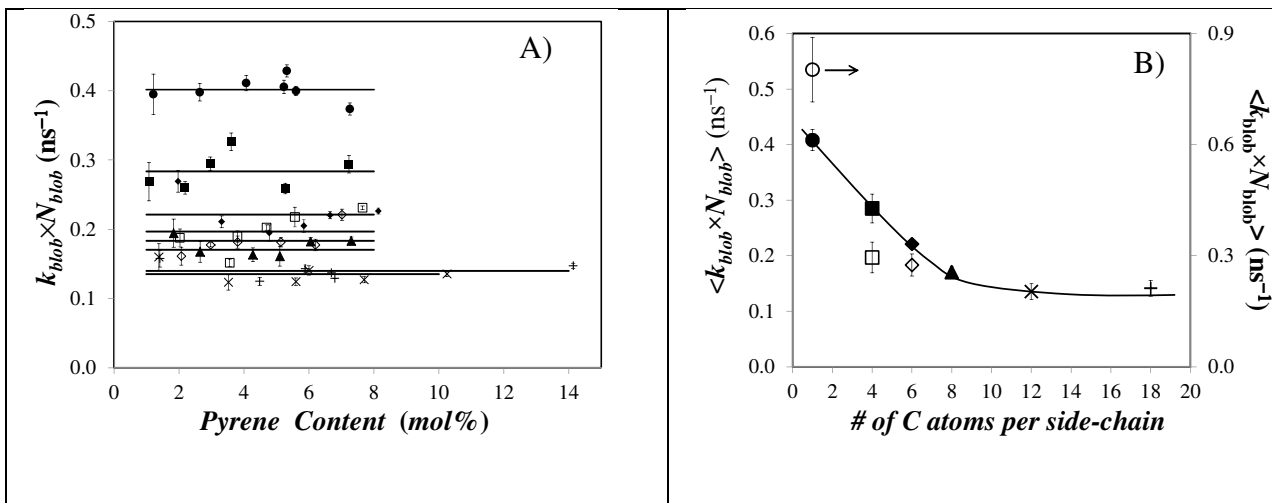


Figure 2.7: A) Plot of $k_{\text{blob}} \times N_{\text{blob}}$ as a function of pyrene content for all poly(alkyl methacrylates). B) Plot of $\langle k_{\text{blob}} \times N_{\text{blob}} \rangle$ versus the number of carbon atoms per side-chain.

(●) Py-PC1MA, (■) Py-PC4MA, (□) Py-PC4TMA, (◆) Py-PC6MA, (◇) Py-PC6CyMA, (▲) Py-PC8MMA, (×) Py-PC12MA, (+) Py-PC18MA, (○) Py-PC1A.

The $\langle k_{\text{blob}} \times N_{\text{blob}} \rangle$ value of $0.80 \pm 0.09 \text{ ns}^{-1}$ obtained for Py-PC1A can also be compared to that of $0.53 \pm 0.02 \text{ ns}^{-1}$ obtained for Py-PS in THF,¹⁸ a copolymer of styrene and 1-pyrenebutyl acrylate. Based on the results obtained with $\langle k_{\text{blob}} \times N_{\text{blob}} \rangle$, replacing the methyl ester group of poly(methyl acrylate) with the bulkier and more rigid phenyl substituent of polystyrene (PS) reduces the mobility of the PS backbone substantially when

compared to that of PC1A. This result agrees with the T_g values of PS and PC1A reported to equal 100 and 10 °C, respectively. However, the decrease in the $\langle k_{\text{blob}} \times N_{\text{blob}} \rangle$ values from 0.53 ± 0.02 to $0.41 \pm 0.02 \text{ ns}^{-1}$ for, respectively, Py-PS and Py-PC1MA, disagrees somewhat with the similar T_g values of 100 and 105 °C reported for PS and PC1MA. One reason for this discrepancy might be the existence of π - π interactions between the benzene rings of PS in the bulk which are absent in solution. These interactions could result in an anomalously large T_g value for PS. This explanation rationalizes why chain flexibility decreases as PC1A > PS > PC1MA for the polymers in solution based on the $\langle k_{\text{blob}} \times N_{\text{blob}} \rangle$ values, whereas it decreases as PC1A > PS \approx PC1MA for the polymers in the bulk based on the T_g values.

2.5 Conclusions

The aim of this study was to utilize fluorescence to probe the PCD of different polymer backbones in solution as a function of different structural parameters known to affect PCD. To this end, several series of pyrene labeled poly(alkyl methacrylate)s were prepared and their ability to form excimer was characterized by steady-state and time-resolved fluorescence. Analysis of the steady-state fluorescence spectra to determine the slope $m(I_E/I_M)$ showed that excimer formation decreased with increasing side-chain length of the poly(alkyl methacrylate)s from Py-PC1MA to Py-PC12MA, after which it remained constant for Py-PC18MA. Changing the side-chains from a flexible *n*-butyl or *n*-hexyl to a more rigid *tert*-butyl or cyclohexyl side-chain led to a decrease in the parameter $m(I_E/I_M)$. Also, removal of the α -methyl of PC1MA to yield the fluorescently labeled Py-PC1A series resulted in a

large increase in $m(I_E/I_M)$ reflecting an enhancement in chain flexibility, as expected from T_g measurements on the non-fluorescently labeled polymers in the bulk. While these trends are interesting, they can be made more accurate if those pyrene labels that form excimer by diffusion can be isolated through FBM analysis of the fluorescence decays.

To this end, time-resolved fluorescence decays of the pyrene monomer and excimer of all the poly(alkyl methacrylate)s labeled with pyrene were acquired and analyzed with the FBM. These analyses yielded N_{blob} and $\langle k_{blob} \times N_{blob} \rangle$, which could be related to the PCD of the different polymer samples. N_{blob} decreased from 59 ± 5 repeat units per *blob* for Py-PC1MA to 16 ± 1 repeat units per *blob* for Py-PC18MA. The reason for the decrease in N_{blob} could be explained by a decrease in backbone flexibility due to an increase in side-chain length. However, N_{blob} for Py-PC1MA and Py-PC1A were found to take a same value of 59 units. This result was surprising at first, since the PC1A backbone without the α -methyl substituent is known to be much more flexible than the PC1MA backbone, and T_g decreases from 105 °C for PC1MA to 10 °C for PC1A. This result was rationalized by noting that N_{blob} provides a physical measure of the volume probed by an excited pyrene, but not about the velocity at which the excited pyrene searches for a ground-state pyrene within the volume of a *blob*. This measure is obtained from the product $\langle k_{blob} \times N_{blob} \rangle$, which was plotted in Figure 2.6B as a function of side-chain length. $\langle k_{blob} \times N_{blob} \rangle$ was found to decrease with decreasing backbone flexibility. Changing an *n*-alkyl side-chain with a more rigid side-chain containing the same number of carbon atoms led to a decrease in backbone mobility. Most importantly, the value of $\langle k_{blob} \times N_{blob} \rangle$ for Py-PC1A was doubled that for Py-PC1MA reflecting the enhanced mobility of the PC1A backbone.

This study carried out with no less than nine different polymer series demonstrates that the characterization of excimer formation between pyrene labels covalently attached onto a polymer via FBM analysis of their fluorescence decays provides a reliable tool to probe PCD in solution quantitatively. In particular, the parameter $\langle k_{\text{blob}} \times N_{\text{blob}} \rangle$ was shown to report faithfully on the PCD of several polymers in solution in a manner similar to the T_g for polymers in the bulk. This study can now be used as a reference against which the PCD of other polymer backbones in solution can be compared. Considering the importance of PCD in a large number of phenomena encountered in polymer solutions, the methodology introduced in this study is expected to open new venues of research where quantitative characterization of PCD is required to rationalize phenomena involving solutions of macromolecules.

Chapter 3

A Pyrenyl Derivative with a Four Atom-Linker that Can Probe the Local Polarity of Pyrene-Labeled Macromolecules

Reproduced with permission from Farhangi, S.; Duhamel, J. A Pyrenyl Derivative with a Four Atom-Linker that Can Probe the Local Polarity of Pyrene-Labeled Macromolecules. *J. Phys. Chem. B.* **2016**, *120*, 834-842. Copyright 2016, American Chemical Society.

3.1 Overview

The fluorescent probe 1-pyrenemethoxyethanol (PyMeEGOH) was designed to replace commercially available 1-pyrenebutanol (PyButOH) as an alternative fluorescent label to probe the internal dynamics and interior polarity of macromolecules by steady-state and time-resolved fluorescence. While excimer formation and sensitivity to solvent polarity are two well recognized properties of pyrene, much less known is that these properties are often mutually exclusive when a 1-pyrenebutyl derivative is used to prepare pyrene-labeled macromolecules (PyLMs). Since the sensitivity of pyrene to solvent polarity is a result of its symmetry, attaching a butyl group to pyrene breaks the symmetry of pyrene so that the 1-pyrenebutyl derivatives are much less sensitive to the polarity of their environment as compared to unmodified pyrene. This report demonstrates that replacement of a methylene group in the β -position of PyButOH by an oxygen atom such as in PyMeEGOH restores the sensitivity of this pyrene derivative to the polarity of its local environment to the same level as that of molecular pyrene, without impeding pyrene excimer formation upon incorporation into PyLMs.

3.2 Introduction

As stated by F. M. Winnik in 1993¹ and supported by more recent reviews,²⁻⁴ “pyrene is by far the most commonly used dye to study macromolecules”, due to its ability to form excimer readily upon encounter between an excited and a ground-state pyrene, and to its sensitivity to the polarity of its local environment. Interactions of PyLMs with themselves and other macromolecules,⁵⁻⁸ surfactants or surfactant micelles,⁹⁻¹² or latex particles¹³⁻¹⁵ lead to changes in the polarity of the local environment of the pyrene probe and its ability to form an excimer. Both effects can be quantified from the ratio of the fluorescence intensity of the excimer over that of the monomer, namely the I_E/I_M ratio, to characterize the efficiency of pyrene excimer formation,^{1-4,16} or the ratio of the fluorescence intensity of the first band in the fluorescence spectrum of the pyrene monomer over that of the third band, namely the I_1/I_3 ratio, used to describe the medium polarity.¹⁷⁻¹⁹ While these two features have been well advertised in the scientific literature,^{1-4,16-19} much less mentioned is the fact that the ability of pyrene to probe the polarity of its local environment is strongly reduced upon labeling with one of the many commonly used 1-pyrenebutyl derivatives. Since the variation in the I_1/I_3 ratio with the polarity of the local environment is due to the fact that the band corresponding to the I_1 intensity in the fluorescence spectrum of pyrene is symmetry forbidden, the loss in symmetry induced by the chemical modification of pyrene to generate the 1-pyrenebutyl derivatives is associated with a substantial sensitivity loss of the I_1/I_3 ratio to polarity. This report demonstrates that 1-pyrenemethoxyethanol (PyMeEGOH), which is the chemical equivalent of 1-pyrenebutanol (PyButOH) except for the oxygen atom in the β -position of the spacer, can be used as conveniently as PyButOH to label a macromolecule and study its internal dynamics by pyrene excimer fluorescence, but contrary to PyButOH, it can probe the

local environment of a macromolecule as reliably as molecular pyrene. This work confirms the insight of earlier reports which suggested but never conclusively demonstrated that the introduction of a heteroatom in the β -position of an alkyl substituent of pyrene re-symmetrizes its electronic wavefunction and restores the sensitivity of pyrene to solvent polarity.^{20,21}

3.3 Experimental

Materials: 2-Iodoethanol, 1-pyrenemethanol, triethylamine, methacryloyl chloride, butyl methacrylate, and ethylene glycol anhydrous were purchased from Sigma-Aldrich (Reagent Grade). Distilled in glass tetrahydrofuran (THF), toluene, cyclohexane, 2-propanol, and acetonitrile were provided by Caledon Laboratories. HPLC grade ethanol and ethyl acetate were supplied by Fisher Scientific. HPLC grade acetone, 2-butanone, butylalcohol, benzyl alcohol, cyclopentanone, 1,2-dichloroethane, DMF, DMSO, methanol, and o-xylene were obtained from Sigma-Aldrich. HPLC grade hexane and dichloromethane (DCM) were purchased from OmniSolv. All chemicals were used as received.

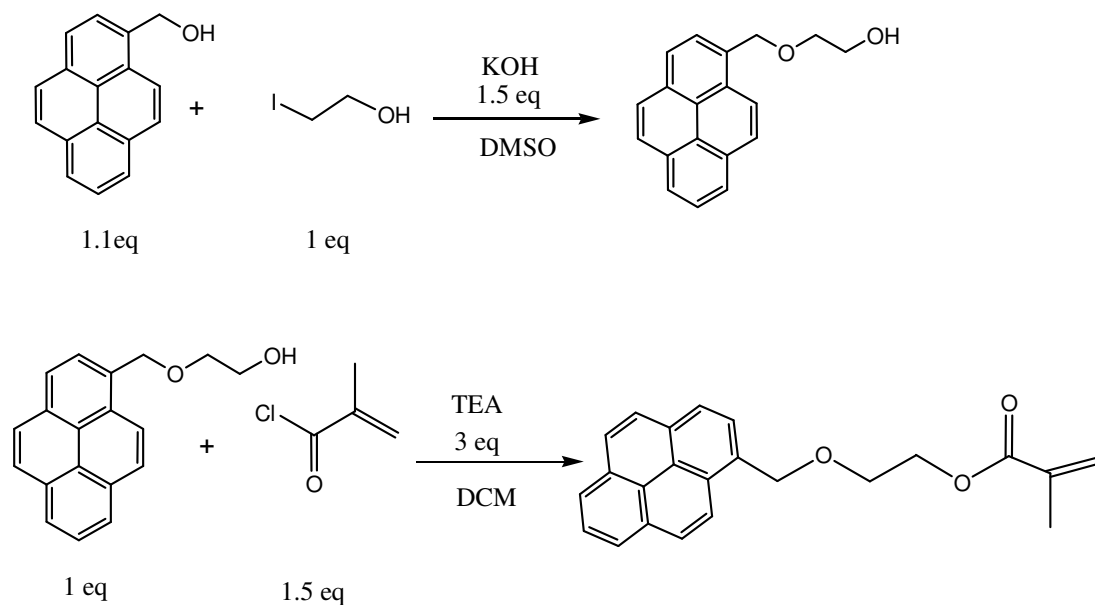
Synthesis of 2-(1-pyrenemethoxy)ethanol (PyMeEGOH): 1-Pyrenemethanol (1.50 g, 6.46 mmol) and ground potassium hydroxide (KOH) (0.50 g, 8.9 mmol) were dissolved in 25 mL of dimethyl sulfoxide (DMSO) and transferred to a 100 mL round bottom flask under N₂ flow. The solution was purged with N₂ for 30 minutes. 2-Iodoethanol (1.00 g, 5.82 mmol) was added drop wise to the reaction mixture. The solution was stirred under N₂ at room temperature for 24 hrs. After the reaction was complete, the solution was washed with 0.5 M HCl, a saturated sodium chloride aqueous solution, and water in that sequence. The solvent

was removed with a rotary evaporator. The yellow remaining crude product was dissolved in a minimum amount of DCM before being purified on a silica gel column using a 55:45 ethyl acetate:hexane mixture. The solid PyMeEGOH was then re-crystallized using a 1:10 ethyl acetate:hexane mixture and a pale-yellow solid was obtained in a 38% yield.

300 MHz ^1H NMR (DMSO-d_6) *PyMeEGOH*: δ 3.56-3.7 (m, 4H, $-\text{CH}_2-\text{CH}_2-\text{OH}$), δ 4.6 (t, 1H, OH), δ 5.2 (s, 2H, $-\text{CH}_2-\text{O}$), δ 7.9-8.4 (m, 9H, Py H's). ^1H NMR spectrum of PyMeEGOH is shown in Figure SI2.1 in Supporting Information (SI).

Synthesis of 2-(1-pyrenemethoxy) ethyl methacrylate (PyMeEG-MA): PyMeEGOH (1.00 g, 4.31 mmol) was dissolved in the presence of distilled triethylamine (1.30 g, 13 mmol) in 20 mL of dichloromethane (DCM) and transferred to a 50 mL round bottom flask. The solution was cooled to 5°C and purged with N_2 for 20 minutes. Methacryloyl chloride (0.68 g, 6.45 mmol) was added drop wise. The solution was stirred under N_2 at room temperature for 24 hr. When the reaction was complete, the reaction mixture was washed with 0.5 M HCl, saturated sodium carbonate aqueous solution, and water in that sequence. A rotary evaporator was used to remove the solvent. The remaining crude product was yellow and it was dissolved in a minimum amount of DCM before being purified by silica gel column using a 60:40 DCM:hexane mixture. The solid was then re-crystallized in methanol to obtain a pale-yellow solid in 85% yield. The overall synthetic procedure is shown in Scheme 1.

300 MHz ^1H NMR (CDCl_3) for PyMeEG-MA: δ 1.89 (s, 3H, CH_3 -), δ 3.8-4.4 (m, 4H, $\text{O}-\text{CH}_2-\text{CH}_2-\text{O}$), δ 3.39 (t, 2H, Py- CH_2 -), δ 5.5 (s, 1H, $=\text{CH}_2$), δ 6.1 (s, 1H, $=\text{CH}_2$), δ 7.9-8.4 (m, 9H, Py H's). ^1H NMR spectrum of PyMeEG-MA is shown in Figure SI2.2.

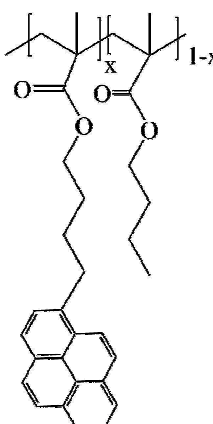
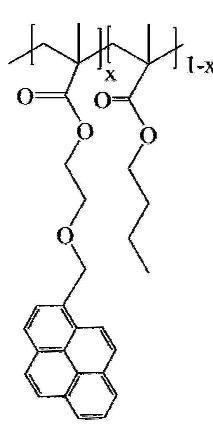


Scheme 3.1: Synthetic procedure applied to prepare PyMeEG-MA.

Random copolymerization: The pyrene-labeled poly(butyl methacrylate)s (Py-PBMAs) were prepared by radical copolymerization of 1-pyrenebutyl methacrylate (PyBut-MA) or PyMeEG-MA with *n*-butyl methacrylate (BMA) to yield PyBut-PBMA or PyMeEG-PBMA, respectively. Their chemical structure is shown in Table 3.1. The overall number of moles of BMA was kept constant while the ratio of PyBut-MA or PyMeEG-MA to BMA monomer was altered to achieve different molar percentages of pyrene contents ranging between 1 and 10 mol%. The copolymerization was carried out in an oil bath at 65 °C using AIBN as the initiator. The MEHQ stabilizer present in the BMA supplied by Sigma-Aldrich was removed with an inhibitor-remover column. The reaction mixture was outgassed for 20 minutes with a gentle flow of nitrogen to remove all oxygen, a well-known inhibitor of radical polymerization. The copolymerization was stopped at a conversion of 0.2 or less to avoid any possible compositional drift during the copolymerization. ¹H NMR was used to follow the conversion as a function of reaction time. Once the desired conversion was achieved, the

reaction vessel was cooled on ice and the polymer was precipitated in methanol, re-dissolved in THF, and re-precipitated in methanol 5-7 times to remove any unreacted PyMeEG-MA monomer. The final yield was approximately 10% in each copolymerization. The same protocol described in an earlier publication was applied to prepare the PyBut-PBMA samples.²¹

Table 3.1: Chemical structure, pyrene content, absolute M_n , and PDI values of the PyBut-PBMA and PyMeEG-PBMA samples.

Chemical Structure PyBut-PBMA	x mol %	M_n kg/mol	\bar{D}	Chemical Structure PyMeEG-PBMA	x , mol %	M_n kg/mol	\bar{D}
	0.6	163	1.9		0.3	135	2.0
	2.2	296	1.4		1.8	160	1.8
	3.0	197	1.4		2.7	117	2.0
	3.6	264	1.7		3.8	100	2.2
	5.3	275	2.0		4.6	190	1.7
	7.2	416	1.8		5.4	303	1.5

Molecular weight determination: The absolute molecular weight of the polymers was determined using Gel Permeation Chromatography (GPC) with a Viscotek instrument equipped with a 305 Triple Detector Array that combined refractive index (DRI), viscosity, and UV-Vis absorption detectors. Typical GPC traces collected with a PyMeEG-PBMA

sample having a pyrene content of 3.8 mol% (PyMeEG(3.8)-PBMA) are provided in Figure SI2.3 in SI2. GPC analysis was also applied to establish that the sample of pyrene-labeled PBMA was free of any unreacted pyrene-labeled monomer. The pyrene content, absolute number-average molecular weight (M_n), and the polydispersity index (PDIs) of all the samples studied in this report have been listed in Table 3.1.

Pyrene content determination: The pyrene content of the samples was determined by UV-Vis spectroscopy with a Varian Cary 100 Bio spectrophotometer. The sharp absorption peak at 344 nm of the pyrene derivatives was used to calculate the pyrene content λ_{py} of the Py-PBMA samples. To this end, the Py-PBMA samples were dissolved in THF to generate a polymer solution of known massic concentration [Poly] in g/L. After diluting the polymer solution to bring the absorbance of the pyrene label at 344 nm below 2.0, the molar concentration of pyrene [Py] in mol/L was determined from the molar absorption coefficient of 1-PyButOH and 1-PyMeEGOH found to equal 42,000 and 45,000 $M^{-1}cm^{-1}$ in THF, respectively. λ_{py} was obtained by taking the ratio [Py]/[Poly] from the diluted polymer solutions used to acquire the absorption spectra. The molar fraction of pyrene labeled monomer in the polymer expressed as (x) could be determined using Equation 3.1 where M and M_{Py} represent the molar mass of the unlabeled and pyrene-labeled monomer, respectively.

$$x = \frac{M}{M - M_{Py} + 1/\lambda_{py}} \quad (3.1)$$

In Equation 3.1, M for BMA equals 142 g/mol and M_{Py} equals 342 or 344 g/mol for PyBut-MA or PyMeEG-MA, respectively.

Steady-state fluorescence measurements: Steady-state fluorescence spectra were acquired on a Photon Technology International LS-100 equipped with an Ushio UXL-75 Xenon lamp and a PTI 814 photomultiplier detection system. The spectra of all pyrene derivatives were obtained using the right angle geometry. Firstly, the solution was diluted to an optical density of ~ 0.1 corresponding to a pyrene concentration of $\sim 2.5 \times 10^{-6}$ M, that is low enough to avoid any possible interchain interactions. The solution was degassed with a gentle flow of N_2 for approximately 30 minutes in order to remove oxygen, which is a known quencher of pyrene fluorescence. The degassed solution was sealed and excited at 344 nm. The emission spectrum was acquired from 350 to 600 nm. The fluorescence intensity of the monomer (I_M) and excimer (I_E) were calculated by integrating the fluorescence spectrum from 372 to 378 nm and from 500 to 530 nm, respectively. The I_E/I_M ratio is a qualitative measure of the efficiency of excimer formation for the pyrene-labeled polymer. The ratio I_1/I_3 was obtained by taking the ratio of the peak intensity at about 375 nm over that at about 386 nm. The exact peak position varied slightly depending on the organic solvents used to prepare the Py-PBMA solutions.

Time-resolved fluorescence measurements: The solutions that were prepared to acquire the fluorescence spectra were used to acquire the fluorescence decays. An IBH Ltd. time-resolved fluorometer equipped with an IBH 340 nm NanoLED was used to excite the solutions at 344 nm. The monomer and excimer fluorescence decays were acquired by monitoring the emission at 375 and 510 nm with cut off filters of, respectively, 370 and 480 nm, to minimize the detection of light scattered by the solution.

Fluorescence Decay Analysis – The Fluorescence Blob Model. The fluorescence decays of the pyrene monomer and excimer were fit globally according to the Fluorescence Blob Model (FBM), based on equations that have been derived earlier and which are provided as supporting information in details in Appendices, Supporting Information for Chapter 3 (SI3), (see Equation SI3.1-SI3.2 in SI3).²³⁻²⁵ More background information on the FBM has been provided in SI3. The FBM retrieves the molar fraction f_{diff} , f_{k2} , f_{free} , f_{E0} , and f_{EL} of all the pyrene species in solution. These are the pyrenes that are diffusing in the solution according to the motion of the structural units of the polymer, that they are bounded to (Py_{diff}), that are close to each other and rearrange rapidly with a rate constant $k_2(Py_{k2})$, that are isolated in pyrene-poor domains of the PyLM where they cannot form excimer and emit with the lifetime of the pyrene derivative $\tau_M(Py_{free})$, that are present as a properly stacked ground-state dimer that can generate an excimer upon direct excitation ($E0$) that emits with a lifetime τ_{E0} , and found as improperly stacked dimer that leads upon direct excitation to the formation of a long-lived excited dimer (EL) that emits with a lifetime τ_{EL} .

Within the framework of the FBM, the polymer coil is divided into a cluster of identical *blobs*. Diffusive motion of Py_{diff} is described by the three parameters k_{blob} , $\langle n \rangle$, and $k_e \times [blob]$ which are the rate constant of encounter between two structural units bearing a pyrene label which are both inside a same *blob*, the average number of pyrenes per *blob*, and the product of the rate constant of exchange of pyrene moieties between neighboring *blobs* in the polymer coil. The parameters were optimized with the Marquardt Levenberg–algorithm.²⁶ Fits were deemed satisfactory if the χ^2 value was smaller than 1.3 and the residuals and autocorrelation function of the residuals were randomly distributed around zero.

3.4 Results and Discussion

Pyrene derivatives are ubiquitous fluorescent probes used to provide information about the internal dynamics of macromolecules or the polarity of their microenvironment. Consequently, the characterization of a new pyrene derivative such as PyMeEGOH developed for the fluorescent labeling of macromolecules must include a study of its response to solvent polarity and ability to report on the internal dynamics of macromolecules. To this end, the steady-state fluorescence spectra of PyMeEGOH and PyButOH were acquired in 21 solvents covering a wide range of dielectric constants between 1.9 for hexane and 78.5 for water. They are shown in Figure 3.1. The fluorescence spectra were normalized to an arbitrary value of 100 at 375 nm, which corresponds to the 0-0 transition of pyrene.

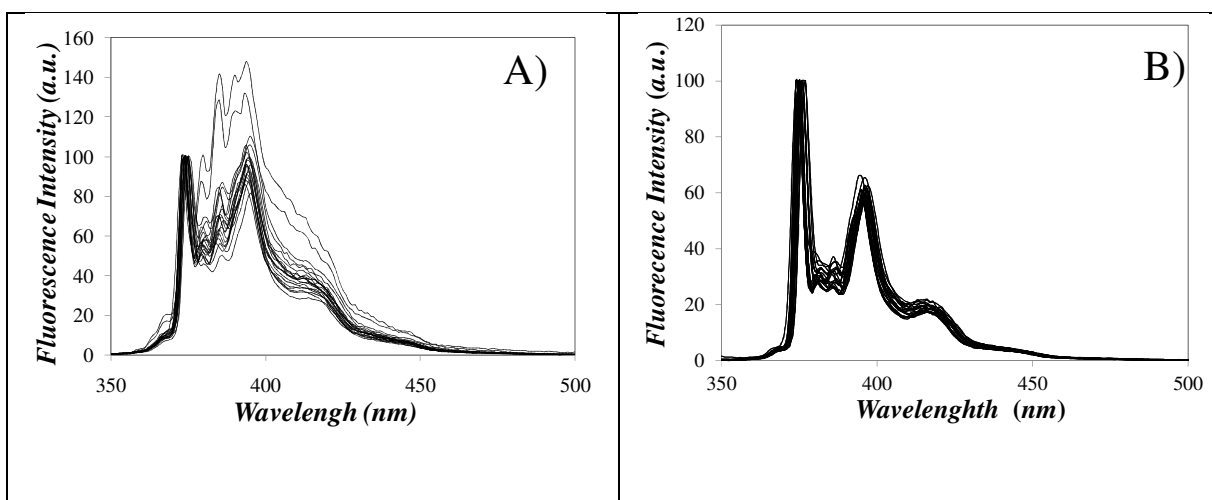


Figure 3.1: Steady-state fluorescence spectra of A) PyMeEGOH and B) PyButOH in the 21 solvents listed in Table 3.2. The solvent polarity increases from top to bottom in Figure 3.1A). $[Py] = 2.5 \times 10^{-6}$ M, $\lambda_{ex} = 344$ nm.

The I_1/I_3 ratio for each steady-state fluorescence spectrum was used to characterize the response of the pyrene derivatives to solvent polarity. Rapid visual inspection of Figure

3.1A indicates that the spectral features of PyMeEGOH, and thus the I_1/I_3 ratios, change substantially with solvent polarity but that these changes are much smaller for PyButOH, implying that the former pyrene derivative is a much better probe to monitor the polarity of its environment than the latter. In the fluorescence spectra shown in Figure 3.1, the intensities I_1 and I_3 correspond to the intensity of the 0-0 and 0-2 transitions of pyrene at about 375 nm and about 386 nm, respectively (see Figure SI3.4).

The I_1/I_3 ratios for PyMeEGOH and PyButOH have been listed in Table 3.2 for the 21 solvents used. The I_1/I_3 ratios of PyMeEGOH and PyButOH were also compared in Figure 3.2 to those of molecular pyrene reported by J. K. Thomas¹⁷ and M. A. Winnik.¹⁹ Whereas the I_1/I_3 ratio of PyButOH increases from 2.38 in cyclohexane to 3.86 in DMSO, a 60 % increase, the I_1/I_3 ratio of PyMeEGOH increased from 0.65 in hexane to 1.99 in DMSO, a more than 200% increase representing a range wide enough to easily assess the micropolarity of an environment probed by PyMeEGOH. Most interestingly, the I_1/I_3 ratios obtained for PyMeEGOH were comparable to those of molecular pyrene with a slope in Figure 3.2 of 1.1, and thus close to unity, and a close to zero intercept of 0.25. This result demonstrates that PyMeEGOH is endowed with the same ability to probe the polarity of microenvironments in solution as molecular pyrene, with the added benefit that PyMeEGOH can be covalently attached onto macromolecules thanks to its hydroxyl group. This feature was taken advantage of to prepare a series of PBMA samples labeled with different amounts of PyMeEGOH. The ability of the PyMeEG-PBMA series to probe the internal dynamics of PBMA in solution was investigated by comparing its response in terms of pyrene excimer formation to that obtained for a series of more traditional PyBut-PBMA samples which had

been prepared for an earlier study.²¹ The characteristics of both Py-PBMA samples in terms of M_n , PDI, and molar fraction of pyrene-labeled monomer (x) were provided in Table 3.1.

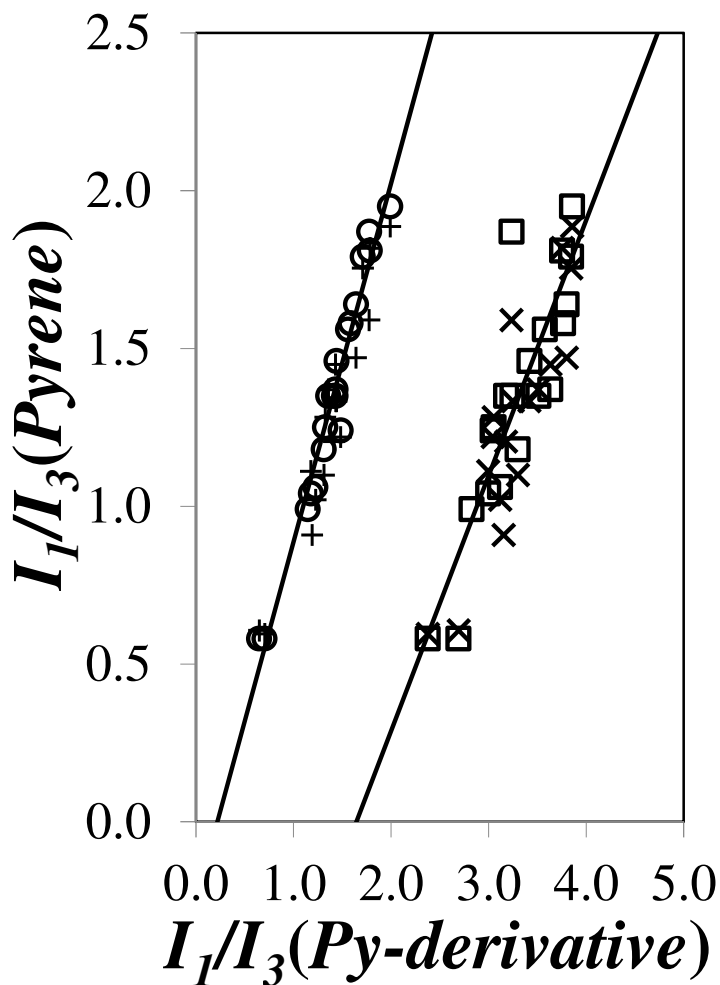


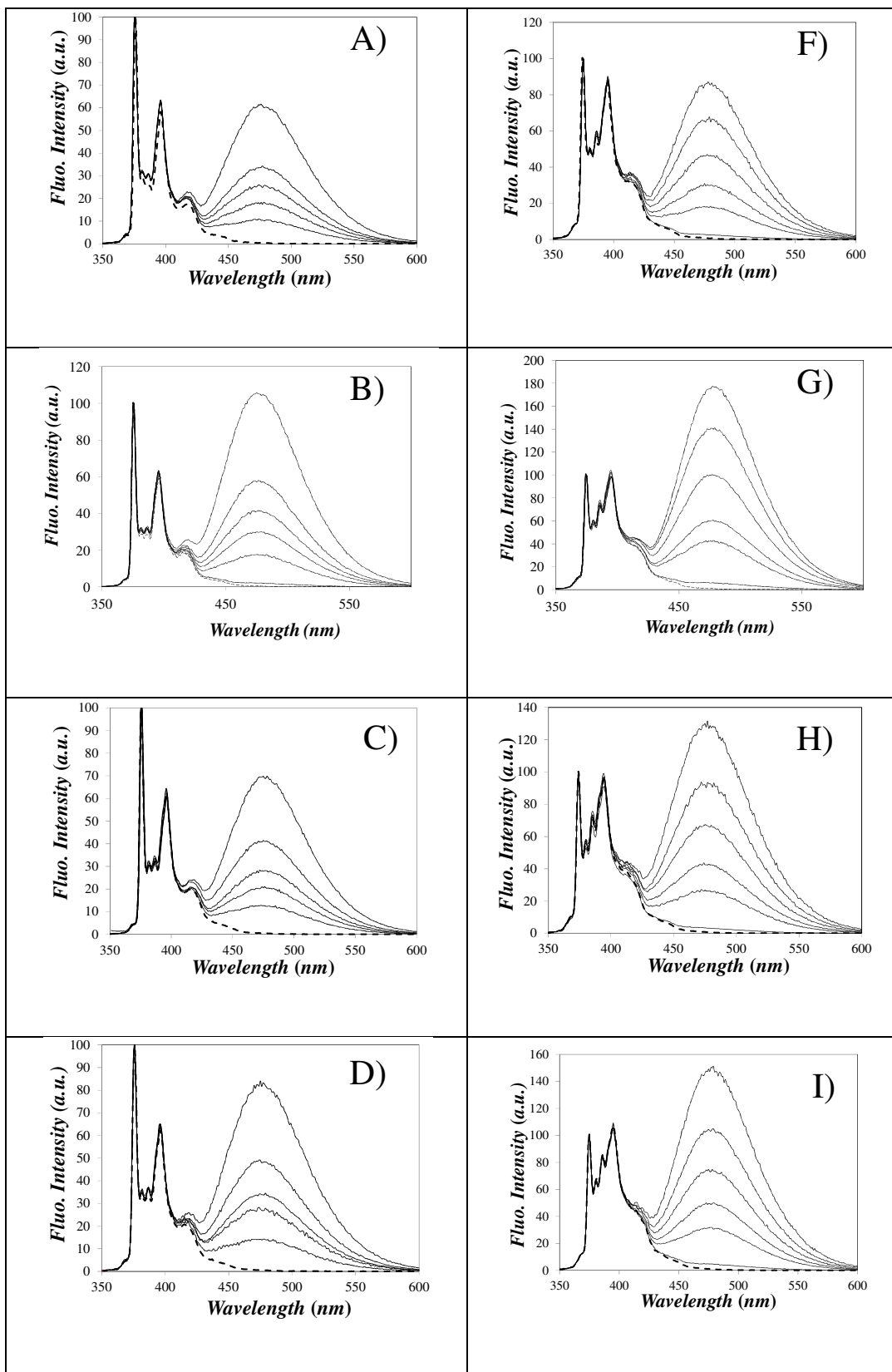
Figure 3.2: Comparison of the I_1/I_3 ratios of molecular pyrene reported by Thomas (+,x)¹⁷ and Winnik (O,□)¹⁹ as a function of the I_1/I_3 ratio of (+,O) PyMeEGOH and (x,□) PyButOH.

The fluorescence spectra of the PyMeEG-PBMA and PyBut-PBMA samples were acquired in cyclohexane ($\epsilon = 2.0$), toluene ($\epsilon = 2.4$), THF ($\epsilon = 7.5$), DCM ($\epsilon = 8.9$), and DMF

($\epsilon = 38.3$)¹⁶ and they are shown in Figure 3.2. The PyMeEG-PBMA samples were found to form excimer as effectively as the PyBut-PBMA samples, the main difference in the spectra being the strong I_1 peak in Figures 3.3A-E resulting from the less symmetry forbidden 0-0 transition of the PyButOH derivative.

Table 3.2: Natural lifetime τ_M and I_1/I_3 ratios of PyButOH and PyMeEGOH in 21 solvents.

Solvent	Dielectric constant (ϵ)	τ_M (ns) PyMeEGOH	τ_M (ns) PyButOH	$\Delta\tau_M$ (ns)	I_1/I_3 PyMeEGOH	I_1/I_3 PyButOH
Water	78.5	195	126	69	1.77	3.23
Dimethyl Sulfoxide	47.2	193	130	63	1.99	3.58
Dimethyl Formamide	38.3	230	163	67	1.78	3.57
Acetonitrile	36.6	273	192	81	1.71	3.84
Methanol	32.7	301	225	76	1.43	3.25
Ethanol	24.6	307	224	83	1.31	3.20
Acetone	19.7	277	195	82	1.64	3.80
Butylalcohol	17.3	295	220	75	1.23	3.12
Cyclopentanone	13.6	193	142	51	1.56	3.57
2-Butanone	13.5	260	187	73	1.58	3.76
2-Propanol	13.4	306	229	77	1.19	3.15
Benzyl Alcohol	11.9	203	145	58	1.48	3.04
1,2-Dichloroethane	10.4	119	80	39	1.44	3.42
Dichloromethane	8.9	155	105	50	1.36	3.36
Tetrahydrofuran	7.5	270	200	70	1.47	3.18
Ethyl Acetate	6.1	266	189	77	1.43	3.63
Chloroform	4.8	121	66	55	1.33	3.05
Toluene	2.4	253	179	74	1.18	2.99
o-Xylene	2.4	218	166	52	1.15	2.82
Cyclohexane	2.0	325	239	86	0.71	2.84
Hexane	1.9	337	257	80	0.65	2.69



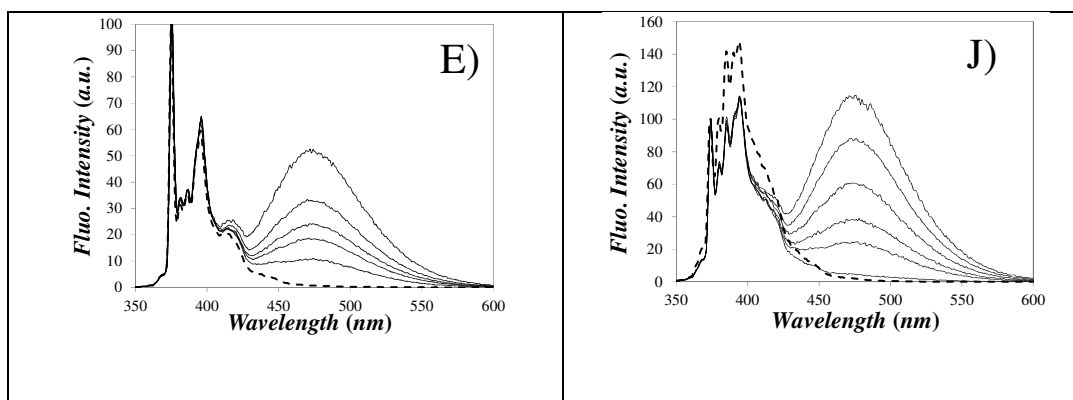


Figure 3.3: Steady-state fluorescence spectra of PyBut-PBMA labeled with 2.2, 3.0, 3.6, 5.3, and 7.2 mol% pyrene (from bottom to top) in A) DMF, B) DCM, C) THF, D) toluene, and E) cyclohexane and PyMeEG-PBMA labeled with 1.8, 2.7, 3.8, 4.6, and 5.4 mol% pyrene (from bottom to top) in F) DMF, G) DCM, H) THF, I) toluene, and J) cyclohexane. $[Py] = 2.5 \times 10^{-6}$ M, $\lambda_{ex} = 344$ nm. Traces with a dashed line in Figures A-E are for PyButOH and in Figures F-J are for PyMeEGOH.

The nice overlay of the fluorescence spectra in the range of wavelengths where the pyrene monomer emits, namely from 370 to 430 nm, suggests that the I_1/I_3 ratio did not change much with pyrene content. Indeed, the I_1/I_3 ratios averaged over all five Py-PBMA samples were determined to equal 1.03 ± 0.03 , 1.18 ± 0.01 , 1.37 ± 0.06 , 1.34 ± 0.03 , and 1.70 ± 0.04 for PyMeEG-PBMA and 2.71 ± 0.05 , 2.74 ± 0.05 , 3.05 ± 0.11 , 3.18 ± 0.04 , and 3.22 ± 0.07 for PyBut-PBMA in cyclohexane, toluene, THF, DCM, and DMF, respectively, showing very little variation with pyrene content. In all solvents studied, the I_1/I_3 ratios obtained for the PyBut-PBMA samples were in relatively good agreement with those obtained for PyButOH and found to equal 2.84, 2.99, 3.18, 3.36, and 3.57 in cyclohexane, toluene, THF, DCM, and DMF, respectively. Except for cyclohexane in Figure 3.3J, good agreement was also found for the I_1/I_3 ratios of the PyMeEG-PBMA samples in toluene,

THF, DCM, and DMF and those of PyMeEGOH found to equal 1.18, 1.47, 1.36, and 1.78, respectively.

In cyclohexane, the fluorescence spectrum of PyMeEGOH differed greatly from that of the pyrene monomer of the PyMeEG-PBMA samples in Figure 3.3J. This observation was reflected in the I_1/I_3 ratio of PyMeEGOH and PyMeEG-PBMA that equalled 0.71 and 1.03 ± 0.03 , respectively. This led to the conclusion that the PyMeEG label probed an environment that was much more polar than cyclohexane, possibly that of the ester bonds of PBMA. These interactions between pyrene and the PBMA backbone were further favored by the poor solvent quality of cyclohexane toward PBMA as inferred from intrinsic viscosity measurements. The intrinsic viscosity $[\eta]$ of an unlabeled PBMA sample ($M_n = 337,000$, PDI = 1.48) was found to equal 50.9 ± 0.9 , 50.1 ± 0.9 , and $56.5 \pm 1.2 \text{ mL.g}^{-1}$ in toluene, THF, and DCM, respectively, but only $20.4 \pm 0.3 \text{ mL.g}^{-1}$ in cyclohexane and $25.9 \pm 0.4 \text{ mL.g}^{-1}$ in DMF (see Table SI3.2 in SI3). The much smaller $[\eta]$ values obtained for PBMA in cyclohexane and DMF demonstrate that these two solvents are poor solvents for PBMA, whereas toluene, THF, and DCM are good solvents for PBMA. The poor solvent quality of cyclohexane toward PBMA implies that the polymer coil in cyclohexane and DMF has a higher density of ester bonds compared to the other good solvents, and that the PyMeEG label in cyclohexane responds strongly to this more polar environment. This conclusion is based on the comparison of the I_1/I_3 ratio of PyMeEGOH equal to 0.71 in cyclohexane and 1.43 in ethyl acetate, the latter solvent being rich in ester bonds resulting in a I_1/I_3 ratio for PyMeEGOH that was twice larger than in cyclohexane. The same effect was not observed in

DMF, certainly due to the relatively smaller difference in the I_1/I_3 ratio between DMF (1.78) and ethyl acetate (1.43).

The spectra shown in Figure 3.3 demonstrated that the PyMeEG-PBMA samples formed excimer, but the difference in monomer fluorescence induced by polarity changes prevented a direct comparison of the kinetics of pyrene excimer formation based on the I_E/I_M ratio, since the intensity of the 0-0 band at ~ 375 nm, that is more sensitive to solvent polarity, is used for I_M to avoid any overlap with the excimer fluorescence. To date, a direct comparison of the efficiency of pyrene excimer formation in the Py-PBMA samples can only be achieved by applying the Fluorescence Blob Model (FBM) analysis to the monomer and excimer fluorescence decays.^{3,4,23} To this end, the fluorescence decays of the pyrene monomer and excimer of all PyMeEG-PBMA and PyBut-PBMA samples were acquired in cyclohexane, toluene, THF, DCM, and DMF and they were analyzed globally according to the FBM, which has been described in details in the Supporting Information (SI3). For both Py-PBMA series, the monomer and excimer decays were fitted globally with Equations provided in the SI3.1 and SI3.2. In a first round of fit, the rate constant k_2 for rearrangement of the pyrene labels was allowed to float. Its value obtained for all the constructs of a same polymer series was averaged, and the average was fixed in a second round of FBM fitting of the decays. The decay fits were excellent and this analysis yielded N_{blob} , the average number of BMA monomers in a *blob* and k_{blob} , the rate constant describing the diffusive motions inside a *blob* of two monomers bearing a pyrene label. The results of this analysis are discussed hereafter.

The first step in the FBM analysis of the decays consisted in determining the lifetime τ_M of the fluorescent label. To this end, a Py-PBMA sample was prepared with a low (<0.6

mol%) pyrene content, whose monomer decay had a strong (> 80%) contribution of a long-lived pyrene species that was attributed to unquenched pyrene labels that did not form excimer (P_{yfree}). This decay time was selected as the natural lifetime τ_M of the pyrene label attached to the polymer. τ_M was found to equal 288, 246, 270, 155, and 228 ns for PyMeEG-PBMA and 224, 180, 195, 110, and 160 ns for PyBut-PBMA in cyclohexane, toluene, THF, DCM, and DMF, respectively. These τ_M values were close to those found for PyMeEGOH and PyButOH in the same solvents (see Table 3.2), the larger discrepancy in τ_M being observed in cyclohexane for PyMeEG-PBMA. As explained earlier based on the analysis of the I_1/I_3 ratios of PyMeEGOH and PyMeEG-PBMA in cyclohexane, the difference in τ_M value for PyMeEG-PBMA in cyclohexane is due to the sensitivity of this pyrene derivative to the more polar environment generated by the ester bonds of the PBMA backbone (see Figure 3.3J). It was interesting to note that τ_M for PyMeEGOH in Table 3.2, determined for all 21 solvents, was on average 67 ± 13 ns longer than for PyButOH. This represents another major advantage of using PyMeEGOH instead of PyButOH as a fluorescent label, as its longer lifetime offers a longer temporal window to probe the slow dynamics observed in macromolecules.

Fits of the decays yielded $\langle n \rangle$, the average number of pyrene labels per *blob*, which was used to determine N_{blob} according to Equation SI3.4. Within experimental error, the N_{blob} values obtained for all the constructs of a given Py-PBMA series did not depend much on pyrene content, as demonstrated in Figure SI3.6. They were averaged and $\langle N_{\text{blob}} \rangle$ was plotted as a function of the inverse of viscosity (η^{-1}) in Figure 3.4A. The $\langle N_{\text{blob}} \rangle$ values

obtained for both Py-PBMA series were comparable, although they might appear to be slightly smaller for the PyBut-PBMA constructs despite the relatively large error bars.

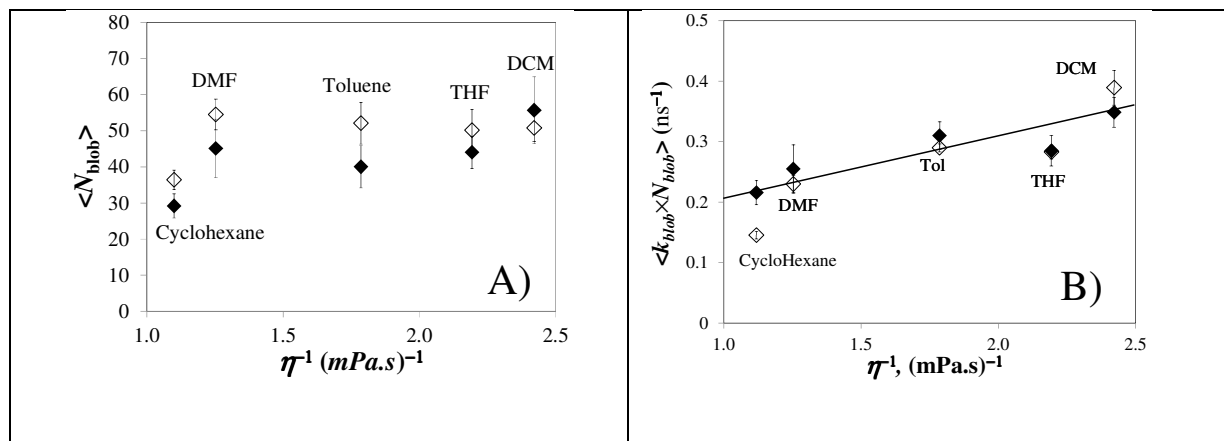


Figure 3.4: Plot of A) $\langle N_{blob} \rangle$ and B) $\langle k_{blob} \rangle \times \langle N_{blob} \rangle$ as a function of η^{-1} for the Py-PBMA samples in different solvents. (◆)PyBut-PBMA, (◇)PyMeEG-PBMA.

Since the PyMeEGOH derivative, with its larger lifetime, could probe a larger *blob* volume (V_{blob}) inside the polymer coil, resulting in a larger $\langle N_{blob} \rangle$ value, quenching experiments were carried out to investigate the effect of lifetime on $\langle N_{blob} \rangle$. Nitromethane, a well-known quencher²⁷ of pyrene, was added to the PyMeEG-PBMA solutions in THF to decrease τ_M . Using sample PyMeEG(0.3)-PBMA, which was labeled with a very small amount of pyrene, quenching of this sample with nitromethane yielded a bimolecular quenching rate constant k_q equal to $1.12 \times 10^9 \text{ M}^{-1} \cdot \text{s}^{-1}$ (see Figure SI3.7 in SI3). Knowing k_q , the nitromethane concentration required to obtain a desired lifetime τ_M for the pyrene label was found from the relationship shown in Equation 3.2, where $\tau_M^o = 270 \text{ ns}$ represents the natural lifetime of PyMeEG(0.3)-PBMA in THF without nitromethane.

$$[Q] = \frac{1}{k_q} \times \left(\frac{\tau_M^o}{\tau_M} - 1 \right) \quad (3.2)$$

The pyrene monomer and excimer fluorescence decays of the PyMeEG-PBMA series were acquired at nitromethane concentrations of 0.0, 1.2, 2.6, 5.6, and 14.0 mmol.L⁻¹, to reduce the natural lifetime of the PyMeEG derivative attached onto PBMA from 270 ns without nitromethane to 200, 150, 100, and 50 ns, respectively. For each nitromethane concentration, the FBM analysis was applied to the decays of the five PyMeEG-PBMA constructs to yield the parameters $\langle N_{\text{blob}} \rangle$ and the product $\langle k_{\text{blob}} \times N_{\text{blob}} \rangle$ as a function of τ_M . A plot of $\langle N_{\text{blob}} \rangle$ as a function of τ_M is shown in Figure 3.5A. As τ_M decreased, so did $\langle N_{\text{blob}} \rangle$, as the volume probed by the shorter-lived PyMeEG derivative decreased. However, $\langle N_{\text{blob}} \rangle$ in Figure 3.4A did not change much when τ_M decreased from 270 to 150 ns, a range of τ_M values representative of those used to fit the decays obtained for solutions of the two Py-PBMA constructs in five different solvents.

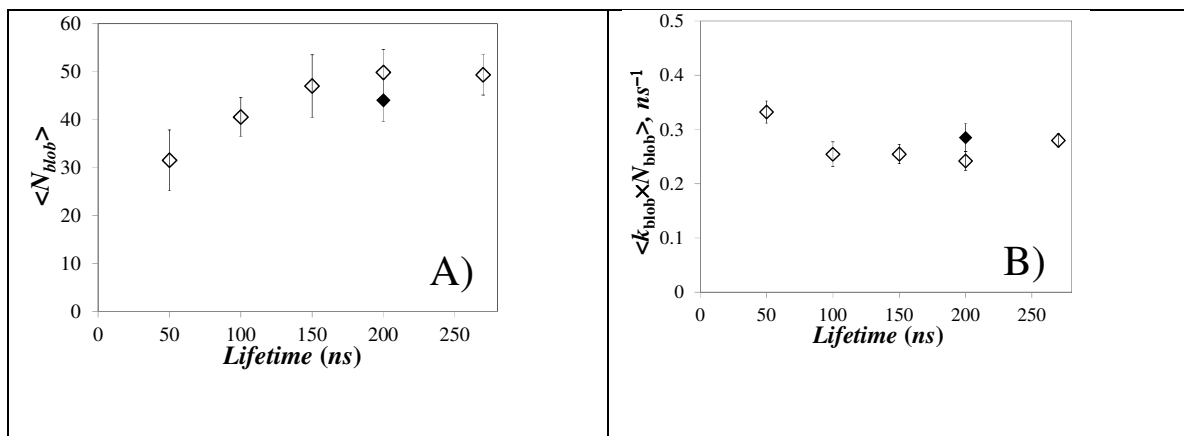


Figure 3.5: Plots of A) $\langle N_{\text{blob}} \rangle$ and B) $\langle k_{\text{blob}} \times N_{\text{blob}} \rangle$ as a function of pyrene lifetime for the Py-PBMA samples in THF. (◆)PyBut-PBMA, (◇)PyMeEG-PBMA. The lifetime of the PyMeEG-PBMA samples was adjusted by addition of nitromethane.

Only with a τ_M value of 50 ns was a significant decrease in $\langle N_{\text{blob}} \rangle$ observed. The $\langle N_{\text{blob}} \rangle$ value determined for the PyBut-PBMA series are also given in Figure 3.5A. The $\langle N_{\text{blob}} \rangle$ values obtained for the two constructs at a same lifetime $\tau_M=200$ ns were comparable in THF within experimental error. Figure 3.5A also suggests that despite the variations in τ_M resulting from the solvent used to prepare the Py-PBMA solutions, the different τ_M values obtained in these solvents are not expected to affect the $\langle N_{\text{blob}} \rangle$ values much.

Beside τ_M , viscosity is also expected to slow down the motions of a fluorescent label, which in turn should reduce V_{blob} and thus N_{blob} .²⁸ Little indication of this effect was observed in Figure 3.4A, where $\langle N_{\text{blob}} \rangle$ did not change much as a function of η^{-1} . Among possible reasons for the apparent lack of response of $\langle N_{\text{blob}} \rangle$ to η^{-1} might be solvent quality toward the polymer.²⁹ It is noticeable that in Figure 3.4A, the higher viscosity solvents DMF

($\eta=0.802$ mPa.s at 25°C) and cyclohexane ($\eta=0.894$ mPa.s at 25°C) are also the two poorest solvents toward PBMA based on the intrinsic viscosity measurements described earlier. Poorer solvents result in denser polymer coils and thus higher N_{blob} values, that would offset the effect imparted by the increased viscosity of DMF and cyclohexane onto N_{blob} . Such effects have been discussed in great details in earlier publications^{22,24} and are beyond the scope of this report, which focuses on the comparison of the results obtained from the fluorescence response of the PyMeEG-PBMA and PyBut-PBMA series. At this stage, the $\langle N_{\text{blob}} \rangle$ values presented in Figure 3.4A suggest that this quantity is similar for PyMeEG-PBMA and PyBut-PBMA, and that it does not change much with viscosity for the range of solvent viscosities investigated.

The rate constant of pyrene excimer formation inside a *blob*, k_{blob} , was also retrieved from the FBM analysis of the decays and it was used to determine the product $k_{\text{blob}} \times N_{\text{blob}}$. The product $k_{\text{blob}} \times N_{\text{blob}}$ has been found to represent polymer chain dynamics in solution more faithfully than N_{blob} .^{22,24,25} As for N_{blob} , the products $k_{\text{blob}} \times N_{\text{blob}}$ were insensitive to pyrene content as shown in Figure SI3.6. They were averaged over all the constructs for a given Py-PBMA series to yield $\langle k_{\text{blob}} \times N_{\text{blob}} \rangle$, which was plotted as a function of η^{-1} in Figure 3.4B. Except in cyclohexane, perfect agreement between the two Py-PBMA series was obtained for $\langle k_{\text{blob}} \times N_{\text{blob}} \rangle$. The difference in $\langle k_{\text{blob}} \times N_{\text{blob}} \rangle$ observed in cyclohexane could not be attributed to different τ_{M} values, as the quenching experiment conducted with PyMeEG-PBMA in THF showed in Figure 3.5B that $\langle k_{\text{blob}} \times N_{\text{blob}} \rangle$ remained constant within experimental error for τ_{M} values between 100 and 270 ns. We suspect that the difference in $\langle k_{\text{blob}} \times N_{\text{blob}} \rangle$ values found in cyclohexane between PyMeEG-PBMA and PyBut-PBMA is

due to stronger interactions in cyclohexane between the ether bond in the linker of the PyMeEG derivative and the ester bonds of PBMA, that hold the pyrene label close to the PBMA backbone. These interactions would hinder the mobility of PyMeEG, as reflected by the lower $\langle k_{\text{blob}} \times N_{\text{blob}} \rangle$ value obtained in Figure 3.4B in cyclohexane. As a matter of fact, an upcoming study provides evidence that, as the length of the spacer connecting pyrene to the polymeric backbone decreases, the pyrene label probes a smaller V_{blob} .³⁰ The more polar DMF, which like cyclohexane is a poor solvent for PBMA, but unlike cyclohexane does not prevent the deployment of the pyrene label into the solution, yields the same $\langle k_{\text{blob}} \times N_{\text{blob}} \rangle$ value for both the PyMeEG-PBMA and PyBut-PBMA constructs.

The uptick observed for $\langle k_{\text{blob}} \times N_{\text{blob}} \rangle$ for a τ_M value of 50 ns in Figure 3.5B is a direct consequence of the scaling laws that apply to polymers in solution.³¹ Since k_{blob} is the rate constant for diffusive encounters between an excited pyrene and a ground-state pyrene located inside a same *blob*, k_{blob} is a pseudo-unimolecular rate constant equal to the product of the bimolecular rate constant of diffusive encounters k_{diff} times the local pyrene concentration equivalent to one ground-state pyrene inside a *blob* ($k_{\text{blob}} = k_{\text{diff}} \times (1/V_{\text{blob}})$). Using a scaling argument where $V_{\text{blob}} \sim N_{\text{blob}}^{3\nu}$ with ν being Flory's exponent,^{31,32} the product $k_{\text{blob}} \times N_{\text{blob}}$ is found to scale as $N_{\text{blob}}^{1-3\nu}$. Since ν equals 0.5 in a θ -solvent and 0.6 in a good solvent, $1-3\nu$ is negative, which implies that $k_{\text{blob}} \times N_{\text{blob}}$ decreases with increasing N_{blob} , as is being observed in Figure 3.5B when τ_M decreases for the PyMeEG series in THF. The product $\langle k_{\text{blob}} \times N_{\text{blob}} \rangle$ obtained for the PyBut-PBMA sample was also given in Figure 3.5B. Within experimental error, the values of $\langle N_{\text{blob}} \rangle$ and $\langle k_{\text{blob}} \times N_{\text{blob}} \rangle$ for PyBut-PBMA are similar to those obtained for PyMeEG-PBMA in THF for a lifetime τ_M of 200 ns.

Besides differences in $\langle k_{\text{blob}} \times N_{\text{blob}} \rangle$ in cyclohexane, induced by the poor solvent quality of cyclohexane towards PBMA and interactions between the ether linker of the PyMeEG derivative and the ester bonds of the PBMA backbone, similar $\langle k_{\text{blob}} \times N_{\text{blob}} \rangle$ values were obtained for the PyMeEG-PBMA and PyBut-PBMA series in all the other solvents that were examined in this study. Furthermore, $\langle k_{\text{blob}} \times N_{\text{blob}} \rangle$ was found to increase with increasing η^{-1} in Figure 3.4B, as would be expected for a diffusion-controlled process of pyrene excimer formation. Since $\langle k_{\text{blob}} \times N_{\text{blob}} \rangle$ has been shown to faithfully represent the internal dynamics of polymers in solution,^{22,24,25} this result demonstrates that the PyMeEGOH derivative used to label PBMA yields the same dynamic information on a polymer in solution, as PyButOH does as would be expected, since the linker connecting the pyrene derivatives to the PBMA backbone is constituted of a same number of (four) atoms. The main difference between these two pyrene derivatives is the ability of PyMeEGOH to probe the polarity of its local environment, with a sensitivity that is similar to that of molecular pyrene (see Figures 3.1A and 3.2), a feature of this dye whose importance is rooted in the fact that the paper introducing this effect for the first time has been cited more than 1800 times since 1977 according to scifinder!¹⁷ This feature was particularly useful in this study to rationalize why $\langle k_{\text{blob}} \times N_{\text{blob}} \rangle$ took a lower value for PyMeEG-PBMA than for PyBut-PBMA in cyclohexane. As shown in Figures 3.1B and 3.3A-E, the fluorescence spectrum of PyButOH responds much more poorly to the polarity of its local environment in comparison to that of PyMeEGOH.

3.5 Conclusions

Macromolecules labeled with a 1-pyrenebutyl derivative are mostly characterized by monitoring changes in pyrene excimer formation, since such probes are not very sensitive to the polarity of their environment, as illustrated by the present study (see Figures 3.1B and 3.3A-E). By comparison, PyMeEGOH differs from PyButOH by the oxygen replacement of the methylene unit in the β -position of the butanol side chain attached in the 1-position of pyrene. Macromolecules labeled with PyMeEGOH report not only on the fluidity of their local environment probed by pyrene excimer formation as efficiently as macromolecules labeled with PyButOH would (see Figure 3.4), but also on the polarity of the local environment experienced by pyrene in the macromolecule, by taking advantage of the excellent fluorescence response to polarity exhibited by PyMeEGOH. Most interestingly, the response to polarity observed for PyMeEGOH was found to be as strong as that of molecular pyrene (Figure 3.2). Based on these results, PyMeEGOH promises to be a most valuable fluorescent probe to study the internal dynamics and the polarity of the microenvironment generated by macromolecules in solution.

Chapter 4

Probing Side Chain Dynamics of Branched Macromolecules by Pyrene Excimer Fluorescence

Reproduced with permission from Farhangi, S.; Duhamel, J. Probing Side Chain Dynamics of Branched Macromolecules by Pyrene Excimer Fluorescence. *Macromolecules* **2015**, *49*, 353-361. Copyright 2015, American Chemical Society.

4.1 Overview

Four different pyrene-labeled polymers were prepared by radical copolymerization of n-butylmethacrylate (BMA) and 1-pyrenemethyl methacrylate (PyEG₀MA), 1-pyrenemethoxyethyl methacrylate (PyEG₁MA), 1-pyrenemethoxyethoxyethyl methacrylate (PyEG₂MA), and 1-pyrenemethoxydiethoxyethyl methacrylate (PyEG₃MA) to yield PyEG₀-PBMA, PyEG₁-PBMA, PyEG₂-PBMA, and PyEG₃-PBMA, respectively. The only structural difference between the polymers was the length of the oligo(ethylene glycol) spacer separating the pyrene label from the main chain. Steady-state and time-resolved fluorescence were applied to investigate how the length of the spacer affected the photophysical properties of the pyrene-labeled polymers. Excimer formation between an excited and a ground-state pyrene was enhanced by a longer spacer, which increased the probability of encounter between two pyrene labels. This conclusion was supported through the analysis of the fluorescence decays of the polymers according to the Fluorescence Blob Model (FBM), which yielded the number (N_{blob}) of monomers constituting the volume in the polymer coil probed by an excited pyrene and the rate constant of excimer formation, k_{blob} , inside a *blob*. N_{blob} increased more or less linearly with increasing spacer length, reflecting a larger *blob* volume. The parameter k_{blob} for PyEG₀-PBMA was small due to steric hindrance, while k_{blob} took a larger but similar value within experimental error for all polymers labeled with pyrene derivatives having oligo(ethylene glycol) spacers. These experiments demonstrate that for a branched macromolecule, the volume probed by the tip of a side chain and its dynamics can be characterized quantitatively by monitoring pyrene excimer fluorescence. They are expected to provide important dynamic and structural information about the numerous highly branched macromolecules that are currently under intense scientific scrutiny.

4.2 Introduction

Polymeric bottlebrushes,¹⁻³ dendrimers,^{4,5} or comb⁶ and arborescent⁷ polymers are all examples of highly branched macromolecules (HBMs) that can be prepared in a well-defined manner and whose architecture endows them with a broad range of highly sought after properties for catalysis,⁴ drug delivery,⁵ or enhanced lubrication at interfaces,⁸ as contrast agents for imaging,⁹ or associative thickeners in paints.¹⁰ If one focuses on anisotropic HBMs such as comb polymers or polymeric bottlebrushes, their characterization presents experimentalists with an additional challenge as compared to linear chains. Their characterization should be conducted along two perpendicular directions, one running axially along the main chain and the other running perpendicularly to the main axis along the side chains. In practice, the characterization of HBMs relies usually on the determination of their overall mass by a combination of techniques such as NMR, gel permeation chromatography, or static light scattering followed by the characterization of their dimensions in solution by scattering or intrinsic viscosity measurements.¹¹⁻¹³ While such studies provide an accurate description of the averaged properties of HBMs in terms of their hydrodynamic or gyration radii for example, they do not yield much detailed information about the actual behavior of the side chains. Microscopy, which provides the dimensions of polymeric bottle brushes adsorbed onto a substrate along their main and secondary axes, might be currently the only technique to characterize HBMs adsorbed onto a two-dimensional substrate along two different axes,¹³ but it does not provide much information about the behavior of the side chains of HBMs adopting their natural three-dimensional conformation in solution.

Over the years, experiments on linear chains labeled randomly or at their ends with the dye pyrene have established that polymer chain dynamics and the volume probed by an excited pyrene could be measured quantitatively by characterizing the kinetics of excimer formation between an excited and a ground-state pyrene according to the Fluorescence Blob Model (FBM) for randomly labeled polymers,¹⁴⁻¹⁷ or Birks' scheme for end-labeled chains.^{18,19} The present chapter investigates whether pyrene excimer fluorescence, which enables the thorough characterization in solution of the internal dynamics of linear chains labeled with pyrene, could also probe the dynamics of side chains in the direction perpendicular to the main chain. To this end, four series of poly(butyl methacrylate) (PBMA) were prepared by copolymerizing BMA with four pyrene-labeled monomers, where a 1-pyrenemethoxide label was connected to a methacrylate monomer via 0 – 3 ethylene glycol units. In so doing, the pyrene label was held at increasing distances from the main chain and its efficiency at forming excimer was characterized as a function of side chain length. Surprisingly, increasing the side chain length was found to dramatically enhance the ability of the pyrene-labeled PBMA constructs to form excimer. The cause for the large enhancement in pyrene excimer formation was clearly identified by analyzing the fluorescence decays of the four series of pyrene-labeled PBMA with the FBM. With increasing side chain length the pyrene labels were held further away from the slow moving main chain, allowing them to experience enhanced mobility and an increased probability of undergoing pyrene–pyrene encounters due to the longer reach of the spacer. Based on these results, the experiments described herein suggest that pyrene excimer fluorescence represents an effective means to probe in solution the dynamics of the side chains of the many HBMs that are currently under investigation.

4.3 Experimental

Materials: 1-(Bromomethyl)pyrene, 1-pyrenemethanol, silver(I) oxide (Ag_2O), diethylene glycol (DEG), and triethylene glycol (TEG) were purchased from Sigma-Aldrich. Celite 545 Filter Aid Powder was provided by Fisher Scientific. Distilled in glass tetrahydrofuran (THF) was supplied by Caledon Laboratories. Four PBMA standards with narrow molecular weight polydispersity (M_n in $\text{kg}\cdot\text{mol}^{-1}$ (PDI) = 7.0 (1.6), 13 (1.12), 24 (1.25), and 38 (1.15)) were purchased from Polymer Source and one PBMA standard ($M_n = 2.8 \text{ kg}\cdot\text{mol}^{-1}$, PDI=1.15) from PSS. All chemicals were used as received.

Synthesis of 1-pyrenemethoxyethyl methacrylate (PyEG₁-MA): The synthesis of this pyrene-labeled monomer has been described elsewhere.²¹

Synthesis of 1-pyrenemethoxyethoxyethanol (PyEG₂-OH) and 1-pyrenemethoxydiethoxy ethanol (PyEG₃-OH): The same procedure was applied for both compounds. Only the synthesis of PyEG₂-OH is described in details hereafter. DEG (1.00g, 5.82 mmol) was added to a suspension of Ag_2O (1.97 g, 8.5 mmol) in 25 mL of dichloromethane (DCM) under a flow of nitrogen and the solution was stirred for 45 minutes under nitrogen. 1-(Bromomethyl) pyrene (1.83 g, 6.20 mmol) was dissolved in 5 mL DCM and the solution was added drop wise to the reaction mixture. The reaction was stirred under nitrogen at room temperature for 72 hr. After the reaction, the solution was filtered through a Celite® bed. The solvent was removed with a rotary evaporator and the yellow remaining residue was purified by silica gel column chromatography using a 55:45 ethyl acetate-to-hexane mixture. A pale-yellow oil was obtained in a 45% yield. The ¹H NMR spectra of PyEG₂-OH and PyEG₃-OH are shown

in details in Appendices, Supporting Information for Chapter 4 (SI4), Figures SI4.1 and SI4.2, respectively.

300 MHz ^1H NMR (DMSO- d_6) for PyEG₂-OH: δ 3.41-3.71 (m, 8H, O-CH₂-CH₂-O-CH₂-CH₂-O), δ 4.6 (t, 1H, OH), δ 5.2 (s, 2H, py-CH₂-O), δ 8.0-8.4 (m, 9H, Py H's).

300 MHz ^1H NMR (DMSO- d_6) for PyEG₃-OH: δ 3.37-3.72 (m, 12H, O-CH₂-CH₂-O-CH₂-CH₂-O-CH₂-CH₂-OH), δ 4.56 (t, 1H, OH), δ 5.2 (s, 2H, -CH₂-O), δ 7.9-8.4 (m, 9H, Py H's).

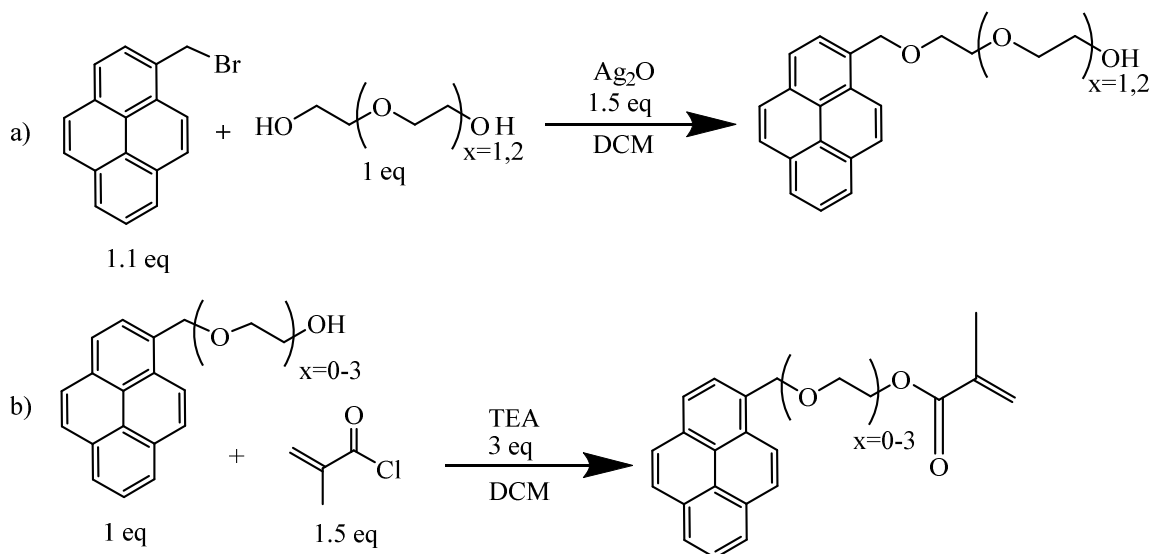
Synthesis of 1-pyrenemethyl methacrylate (PyEG₀-MA), 1-pyrenemethoxyethoxyethyl methacrylate (PyEG₂-MA), and 1-pyrenemethoxyethoxydiethyl methacrylate (PyEG₃-MA):

Only the synthesis of PyEG₂MA is described in detail since a similar procedure was applied for the synthesis of PyEG₀-MA and PyEG₃-MA. PyEG₂-OH (1.10 g, 3.43 mmol) was dissolved in 30 mL of DCM in a 100 mL round bottom flask. Freshly distilled trimethylamine (1.04 g, 12 mmol) was added to the reaction mixture. The solution was purged with nitrogen for 20 minutes and kept on dry ice. Methacryloyl chloride (0.62 g, 6.0 mmol) was added drop wise. The reaction mixture was brought to room temperature and the solution was stirred under nitrogen for 24 hr. After the reaction was complete, the mixture was washed with an aqueous solution of 0.5 M HCl, saturated sodium carbonate, and saturated sodium chloride, followed by water in that sequence. A rotary evaporator was used to remove the solvent. The remaining crude product was purified by silica gel column chromatography using a 60:40 ethyl acetate-to-hexane mixture to obtain a yellow oil in 90% yield. The overall synthetic procedure is shown in Scheme 4.1. The ^1H NMR spectra of PyEG₀-MA, PyEG₂-MA, and PyEG₃-MA are shown in Figures SI4.3, SI4.4, and SI4.5, respectively.

300 MHz ^1H NMR (CDCl_3) for PyEG₀-MA: δ 1.95 (s, 3H, CH_3 -), δ 5.5 (s, 1H, $=\text{CH}_2$), δ 5.9 (s, 2H, Py- CH_2 -), δ 6.4 (s, 1H, $=\text{CH}_2$), δ 7.9-8.3 (m, 9H, Py H's).

300 MHz ^1H NMR (CDCl_3) for PyEG₂-MA: δ 1.81 (s, 3H, CH_3 -), δ 3.73-3.77 (m, 6H, $-\text{CH}_2-\text{O}-\text{CH}_2-\text{CH}_2-\text{O}-$), δ 4.29-4.32 (m, 2H, $\text{COO}-\text{CH}_2$ -), δ 5.2 (s, 2H, Py- CH_2 -), δ 5.5 (s, 1H, $=\text{CH}_2$), δ 6.1 (s, 1H, $=\text{CH}_2$), δ 7.9-8.4 (m, 9H, Py H's).

300 MHz ^1H NMR (CDCl_3) for PyEG₃-MA: δ 1.89 (s, 3H, CH_3 -), δ 3.8-4.4 (m, 8H, $\text{CH}_2-\text{O}-\text{CH}_2-\text{CH}_2-\text{O}-\text{CH}_2-\text{CH}_2-\text{O}$), δ 4.21-4.28 (m, 2H, $\text{COO}-\text{CH}_2$ -), δ 5.2 (s, 2H, Py- CH_2 -), δ 5.5 (s, 1H, $=\text{CH}_2$), δ 6.1 (s, 1H, $=\text{CH}_2$), δ 7.9-8.4 (m, 9H, Py H's).

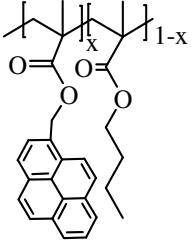
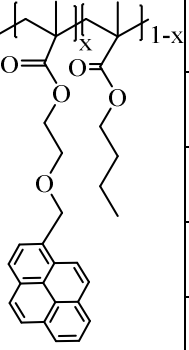
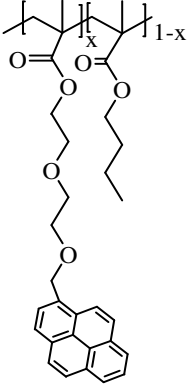
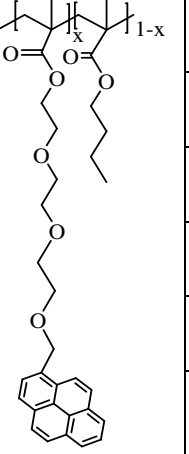


Scheme 4.1: Synthetic procedure applied to prepare a) PyEG₂-OH and PyEG₃-OH, and b) the monomer series PyEG_x-MA with $x = 0 - 3$.

Random copolymerization: The pyrene-labeled poly(butyl methacrylate)s (Py-PBMA) were prepared by radical copolymerization of PyEG₀MA, PyEG₁MA, PyEG₂MA, or PyEG₃MA with butyl methacrylate (BMA) to yield PyEG_x-PBMA with $x = 0 - 3$ (structures shown in

Table 4.1) according to a procedure that was developed earlier.^{20,21} The synthesis and purification of the PyEG_x-PBMA samples with $x = 1$ has been described in detail earlier, and the same procedure was applied to prepare the PyEG_x-PBMA samples with $x = 0, 2,$ and $3.$ ²¹

Table 4.1: Chemical structure, pyrene content, absolute M_n , and PDI values of the PyEG_x-PBMA samples with $x = 0 - 3$.

PyEG ₀ PBMA				PyEG ₁ PBMA			
Chemical Structure	Py-content μmol/g (mol %)	M_n kg/mol	PDI	Chemical Structure	Py-content μmol/g (mol %)	M_n kg/mol	PDI
	25 (0.35)	182	1.92		23 (0.32)	164	2.00
	270 (4.0)	204	1.44		123 (1.8)	160	1.80
	352 (5.3)	170	1.39		184 (2.7)	117	2.00
	412 (6.3)	183	1.92		255 (3.8)	100	2.23
	461 (7.1)	164	1.94		304 (4.6)	190	1.73
	525 (8.1)	138	2.20		354 (5.4)	303	1.46
PyEG ₂ PBMA				PyEG ₃ PBMA			
Chemical Structure	Py-content μmol/g (mol %)	M_n kg/mol	PDI	Chemical Structure	Py-content μmol/g (mol %)	M_n kg/mol	PDI
	22 (0.32)	179	1.96		23 (0.32)	113	1.56
	123 (1.8)	178	1.56		70 (1.0)	201	1.53
	160 (2.3)	173	1.77		126 (1.9)	117	1.60
	215 (3.2)	191	1.74		142 (2.1)	137	1.48
	258 (3.9)	167	1.56		185 (2.8)	195	1.55
	342 (5.3)	178	1.76		274 (4.2)	157	1.82

Molecular weight determination: Gel Permeation Chromatography (GPC) was applied to determine the absolute molecular weight of the pyrene labeled polymers. A Viscotek GPC 305 Triple Detector Array device with a combination of refractive index (DRI), viscosity, and UV-Vis absorption detectors was used. The quality and purity of the fluorescently labeled samples, particularly the confirmation that no free pyrene-labeled monomer eluting with the solvent remained in the polymer sample, was achieved by visual inspection of the traces of the DRI and UV-Vis absorption detectors. Examples of GPC traces of the labeled polymers have been presented in Figure SI4.6 in SI. The pyrene content, absolute number-average molecular weight (M_n), and polydispersity indices (PDIs) have been listed in Table 4.1.

Absorption measurements: The absorption spectra used to determine the pyrene content of the PyEG_x-PBMA samples and the pyrene concentration ($[Py] = 2.5 \times 10^{-6}$ M) for the PyEG_x-PBMA solutions used for fluorescence measurements were acquired with a Varian Cary 100 Bio spectrophotometer. The pyrene contents listed in Table 4.1 were obtained in terms of molar fraction (x) of pyrene-labeled monomer and number of moles of pyrene labeled monomer per gram of polymer (λ_{Py} in $\mu\text{mol.g}^{-1}$). Taking the ratio of the massic polymer concentration in g.L^{-1} over the pyrene concentration in mol.L^{-1} , obtained by applying Beer-Lambert law to the solution absorbance with the molar absorption coefficient of 1-pyrenemethanol in THF ($\epsilon[344 \text{ nm}] = 42,700 \text{ M}^{-1}.\text{cm}^{-1}$), yielded the parameter λ_{Py} . The molar fraction x of pyrene-labeled monomers could be determined by applying Equation 4.1 where M_{BMA} is the molar mass of *n*-butyl methacrylate (142 g.mol^{-1}), and M_{Py} is the molar

mass of the pyrene-labeled monomers equal to 300, 344, 388, and 432 g.mol⁻¹ for PyEG₀-MA, PyEG₁-MA, PyEG₂-MA, and PyEG₃-MA, respectively.

$$x = \frac{M_{BMA}}{1/\lambda_{Py} + M_{BMA} - M_{Py}} \quad (4.1)$$

Steady-state fluorescence: The fluorescence spectra of the dilute PyEG_x-PBMA solutions in THF ([Py] = 2.5×10⁻⁶ M) were acquired with a Photon Technology International LS-100 steady-state fluorometer using the right angle geometry. The solutions were excited at 344 nm with an Ushio UXL-75 Xenon lamp, and the fluorescence monitored with a PTI 814 photomultiplier. The polymer solutions were outgassed with a gentle flow of nitrogen for 30 min. to avoid oxygen quenching. Fluorescence quantum yield measurements were carried out by comparing the fluorescence signal of a polymer sample in THF integrated over the entire fluorescence spectrum with that of 1-pyrenebutanol in THF, taking advantage of its known quantum yield ($\phi_{PyBut} = 0.52$).²² The absorption at 344 nm, where the 1-pyrenemethoxy derivative absorbs for the solutions used for quantum yield measurements, was kept at 0.05.

Time-resolved fluorescence: The same polymer solutions used for steady-state fluorescence measurements were then placed in an IBH Ltd. time-resolved fluorometer to acquire the pyrene monomer and excimer decays at 375 and 510 nm, respectively. The solutions were excited at 344 nm with an IBH 340 nm NanoLED. Cut-off filters were employed at 370 and 495 nm to minimize straight light scattering when collecting the monomer and excimer decays, respectively. The fluorescence decays were fitted globally according to the Fluorescence Blob Model (FBM).^{15-17,20,21} The quality of the fits was assessed from the χ^2

value (< 1.3) and the random distribution around zero of the residuals and autocorrelation of the residuals. The fits yielded the molar fractions of the different pyrene species present in the solution and the FBM parameters. A more detailed description of the FBM analysis can be found in SI.4 and in earlier publications.^{15-17,20,21}

4.4 Results

Three pyrene derivatives (PyEG_x-OH with $x = 1 - 3$) were synthesized by extending the substituent of 1-pyrenemethanol (PyEG₀-OH) with one, two, and three ethylene glycol units. Reaction of the PyEG_x-OH ($x = 0 - 3$) compounds with methacryloyl chloride yielded four pyrene-labeled methacrylate monomers, which after copolymerization with butyl methacrylate yielded four different polymers (PyEG_x-PBMA with $x = 0 - 3$). The fluorescent pyrene label was held at different distances from the main chain by oligo(ethylene glycol) spacers of increasing length, to probe whether the formation of excimer between two pyrene labels attached at the tip of the side chains would be affected by the spacer length. All the fluorescence spectra of the PyEG_x-PBMA samples in THF can be seen in Figure SI4.7. The steady-state fluorescence spectra of dilute THF solutions of the PyEG_x-PBMA with $x = 0 - 3$ having a similar pyrene content of about 4 mol% are shown in Figure 4.1. To avoid intermolecular excimer formation, all the fluorescence experiments were conducted with dilute solutions of the PyEG_x-PBMA samples in THF using a pyrene concentration of 2.5×10^{-6} M. Figure 4.1 demonstrates that increasing the spacer length of the pyrene derivative from three atoms in PyEG₀-MA to 12 atoms in PyEG₃-MA substantially increased the efficiency of pyrene excimer formation. However this conclusion

needs to be adjusted to account for the differences in vibrational structure experienced by the pyrene labels in different polymeric constructs. As can be seen in Figure 4.1, the I_1/I_3 ratio of the pyrene labels equals 1.86 for PyEG₀-PBMA but only 1.25, 1.36, and 1.19 for PyEG₁-PBMA, PyEG₂-PBMA, and PyEG₃-PBMA, respectively. The fluorescence quantum yield was determined for all solutions in Figure 4.1 and found to take a similar value of 0.31 ± 0.05 . The unnormalized fluorescence spectra used for Figure 4.1 are presented in Figure SI4.7 in SI4.

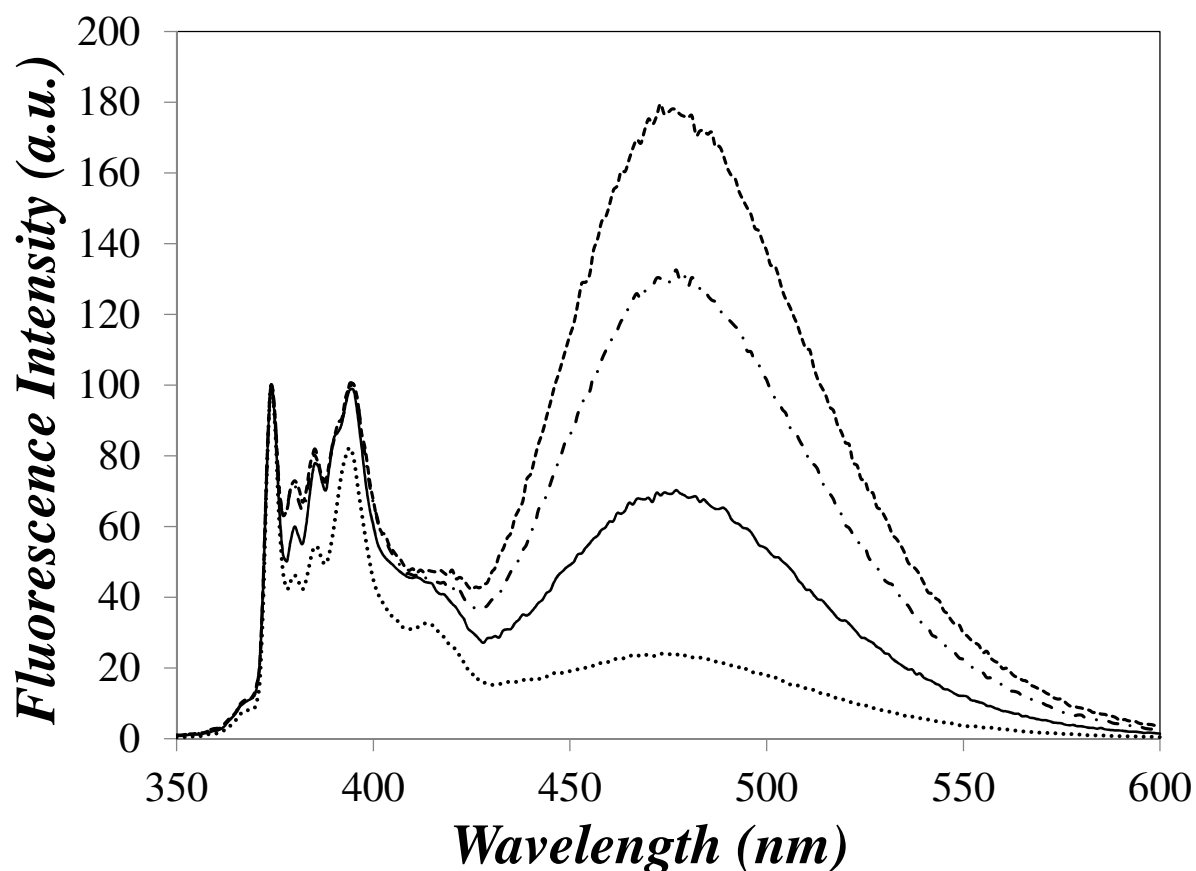


Figure 4.1: Normalized steady-state fluorescence spectra of (....., $\phi_F = 0.38$) Py(4.0)EG₀-PBMA, (---, $\phi_F = 0.27$) Py(3.8)EG₁-PBMA, (-.-, $\phi_F = 0.32$) Py(3.9)EG₂-PBMA, and (----, $\phi_F = 0.28$) Py(4.2)EG₃-PBMA in THF. $[Py] = 2.5 \times 10^{-6}$ M, $\lambda_{ex} = 344$ nm.

As demonstrated in an earlier publication,²⁰ the 1-pyrenemethoxy group of PyEG₁-OH responds effectively to the polarity of its local environment and so do PyEG₂-OH and PyEG₃-OH. The similar I_1/I_3 ratios taken by PyEG_x-PBMA with $x = 1 - 3$ suggests that these three constructs respond in a similar manner to the polarity of THF. Since the I_1/I_3 ratio takes a value substantially larger for PyEG₀-PBMA, it suggests that either the pyrene label of PyEG₀-PBMA probes an environment that is much more polar than THF, or that this pyrene derivative responds differently to the polarity of its environment, resulting in a larger I_1/I_3 ratio. As it turns out, the latter possibility is certainly more likely. 1-Pyrenemethanol and 1-pyrenemethyl methacrylate showed an I_1/I_3 ratio of, respectively, 1.76 and 1.83 in THF, similar to the value of 1.86 obtained for PyEG₀-PBMA in THF. It is certainly the difference in chemical structure between 1-pyrenemethanol (PyEG₀-OH) and the family of PyEG_x-OH ($x = 1 - 3$) constructs that leads to the difference in I_1/I_3 ratio between 1.86 for the former and 1.27 ± 0.09 for the latter, a result of the sensitivity of the 0-0 transition of pyrene to the polarity of the environment. In turn, this effect makes it difficult to assess the efficiency of excimer formation for the PyEG₀-PBMA series, since the larger I_1 peak of PyEG₀-PBMA makes the excimer signal of this polymer series appear smaller in Figure 4.1. Nevertheless, the I_E/I_M ratios of all fluorescence spectra were determined by taking the ratio of the integrals between 500 and 530 nm and between 372 and 378 nm for I_E and I_M , respectively. The I_E/I_M ratios were plotted in Figure 4.2A as a function of pyrene content.

For each polymer series, the I_E/I_M ratio increased with increasing pyrene content as expected, since a larger pyrene content enabled more pyrene encounters and thus more excimer formation. The trend observed in Figure 4.1 for a pyrene content close to 4 mol%, that showed an increase in excimer formation with increasing number of EG units (x), could

be generalized since the I_E/I_M ratio in Figure 4.2A was shown to increase with increasing x value at any pyrene content. Approximating the trends obtained in Figure 4.2A for the plots of I_E/I_M versus pyrene content as straight lines, the slopes $m(I_E/I_M)$ of these lines were plotted in Figure 4.2B as a function of the number of atoms in the side chain. The slope $m(I_E/I_M)$ increased linearly with increasing number of atoms in the side chain, thus demonstrating enhanced efficiency of excimer formation displayed by the polymer series prepared with larger oligo(ethylene glycol) linkers. It appears that a larger spacer enabled an excited pyrene to sample a larger volume in the polymer coil, thus leading to a greater probability of encountering a ground-state pyrene and forming an excimer. However since the I_1/I_3 ratio of the PyEG₀-PBMA series was much larger than that of the other polymers, these conclusions were true for the three PyEG_{*x*}-PBMA series with $x= 1 - 3$, that all exhibited a similar I_1/I_3 ratio but might not fully hold for the PyEG₀-PBMA series, whose I_1 peak was enhanced. By comparison, the time-resolved fluorescence experiments, are more straightforward to interpret since their analysis is impervious to the polarity of the environment, as it solely reflects the kinetics of pyrene excimer formation. Furthermore, the analysis of the fluorescence spectra of the pyrene-labeled polymers in solution only provides a qualitative measure of their ability to form an excimer, since they do not distinguish between the different pyrene species present in solution. These pyrene species are those that are attached onto macromolecular units that diffuse slowly ($P_{y_{diff}}$), rearrange quickly with a large rate constant k_2 to form an excimer after two slowly diffusing pyrene-bearing macromolecular units have been brought into close proximity ($P_{y_{k2}}$), cannot form excimer because they are located in pyrene-poor regions of the polymer coil and behave as if they were free in solution ($P_{y_{free}}$), or are pre-associated and form an excimer (E^*) or an excited long-lived dimer (D^*)

instantaneously upon direct excitation of a pyrene dimer. Since the global FBM analysis of the monomer and excimer fluorescence decays can distinguish between those different pyrene species, it can isolate the contribution of Py_{diff} , to provide a quantitative measure of the rate constant of diffusive encounters (k_{blob}) between two macromolecular units bearing a pyrene label, and the number of backbone monomers encompassing a *blob* (N_{blob}).^{15-17,20,21}

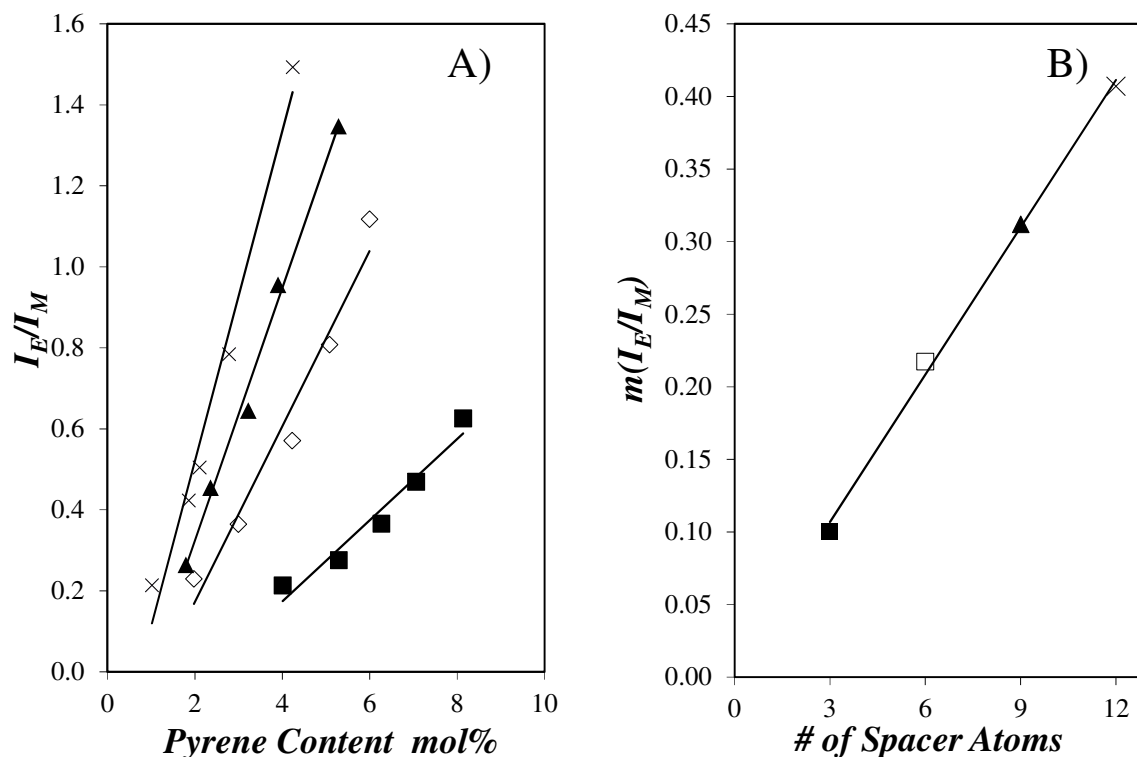


Figure 4.2: A) Comparison of the I_E/I_M ratios of (■)PyEG₀-PBMA labeled with 4.0, 5.3, 6.3, 7.1, and 8.1 mol% pyrene, (◇)PyEG₁-PBMA labeled with 1.8, 2.7, 3.8, 4.6, and 5.4 mol% pyrene, (■)PyEG₂-PBMA with 1.8, 2.3, 3.2, 3.9, and 5.3 mol% pyrene, and (x)PyEG₃-PBMA labeled with 1.0, 1.8, 2.1, 2.7, and 4.3 mol% pyrene. B) $m(I_E/I_M)$ for the same polymers in THF. $[Py] = 2.5 \times 10^{-6}$ M, $\lambda_{\text{ex}} = 344$ nm.

Consequently, the fluorescence decays of the pyrene monomer and excimer of all the pyrene labeled polymer series were acquired and fitted globally with Equations SI4.1 and SI4.2 according to the FBM analysis. This analysis yielded k_{blob} and N_{blob} , the number of monomers constituting the polymer segment encompassed inside V_{blob} , the volume of a blob, and these parameters will be discussed in detail hereafter. The fits of the decays were excellent, as can be seen in Figure SI4.9 in SI. All the parameters retrieved from the FBM analysis of the fluorescence decays have been listed in Tables SI4.3-5 in SI4. A more complete description of the FBM can be found in earlier publications.^{20,21} The largest molar fractions were f_{diff} and f_{k2} , whose combined value ($f_{\text{diff}} + f_{k2}$) for all PyEG_x-PBMA polymers averaged 0.87 ± 0.03 , indicating that the vast majority of pyrene labels formed excimer by diffusion. Thus these fluorescence experiments reflected the diffusive motions of the pyrene-terminated side chains.

The FBM analysis of the fluorescence decays also yielded the average number of pyrenes per *blob*, $\langle n \rangle$. Using the known pyrene content (λ_{py}) of the polymers listed in Table 4.1, the number of monomer units encompassed inside a *blob*, N_{blob} , could be determined according to Equation 4.2.

$$N_{\text{blob}} = \frac{1}{(1 - f_{M\text{free}})} \times \frac{\langle n \rangle}{x} \quad (4.2)$$

In Equation 4.2, x is the molar fraction of pyrene-labeled monomer of the PyEG_x-PBMA samples listed in Table 4.1. The FBM parameters N_{blob} , k_{blob} , and the product $k_{\text{blob}} \times N_{\text{blob}}$ obtained from the FBM analysis of the fluorescence decays acquired with each PyEG_x-

PBMA polymer are shown as a function of pyrene content for the four polymer series in Figures 4.3A-C. Within experimental error, these parameters remained constant with pyrene content. As usually done in such a situation,^{15-17,20,21} their values were then averaged for each polymer series and $\langle N_{\text{blob}} \rangle$, $\langle k_{\text{blob}} \rangle$, and $\langle k_{\text{blob}} \times N_{\text{blob}} \rangle$ were plotted in Figures 4.3D-F as a function of the linker length connecting pyrene to the PBMA chain.

In Figure 4.3D, $\langle N_{\text{blob}} \rangle$ was found to increase linearly with increasing linker length from 40.5 ± 2.3 for PyEG₀-PBMA to 82.7 ± 3.7 for PyEG₃-PBMA. This trend indicated that the volume probed by an excited pyrene V_{blob} increased with increasing spacer length as would be expected, since a longer spacer allows an excited pyrene to probe a larger volume inside the polymer coil. The smallest N_{blob} value was obtained for the short 3 atom spacer of the PyEG₀-PBMA series, which restricted the mobility of the excited pyrene label so that it probed the smallest volume V_{blob} of all other constructs.

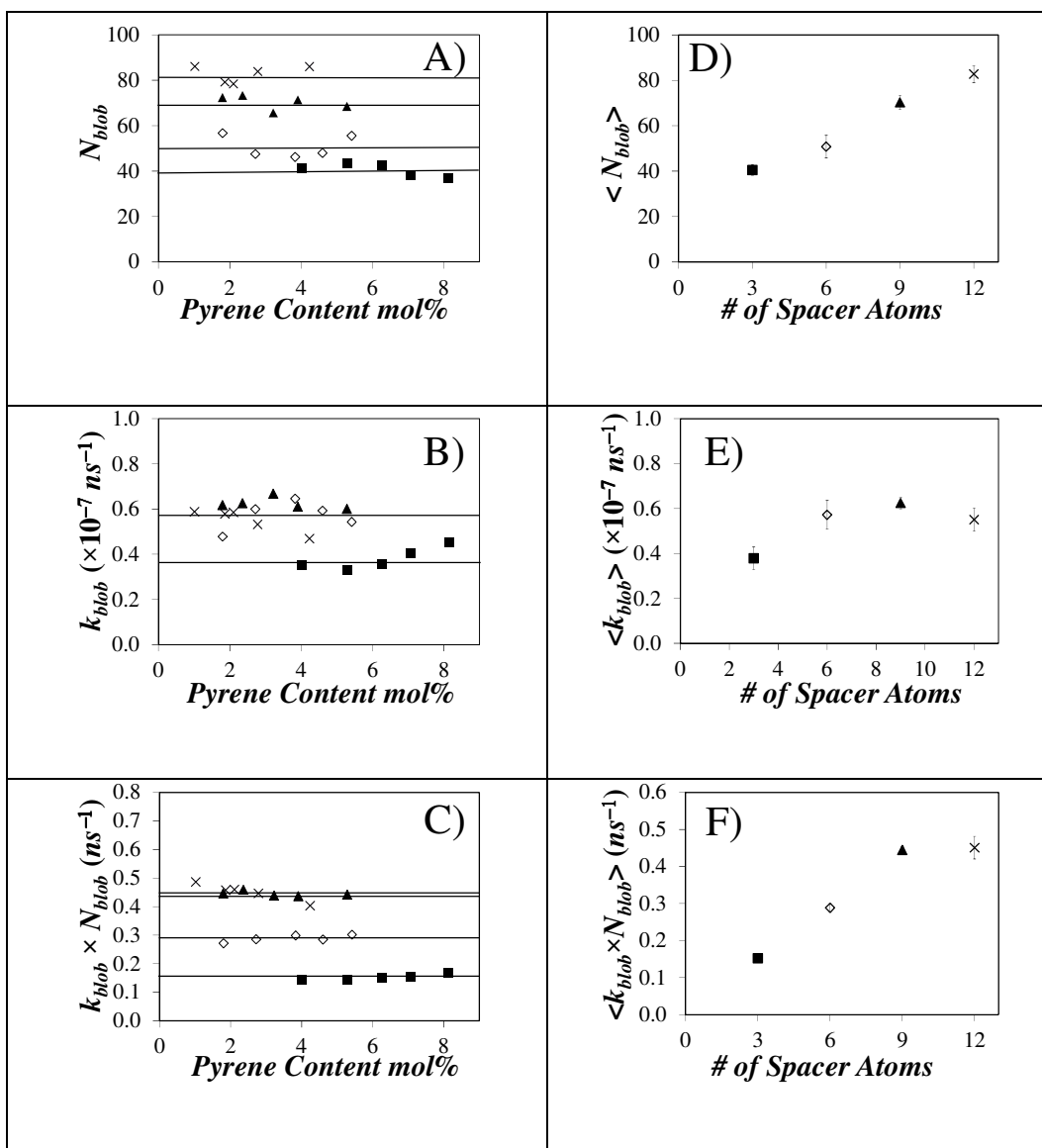


Figure 4.3: Plot of A) N_{blob} , B) k_{blob} , and C) $k_{blob} \times N_{blob}$ as a function of pyrene content and D) $\langle N_{blob} \rangle$, E) $\langle k_{blob} \rangle$, and F) $\langle k_{blob} \times N_{blob} \rangle$ as a function of the number of spacer atoms for (■)PyEG₀PBMA labeled with 4.0, 5.3, 6.3, 7.1, and 8.1 mol% pyrene, (◇)PyEG₁PBMA labeled with 1.8, 2.7, 3.8, 4.6 and 5.4 mol% pyrene, (■)PyEG₂PBMA with 1.8, 2.3, 3.2, 3.9, and 5.3 mol% pyrene, and (×)PyEG₃PBMA labeled with 1.0, 1.8, 2.1, 2.7, and 4.3 mol% pyrene in THF. $[Py] = 2.5 \times 10^{-6}$ M, $\lambda_{ex} = 344$ nm.

The behavior of $\langle k_{\text{blob}} \rangle$ plotted as a function of the linker length in Figure 4.3E was quite remarkable. By definition, k_{blob} is equal to the product $k_{\text{diff}} \times [\text{Py}]_{\text{blob}}$, where k_{diff} is the bimolecular rate constant for diffusive encounters between two monomers bearing a pyrene group, and $[\text{Py}]_{\text{blob}}$ is the local concentration equivalent to one ground-state pyrene inside a *blob* ($[\text{Py}]_{\text{blob}} = 1/V_{\text{blob}}$). Since V_{blob} scales as $N_{\text{blob}}^{3\nu}$ where ν is the Flory exponent^{23,24} equal to 0.6 in a good-solvent for PBMA like THF,²⁰ k_{blob} is expected to decrease with increasing N_{blob} as has been observed in a number of examples.^{25,26} Yet instead of decreasing as the spacer length increased from 3 to 12 atoms and N_{blob} increased linearly from 40.5 for PyEG₀-PBMA to 82.7 for PyEG₃-PBMA, k_{blob} increased from $0.38 (\pm 0.05) \times 10^7 \text{ s}^{-1}$ for PyEG₀-PBMA to $0.57 (\pm 0.06) \times 10^7 \text{ s}^{-1}$ for PyEG₁-PBMA and it remained relatively constant and equal to $0.57 (\pm 0.05) \times 10^7 \text{ s}^{-1}$ for the PyEG_{*x*}-PBMA series with spacer length *x* equal to 1 – 3. This unexpected trend was attributed to the enhanced mobility afforded by the flexible oligo(ethylene glycol) linker.

With 1-pyrenemethanol used to prepare PyEG₀-PBMA, the pyrenyl unit is tightly held via an ester bond close to the PBMA backbone, severely hindering its mobility and ability to form an excimer, and thus strongly reducing k_{diff} and resulting in a small k_{blob} value. Introducing one ethylene glycol unit in the linker of PyEG₀-PBMA to obtain PyEG₁-PBMA enhances the mobility of the pyrene label considerably. This enhanced mobility is reflected by a much larger k_{diff} that counteracts the decrease in $[\text{Py}]_{\text{loc}}$ associated with the longer spacer, thus resulting in the increase of k_{blob} from $0.38 (\pm 0.05) \times 10^7 \text{ s}^{-1}$ for PyEG₀-PBMA to $0.57 (\pm 0.06) \times 10^7 \text{ s}^{-1}$ for PyEG₁-PBMA. Addition of a second and third ethylene glycol unit further releases the steric constraints imposed by the main chain, but this effect decreases

with each addition of an ethylene glycol unit in the spacer. Assuming that $[Py]_{loc}$ scales as $N_{blob}^{-1.8}$ ($[Py] = 1/V_{blob} \sim N_{blob}^{-3v}$), the effect that adding one ethylene glycol unit has on k_{diff} can be estimated by applying Equation 4.3, where x represents the number of ethylene glycol units in the linker.

$$\frac{k_{diff,x+1}}{k_{diff,x}} = \frac{k_{blob,x+1}}{k_{blob,x}} \times \left(\frac{N_{blob,x+1}}{N_{blob,x}} \right)^{1.8} \quad (4.3)$$

Based on the FBM parameters retrieved from the decay analysis, and whose average values are shown in Figures 4.3D and 4.3E, Equation 4.3 predicts that k_{diff} increases by 2.3 ± 0.3 , 2.0 ± 0.2 , and 1.2 ± 0.1 when the linker length is increased from PyEG₀-PBMA to PyEG₁-PBMA, from PyEG₁-PBMA to PyEG₂-PBMA, and from PyEG₂-PBMA to PyEG₃-PBMA, respectively. According to this trend, the addition of two ethylene glycol units to obtain PyEG₂-PBMA appears to provide the pyrene label with sufficient mobility to no longer sense the hindrance from the main chain, as adding a third ethylene glycol unit to the linker of PyEG₂-PBMA to generate PyEG₃-PBMA hardly changes k_{diff} , with the ratio $k_{diff,3}/k_{diff,2}$ taking a value close to unity (1.2 ± 0.1). While reducing steric hindrance enhances pyrene excimer formation, it must be pointed out that it also reduces the response of pyrene to the dynamics of the main chain. Consequently, these results indicate that in the case of PBMA using a linker with 6 or less spacer atoms such as for PyEG₀-PBMA and PyEG₁-PBMA, pyrene excimer formation probes the dynamics of the main chain, whereas when using a linker with 9 or more spacer atoms such as for PyEG₂-PBMA and PyEG₃-PBMA, pyrene excimer formation is more representative of the dynamics of the side chains rather than the

dynamics of the main chain. This information might be of particular interest for applying pyrene excimer formation to the study of branched macromolecules such as polymeric bottlebrushes, where the side chains can be much longer than the longest spacer employed in this study for PyEG₃-PBMA.

The main consequence of having k_{blob} taking a larger but constant value for linkers made of a number x of EG units comprised between 1 and 3 is that the product $\langle k_{\text{blob}} \times N_{\text{blob}} \rangle$ increased almost linearly with increasing linker length up to $x=2$, before plateauing in Figure 4.3F for $x=3$ instead of decreasing as $k_{\text{diff}} \times N_{\text{blob}}^{1-3\nu}$ as could be expected based on scaling arguments alone.^{25,26} While the interpretation of the trend obtained with $\langle k_{\text{blob}} \times N_{\text{blob}} \rangle$ in Figure 4.3E is complicated by the fact that k_{blob} depends both on the *blob* volume via N_{blob} , and the flexibility of the oligo(ethylene glycol) linker via k_{diff} , the trend obtained with N_{blob} in Figure 4.3D is more straightforward to interpret since N_{blob} relies solely on the volume V_{blob} probed by an excited pyrene label.

As a matter of fact, knowledge of the Mark-Houwink-Sakurada (MHS) parameters K and a for PBMA in THF enables the use of N_{blob} to estimate the hydrodynamic radius of a *blob*, R_{blob} , as a function of the number x of ethylene glycol units linking pyrene to the PBMA chain. Since N_{blob} values ranging from 40 to 83 monomers would be equivalent to low molecular weight PBMA samples for which the MHS parameters were unavailable in THF at room temperature, they were determined by measuring the intrinsic viscosity at 25 °C of five PBMA samples having a narrow molecular weight distribution, and with M_n values ranging between 2.5 and 38 K. The intrinsic viscosity experiments were conducted in THF at 25 °C. A plot of $[\eta]$ as a function of M_n is shown in Figure SI4.10 in SI4. A plot of $\text{Ln}[\eta]$ versus $\text{Ln}(M_n)$ could be well fitted with a straight line and the fit yielded the K and a parameters of

the MHS equation found to equal $2.8 (\pm 0.6) \times 10^{-4}$ mL/g and 1.09 ± 0.03 , respectively. The parameters K and a were then introduced into Equation 4.4 to determine R_{blob} , the equivalent hydrodynamic radius of a *blob*.

$$R_{\text{blob}} = \left(\frac{3KN_{\text{blob}}^{a+1}}{10\pi N_A} \right)^{1/3} \quad (4.4)$$

A plot of R_{blob} as a function of the linker length is shown in Figure 4.4 within experimental error, R_{blob} increased linearly by an increment δr of 0.32 ± 0.06 nm per ethylene glycol unit added to the linker.

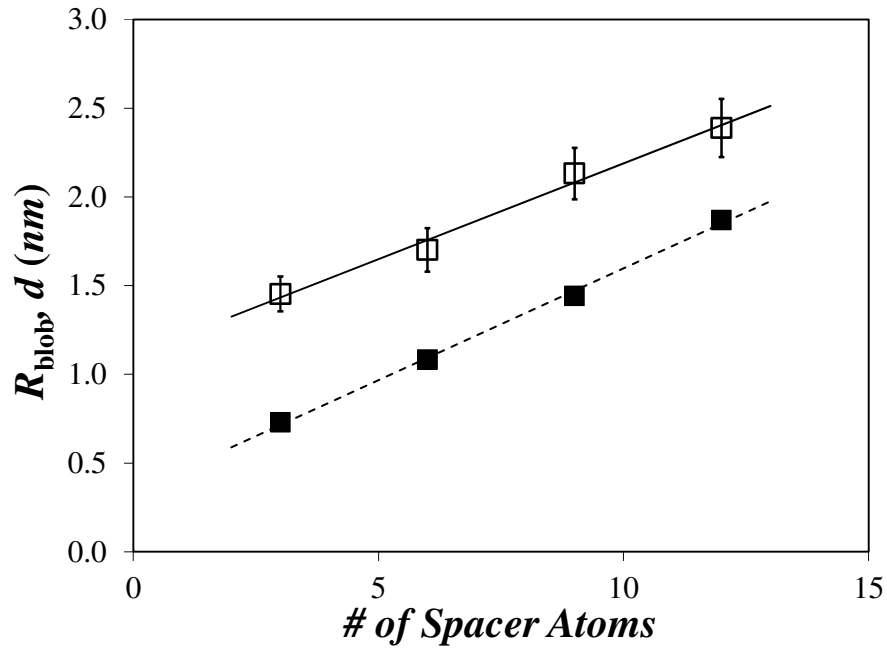


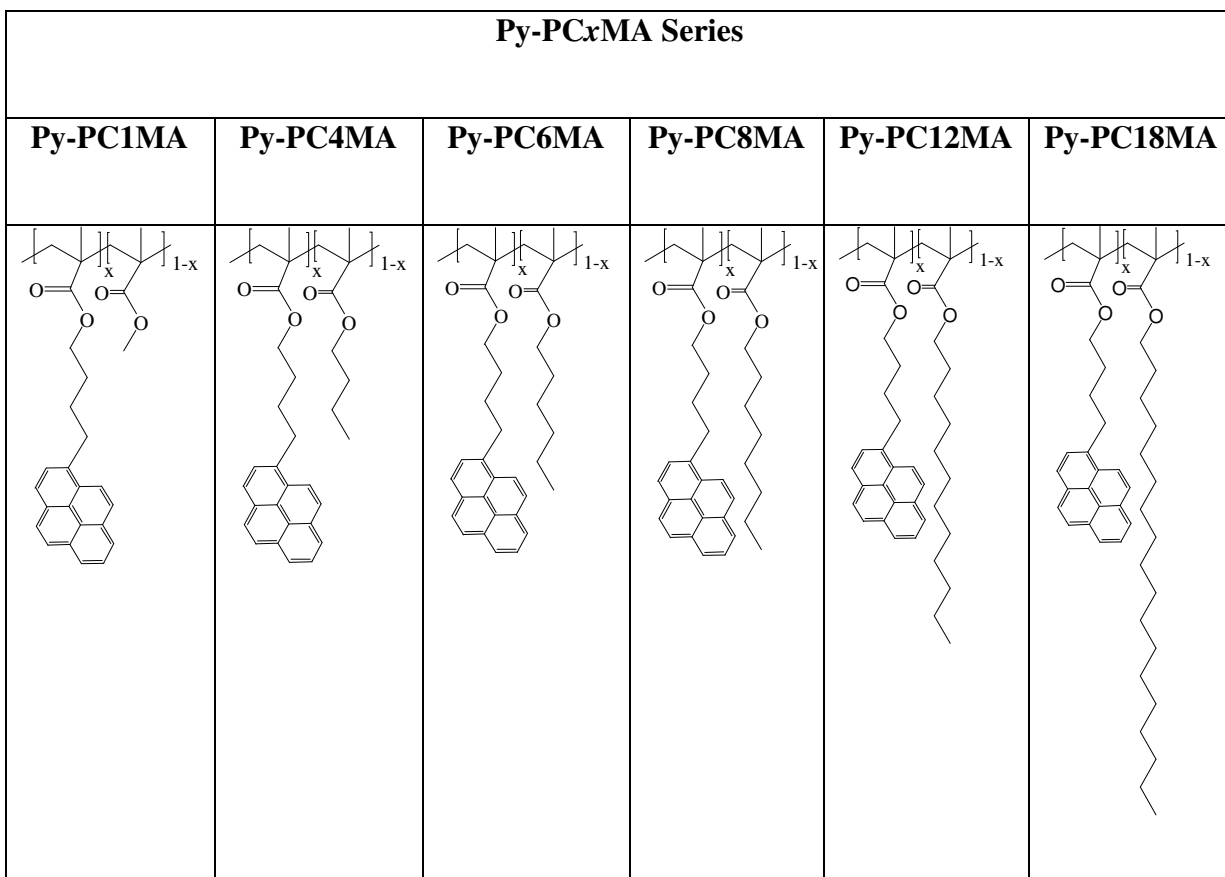
Figure 4.4: Comparison of R_{blob} (□) and the spacer length d (■) for the PyEG_x-PBMA series.

The increase in R_{blob} with increasing linker length could be accounted for, in part, by considering the end-to-end distance of the stretched oligo(ethylene glycol) spacer (d) between the carbon in the main PBMA chain bearing the carbonyl group to the center of the pyrene molecule. The distance d was calculated by conducting molecular mechanics optimizations with HyperChem. The constructs generated through these optimizations can be viewed in Table SI4.2. Plotting d as a function of the number of linker atoms yielded a straight line in Figure 4.4, with a slope of 0.126 nm/side chain atom, representing an increment δr of 0.38 nm per ethylene glycol unit, similar to that found for R_{blob} (0.32 ± 0.06 nm per ethylene glycol unit). Since R_{blob} and d increased in a similar manner with increasing number of linker atoms, it strongly suggests that the increase in R_{blob} shown in Figure 4.4D was directly related to the increase $\delta r = 0.38$ nm in linker length brought about by each addition of an ethylene glycol unit.

4.5 Discussion

The present study enables one to draw a direct comparison between the dynamics experienced by pyrene labels distributed randomly in a macromolecule according to two orthogonal structural arrangements. In the first arrangement, the pyrene labels are randomly distributed along a main chain, but held at the same distance from the main chain via a butyl spacer, while the length of the side chains increases from a methyl to a stearyl units (see Figure 4.5). To obtain this structural arrangement, 1-pyrenebutyl methacrylate was copolymerized with a series of alkyl methacrylates to yield the polymer samples Py-PcxMA, where Cx represents a linear alkyl side chain with x carbon atoms. The results of this study

have been already published.²¹ The second structural arrangement corresponds to the present study, whereby a PBMA, main chain is labeled randomly with pyrene held at increasing distances from the main chain via an oligo(ethylene glycol) spacer. These samples were referred to as PyEG_x-PBMA, where $x = 0 - 3$ represents the number of ethylene glycol units in the side chain. As a matter of fact, the Py-PC_xMA constructs enable one to monitor the dynamics experienced by a main chain as longer side chains are incorporated into the polymer, while the PyEG_x-PBMA series enables one to probe the dynamics experienced by the tip of a side chain growing perpendicularly to the main chain.



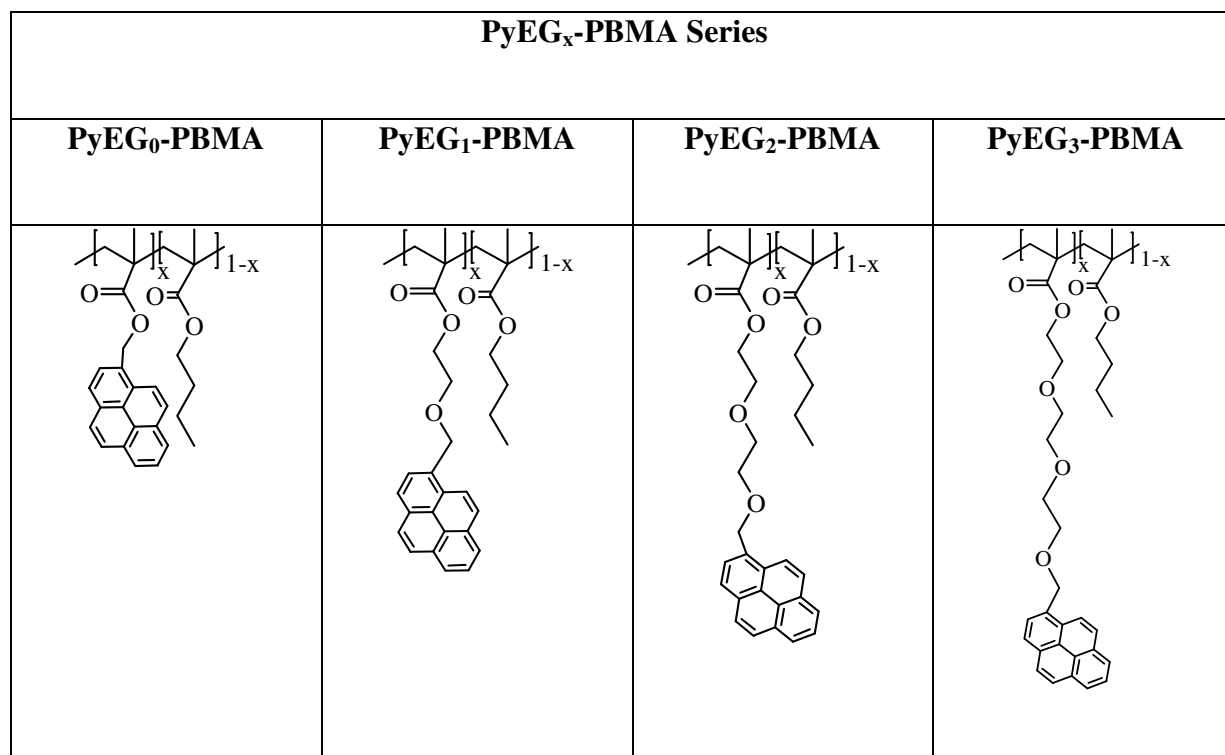


Figure 4.5: Comparison of the chemical structure of the Py-PC_xMA and PyEG_x-PBMA samples that were studied in ref 21 and in the present report, respectively.

As shown in Figure 4.6, all the parameters retrieved from the analysis of the fluorescence data show strikingly different trends depending on the structural arrangement of the pyrene labels, when plotted as a function of the number of side chain atoms. All the parameters indicate that excimer formation is strongly reduced when the side chain length is increased for the Py-PC_xMA series. As the side chain length increases, the efficiency of excimer formation reflected by $m(I_E/I_M)$ decreases in Figure 4.6A. This effect is due to the smaller *blob* volume V_{blob} , as reflected by the decreasing N_{blob} value in Figure 4.6B, probed by an excited pyrene as the motion of the label is hindered by the bulkier substituents and

slower main chain mobility. Similarly, the dynamics of the main chain probed by the decreasing $\langle k_{\text{blob}} \times N_{\text{blob}} \rangle$ product in Figure 4.6C are strongly slowed down by the larger substituents.

By comparison, an increase in the length of the oligo(ethylene glycol) side chain bearing the 1-pyrenemethoxy label in the PyEG_x-PBMA series is associated with a substantial enhancement in excimer formation as illustrated in Figure 4.6A for $m(I_E/I_M)$. The reason for this increased excimer formation is the larger reach of the tip of the side chain that allows an excited pyrene to probe a larger V_{blob} , reflected by a larger N_{blob} in Figure 4.6B, as well as faster dynamics due to reduced steric hindrance from the main chain, as illustrated in Figure 4.6C, where the product $\langle k_{\text{blob}} \times N_{\text{blob}} \rangle$ increased with increasing side chain length. Based on the trends described in Figure 4.6, the substantial difference in behaviour observed between the fluorescence data obtained from the Py-PC_xMA and PyEG_x-PBMA series represents a strong indication that pyrene excimer fluorescence measurements can provide valuable information about the dynamics experienced by a HBM along and perpendicularly to its main chain.

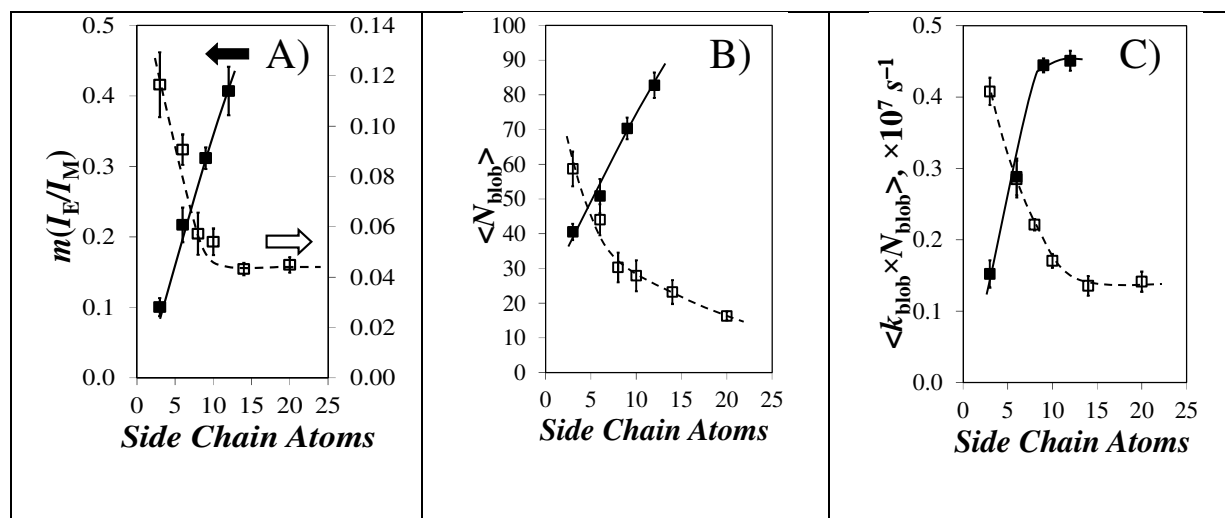


Figure 4.6: Plot of $m(I_E/I_M)$, $\langle N_{\text{blob}} \rangle$, and $\langle k_{\text{blob}} \times N_{\text{blob}} \rangle$ as a function of side chain atoms for the (□)Py-PC_xMA and (■)PyEG_x-PBMA series.

4.6 Conclusions

This study has demonstrated that excimer formation between pyrene labels covalently attached to the tip of side chains responds quite strongly to the size of the linker connecting pyrene to the main chain in terms of both increased mobility characterized by k_{blob} , and enhanced reach within the polymer coil as described by R_{blob} . Both effects contributed to dramatically increase pyrene excimer formation, as found from the analysis of the steady-state fluorescence spectra through the I_E/I_M ratio (Figures 4.1 and 4.2). As a matter of fact, increasing the length of the linker connecting pyrene to the PBMA backbone resulted in the decoupling of the motion of the pyrene label in solution from that of the polymer main chain. The measurements described herein suggest that two ethylene glycol units between the pyrenemethoxy label and the polymethacrylate backbone are required to achieve this decoupling. For linkers made of two or more ethylene glycol units, k_{blob} retrieved from the global FBM analysis of the fluorescence decays described mainly the diffusive motions of

the side chains, whereas N_{blob} provided a measure of the volume probed by the tip of the side chains. For shorter side chains, k_{blob} reflected the diffusive motions of the main chain. These observations are important to design a proper linker between a dye and a linear polymer, depending on the element of a macromolecule (main chain versus side chain) being investigated.

The volume described by the tip of the side chains within the polymer coil could be determined quantitatively by applying the MHS equation to the N_{blob} values retrieved from the FBM analysis of the decays to yield R_{blob} , the hydrodynamic radius of a *blob*. While k_{blob} increased with increasing side chain length due to the relaxation of the dye as it was more separated from the main chain, the increase in R_{blob} by an increment of 0.38 nm per added ethylene glycol unit with increasing linker length could be mostly accounted for by considering the increase in length of the extended linker determined from molecular mechanics optimizations carried out with HyperChem.

The conclusions reached in the present study regarding the volume probed by the tip of a side chain and its dynamics were enabled by the FBM, whose framework readily distinguishes between the contributions of the different pyrene species present in solution and the process of excimer formation due to the different length and time scales experienced by an excited pyrene attached to the tip of a series of side chains. The results presented herein suggest that pyrene excimer formation should be a powerful tool for the study of HBMs such as comb polymers or polymeric bottlebrushes. Using a short and long linker to connect pyrene to the macromolecule enables the experimentalist to probe the dynamics along and perpendicularly to the main chain, respectively, a feature that should prove extremely useful to the many scientists interested in characterizing HBMs at the molecular level.

Chapter 5

Characterization of the Long Range Internal Dynamics of Pyrene-Labeled
Macromolecules by Pyrene Excimer Fluorescence

5.1 Overview

The Long Range Internal Dynamics (LRID) of 74 Pyrene-Labeled Macromolecules (PyLMs) was characterized in four solvents representing a broad range of dielectric constants equal to 2.4 (toluene), 7.6 (tetrahydrofuran, THF), 37.8 (*N,N*-dimethylformamide, DMF) and 46.7 (dimethylsulfoxide, DMSO). The LRID of the PyLMs were quantified based on the parameters retrieved from the Model Free Analysis (MFA) of the time-resolved fluorescence (TRF) decays of the pyrene monomer and excimer. These parameters were combined to yield $\langle k \rangle$, the average rate constant of pyrene excimer formation in the PyLMs, and $(I_E/I_M)^{\text{TRF}}(f_{\text{free}}=0)$, the ratio of excimer to monomer fluorescence intensity obtained in the absence of pyrene labels that do not form excimer. $(I_E/I_M)^{\text{TRF}}(f_{\text{free}}=0)$ was found to increase linearly with increasing $\langle k \rangle$ values over three orders of magnitude in the four solvents studied, with a slope that equaled the lifetime of the pyrene excimer (τ_E). The $\langle k \rangle$ values obtained to build these master curves could be correlated back to the expected LRID of the macromolecules, with the end-labeled linear chains holding the pyrene groups far apart yielding the lowest $\langle k \rangle$ values, whereas branched macromolecules bringing the pyrene labels close to each other yielded the larger $\langle k \rangle$ values. Furthermore, the fact that these linear master curves were observed for so many different PyLMs in the four solvents covering such a broad range of solvent polarity suggests that this relationship represents a general physical phenomenon that applies to all PyLMs. Considering the importance of characterizing the LRID of macromolecules in solution, the $(I_E/I_M)^{\text{TRF}}(f_{\text{free}}=0)$ -vs.- $\langle k \rangle$ plots presented in this report can be viewed as calibration curves against which the LRID of any PyLM can now be compared. Thus the 3-order of magnitude range found for these master curves offers the

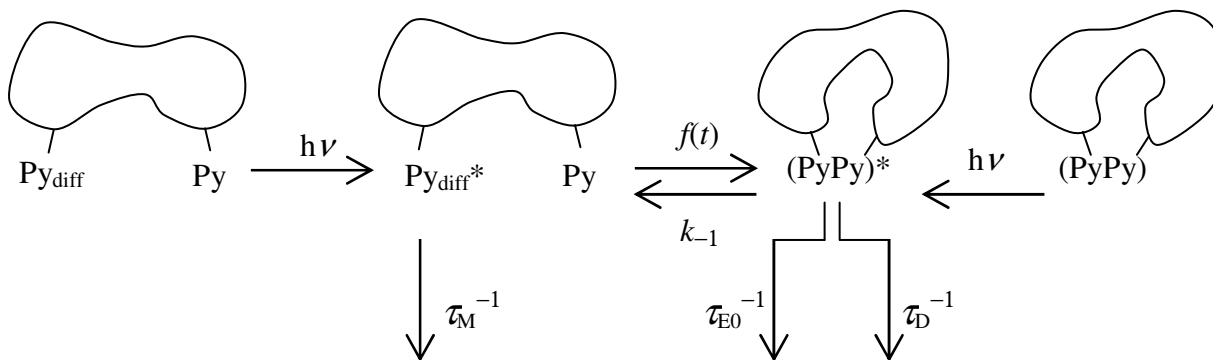
scientific community an impressive analytical opportunity to gauge the LRID of macromolecules in solution.

5.2 Introduction

The rate constant of excimer formation through the diffusive encounter of an excited and a ground-state pyrene covalently attached onto a macromolecule provides a direct measure of the Long Range Internal Dynamics (LRID) of macromolecules in solution.^{1,2} Compared to many other techniques that yield the rotational diffusion coefficient of a specific unit of a macromolecule such as NMR,³ dynamic light scattering,⁴ or fluorescence anisotropy⁵ to name a few, pyrene excimer formation offers the much rarer feature of probing translational diffusion, whereby two pyrene molecules covalently attached to different segments of a macromolecule diffuse through space until they come within 1 nm of each other to form an excimer.⁶ Thus pyrene excimer formation is ideally suited to describe the LRID of macromolecules, as it provides a direct measure of how different segments of a macromolecule diffuse within a given macromolecular volume. As a result, numerous macromolecules have been pyrene-labeled in a variety of ways, at the ends of linear monodisperse chains,⁷ at the termini of highly branched dendrimers,⁸ randomly along a chain,⁹ or at specific internal positions in proteins^{10,11} or polymers.^{12,13} Unfortunately, this variety in pyrene-labeling schemes has substantially complicated the quantitative analysis of fluorescence data acquired with PyLMs.

As it turns out, all but one of the photophysical process depicted in Scheme 5.1, which is the accepted kinetic scheme to describe excimer formation in pyrene-labeled

macromolecules (PyLMs), are well understood in the literature. Upon absorption of a photon, an excited pyrene monomer can either fluoresce with its natural lifetime τ_M or form one of two possible excimers, referred to as $E0^*$ or D^* , upon encounter with a ground-state pyrene.¹⁴ The existence of a second excimer D^* is usually observed when excimer formation occurs in restricted geometries that hinder the mobility of pyrene which, in turn, leads to poor stacking of two pyrenyl moieties. Such conditions can be encountered in PyLMs. Once formed excimers $E0^*$ and D^* can dissociate, but since the dissociation rate constant (k_{-1}) is usually small when compared to the inverse of their lifetime ($k_{-1} \ll \tau_{E0}^{-1}$ or τ_D^{-1}), k_{-1} is often neglected when modelling the process of pyrene excimer formation.



Scheme 5.1: Excimer formation between pyrenyl groups covalently attached onto a PyLM.

Compared to all these photophysical processes, the one process that remains most difficult to handle mathematically is the time-dependent rate constant of pyrene excimer formation described by the function $f(t)$ in Scheme 5.1. When excimer formation is monitored between several pyrene labels covalently attached to a macromolecule, each contour length separating every pair of pyrene labels is expected to generate one rate constant, so that pyrene excimer formation must be described by a distribution of rate

constants (DRC) reflecting the distribution of contour lengths. While much effort has been devoted over the past four decades to carefully determine the exact expression of the DRC in fluorescently labeled macromolecules, the DRC being unimodal and monodisperse for a monodisperse linear end-labeled polymer (one contour length yields one rate constant)⁷ or Poisson for randomly labeled macromolecules,⁹ the average rate constant $\langle k \rangle$ of the DRC for pyrene excimer formation is usually the most important information required to describe the main dynamical features of a macromolecule. It is in this context that the Model Free Analysis (MFA)^{1,2,8} becomes particularly appealing, especially when considering the simplicity of its derivation as shown hereafter.

The MFA is based on the observation that regardless of the nature of the PyLM (linear, branched, or helical) and the strategy selected for pyrene-labeling (randomly or at specific positions), the fluorescence decays of the pyrene monomer can always be fitted with a sum of exponentials as shown in Equation 5.1.¹⁵ Starting from this insight, an expression for the excimer decay is derived in a remarkably straightforward manner. Rearranging Equation 5.2 yields an expression for the time-dependent rate constant $f(t)$, which takes the form of a sum of exponentials which represents best the DRC. The expression for the rate constant $f(t)$ can then be introduced into Equation 5.3 to provide, after integration, the equation describing the excimer fluorescence decay, which is a sum of exponentials that includes the same pre-exponential factors a_i and decay times τ_i used in Equation 5.1. The mathematical derivation presented in Equations 5.1-5.3 can be easily expanded to include a second excimer D^* if required.

$$[M^*]=[M^*]_o \sum_{i=1}^n a_i \times \exp(-t/\tau_i) \quad (5.1)$$

$$\frac{d[M^*]}{dt} = -f(t) - \frac{1}{\tau_M} [M^*] \quad (5.2)$$

$$\frac{d[E^*]}{dt} = f(t) - \frac{1}{\tau_E} [E^*] \quad (5.3)$$

The sums of exponentials obtained for $[M^*]$ and $[E^*]$ are used to fit globally the monomer and excimer decays of a PyLM, where both the a_i and τ_i parameters are optimized simultaneously in the expressions for $[M^*]$ and $[E^*]$. Surprisingly, this apparently innocuous analytical detail represented a major departure from all other global analyses of monomer and excimer fluorescence decays of PyLMs conducted outside this laboratory, because these other analyses optimized τ_i as the same parameter in the expressions of $[M^*]$ and $[E^*]$, but not the a_i coefficients which were optimized separately in the monomer and excimer decays. Since optimization programs seek out a best fit without regard for the physical meaning of the parameters retrieved, the global fit of the monomer and excimer decays yielded usually different values for the set of a_i coefficients, resulting in rather laborious, sometimes erroneous, and often impossible interpretations of the decay analysis results. These considerations have been documented in an earlier publication.¹⁶ By contrast, implementation of the MFA only yields meaningful a_i and τ_i parameters thanks to the additional constraints imposed during their optimization. In turn, the a_i and τ_i parameters are applied to determine $\langle k \rangle$ and the absolute ratio of excimer over monomer, namely the $(I_E/I_M)^{\text{TRF}}$ ratio, obtained by time-resolved fluorescence (TRF) according to Equations 5.4 and 5.5, respectively.¹⁵ In

Equations 5.4 and 5.5, $\langle \tau \rangle$ is the number average lifetime of the monomer decay accounting for all decay times τ_i , other than τ_M , that represents those pyrene labels that do not form excimer and emit as if they were free in solution. The molar fractions f_{free} , f_{diff}^{E0} , f_{diff}^D , f_{E0} , and f_D used in Equation 5.5 represent those pyrene species that do not form excimer, form the excimer $E0^*$ or D^* by diffusion, and form the excimer $E0^*$ or D^* quasi-instantaneously upon direct excitation of a pyrene aggregate, respectively. When f_{free} is set to zero to represent the $(I_E/I_M)^{\text{TRF}}$ ratio in the absence of those pyrene labels that do not form excimer, the $(I_E/I_M)^{\text{TRF}}$ ratio is referred to as $(I_E/I_M)^{\text{TRF}}(f_{\text{free}}=0)$.^{16,17}

$$\langle k \rangle = \frac{\sum_{i=1}^n a_i}{\sum_{i=1}^n a_i \tau_i} - \frac{1}{\tau_M} = \frac{1}{\langle \tau \rangle} - \frac{1}{\tau_M} \quad (5.4)$$

$$(I_E/I_M)^{\text{TRF}} = \frac{(f_{\text{diff}}^{E0} \tau_{E0} + f_{\text{diff}}^D \tau_D) \langle k \rangle \langle \tau \rangle + f_{E0} \tau_{E0} + f_D \tau_D}{(f_{\text{diff}}^{E0} + f_{\text{diff}}^D) \langle \tau \rangle + f_{\text{free}} \tau_M} \quad (5.5)$$

In a study conducted on 32 PyLMs, representing the largest number and variety in structure of PyLMs in THF that have been studied to date, all $(I_E/I_M)^{\text{TRF}}(f_{\text{free}}=0)$ and $\langle k \rangle$ values were found to line up on a master straight line that spanned three orders of magnitude, as long as all the pyrene labels of the PyLMs formed excimer by diffusion. The slope of this master straight line equaled the excimer lifetime in the solvent considered. The PyLMs composed of a more flexible backbone or exhibiting a larger local pyrene concentration were found to take the largest $(I_E/I_M)^{\text{TRF}}(f_{\text{free}}=0)$ and $\langle k \rangle$ values. Consequently, this master curve

obtained for a series of PyLMs in THF provided a means to rank these PyLMs according to their ability to form excimer which reflected their compactness and LRID in that solvent.

Recognizing the importance of having a robust experimental means to rank quantitatively macromolecules according to the magnitude of their LRID, this chapter demonstrates the general nature of the master straight line obtained between $(I_E/I_M)^{\text{TRF}}(f_{\text{free}}=0)$ and $\langle k \rangle$, that was first established for PyLMs in THF,¹⁶ by showing that similar master straight lines can be generated not only in THF, but also in less polar toluene and more polar *N,N*-dimethylformamide (DMF) and dimethyl sulfoxide (DMSO). This study also expands on the range of PyLMs being characterized earlier, by including nine series of poly(alkyl methacrylate)s, amylose, amylopectin, and polystyrene that were randomly labeled with 1-pyrenebutyl derivatives and one series of pyrene end labeled poly(ethylene oxide)s. DiPyMe, pyrene end-labeled dendrimers, poly(1-pyrenebutyl methacrylate), and poly(1-pyrenemethoxydiethoxydiethyl methacrylate) were also added to this study as representatives of macromolecules with high pyrene contents, capable of forming excimer very efficiently. Together 74 PyLMs were investigated, which represents by far the largest set of PyLMs ever investigated in the literature. The fact that the same behavior was found for such a large group of PyLMs, with such a broad range of architectures, demonstrates that the MFA is a robust and versatile analytical tool to study any type of PyLM.

The four master straight lines established in solvents having dielectric constants at 25 °C equal to 2.4 (toluene), 7.6 (THF), 37.8 (DMF), and 46.7 (DMSO) cover a broad range of solvent polarity. This wide range of solvent polarity implies that at least one of these four solvents should be able to dissolve any PyLM whose LRID can then be characterized from its $\langle k \rangle$ value. Since $\langle k \rangle$ can be easily determined for any PyLM from Equation 5.4, by

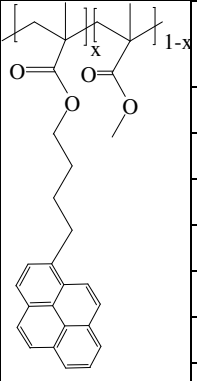
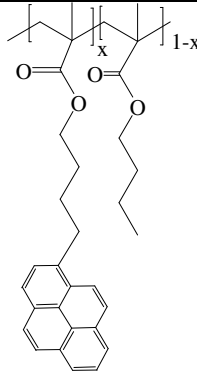
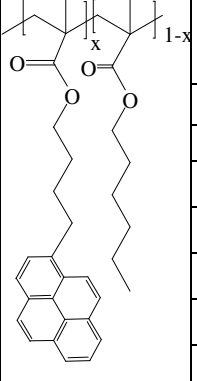
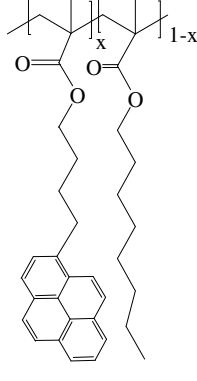
fitting the monomer decay with a sum of exponentials, where the longest decay time is fixed to equal the lifetime (τ_M) of the pyrene derivative used to prepare the PyLM, the master straight lines obtained in the four solvents provide the scientific community with a means to gauge the magnitude of the LRID of any new PyLM, by determining and comparing its $\langle k \rangle$ value to those obtained in this study.

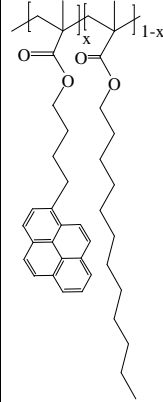
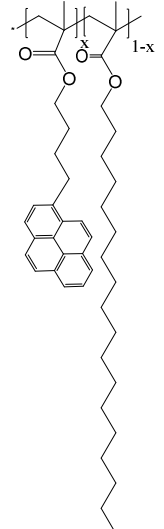
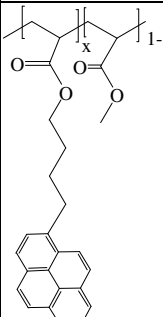
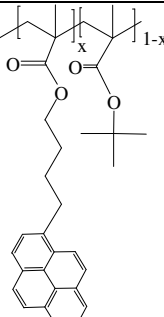
5.3 Experimental

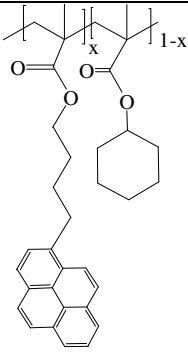
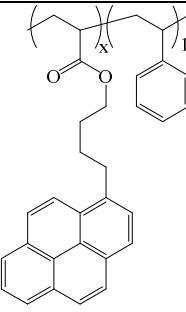
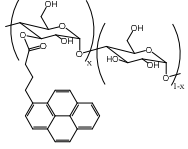
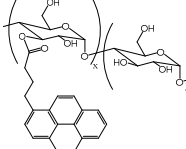
Materials: Dimethyl sulfoxide (DMSO) was purchased from Sigma-Aldrich. Distilled in glass toluene, tetrahydrofuran (THF), and dimethylformamide (DMF) were supplied by Caledon.

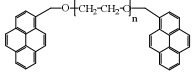
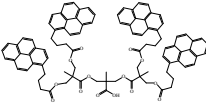
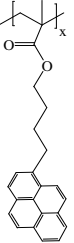
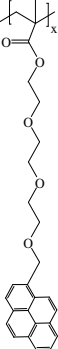
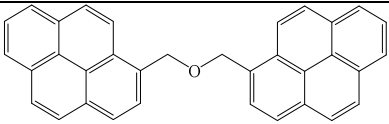
The chemical structures of all the pyrene-labeled constructs are presented in Table 5.1. All these PyLMs have been prepared for previous studies¹⁷⁻¹⁸ and their synthesis and characterization has been described in detail earlier.

Table 5.1: Chemical structure, pyrene content in mol%, λ_{py} in $\mu\text{mol/g}$, number-average molecular weights, and PDIs of the pyrene-labeled constructs used in this study.

Chemical Structure	Py-PC1MA				Chemical Structure	Py-PC4MA			
	Pyrene Content	λ_{py}	M_n	PDI		Pyrene Content	λ_{py}	M_n	PDI
	(mol %)	($\mu\text{mol/g}$)	(kg/mol)	[-]		[mol %]	($\mu\text{mol/g}$)	(kg/mol)	[-]
	2.6	248	200	1.33		2.2	149	296	1.44
	4.1	371	135	1.60		3.0	200	197	1.39
	5.2	464	206	1.70		3.6	242	264	1.68
	5.3	471	101	2.10		5.3	345	275	1.97
	5.6	491	170	1.55		7.2	461	416	1.76
7.3	618	176	1.80						
Chemical Structure	Py-PC6MA				Chemical Structure	Py-PC8MA			
	Pyrene Content	λ_{py}	M_n	PDI		Pyrene Content	λ_{py}	M_n	PDI
	(mol %)	($\mu\text{mol/g}$)	(kg/mol)	[-]		(mol %)	($\mu\text{mol/g}$)	(kg/mol)	[-]
	2.0	113	139	1.93		2.7	131	312	1.75
	3.3	188	125	1.95		4.3	209	146	2.04
	4.7	268	151	1.97		5.1	258	371	1.83
	5.8	324	183	1.84		6.1	292	234	1.88
	6.7	366	116	1.76		7.3	350	271	2.07
8.1	442	179	1.97						

Chemical Structure	Py-PC12MA				Chemical Structure	Py-PC18MA			
	Pyrene Content	λ_{py}	M_n	PDI		Pyrene Content	λ_{py}	M_n	PDI
	(mol %)	($\mu\text{mol/g}$)	(kg/mol)	[-]		(mol %)	($\mu\text{mol/g}$)	(kg/mol)	[-]
	1.4	54	265	1.70		1.4	42	810	1.52
	3.5	137	244	2.43		4.5	132	480	1.44
	5.6	216	507	1.70		5.9	174	663	1.42
	6.0	232	174	2.17		6.8	201	705	1.41
	7.7	295	662	2.10		6.7	198	719	1.49
10.2	389	265	1.68	14.2	417	770	1.45		
Chemical Structure	Py-PC1A				Chemical Structure	Py-PC4TMA			
	Pyrene Content	λ_{py}	M_n	PDI		Pyrene Content	λ_{py}	M_n	PDI
	(mol %)	($\mu\text{mol/g}$)	(kg/mol)	[-]		(mol %)	($\mu\text{mol/g}$)	(kg/mol)	[-]
	1.7	193	148	2.00		3.6	239	127	1.72
	2.6	284	236	1.40		3.8	254	183	1.56
	2.6	284	313	1.40		4.7	310	233	1.25
	5.0	342	138	2.08		5.6	363	147	1.65
6.7	655	870	2.40	7.6	486	141	2.19		

Chemical Structure	Py-PC6CyMA				Chemical Structure	Py-CoE-PS			
	Pyrene Content	λ_{py}	M_n	PDI		Pyrene Content	λ_{py}	M_n	PDI
	(mol %)	($\mu\text{mol/g}$)	(kg/mol)	[-]		(mol %)	($\mu\text{mol/g}$)	(kg/mol)	[-]
	2.0	121	187	1.61		2.1	190	46	1.65
	3.0	172	206	2.00		3.1	280	43	1.67
	3.8	218	244	2.14		4.5	390	49	1.62
	5.1	290	263	2.19		5.4	467	53	1.69
	6.2	346	192	2.04		6.0	510	46	1.68
	7.0	389	268	1.67					
Chemical Structure	Py-Amylose				Chemical Structure	Py-Amylopectin			
	Pyrene Content	λ_{py}	M_n	PDI		Pyrene Content	λ_{py}	M_n	PDI
	(mol %)	($\mu\text{mol/g}$)	(kg/mol)	[-]		(mol %)	($\mu\text{mol/g}$)	(kg/mol)	[-]
	5.1	289				4.1	237		
	5.6	314				5.7	321		
	5.6	318				8.7	470		
	7.5	410				9.6	510		
10.1	532			12.0	618				

Chemical Structure	Py ₂ -PEO(X) X = 3.4, 5, and 6K				Chemical Structure	Pyn-GX-PP N = 4, 8, 16; X = 2 – 3			
	Pyrene Content	λ_{py}	M_n	PDI		Pyrene Content	λ_{py}	M_n	PDI
	(mol %)	($\mu\text{mol/g}$)	(kg/mol)	[-]		(mol %)	($\mu\text{mol/g}$)	(kg/mol)	[-]
PEO(3.4K)	n.a.	522	3.1	1.0	PP-G2-BuPy4	n.a.	2,766	1.45	1.0
PEO(5K)	n.a.	368	5	1.0	PP-G3-BuPy8	n.a.	2,676	2.99	1.0
PEO(6K)	n.a.	311	6	1.0	PP-G4-BuPy16	n.a.	2,632	6.08	1.0
Chemical Structure	Poly(PyBuMA)				Chemical Structure	Poly(PyEG ₃ MA)			
	Pyrene Content	λ_{py}	M_n	PDI		Pyrene Content	λ_{py}	M_n	PDI
	(mol %)	($\mu\text{mol/g}$)	(kg/mol)	[-]		(mol %)	($\mu\text{mol/g}$)	(kg/mol)	[-]
	100	2920	71	1.67		100	2312	30	1.6
Chemical Structure	DiPyMe								
	Pyrene Content	λ_{py}	M_n	PDI					
	(mol %)	($\mu\text{mol/g}$)	(g/mol)	[-]					
	n.a	4479	446.56	-					

The nine series of pyrene-labeled poly(alkyl methacrylate)s were prepared by copolymerizing 1-pyrenebutyl methacrylate with either methyl methacrylate, *n*-butyl methacrylate, *n*-hexyl methacrylate, *n*-octyl methacrylate, *n*-dodecyl methacrylate, *n*-stearyl methacrylate, *tert*-butyl methacrylate, or cyclohexyl methacrylate to yield Py-PC1MA, Py-PC4MA, Py-PC6MA, Py-PC8MA, Py-PC12MA, Py-PC18MA, Py-PC4TBMA, or Py-PC6CyMA, respectively.¹⁸ Py-PC1A was obtained by copolymerizing 1-pyrenebutyl acrylate with methyl acrylate.¹⁸ Similarly, a series of polystyrenes randomly labeled with pyrene was

synthesized by copolymerizing 1-pyrenebutyl acrylate with styrene to yield Py-CoE-PS.¹⁹ Amylose and amylopectin were randomly labeled with pyrene by reacting their hydroxyl groups with 1-pyrenebutyric acid in the presence of diisopropylcarbodiimide, to yield Py-Amylose and Py-Amylopectin, respectively.²⁰ Three pyrene end-capped monodisperse poly(ethylene oxide)s were obtained by reacting 1-pyrenemethoxide onto the corresponding tosylated PEOs to yield the Py₂-PEO series.²¹ The reaction of 1-pyrenemethoxide with 1-pyrenemethyl chloride yielded DiPyMe.²² A series of bis(hydroxymethyl)propionic acid of generation 2 – 4 dendrons end-labeled with 1-pyrenebutyric acid (PP-G2-BuPy₄, PP-G3-BuPy₈, PP-G4-BuPy₁₆) were also investigated.¹⁷ PPyBuMA and PPyEG₃MA were homopolymers of 1-pyrenebutyl methacrylate and 1-pyrenemethoxydiethoxyethyl methacrylate prepared by radical polymerization.²³

Steady-state fluorescence: The steady-state fluorescence measurements were carried out on a Photon Technology International (PTI) LS-100 steady-state fluorometer equipped with an Ushio UXL-75Xe Xenon lamp and a PTI 814 photomultiplier detection system. To avoid intermolecular interactions between the PyLMs, all the fluorescence spectra were acquired with dilute PyLMs solutions having a pyrene concentration of 2.5×10^{-6} M. For all the solvents beside DMSO, the PyLM solutions were deoxygenated by passing a gentle stream of nitrogen through the solution for 30 minutes before sealing the solution for the fluorescence experiments. The PyLM solutions were excited at the S₂⁰ transition, at about 344 nm, with some variation depending on the solvent, and the fluorescence spectra were acquired between 350 and 600 nm.

Time-resolved fluorescence: The same solutions used to acquire the fluorescence spectra were then placed in an IBH Ltd. time-resolved fluorometer equipped with an IBH 340 nm NanoLED. The PyLM solutions were excited at 344 nm and the monomer and excimer

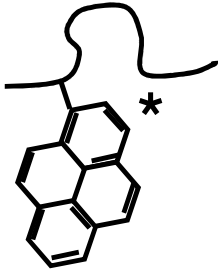
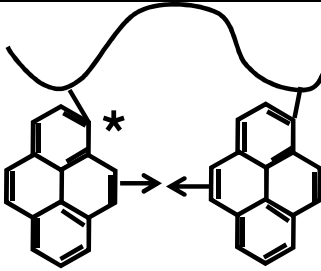
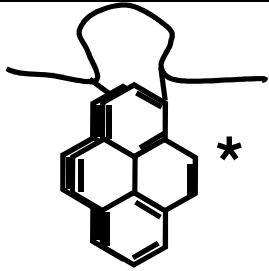
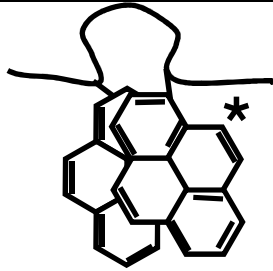
fluorescence emission were monitored at 375 and 510 nm, respectively. All the acquired decays were fitted according to the MFA, with the equations used for the monomer and excimer fluorescence decays which are provided in Supporting Information (SI.5). All the parameters retrieved from the MFA of the fluorescence decays including the pre-exponential factors and decay times, have been listed in Appendices, Supporting Information for Chapter 5 (SI5), Tables SI5.1-SI5. The quality of the fits was evaluated from the random distribution of the residuals and the autocorrelation of the residuals and the χ^2 value smaller than 1.30.

5.4 Results and Discussion

The fluorescence spectra of the 74 PyLMs listed in Table 5.1 have already been acquired in a few solvents¹⁷⁻²³ and their features will not be discussed again in this chapter, which focuses on the characterization of their LRID through the global MFA of their monomer and excimer fluorescence decays. As it turns out, the analysis of the fluorescence spectra obtained with PyLMs is plagued by the fact that the spectra represent the entire population of pyrene species and do not distinguish which one among them forms excimer by diffusion, which is the only pyrene species that matters to characterize the LRID of a PyLM. In fact, work from this and other laboratories has established that at least four different pyrene species contribute to the fluorescence spectra.^{1,2,24} The inability of steady-state fluorescence experiments to distinguish quantitatively between the different pyrene species makes it particularly difficult to obtain quantitative information about the LRID of PyLMs based on the analysis of fluorescence spectra alone. These species were already presented in the Introduction and are depicted in Table 5.2. The first entry on the left of Table 5.2 represents those pyrene labels of a PyLM that are isolated, either because the LRID of the

macromolecules are too slow, the solvent is too viscous, or the pyrene content is too low. These pyrene labels cannot form excimer and they fluoresce as if they were free in solution with the natural lifetime τ_M of pyrene. They are referred to as Py_{free}^* .

Table 5.2: Diagrams of the four excited pyrene species often encountered in PyLMs.

			
Py_{free}^*	Py_{diff}^*	EO^*	D^*

The second species in Table 5.2 concerns those pyrenyl groups that form excimer by diffusion. Because the pyrenyl groups are often sterically hindered when attached onto a macromolecule, diffusive encounters between an excited and a ground-state pyrene can result in the formation of one of two excimers referred to as EO^* or D^* in Table 5.2. EO^* is an excimer emitting with a lifetime τ_{E0} , generated by the proper stacking of two pyrene monomers, whereas D^* is an excimer emitting with a lifetime τ_D , resulting from the improper stacking of two pyrene labels. EO^* and D^* can be generated by either the direct excitation of a pyrene aggregate or the diffusive encounter between a ground-state and an excited pyrene,

referred to as Py_{diff}^{E0*} and Py_{diff}^D* , depending on whether they will form an $E0^*$ or D^* excimer type, respectively. Since the Py_{diff}^{E0*} and Py_{diff}^D* species are indistinguishable in the pyrene monomer fluorescence decays, they are referred to as Py_{diff}^* in Table 5.2. Fitting globally the monomer and excimer fluorescence decays according to the MFA yields the molar fractions f_{free} , f_{diff}^{E0} , f_{diff}^D , f_{E0} , and f_D for the pyrene species Py_{free}^* , Py_{diff}^{E0*} , Py_{diff}^D* , $E0^*$, and D^* , respectively. In some cases, a single excimer species $E0^*$ is required to fit the decays, but it is often necessary to introduce the second excimer D^* . Fitting of the monomer and excimer decays with the MFA proceeds in a stepwise fashion, whereby the excimer decays are fitted first assuming one excimer $E0^*$ with contributions f_{diff}^{E0} and f_{E0} , then with a second excimer D^* with a contribution f_D only, and finally with a second excimer D^* with contributions f_{diff}^D and f_D . Only if a notable improvement in the quality of the fit is observed in terms of reduced χ^2 or a better random distribution of the residuals and autocorrelation function of the residuals around zero, would an additional parameter be included in the analysis of the fluorescence decays. As shown in Figure 5.1 for the Py(5.0)-PC1A sample in DMF, the fits of the monomer and excimer fluorescence decays acquired with the PyLMs were excellent and all the parameters retrieved from the global MFA of the monomer and excimer decays have been listed in Tables SI5.1-5.12 as SI5.

Due to the immense benefit associated with having access to a calibration curve that would enable the ranking of PyLMs according to their LRID, PyLMs were selected for their solubility in solvents having a broad range of polarity, from low polarity toluene to high polarity DMSO, and including solvents of intermediate polarity such as THF and DMF. The

series of $\text{Py}_2\text{-PEO}$ and $\text{Py}_n\text{-GX-PP}$ constructs and DiPyMe, poly(PyBuMA), and poly(PyEG₃MA) were found to be soluble in all four solvents. The poly(alkyl methacrylate)s Py-PC1MA and Py-PC4MA were soluble in toluene, THF, and DMF but not in more polar DMSO. The more polar Py-PC1A was soluble in THF, DMF and DMSO but not in toluene. All other poly(alkyl methacrylate)s were studied in THF only. Finally, amylose and amylopectin were studied in polar DMF and DMSO but could not be dissolved in toluene and THF. By adjusting the polarity of PyLMs and solvents, a sufficiently large number of PyLM/solvent pairs could be assembled in toluene, THF, DMF, and DMSO to build a calibration curve describing the LRID of these PyLMs in each solvent.

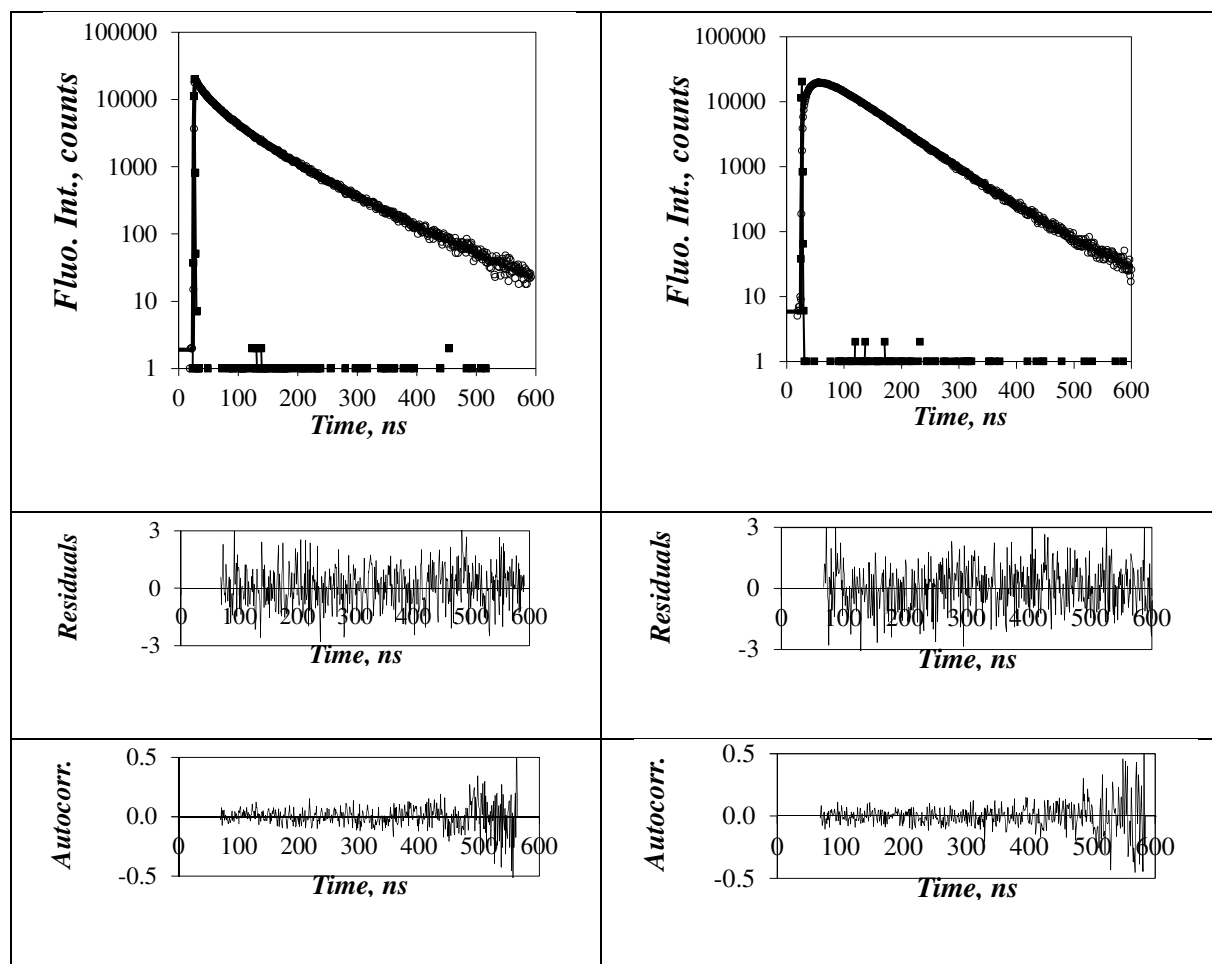


Figure 5.1: MFA of the monomer (left, $\lambda_{\text{ex}} = 344 \text{ nm}$, $\lambda_{\text{em}} = 375 \text{ nm}$) and excimer (right, $\lambda_{\text{ex}} = 344 \text{ nm}$, $\lambda_{\text{em}} = 510 \text{ nm}$) fluorescence decays of Py(5.0)-PC1A in DMF. $\chi^2 = 1.1$.

To this end, the parameters retrieved from the MFA were employed to calculate $\langle k \rangle$ and $(I_E/I_M)^{\text{TRF}}(f_{\text{free}}=0)$ for all 74 PyLMs in the solvent where they were soluble, and $\langle k \rangle$ and $(I_E/I_M)^{\text{TRF}}(f_{\text{free}}=0)$ were plotted against each other in Figure 5.2. In the plots obtained for the four solvents, $(I_E/I_M)^{\text{TRF}}(f_{\text{free}}=0)$ increased linearly with increasing $\langle k \rangle$, and this linear relationship was found to hold over 3 orders of magnitude, which represents an impressive dynamic range.

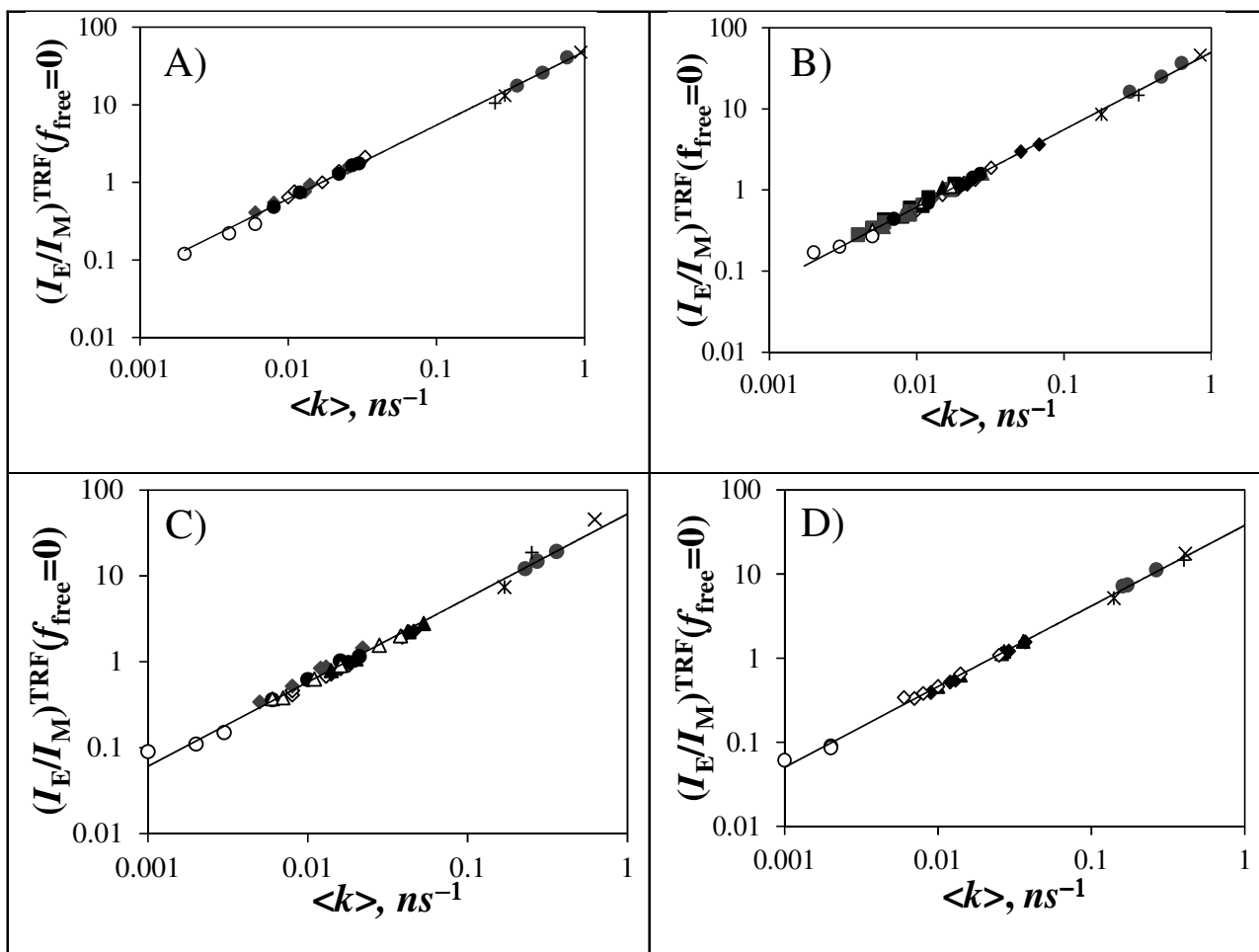


Figure 5.2: Plots of $(I_E/I_M)^{\text{TRF}}(f_{\text{free}}=0)$ as a function of $\langle k \rangle$ in A) degassed toluene, B) degassed THF, C) degassed DMF, and D) aerated DMSO. (\blacklozenge) Py-PC1A in B-D, (\blacklozenge) Py-PC1MA in A-C, (\blacklozenge) Py-PC4MA in A-C, (\blacksquare) Py-PC4TMA in B), (\square) Py-PC6MA in B), (\blacksquare) Py-PC6CyMA in B), (\blacktriangle) Py-PC8MA in B) or Py-Amylose in C-D, (\triangle) Py-PC12MA in B) or Py-Amylopectin in C-D, (\blacktriangle) Py-PC18MA in B, (\bullet) Py-CoE-PS in A-C, (\circ) Py₂-PEO in A-D, (\bullet) Py_n-GX-PP in A-D, (\times) PPyBuMA in A-D, (\oplus) PPyEG₃MA in A-D, and (\ast) DiPyMe in A-D.

Considering the complicated expression for $(I_E/I_M)^{\text{TRF}}$ in Equation 5.5, the linear relationship observed in Figure 5.2 between $\langle k \rangle$ and $(I_E/I_M)^{\text{TRF}}(f_{\text{free}}=0)$ might appear fortuitous. But under ideal conditions where all the pyrene labels of a PyLM form one excimer $E0^*$ by diffusion, the molar fractions f_{free} , f_{diff}^D , f_{E0} , and f_D equal zero and f_{diff}^{E0} equals unity. Under this condition, the expression for $(I_E/I_M)^{\text{TRF}}$ in Equation 5.5 simplifies remarkably to give Equation 5.6.

$$(I_E/I_M)^{\text{TRF}} = \langle k \rangle \times \tau_{E0} \quad (5.6)$$

As it turns out, Equation 5.6 is predicted by Birks' scheme,²⁵ when excimer formation can be described by a single rate constant (k_1) so that $\langle k \rangle = k_1$ and the excimer dissociation rate constant (k_{-1}) is negligible ($k_{-1} = 0$). Since the PyLMs are prepared to favor pyrene excimer formation by diffusion, f_{free} , f_{diff}^D , f_{E0} , and f_D are often much smaller than f_{diff}^{E0} which approaches unity. However some precautions still have to be taken, particularly for those PyLMs that form excimer on very short time scales, such as the $\text{Py}_n\text{-GX-PP}$ dendrimer series. In this case, the pyrene monomer is extremely short-lived and $\langle \tau \rangle$ in the denominator of Equation 5.5 becomes very small, so small in fact that even a small f_{free} value can lead to major errors in the $(I_E/I_M)^{\text{TRF}}$ value since τ_M is then orders of magnitude larger than $\langle \tau \rangle$.¹⁷ It is to avoid this complication that $(I_E/I_M)^{\text{TRF}}(f_{\text{free}}=0)$ was plotted as a function of $\langle k \rangle$ in Figure 5.2. Other macromolecules that were fairly compact, such as helical amylose and branched

amylopectin, or had very high pyrene contents, such as poly(PyBuMA) or poly(PyEG₃MA), were found to yield large f_{E0} and f_D values in DMF and DMSO, an indication of residual pyrene aggregation in these solvents. Since $\langle k \rangle$ only reports on those pyrene labels that lead to excimer formation by diffusion, f_{E0} and f_D were set equal to zero for these PyLMs in DMF and DMSO.

Since the plots shown in Figure 5.2 covered a dynamic range going over three orders of magnitude, the trends were fitted according to Equation 5.7, where τ_E represents an equivalent excimer lifetime and α is a scaling exponent. The values of τ_E and α were obtained by fitting the data shown in Figure 5.2, and their values obtained in the four solvents are listed in Table 5.3.

$$(I_E/I_M)^{TRF}(f_{free}=0) = \tau_E \times \langle k \rangle^\alpha \quad (5.7)$$

In all cases, α approached unity within experimental error, confirming the linear relationship that appears to exist between $\langle k \rangle$ and $(I_E/I_M)^{TRF}(f_{free}=0)$ in Figure 5.2. The excimer lifetime τ_E was found to equal 49, 50, and 53 ns in toluene, THF, and DMF, respectively. These excimer lifetimes are typical of what would be expected for pyrene derivatives in degassed organic solvents. The τ_E value of 50 (± 1) ns obtained in THF with these PyLMs matches that of 51 ns obtained earlier in THF for 32 PyLMs. In aerated DMSO, a slightly shorter excimer

lifetime of 38 ns was obtained, certainly due to oxygen quenching. The values of these excimer lifetimes are reasonable when compared to published results for pyrene.

The plots presented in Figure 5.2 revealed some general features for the LRID of PyLMs. For all series of PyLMs and regardless of the macromolecular architecture, the most important parameter that influenced excimer formation was the average contour length $\langle A_{\text{Py}} \rangle$ separating every two pyrene labels. Indeed, $\langle k \rangle$ and $(I_{\text{E}}/I_{\text{M}})^{\text{TRF}}(f_{\text{free}}=0)$ always decreased with increasing $\langle A_{\text{Py}} \rangle$. In the case of the Py₂-PEO series where $\langle A_{\text{Py}} \rangle$ equals the length of the fully extended PEO chain, a larger $\langle A_{\text{Py}} \rangle$ was associated with a longer PEO chain and $(I_{\text{E}}/I_{\text{M}})^{\text{TRF}}(f_{\text{free}}=0)$ or $\langle k \rangle$ were found to decrease with increasing chain length for the pyrene end-labeled linear chains. In the case of the Py_n-GX-PP series, a higher dendrimer generation resulted in a smaller $\langle A_{\text{Py}} \rangle$, which in turn led to more excimer formation. For the randomly labeled polymers, a higher pyrene content meant a smaller $\langle A_{\text{Py}} \rangle$ resulting in larger $(I_{\text{E}}/I_{\text{M}})^{\text{TRF}}(f_{\text{free}}=0)$ and $\langle k \rangle$ values.

Table 5.3: Parameters τ_E and α used to fit $(I_E/I_M)^{\text{TRF}}(f_{\text{free}}=0)$ as $\tau_E \times \langle k \rangle^\alpha$.

Solvent	τ_E (ns)	$\Delta\tau_E$ (ns)	α	$\Delta\alpha$
Toluene (degassed)	49	± 2	0.95	± 0.01
THF (degassed)	50	± 1	0.95	± 0.01
DMF (degassed)	53	± 2	0.98	± 0.02
DMSO (aerated)	38	± 1	0.96	± 0.01

Compared to all other PyLMs, DiPyMe was the construct where the pyrene moieties were held in closest proximity to each other. In all solvents, its $\langle k \rangle$ value was larger than for the pyrene-labeled linear chains but smaller than for the branched macromolecules. This result indicates that proximity of the pyrene labels is not the sole factor controlling the efficiency of pyrene excimer formation, but that the conformation of the macromolecule must play a part as well. As shown in Figure 5.2, the branched macromolecules provided better opportunities for having pyrene-pyrene encounters than in DiPyMe.

The macromolecular architecture of the PyLMs was also found to affect pyrene excimer formation. The pyrene end-labeled linear chains held the pyrene labels far apart, limiting pyrene-pyrene encounters and resulting in the smallest $(I_E/I_M)^{\text{TRF}}(f_{\text{free}}=0)$ or $\langle k \rangle$ values. The branched PyLMs such as the pyrene-labeled dendrimers, poly(PyBuMA), and poly(PyEG₃MA) all yielded large $(I_E/I_M)^{\text{TRF}}(f_{\text{free}}=0)$ or $\langle k \rangle$ values since their branched architecture brought the pyrene labels closer to each other in a conformation that favored

pyrene-pyrene encounters. The randomly labeled linear chains took $(I_E/I_M)^{\text{TRF}}(f_{\text{free}}=0)$ or $\langle k \rangle$ values that were intermediate between those obtained for the end-labeled Py₂-PEOs and Py₂-GX-PP dendrimers.

Within a series of similar polymers randomly labeled with pyrene such as for the Py-PCXMA series with $X = 1 - 18$, the $\langle k \rangle$ values reported in Figure 5.2B for THF could be employed to draw conclusions on the effect of the side chain length on the LRID of the poly(alkyl methacrylate)s. Since these polymers were randomly labeled with pyrene, this effect has already been described by applying the Fluorescence Blob Model Analysis (FBMA) to the fluorescence decays.¹⁸ Based on this analysis, the product $\langle k_{\text{blob}} \times N_{\text{blob}} \rangle$ which reflects the magnitude of the LRID of polymers randomly labeled with pyrene was found to decrease continuously with increasing side chain length. Since $\langle k \rangle$ obtained from the MFA of the fluorescence decays can be mathematically rearranged into $\langle k^{\text{MF}} \rangle^{\text{blob}}$, which has been shown to mimic the product $\langle k_{\text{blob}} \times N_{\text{blob}} \rangle$.¹⁶ The $\langle k \rangle$ values obtained in Figure 5.2B for the poly(alkyl methacrylate)s in THF were rearranged to yield $\langle k^{\text{MF}} \rangle^{\text{blob}}$ according to Equation 5.8.

$$\langle k^{\text{MF}} \rangle^{\text{blob}} = \frac{1 - f_{\text{Mfree}}}{x} \langle k \rangle \quad (5.8)$$

In Equation 5.8, f_{Mfree} represents the molar fraction of the $\text{Py}_{\text{free}}^*$ species in Table 5.2 that contribute to the monomer decays, and x is the molar fraction of structural units bearing a pyrene label. Figure 5.3 shows a plot of $\langle k^{\text{MF}} \rangle^{\text{blob}}$ as a function of the molar percentage of

pyrene-labeled monomers in the pyrene-labeled poly(alkyl methacrylate)s. Despite the scatter in the data points, a general trend was observed where Py-PC1MA with the shortest side chain took the largest $\langle k^{\text{MF}} \rangle^{\text{blob}}$ value, and $\langle k^{\text{MF}} \rangle^{\text{blob}}$ was found to decrease continuously with increasing side chain length. The average $\langle k^{\text{MF}} \rangle^{\text{blob}}$ values were plotted in Figure 5.3B as a function of the number of carbon atoms in the side chains. After a substantial decrease for short side chains, the $\langle k^{\text{MF}} \rangle^{\text{blob}}$ was found to stabilize for side chains made of 12 and more carbon atoms. For these longer side chains, a further increase in side chain length resulted in a marginal decrease in LRID.

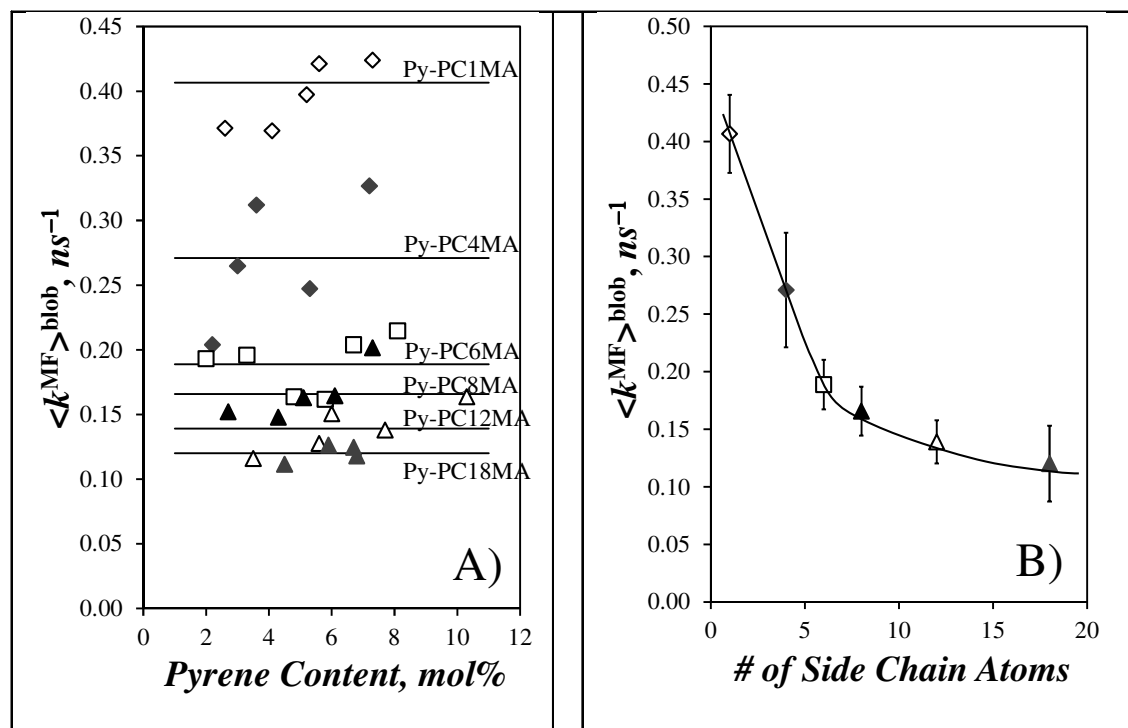


Figure 5.3: Plot of $\langle k^{MF} \rangle^{blob}$ versus A) pyrene content and B) the number of side chain atoms for a series of poly(alkyl methacrylate)s randomly labeled with pyrene in THF. (\diamond) Py-PC1MA, (\blacklozenge) Py-PC4MA, (\square) Py-PC6MA in B), (\blacktriangle) Py-PC8MA, (\triangle) Py-PC12MA, (\blacktriangle) Py-PC18MA.

$\langle k^{MF} \rangle^{blob}$ was also calculated for the Py-C1A, Py-PC4TMA, and Py-PC6CyMA constructs and was found to equal 0.88 ± 0.14 , 0.19 ± 0.04 , and 0.17 ± 0.04 ns⁻¹, respectively. Removal of the methyl substituent from the Py-PC1MA backbone resulted in a much larger $\langle k^{MF} \rangle^{blob}$ value of 0.88 ns⁻¹ for the Py-PC1A series instead of 0.41 ± 0.03 ns⁻¹ for Py-PC1MA. This doubling in $\langle k^{MF} \rangle^{blob}$ value from Py-PC1MA to Py-PC1A reflects the

faster LRID of the polyacrylate backbone. Similarly, stiffening of the side chain resulted in slower LRID. Indeed, $\langle k^{\text{MF}} \rangle^{\text{blob}}$ was found to decrease from $0.27 \pm 0.05 \text{ ns}^{-1}$ for Py-PC4MA to $0.19 \pm 0.04 \text{ ns}^{-1}$ for Py-PC4TMA and from $0.19 \pm 0.02 \text{ ns}^{-1}$ for Py-PC6MA to $0.17 \pm 0.04 \text{ ns}^{-1}$ for Py-PC6CyMA. These results match how the LRID are expected to vary with the nature of the side chain, and are in complete agreement with earlier conclusions drawn from the FBMA of the fluorescence decays acquired with the pyrene-labeled poly(alkyl methacrylate)s in THF.¹⁷

5.5 Conclusions

The trends shown in Figure 5.2 in four different solvents for 74 PyLMs demonstrate that the kinetics of excimer formation between pyrene labels covalently attached onto a macromolecule follow some very general physical principles, regardless of the architecture of the macromolecule (linear versus branched) and the selection of the pyrene labeling scheme (at specific positions versus randomly). This study has demonstrated that the rate constant $\langle k \rangle$ can be used to describe quantitatively the LRID of macromolecules in solution. In fact, the plots presented in Figure 5.2 offer researchers a unique means of gauging the LRID of a macromolecule of interest with the LRID of other PyLMs, by simply pyrene-labeling the macromolecule and determining $\langle k \rangle$ according to Equation 5.4, with the parameters retrieved from fitting the monomer fluorescence decay with a sum of exponentials where the longest decay time is fixed to equal the lifetime (τ_{M}) of the pyrene monomer. The broad range of solvent polarity selected for the present study with dielectric constants equal to 2.4, 7.6, 37.8, and 46.7 for, respectively, toluene, THF, DMF, and DMSO

ensures that any macromolecule should be soluble in at least one of these four solvents, and that the corresponding $\langle k \rangle$ value can be determined and compared to that of the other PyLMs used to build the calibration curves presented in Figure 5.2.

Chapter 6

Concluding Remarks and Future Work

6.1 Summary of Accomplished Work

This thesis has illustrated how the excimer fluorescence from pyrene labeled polymers (PyLPs) can be analyzed to provide valuable information on the internal dynamics (ID) of macromolecules. The information obtained from these studies was either qualitative or quantitative depending on whether it was being retrieved from the analysis of the steady-state fluorescence spectra or the time-resolved fluorescence decays acquired with solutions of the PyLPs, respectively.¹⁻⁴ The first study completed in the 2nd chapter of this thesis aimed to characterize the ID of a series of poly(alkyl methacrylate)s randomly labeled with pyrene using the Fluorescence Blob Model (FBM).⁵⁻⁹ This was accomplished by synthesizing eight series of fluorescently labeled polymers via the radical copolymerization of 1-pyrenebutylmethacrylate and an alkyl methacrylate bearing a C1 –C18 side chain to yield the desired Py-PC1MA, Py-PC4MA, Py-PC6MA, Py-PC8MA, Py-PC12MA, Py-PC18MA, Py-PC4TBMA, or Py-PC6CyMA samples with pyrene contents ranging between 1 and 14 mol%.⁹ These samples were referred to as Py-PCXMA with $X = 1 - 18$.

The steady-state fluorescence spectra were acquired in tetrahydrofuran (THF) which was a suitable solvent for all the Py-PCXMA samples. In all these fluorescence measurements, the pyrene concentration was kept below 3×10^{-6} M to avoid intermolecular interactions so that excimer formation by diffusion took place intramolecularly. Excimer formation was found to increase with increasing pyrene content for any given Py-PCXMA series. The ratio of the fluorescence intensity of the excimer over that of the monomer, namely the I_E/I_M ratio, increased linearly with increasing pyrene content and the corresponding slope ($m(I_E/I_M)$) of these straight lines could be viewed as a measure of the efficiency of the Py-PCXMA series at forming excimer. The slope $m(I_E/I_M)$ decreased with

increasing side chain length before plateauing for side chain length greater than 12 carbon atoms. This decrease reflected the reduction in ID experienced by the Py-PCXMA samples having longer side chains. Quantitative information on the ID of the Py-PCXMA samples could be obtained through the FBM analysis of the fluorescence decays acquired with these samples. Global FBM analysis of the pyrene monomer and excimer fluorescence decays yielded N_{blob} , the number of monomers encompassed inside a *blob*, which represents the volume probed by an excited pyrene during its lifetime, and the product of N_{blob} and the rate constant (k_{blob}) of excimer formation between two pyrene labels located inside a same *blob*, namely $k_{\text{blob}} \times N_{\text{blob}}$. The parameters N_{blob} and $k_{\text{blob}} \times N_{\text{blob}}$ of each Py-PCXMA series remained constant with pyrene content, but their values averaged over all pyrene contents ($\langle N_{\text{blob}} \rangle$ and $\langle k_{\text{blob}} \times N_{\text{blob}} \rangle$) decreased with increasing side chain length due to the slower ID of the PCXMA chains. This work demonstrated that an increase in side chain length and bulkiness resulted in a pronounced decrease in chain mobility which could be characterized quantitatively by the FBM analysis of the fluorescence decays.

Contrary to the traditional studies dealing with pyrene end-labeled monodisperse polymers that require more advanced synthetic techniques based on living polymerization, the study on the Py-PCXMA samples took advantage of the synthetic simplicity of free radical polymerization which yields polydisperse samples. The polydispersity of the Py-PCXMA samples was not a problem for the FBM analysis, as it focuses on the characterization of a polymeric *blob*, which represents the domain in the polymer coil where pyrene excimer formation takes place. The polydispersity of the polymers can be handled by dividing the polymer coils into different numbers of *blobs*, a longer chain being composed of more *blobs* than a shorter chain. The *blobs* are then used as unit volume to compartmentalize

the polymer coils into clusters of *blobs* where the randomly attached pyrene labels distribute themselves randomly among the *blobs*. Therefore, the FBM analysis allows one to gain quantitative information on the ID of polydisperse polymers whose preparation is much simpler than that of monodisperse end-labeled polymers.

Another advantage of the FBM analysis of fluorescence decays is that it enables one to distinguish between the different pyrene species present in solutions of the Py-PCXMA samples. In particular, the FBM isolates the $P_{y_{\text{diff}}}^*$ species, which leads to excimer formation by diffusion and whose contribution to the fluorescence decays is used to describe the ID of the polymers in solution. The FBM analysis could also determine the molar fraction of isolated pyrene labels $P_{y_{\text{free}}}^*$ which never formed excimer, emitted with the natural lifetime τ_M of the pyrene label, and behaved as if they were free in solution. This fraction, referred to as f_{free} , was found to decrease with increasing pyrene content as a larger pyrene content brought the pyrene labels closer to each other allowing them to form excimer.

The glass transition temperature (T_g) is a parameter that is used as an experimental means to characterize the ID of polymer in the bulk, a polymer with a low T_g being usually more flexible than a polymer with a high T_g . Because T_g has been described as being the single most important parameter that determines what an amorphous polymer will be used for, T_g has been measured for a large number of polymers and the effect that various molecular parameters such as backbone rigidity, side chain bulkiness, or hydrogen bonding have on their T_g has been investigated. The fourth chapter of this thesis focused on preparing different pyrene-labeled PBMA s where the pyrene label was held away from the main chain with spacers made of different numbers of ethylene glycol unit. In total, four Py-PBMA series were prepared which were referred to as PyEG_x-PBMA with $x = 0 - 4$. Steady-state

fluorescence was applied to characterize qualitatively the efficiency of excimer formation in the pyrene-labeled constructs, while time-resolved fluorescence was applied to probe how the length of the oligo(ethylene glycol) spacer would affect the response of the FBM analysis in probing the ID of PBMA. The FBM parameters, N_{blob} and k_{blob} , remained constant within experimental error with pyrene content and they were averaged. $\langle N_{\text{blob}} \rangle$ increased linearly with increasing spacer length from 40.5 ± 2.3 for PyEG₀-PBMA to 82.7 ± 3.7 for PyEG₃-PBMA, indicating that a larger volume was being probed by the excited pyrene as the oligo(ethylene glycol) spacer length increased.

Both $\langle N_{\text{blob}} \rangle$ and $\langle k_{\text{blob}} \rangle$ were small for PyEG₀-PBMA, reflecting the restricted motion of the pyrene label due to steric hindrance induced by the short 3 atom spacer (-CO-O-CH₂-). Interestingly, $\langle k_{\text{blob}} \rangle$ was larger for PyEG₁-PBMA but took similar values for PyEG₂-PBMA and PyEG₃-PBMA within experimental error. The $\langle N_{\text{blob}} \rangle$ and $\langle k_{\text{blob}} \rangle$ values obtained from the global FBM analysis of the PyEG_x-PBMA samples described the ID probed by pyrenes that reflected the diffusive motion of the main chain and the oligo(ethylene glycol) side chains. They were combined to yield the bimolecular rate constant k_{diff} describing the diffusive motion of the pyrene labels attached to the PyEG_x-PBMA constructs. The k_{diff} value was found to increase by 2.3 ± 0.3 , 2.0 ± 0.2 , and 1.2 ± 0.1 between PyEG₀-PBMA and PyEG₁-PBMA, PyEG₁-PBMA and PyEG₂-PBMA, and PyEG₂-PBMA and PyEG₃-PBMA, respectively. These results indicated that the pyrene label attached to PyEG₀-PBMA and PyEG₁-PBMA was sterically hindered by the polymeric backbone, but that adding ethylene glycol units to the spacer reduced steric hindrance to the point where it became insignificant for PyEG₂-PBMA and PyEG₃-PBMA for which k_{diff} took a similar value within experimental error.

$\langle N_{\text{blob}} \rangle$ was employed to estimate the hydrodynamic radius of a *blob*, R_{blob} . To this end, the Mark-Houwink-Sakurada (MHS) parameters K and a were determined for PBMA using PBMA standards with M_n values ranging between 2.5 and 38 K which would cover the range of 40 to 83 monomers corresponding to the experimental $\langle N_{\text{blob}} \rangle$ values. The MHS parameters were then used to determine R_{blob} . R_{blob} was found to increase linearly with increasing spacer length thus demonstrating the direct relationship that exists between the increased volume probed by an excited pyrene at the tip of an oligo(ethylene glycol) side chain and the spacer length.

In summary, FBM analysis of the fluorescence decays acquired with the PyEG_x-PBMA constructs demonstrated that both the reach of and the dynamics experienced by the pyrenyl label at the tip of the side chain could be described quantitatively by the FBM parameters. This study suggests that pyrene excimer fluorescence could be applied effectively to probe branched polymers such as comb polymers and polymeric bottlebrushes. In fact, this study demonstrated that the FBM is a powerful tool to probe the dynamics not only of a main chain but also of the side chains extending perpendicularly to the main chain.⁷

While the previous three chapters focused on characterizing the ID of linear chains from the FBM parameters N_{blob} , k_{blob} , and their product $k_{\text{blob}} \times N_{\text{blob}}$, the fourth chapter aimed to derive more general trends that would describe the ID of any type of pyrene-labeled macromolecule. This was achieved by determining the $(I_E/I_M)^{\text{TRF}}$ ratio which represents the absolute ratio of the fluorescence intensity of the excimer over that of the monomer and $\langle k \rangle$ which is the average rate constant of pyrene excimer formation from the Model Free Analysis (MFA) of the fluorescence decays of the monomer and excimer acquired with no less than 74 pyrene-labeled macromolecules. To this end, steady-state fluorescence spectra

and time-resolved fluorescence decays were acquired for eight series of poly(alkyl methacrylate)s, poly(methyl acrylate), amylose, amylopectine, and polystyrene which were all randomly labeled with pyrene, pyrene end-labeled poly(ethylene oxide)s, three generations of pyrene end-labeled bis(hydroxymethyl)propionic acid dendrons, poly(pyrenebutyl methacrylate), poly(pyrenemethoxydiethoxyethyl methacrylate), and DiPyMein four different solvents, namely THF, toluene, DMF, and DMSO.

The parameters retrieved from the MFA of the fluorescence decays were combined to yield the $(I_E/I_M)^{\text{TRF}}$ ratios and the $\langle k \rangle$ rate constants. However, the $(I_E/I_M)^{\text{TRF}}$ ratios were found to be quite sensitive to the contribution from those pyrene labels that did not form excimer by diffusion such as the species Py_{free}^* and $E0^*$. Fortunately, global analysis of the monomer and excimer fluorescence decays could isolate the Py_{diff}^* species from the other which allowed the determination of the $(I_E/I_M)^{\text{TRF}}(f_{\text{free}}=0)$ ratio. $(I_E/I_M)^{\text{TRF}}(f_{\text{free}}=0)$ and $\langle k \rangle$ showed a linear relationship over three orders of magnitude in the four different solvents, thus providing a calibration curve to characterize the ID of macromolecules in solution.

The average chain length separating every two pyrene labels was found to be the main parameter determining the magnitude of $(I_E/I_M)^{\text{TRF}}(f_{\text{free}}=0)$ and $\langle k \rangle$. The pyrene end-labeled dendrimers, poly(pyrenebutyl methacrylate), and poly(pyrenemethoxydiethoxyethyl methacrylate) with their short average chain length separating every two pyrene labels yielded the largest $(I_E/I_M)^{\text{TRF}}(f_{\text{free}}=0)$ and $\langle k \rangle$ values. In contrast, the pyrene end-labeled PEOs held the pyrene labels the furthest apart from each other and as a result, yielded the lowest $(I_E/I_M)^{\text{TRF}}(f_{\text{free}}=0)$ and $\langle k \rangle$ values. The randomly labeled linear polymers with their intermediate average chain length between every two pyrene labels displayed an intermediate behavior between the pyrene end-labeled dendrimers and PEOs. The trends obtained in this

chapter can now be applied to characterize the ID of any pyrene-labeled macromolecule in solution.^{6, 10-12}

Together, these four studies have demonstrated the value of pyrene excimer fluorescence to describe the ID of macromolecules in solution. They provide a solid scientific basis from which other research laboratories can now design their pyrene derivatives, either with a longer or shorter spacer or with an oxygen atom in the β -position to pyrene, to label their macromolecules of interest and characterize their ID in solution.

6.2 Future Work

The fourth research chapter demonstrated that pyrene excimer fluorescence can not only probe the dynamics of a chain longitudinally but also perpendicularly to the main axis of the chain. This feature might be applicable to the characterization of the ID of polymeric bottlebrushes (PPBs). PPBs are linear chains with a high density of long side chains. As the length of the side chain increases, a point is reached where the main chain can no longer adopt a random coil conformation but rather extends like a tube. The transition has been vividly captured with PPBs adsorbed on mica plates by atomic force microscopy. While these studies provide a compelling demonstration that the transition takes place on a 2-dimensional surface, the question still remains whether and how the conformational transition would occur in the 3-dimensional space offered by a solution. Pyrene excimer fluorescence might be able to provide some insight on this by conducting a series of experiments using the protocols established in this thesis.

The procedure described in Chapter 4 could be applied to generate pyrene end-labeled macromonomers by terminating an oligo(ethylene glycol) chain with a pyrenemethoxy group at one end and a methacrylate monomer at the other end to yield PyEG_x-MA monomers with $x > 3$. By copolymerizing a small amount of PyEG_x-MA and the non-pyrene labeled EG_x-MA equivalent, pyrene-labeled PBBs (Py-PBBs) could be produced. The FBM could then be applied to probe the ID of these Py-PBBs as a function of the side chain length x to investigate if the conformational change expected for non-fluorescently labeled PBBs could be sensed by the Py-PBBs. Such experiments could provide a first means for probing PBBs in solution, a major departure from the vast majority of studies being presently conducted in the scientific literature that focus on the characterization of PBBs adsorbed onto surfaces by microscopy.

Letters of Copyright Permission



Title: Long Range Polymer Chain Dynamics Studied by Fluorescence Quenching
Author: Shiva Farhangi, Jean Duhamel
Publication: Macromolecules
Publisher: American Chemical Society
Date: Sep 1, 2016
Copyright © 2016, American Chemical Society

Logged in as:

Shiva Farhangi

Account #:
3001004201

[LOGOUT](#)

Quick Price Estimate

Permission for this particular request is granted for print and electronic formats, and translations, at no charge. Figures and tables may be modified. Appropriate credit should be given. Please print this page for your records and provide a copy to your publisher. Requests for up to 4 figures require only this record. Five or more figures will generate a printout of additional terms and conditions. Appropriate credit should read: "Reprinted with permission from {COMPLETE REFERENCE CITATION}. Copyright {YEAR} American Chemical Society." Insert appropriate information in place of the capitalized words.

I would like to...

Requestor Type

Portion

Format

Select your currency

Quick Price [Click Quick Price](#)

This service provides permission for reuse only. If you do not have a copy of the article you are using, you may copy and paste the content and reuse according to the terms of your agreement. Please be advised that obtaining the content you license is a separate transaction not involving Rightslink.

[QUICK PRICE](#)

[CONTINUE](#)

To request permission for a type of use not listed, please contact [the publisher](#) directly.



Title: Long Range Polymer Chain Dynamics Studied by Fluorescence Quenching
Author: Shiva Farhangi, Jean Duhamel
Publication: Macromolecules
Publisher: American Chemical Society
Date: Sep 1, 2016
Copyright © 2016, American Chemical Society

Logged in as:
Shiva Farhangi
Account #:
3001004201

[LOGOUT](#)

PERMISSION/LICENSE IS GRANTED FOR YOUR ORDER AT NO CHARGE

This type of permission/license, instead of the standard Terms & Conditions, is sent to you because no fee is being charged for your order. Please note the following:

- Permission is granted for your request in both print and electronic formats, and translations.
- If figures and/or tables were requested, they may be adapted or used in part.
- Please print this page for your records and send a copy of it to your publisher/graduate school.
- Appropriate credit for the requested material should be given as follows: "Reprinted (adapted) with permission from (COMPLETE REFERENCE CITATION). Copyright (YEAR) American Chemical Society." Insert appropriate information in place of the capitalized words.
- One-time permission is granted only for the use specified in your request. No additional uses are granted (such as derivative works or other editions). For any other uses, please submit a new request.

[BACK](#)

[CLOSE WINDOW](#)



Title: Effect of Side-Chain Length on the Polymer Chain Dynamics of Poly(alkyl methacrylate)s in Solution
Author: Shiva Farhangi, Henning Weiss, Jean Duhamel
Publication: Macromolecules
Publisher: American Chemical Society
Date: Dec 1, 2013
Copyright © 2013, American Chemical Society

Logged in as:

Shiva Farhangi

LOGOUT

Quick Price Estimate

Permission for this particular request is granted for print and electronic formats, and translations, at no charge. Figures and tables may be modified. Appropriate credit should be given. Please print this page for your records and provide a copy to your publisher. Requests for up to 4 figures require only this record. Five or more figures will generate a printout of additional terms and conditions. Appropriate credit should read: "Reprinted with permission from {COMPLETE REFERENCE CITATION}. Copyright {YEAR} American Chemical Society." Insert appropriate information in place of the capitalized words.

I would like to... ? reuse in a Thesis/Dissertation ▼

Requestor Type ? Author (original work) ▼

Portion ? Full article ▼

Format ? Print and Electronic ▼

Will you be translating? ? No ▼

Select your currency CAD - \$ ▼

Quick Price Click Quick Price

This service provides permission for reuse only. If you do not have a copy of the article you are using, you may copy and paste the content and reuse according to the terms of your agreement. Please be advised that obtaining the content you license is a separate transaction not involving Rightslink.

QUICK PRICE

CONTINUE

To request permission for a type of use not listed, please contact [the publisher](#) directly.

Copyright © 2016 Copyright Clearance Center, Inc. All Rights Reserved. [Privacy statement](#). [Terms and Conditions](#).
Comments? We would like to hear from you. E-mail us at customer@copyright.com



Title: Effect of Side-Chain Length on the Polymer Chain Dynamics of Poly(alkyl methacrylate)s in Solution

Author: Shiva Farhangi, Henning Weiss, Jean Duhamel

Publication: Macromolecules

Publisher: American Chemical Society

Date: Dec 1, 2013

Copyright © 2013, American Chemical Society

Logged in as:

Shiva Farhangi

LOGOUT

PERMISSION/LICENSE IS GRANTED FOR YOUR ORDER AT NO CHARGE

This type of permission/license, instead of the standard Terms & Conditions, is sent to you because no fee is being charged for your order. Please note the following:

- Permission is granted for your request in both print and electronic formats, and translations.
- If figures and/or tables were requested, they may be adapted or used in part.
- Please print this page for your records and send a copy of it to your publisher/graduate school.
- Appropriate credit for the requested material should be given as follows: "Reprinted (adapted) with permission from (COMPLETE REFERENCE CITATION). Copyright (YEAR) American Chemical Society." Insert appropriate information in place of the capitalized words.
- One-time permission is granted only for the use specified in your request. No additional uses are granted (such as derivative works or other editions). For any other uses, please submit a new request.

BACK

CLOSE WINDOW



Title: Pyrenyl Derivative with a Four-Atom Linker That Can Probe the Local Polarity of Pyrene-Labeled Macromolecules
Author: Shiva Farhangi, Jean Duhamel
Publication: The Journal of Physical Chemistry B
Publisher: American Chemical Society
Date: Feb 1, 2016
Copyright © 2016, American Chemical Society

Logged in as:
Shiva Farhangi

[LOGOUT](#)

Quick Price Estimate

Permission for this particular request is granted for print and electronic formats, and translations, at no charge. Figures and tables may be modified. Appropriate credit should be given. Please print this page for your records and provide a copy to your publisher. Requests for up to 4 figures require only this record. Five or more figures will generate a printout of additional terms and conditions. Appropriate credit should read: "Reprinted with permission from {COMPLETE REFERENCE CITATION}. Copyright {YEAR} American Chemical Society." Insert appropriate information in place of the capitalized words.

I would like to... ?

reuse in a Thesis/Dissertation ▼

Requestor Type ?

Author (original work) ▼

Portion ?

Full article ▼

Format ?

Print and Electronic ▼

Will you be translating? ?

No ▼

Select your currency

USD - \$ ▼

Quick Price

Click Quick Price

This service provides permission for reuse only. If you do not have a copy of the article you are using, you may copy and paste the content and reuse according to the terms of your agreement. Please be advised that obtaining the content you license is a separate transaction not involving Rightslink.

[QUICK PRICE](#)

[CONTINUE](#)

To request permission for a type of use not listed, please contact [the publisher](#) directly.



Title: Pyrenyl Derivative with a Four-Atom Linker That Can Probe the Local Polarity of Pyrene-Labeled Macromolecules

Author: Shiva Farhangi, Jean Duhamel

Publication: The Journal of Physical Chemistry B

Publisher: American Chemical Society

Date: Feb 1, 2016

Copyright © 2016, American Chemical Society

Logged in as:
Shiva Farhangi

[LOGOUT](#)

PERMISSION/LICENSE IS GRANTED FOR YOUR ORDER AT NO CHARGE

This type of permission/license, instead of the standard Terms & Conditions, is sent to you because no fee is being charged for your order. Please note the following:

- Permission is granted for your request in both print and electronic formats, and translations.
- If figures and/or tables were requested, they may be adapted or used in part.
- Please print this page for your records and send a copy of it to your publisher/graduate school.
- Appropriate credit for the requested material should be given as follows: "Reprinted (adapted) with permission from (COMPLETE REFERENCE CITATION). Copyright (YEAR) American Chemical Society." Insert appropriate information in place of the capitalized words.
- One-time permission is granted only for the use specified in your request. No additional uses are granted (such as derivative works or other editions). For any other uses, please submit a new request.

[BACK](#)

[CLOSE WINDOW](#)



Title: Probing Side Chain Dynamics of
Branched Macromolecules by
Pyrene Excimer Fluorescence

Author: Shiva Farhangi, Jean Duhamel

Publication: Macromolecules

Publisher: American Chemical Society

Date: Jan 1, 2016

Copyright © 2016, American Chemical Society

Logged in as:

Shiva Farhangi

LOGOUT

Quick Price Estimate

Permission for this particular request is granted for print and electronic formats, and translations, at no charge. Figures and tables may be modified. Appropriate credit should be given. Please print this page for your records and provide a copy to your publisher. Requests for up to 4 figures require only this record. Five or more figures will generate a printout of additional terms and conditions. Appropriate credit should read: "Reprinted with permission from {COMPLETE REFERENCE CITATION}. Copyright {YEAR} American Chemical Society." Insert appropriate information in place of the capitalized words.

I would like to... ?

reuse in a Thesis/Dissertation ▼

Requestor Type ?

Author (original work) ▼

Portion ?

Full article ▼

Format ?

Print and Electronic ▼

Will you be
translating? ?

No ▼

Select your currency

CAD - \$ ▼

Quick Price

Click Quick Price

This service provides permission for reuse only. If you do not have a copy of the article you are using, you may copy and paste the content and reuse according to the terms of your agreement. Please be advised that obtaining the content you license is a separate transaction not involving Rightslink.

QUICK PRICE

CONTINUE

To request permission for a type of use not listed, please contact [the publisher](#) directly.

Copyright © 2016 Copyright Clearance Center, Inc. All Rights Reserved. [Privacy statement](#), [Terms and Conditions](#).
Comments? We would like to hear from you. E-mail us at customercare@copyright.com



Title: Probing Side Chain Dynamics of Branched Macromolecules by Pyrene Excimer Fluorescence

Author: Shiva Farhangi, Jean Duhamel

Publication: Macromolecules

Publisher: American Chemical Society

Date: Jan 1, 2016

Copyright © 2016, American Chemical Society

Logged in as:

Shiva Farhangi

LOGOUT

PERMISSION/LICENSE IS GRANTED FOR YOUR ORDER AT NO CHARGE

This type of permission/license, instead of the standard Terms & Conditions, is sent to you because no fee is being charged for your order. Please note the following:

- Permission is granted for your request in both print and electronic formats, and translations.
- If figures and/or tables were requested, they may be adapted or used in part.
- Please print this page for your records and send a copy of it to your publisher/graduate school.
- Appropriate credit for the requested material should be given as follows: "Reprinted (adapted) with permission from (COMPLETE REFERENCE CITATION). Copyright (YEAR) American Chemical Society." Insert appropriate information in place of the capitalized words.
- One-time permission is granted only for the use specified in your request. No additional uses are granted (such as derivative works or other editions). For any other uses, please submit a new request.

BACK

CLOSE WINDOW

References

Chapter 1

1. Glass, J. E., Ed.; *Polymers in Aqueous Media: Performance through Association*; Advances in Chemistry Series 226; American Chemical Society: Washington, DC, **1989**.
2. Schulze, D. N.; Glass, J. E., Ed.; *Polymers as Rheology Modifiers*; ACS Symposium Series 462; American Chemical Society: Washington, DC, **1991**.
3. Kwak, J. C. T., Ed.; *Polymer-Surfactant Systems*; Surfactant Science Series 77; Marcel Dekker: New York, **1998**.
4. Goddard, E. O.; Ananthapadamanabham, K. P., Ed.; *Interactions of Surfactants with Polymers and Proteins*; CRC Press: Boca Raton, FL, **1993**.
5. Winnik, M. A.; Yekta, A. Associative Polymers in Aqueous Solution. *Curr. Opin. Colloid Interface Sci.* **1997**, 2, 424-436.
6. Glass, J. E. A Perspective on the History of and Current Research in Surfactant-Modified, Water-Soluble Polymers. *J. Coat. Tech.* **2001**, 73, 79-98.

7. Annabale, T.; Buscall, R.; Ettelaie, R.; Whittlestone, D. The Rheology of Solutions of Associating Polymers: Comparison of Experimental Behavior with Transient Network Theory. *J. Rheol.* **1993**, *37*, 695-726.
8. Tripathi, A.; Tam, K. C.; McKinley, G. H. Rheology and Dynamics of Associative Polymers in Shear and Extension: Theory and Experiments. *Macromolecules* **2006**, *39*, 1981-1999.
9. Zhao, G.; Khin, C. C.; Chen, S. B. Nonionic Surfactant and Temperature Effects on the Viscosity of Hydrophobically Modified Hydroxyethyl Cellulose Solutions. *J. Phys. Chem. B* **2005**, *109*, 14198-14204.
10. Bai, Y. Protein Folding Pathways Studied by Pulsed- and Native-State Hydrogen Exchange. *Chem. Rev.* **2006**, *106*, 1757-1768.
11. Neira, J. L. NMR as a Tool to Identify and Characterize Protein Folding Intermediates. *Archiv. Biochemistry Biophys.* **2013**, *531*, 90-99.
12. Adhikari, A. N.; Freed, K. F.; Sosnick, T. T. Simplified Protein Models: Predicting Folding Pathways and Structure Using Amino Acid Sequences. *Phys. Rev. Lett.* **2013**, *111*, 028103.
13. Plotkin, S. S.; Onuchic, J. N. Understanding Protein Folding with Energy Landscape Theory. Part I: Basic Concepts. *Q. Rev. Biophys.* **2002**, *35*, 111-167.

14. Englander, S. W.; Mayne, L. The Nature of Protein Folding Pathways. *Proc. Natl. Acad. Sci.* **2014**, *111*, 15873-15880.
15. Li, J.; Ngai, T.; Wu, C. The Slow Relaxation Mode: From Solutions to Gel Networks. *Polym. J.* **2010**, *42*, 609-625.
16. Dais, P.; Spyros, A. ¹³C Nuclear Magnetic Relaxation and Local Dynamics of Synthetic Polymers in Dilute Solution and in the Bulk State. *Prog. Nucl. Magn. Res. Spectrosc.* **1995**, *27*, 555-633.
17. Pilař, J. Local Dynamics of Polymers in Solution by Spin-Label ESR. In *Advance ESR Methods in Polymer Research*, Ed. Schlick, S. Wiley, **2006**, pp 133-163.
18. Hyun, K.; Wilhelm, M.; Klein, C. O.; Cho, K. S.; Nam, J. G.; Ahn, K. H.; Lee, S. J.; Ewoldt, R. H.; McKinley, G. H. A Review of Nonlinear Oscillatory Shear Tests: Analysis and Application of Large Amplitude Oscillatory Shear (LAOS). *Porg. Polym. Sci.* **2011**, *36*, 1697-1753.
19. Perkins, T. T.; Quake, S. R.; Smith, D. E.; Chu, S. Relaxation of a Single DNA Molecule Observed by Optical Microscopy. *Science* **1994**, *264*, 822-826.
20. Keshavarz, M.; Engelkamp, H.; Xu, J.; Braeken, E.; Otten, M. B. J.; Uji-i, H.; Schwartz, E.; Koepf, M.; Vananroye, A.; Vermant, J.; Nolte, R. J. M.; De Schryver, F.;

Maan, J. C.; Hofkens, J.; Christianen, P. C. M., Rowan, A. E. Nanoscale Study of Polymer Dynamics. *ACS Nano* **2015**, ASAP.

21. Viovy, J. L.; Monerie, L. Fluorescence Anisotropy Technique Using Synchrotron Radiation as a Powerful Means for Studying the Orientation Correlation Function of Polymer Chains. *Adv. Polym. Sci.* **1985**, *67*, 99-122.

22. Winnik, M. A. End-to-End Cyclization of Polymer Chains. *Acc. Chem. Res.* **1985**, *18*, 73-79.

23. Duhamel, J. New Insights in the Study of Pyrene Excimer Fluorescence to Characterize Macromolecules and their Supramolecular Assemblies in Solution. *Langmuir* **2012**, *28*, 6527-6538.

24. Duhamel, J. Global Analysis of Fluorescence Decays to Probe the Internal Dynamics of Fluorescently Labeled Macromolecules. *Langmuir* **2014**, *30*, 2307-2324.

25. Willemski, G.; Fixman, M. Diffusion-Controlled Intrachain Reactions of Polymers. I Theory. *J. Chem. Phys.* **1974**, *60*, 866-877.

26. Willemski, G.; Fixman, M. Diffusion-Controlled Intrachain Reactions of Polymers. II Results for a Pair of Terminal Reactive Groups. *J. Chem. Phys.* **1974**, *60*, 878-890.

27. Zachariasse, K.; Kühnle, W. Intramolecular Excimers with α,ω -Diarylalkanes. *Z. Phys. Chem. Neue F.* **1976**, *101*, 267-276.
28. Zachariasse, K. A.; Maçanita, A. L.; Kuehnle, W. Chain Length Dependence of Intramolecular Excimer Formation with n-Bis(-1pyrenylcarboxy)alkanes for n=1-16, 22, and 32. *J. Phys. Chem. B* **1999**, *103*, 9356-9365.
29. Cuniberti, C.; Perico, A. Intramolecular Excimers and Microbrownian Motion of Flexible Polymer Molecules in Solution. *J. Eur. Polym.* **1977**, *13*, 369-374.
30. Birks, J. B.; Dyson, D. J.; Munro, I. H. 'Excimer' Fluorescence. II. Lifetime Studies of Pyrene Solutions. *Proc. Roy. Soc. A* **1963**, *275*, 575-588.
31. Birks, J.B. *Photophysics of Aromatic Molecules*; Wiley: New York, NY, USA, **1970**; p. 301.
32. Winnik, M. A.; Redpath, T.; Richards, D. H. The Dynamics of End-to-End Cyclization in Polystyrene Probed by Pyrene Excimer Formation. *Macromolecules.* **1980**, *13*, 328-335.
33. Svirskaya, P.; Danhelka, J.; Redpath, A. E. C.; Winnik, M. A. Cyclization Dynamics of Polymers: 7. Applications of the Pyrene Excimer Technique to the Internal Dynamics of Polydimethylsiloxane Chains. *Polymer* **1983**, *24*, 319-322.

34. Ghiggino, K. P.; Snare, M. J.; Thistlethwaite, P. J. Cyclization Dynamics in Poly(ethylene oxide). Chain Length and Temperature Dependence. *Eur. Polym. J.* **1985**, *21*, 265-272.
35. Boileau, S.; Mechin, F.; Martinho, J. M.; Winnik, M. A. End-to-End Cyclization of a Pyrene End-Capped Poly(bisphenol A-diethylene glycol carbonate). *Macromolecules* **1989**, *22*, 215-220.
36. Ingratta, M.; Hollinger, J.; Duhamel, J. A Case for Using Randomly Labeled Polymers to Study Long Range Polymer Chain Dynamics by Fluorescence. *J. Am. Chem. Soc.* **2008**, *130*, 9420-9428.
37. Chen, S.; Duhamel, J.; Winnik, M. A. Probing End-to-End Cyclization Beyond Willemski and Fixmann. *J. Phys. Chem. B* **2011**, *115*, 3289-3302.
38. Fierz, B.; Kiefhaber, T. End-to-End vs Interior Loop Formation Kinetics in Unfolded Polypeptide Chains. *J. Am. Chem. Soc.* **2007**, *129*, 672-679.
39. Fierz, B.; Satzger, H.; Root, C.; Gilch, P.; Zinth, W.; Kiefhaber, T. Loop Formation in Unfolded Polypeptide Chains on the Picoseconds to Microseconds Time Scale. *Proc. Natl. Acad. Sci.* **2007**, *104*, 2163-2168.

40. Hagen, S. J.; Hofrichter, J.; Szabo, A.; Eaton, W. A. Diffusion-Limited Contact Formation in Unfolded Cytochrome c: Estimating the Maximum Rate of Protein Folding. *Proc. Natl. Acad. Sci.* **1996**, *93*, 11615-11617.
41. Hudgins, R. R.; Huang, F.; Gramlich, G.; Nau, W. M. A Fluorescence-Based Method for Direct Measurement of Submicrosecond Intramolecular Contact Formation in Biopolymers: An Exploratory Study with Polypeptides. *J. Am. Chem. Soc.* **2002**, *124*, 556-564.
42. Huang, F.; Nau, W. M. A Conformational Flexibility Scale for Amino Acids in Peptides. *Angew. Chem. Int. Ed.* **2003**, *42*, 2269-2272.
43. Huang, F.; Hudgins, R. R.; Nau, W. M. Primary and Secondary Structure Dependence of Peptide Flexibility Assessed by Fluorescence-Based Measurement of End-to-End Collision Rates. *J. Am. Chem. Soc.* **2004**, *126*, 16665-16675.
44. Roccatano, D.; Sahoo, H.; Zacharias, M.; Nau, W. M. Temperature Dependence of Looping Rates in a Short Peptide. *J. Phys. Chem. B* **2007**, *111*, 2639-2646.
45. Lapidus, L. S.; Eaton, W. A.; Hofrichter, J. Measuring the Rate of Intramolecular Contact Formation in Polypeptides. *Proc. Natl. Acad. Sci.* **2000**, *97*, 7220-7225.
46. Lapidus, L. J.; Eaton, W. A.; Hofrichter, J. Measuring Dynamic Flexibility of the Coil State of a Helix-Forming Peptide. *J. Mol. Biol.* **2002**, *319*, 19-25.

47. Haas, E. The Study of Protein Folding and Dynamics by Determination of Intramolecular Distance Distributions and Their Fluctuations Using Ensemble and Single-Molecule FRET Measurements. *ChemPhysChem*. **2005**, *6*, 858-870.
48. Bieri, O.; Wirz, J.; Hellrung, B.; Schutkowski, M.; Drewello, M.; Kiefhaber, T. The Speed Limit for Protein Folding Measured by Triplet-Triplet Energy Transfer. *Proc. Natl. Acad. Sci.* **1999**, *96*, 9597-9601.
49. Krieger, F.; Fierz, B.; Bieri, O.; Drewello, M.; Kiefhaber, T. Dynamics of Unfolded Polypeptide Chains as Model for the Earliest Steps in Protein Folding. *J. Mol. Biol.* **2003**, *332*, 265-274.
50. Möglich, A.; Krieger, F.; Kiefhaber, T. Molecular Basis for the Effect of Urea and Guanidinium Chloride on the Dynamics of Unfolded Polypeptide Chains. *J. Mol. Biol.* **2005**, *345*, 153-162.
51. Fierz, B.; Kiefhaber, T. End-to-End vs Interior Loop Formation Kinetics in Unfolded Polypeptide Chains. *J. Am. Chem. Soc.* **2007**, *129*, 672-679.
52. Fierz, B.; Satzger, H.; Root, C.; Gilch, P.; Zinth, W.; Kiefhaber, T. Loop Formation in Unfolded Polypeptide Chains on the Picoseconds to Microseconds Time Scale. *Proc. Natl. Acad. Sci.* **2007**, *104*, 2163-2168.

53. Neuweiler, H.; Löllmann, M.; Doose, S.; Sauer, M. Dynamics of Unfolded Polypeptide Chains in Crowded Environment Studied by Fluorescence Correlation Spectroscopy. *J. Mol. Biol.* **2007**, *365*, 856-869.
54. Neuweiler, H.; Schultz, A.; Böhmer, M.; Enderlein, J.; Sauer, M. Measurements of Submicrosecond Intramolecular Contact Formation in Peptides at the Single-Molecule Level. *J. Am. Chem. Soc.* **2007**, *125*, 5324-5330.
55. McGimpsey, W. G.; Chen, L.; Carraway, R.; Samaniego, W. N. Singlet-Singlet and Triplet-Triplet Energy Transfer in Biochromophoric Peptides. *J. Phys. Chem. A* **1999**, *103*, 6082-6090.
56. Möglich, A.; Joder, K.; Kiefhaber, T. End-to-End Distance Distributions and Intrachain Diffusion Constants in Unfolded Polypeptide Chains Indicate Intramolecular Hydrogen Bond Formation. *Proc. Natl. Acad. Sci.* **2006**, *103*, 12394-12399.
57. Sahoo, H.; Roccatano, D.; Hennig, A.; Nau, W. M. A 10-Å Spectroscopic Ruler Applied to Short Polyprolines. *J. Am. Chem. Soc.* **2007**, *129*, 9762-9772.
58. Jacob, M. H.; Dsouza, R. N.; Ghosh, I.; Norouzy, A.; Schwarzlose, T.; Nau, W. M. Diffusion-Enhanced Förster Resonance Energy Transfer and the Effects of External Quenchers and the Donor Quantum Yield. *J. Phys. Chem. B* **2013**, *117*, 185-198.

59. Norouzy, A.; Assaf, K. I.; Zhang, S.; Jacob, M. H.; Nau, W. M. Coulomb Repulsion in Short Polypeptides. *J. Phys. Chem. B* **2015**, *119*, 33-43.
60. Galoppini, E.; Fox, M. A. Effect of the Electric Field Generated by the Helix Dipole on Photoinduced Intramolecular Electron Transfer in Dichromophoric α -Helical Peptides. *J. Am. Chem. Soc.* **1996**, *118*, 2299-2300.
61. Fox, M. A.; Galoppini, E. Electric Field Effects on Electron Transfer Rates in Dichromophoric Peptides: The Effect of Helix Unfolding. *J. Am. Chem. Soc.* **1997**, *119*, 5277-5285.
62. Ingratta, M.; Mathew, M.; Duhamel, J. How Switching the Substituent of a Pyrene Derivative from a Methyl to a Butyl Affects the Fluorescence Response of Polystyrene Randomly Labeled with Pyrene. *Can. J. Chem.* **2010**, *88*, 217-227.
63. Farhangi, S.; Weiss, H.; Duhamel, J. Effect of Side-Chain Length on the Polymer Chain Dynamics of Poly (alkyl methacrylate)s in Solution. *Macromolecules* **2013**, *46*, 9738-9747.
64. Bandrup, J. ; Immergut, E. H. ; Grulke, E. A. *Polymer Handbook*, 4th ed.; John Wiley & Sons: NY, **1999**, p VII 675-683.
65. Mathew, A.; Siu, H.; Duhamel, J. A *Blob* Model to Study Chain Folding by Fluorescence. *Macromolecules* **1999**, *32*, 7100-7108.

66. Tachiya, M. Stochastic and Diffusion Models of Reactions in Micelles and Vesicles. In *Kinetics of Nonhomogeneous Processes: A Practical Introduction for Chemists, Biologists, Physicists, and Material Scientists*. Ed. G. R. Freeman, Wiley, NY, **1987**, pp575-650.
67. Kanagalingam, S.; Spartalis, J.; Cao, T.-C.; Duhamel, J. Scaling Relations Related to the Kinetics of Excimer Formation between Pyrene Groups Attached onto Poly(N,N-dimethylacrylamide)s *Macromolecules* **2002**, *35*, 8571-8577.
68. Duhamel, J.; Kanagalingam, S.; O'Brien, T.; Ingratta, M. Side-Chain Dynamics of an α -Helical Polypeptide Monitored by Fluorescence. *J. Am. Chem. Soc.* **2003**, *125*, 12810-12822.
69. Teertstra, S. J.; Lin, W. Y.; Gauthier, M.; Ingratta, M. Duhamel, J. Comparison of the Long Range Polymer Chain Dynamics of Polystyrene and *cis*-Polyisoprene Using Polymers Randomly Labeled with Pyrene. *Polymer* **2009**, *50*, 5456-5466.
70. Yip, J.; Duhamel, J.; Qiu, X. P.; Winnik, F. M. Long-Range Polymer Chain Dynamics of Pyrene-Labeled Poly(*N*-isopropylacrylamide)s Studied by Fluorescence. *Macromolecules* **2011**, *44*, 5363-5372.
71. Farhangi, S.; Duhamel, J. Probing Side Chain Dynamics of Branched Macromolecules by Pyrene Excimer Fluorescence. *Macromolecules* **2016**, *49*, 353-361.

72. Ironi, K.; Zhang, M.; Duhamel, J. Study of the Semidilute Solutions of Poly(*N,N*-dimethylacrylamide) by Fluorescence and its Implications to the Kinetics of Coil-to-Globule Transition. *J. Phys. Chem. B* **2006**, *110*, 2628-2637.
73. Levinthal, C. How to Fold Graciously. Mossbauer Spectroscopy in Biological Systems. Proceedings University of Illinois Bulletin (University of Illinois Press, Urbana, IL), **1969**, pp 22–24.
74. Ptitsyn, O. B. Kinetic and Equilibrium Intermediates in Protein Folding. *Protein Eng.* **1994**, *7*, 593-596.
75. Wetlaufer, D. B. Nucleation, Rapid Folding, and Globular Intrachain Regions in Proteins. *Proc. Natl. Acad. Sci. U.S.A.* **1973**, *70*, 697-701.
76. Wetlaufer, D. B. Nucleation in Protein Folding-Confusion of Structure and Process. *Trends Biochem. Sci.* **1990**, *15*, 414-415.
77. Dill, K. A.; Bromberg, S.; Yue, K.; Fiebig, K. M.; Yee, D. P.; Thomas, P. D.; Chan, H. S. Principle of Protein Folding-A Perspective from Simple Exact Model. *Protein Sci.* **1995**, *4*, 561-602.
78. Dill, K. A.; Chan, H. S. From Levinthal to Pathways to Funnels. *Nature Struct. Biol.* **1997**, *4*, 10-19.

79. Dinner, A. R.; Sýali, A.; Smith, L. J.; Dobson, C. M.; Karplus, M. Understanding Protein Folding via Free-Energy Surfaces from Theory to Experiment. *Trends Biochem. Sci.* **2000**, *25*, 331-339
80. Duhamel, J.; Kanagalingam, S.; O'Brien, T.; Ingratta, M. Side-Chain Dynamics of an α -Helical Polypeptide Monitored by Fluorescence. *J. Am. Chem. Soc.* **2003**, *125*, 12810-12822.
81. Ingratta, M.; Duhamel, J. Effect of Side-chain Length on the Side-chain Dynamics of α -Helical Poly(L-glutamic acid) as Probed by a Fluorescence Blob Model. *J. Phys. Chem. B* **2008**, *112*, 9209-9218.
82. Englander, S. W.; Mayne, L. The Nature of Protein Folding Pathways. *Proc. Natl. Acad. Sci.* **2014**, *111*, 15873-15880.
83. Duhamel, J.; Yekta, A.; Winnik, M. A.; Jao, T.-C.; Mishra, M. K.; Rubin, I. D. A Statistical Blob Model for Studying Polymer Chain Dynamics in Solution by Excimer Formation Processes. *J. Phys. Chem.* **1993**, *97*, 13708-13712.
84. Kalyanasundaram, K.; Thomas, J. K. Environmental Effects on Vibronic Band Intensities in Pyrene Monomer Fluorescence and Their Application in Studies of Micellar Systems. *J. Am. Chem. Soc.* **1977**, *99*, 2039-2044.

85. Dong, D. C.; Winnik, M. A. The Py Scale of Solvent Polarities. Solvent Effects on the Vibronic Fine Structure of Pyrene Fluorescence and Empirical Correlations with ET and Y Values. *Photochem. Photobiol.* **1982**, *35*, 17-21.
86. Dong, D. C.; Winnik, M. A. The Py Scale of Solvent Polarities. *Can. J. Chem.* **1984**, *62*, 2560–2565.

Chapter 2

1. Eisenberg, A. in *Physical Properties of Polymers* 2nd Ed., American Chemical Society, Washington, DC, **1993**, pp 61-95.
2. Aklonis, J. J.; MacKnight, W. J. *Introduction to Polymer Viscoelasticity* 2nd Ed., Wiley, NY, **1983**.
3. Winnik, M. A. End-to-End Cyclization of Polymer Chains. *Acc. Chem. Res.* **1985**, *18*, 73-79.
4. Duhamel, J. Internal Dynamics of Dendritic Molecules Probed by Pyrene Excimer Formation. *Polymers* **2012**, *4*, 211-239.
5. Duhamel, J. New Insights in the Study of Pyrene Excimer Fluorescence to Characterize Macromolecules and their Supramolecular Assemblies in Solution. *Langmuir* **2012**, *28*, 6527-6538.
6. Zachariasse, K.; Kühnle, W. Intramolecular Excimers with α,ω -Diarylalkanes. *Z. Phys. Chem. Neue Fol.* **1976**, *101*, 267-276.
7. Cuniberti, C.; Perico, A. Intramolecular Excimers and Microbrownian Motion of Flexible Polymer Molecules in Solution. *Eur. Polym. J.* **1977**, *13*, 369-374.

8. Winnik, M. A.; Redpath, T.; Richards, D. H. The Dynamics of End-to-End Cyclization in Polystyrene Probed by Pyrene Excimer Formation. *Macromolecules* **1980**, *13*, 328-335.
9. Huang, F.; Hudgins, R. R.; Nau, W. M. Primary and Secondary Structure Dependence of Peptide Flexibility Assessed by Fluorescence-Based Measurement of End-to-End Collision Rates. *J. Am. Chem. Soc.* **2004**, *126*, 16665-16675.
10. Neuweiler, H.; Löllmann, M.; Doose, S.; Sauer, M. Dynamics of Unfolded Polypeptide Chains in Crowded Environment Studied by Fluorescence Correlation Spectroscopy. *J. Mol. Biol.* **2007**, *365*, 856-869.
11. Fierz, B.; Satzger, H.; Root, C.; Gilch, P.; Zinth, W.; Kiefhaber, T. Loop Formation in Unfolded Polypeptide Chains on the Picoseconds to Microseconds Time Scale. *Proc. Natl. Acad. Sci.* **2007**, *104*, 2163-2168.
12. Fierz, B.; Kiefhaber, T. End-to-End vs Interior Loop Formation Kinetics in Unfolded Polypeptide Chains. *J. Am. Chem. Soc.* **2007**, *129*, 672-679.
13. Hagen, S. J.; Hofrichter, J.; Szabo, A.; Eaton, W. A. Diffusion-Limited Contact Formation in Unfolded Cytochrome C: Estimating the Maximum Rate of Protein Folding. *Proc. Natl. Acad. Sci.* **1996**, *93*, 11615-11617.

14. Yekta, A.; Xu, B.; Duhamel, J.; Adiwidjaja, H.; Winnik, M. A. Fluorescence Studies of Associating Polymers in Water. Determination of the Chain-End Aggregation Number and a Model for the Association Process. *Macromolecules* **1995**, *28*, 956-966.
15. Mathew, A.; Siu, H.; Duhamel, J. A *Blob* Model to Study Chain Folding by Fluorescence. *Macromolecules* **1999**, *32*, 7100-7108.
16. Duhamel, J. Polymer Chain Dynamics in Solution Probed with a Fluorescence Blob Model *Acc. Chem. Res.* **2006**, *39*, 953-960.
17. Ingratta, M.; Hollinger, J.; Duhamel, J. A Case for Using Randomly Labeled Polymers to Study Long Range Polymer Chain Dynamics by Fluorescence. *J. Am. Chem. Soc.* **2008**, *130*, 9420-9428.
18. Ingratta, M.; Mathew, M.; Duhamel, J. How Switching the Substituent of a Pyrene Derivative from a Methyl to a Butyl Affects the Fluorescence Response of Polystyrene Randomly Labeled with Pyrene. *Can. J. Chem.* **2010**, *88*, 217-227.
19. Yip, J.; Duhamel, J.; Qiu, X. P.; Winnik, F. M. Long-Range Polymer Chain Dynamics of Pyrene-Labeled Poly(*N*-isopropylacrylamide)s Studied by Fluorescence. *Macromolecules* **2011**, *44*, 5363-5372.

20. Press, W. H.; Flannery, B. P.; Teukolsky, S. A.; Vetterling, W. T. *Numerical Recipes. The Art of Scientific Computing (Fortran Version)*; Cambridge University Press: Cambridge, **1992**.
21. Stals, P. J. M.; Li, Y.; Burdyriska, J.; Nicolay, R.; Nese, A.; Palmans, A. R. A.; Meijer, E. W.; Matyjaszewski, K.; Sheiko, S. S. How Far Can We Push Polymer Architectures. *J. Am. Chem. Soc.* **2013**, *135*, 11421-11424.

Chapter 3

1. Winnik, F. M. Photophysics of Preassociated Pyrenes in Aqueous Polymer Solutions and in Other Organized Media. *Chem. Rev.* **1993**, *93*, 587–614.
2. Duhamel, J. Internal Dynamics of Dendritic Molecules Probed by Pyrene Excimer Formation. *Polymers* **2012**, *4*, 211–239.
3. Duhamel, J. New Insights in the Study of Pyrene Excimer Fluorescence to Characterize Macromolecules and their Supramolecular Assemblies in Solution. *Langmuir* **2012**, *28*, 6527-6538.
4. Duhamel, J. Global Analysis of Fluorescence Decays to Probe the Internal Dynamics of Fluorescently Labeled Macromolecules. *Langmuir* **2014**, *30*, 2307-2324.

5. Winnik, M. A.; Li, X.-B.; Guillet, J. E. Cyclization Dynamics of Polymers. 13. Effects of Added Polymer on the Conformation and Dynamics of Polystyrene Containing Evenly Spaced Pyrene Groups. *Macromolecules* **1984**, *17*, 699-702.
6. Nishikawa, K.; Yekta, A.; Pham, H. H.; Winnik, M. A.; Sau, A. C. Fluorescence Studies of Hydrophobically Modified Hydroxyethylcellulose (HMHEC) and Pyrene-Labeled HMHEC. *Langmuir* **1998**, *14*, 7119-7129.
7. Kujawa, P.; Liu, R. C. W.; Winnik, F. M. Do Fluorocarbon, Hydrocarbon, and Polycyclic Aromatic Groups Intermingle? A Study of the Interactions in Water between Fluorocarbon- and Hydrocarbon-Modified Poly(*N*-isopropylacrylamides). *J. Phys. Chem. B* **2002**, *106*, 5578-5585.
8. Anghel, D. F.; Alderson, V.; Winnik, F. M.; Mizusaki, M.; Morishima, Y. Fluorescent Dyes as Model 'Hydrophobic Modifiers' of Polyelectrolytes: A Study of Poly(acrylic acid)s Labeled with Pyrenyl and Naphthyl Groups. *Polymer* **1998**, *39*, 3035-3044.
9. Hu, Y.-Z.; Zhao, C.-L.; Winnik, M. A.; Sundararajan, P. R. Fluorescence Studies of the Interactions of Sodium Dodecyl Sulfate with Hydrophobically Modified Poly(ethylene oxide). *Langmuir* **1990**, *6*, 880-883.

10. Winnik, F. M.; Regismond, S. T. A.; Goddard, E. D. Interactions of an Anionic Surfactant with a Fluorescence Dye-Labeled Hydrophobically-Modified Cationic Cellulose Ether. *Langmuir* **1997**, *13*, 111-114.
11. Anghel, D. F.; Toca-Herrera, J. L.; Winnik, F. M.; Rettig, W.; v. Kliting, R. Steady-State Fluorescence Investigation of Pyrene-Labeled Poly(acrylic acid)s in Aqueous Solution and in the Presence of Sodium Dodecyl Sulfate. *Langmuir* **2002**, *18*, 5600-5606.
12. Relógio, P.; Martinho, J. M. G.; Farinha, J. P. S. Effect of Surfactant on the Intra- and Intermolecular Association of Hydrophobically Modified Poly(*N,N*-dimethylacrylamide). *Macromolecules* **2005**, *38*, 10799-10811.
13. Winnik, M. A.; Egan, L. S.; Tencer, M.; Croucher, M. D. Luminescence Studies on Sterically Stabilized Polymer Colloid Particles: Pyrene Excimer Formation. *Polymer* **1987**, *28*, 1553-1560.
14. Nakashima, K.; Liu, Y. S.; Zhang, P.; Duhamel, J.; Feng, J.; Winnik, M. A. Picosecond Fluorescence Studies of Energy Transfer on the Surface of Poly(butyl methacrylate) Latex Particles. *Langmuir* **1993**, *9*, 2825-2831.
15. Eckert, A. R.; Hsiao, J.-S.; Webber, S. E. Photophysics of Adsorbed and Solution Phase End-Tagged Poly(ethylene oxide). *J. Phys. Chem.* **1994**, *98*, 12025-12031.
16. Birks, J. B. *Photophysics of Aromatic Molecules*; Wiley: New York, **1970**; p 301.

17. Kalyanasundaram, K.; Thomas, J. K. Environmental Effects on Vibronic Band Intensities in Pyrene Monomer Fluorescence and Their Application in Studies of Micellar Systems. *J. Am. Chem. Soc.* **1977**, *99*, 2039-2044.
18. Dong, D. C.; Winnik, M. A. The Py Scale of Solvent Polarities. Solvent Effects on the Vibronic Fine Structure of Pyrene Fluorescence and Empirical Correlations with ET and Y Values. *Photochem. Photobiol.* **1982**, *35*, 17-21.
19. Dong, D. C.; Winnik, M. A. The Py Scale of Solvent Polarities. *Can. J. Chem.* **1984**, *62*, 2560–2565.
20. Zachariasse, K. A.; Vaz, W. L.; Sotomayor, C.; Kühnle, W. Investigation of Human Erythrocyte Ghost Membranes with Intramolecular Excimer Probes. *Biochim. Biophys. Acta* **1982**, *688*, 323-332.
21. Winnik, F. M.; Winnik, M. A.; Ringsdorf, H.; Venzmer, J. Bis(1-pyrenylmethyl) Ether as an Excimer-Forming Probe of Hydrophobically Modified Poly(N-isopropylacrylamides) in Water. *J. Phys. Chem.* **1991**, *95*, 2583-2587.
22. Farhangi, S.; Weiss, H.; Duhamel, J. Effect of Side-Chain Length on the Polymer Chain Dynamics of Poly(alkyl methacrylate)s in Solution. *Macromolecules* **2013**, *46*, 9738-9747.
23. Duhamel, J. Polymer Chain Dynamics in Solution Probed with a Fluorescence Blob Model. *Acc. Chem. Res.* **2006**, *39*, 953-960.

24. Ingratta, M.; Mathew, M.; Duhamel, J. How Switching the Substituent of a Pyrene Derivative from a Methyl to a Butyl Affects the Fluorescence Response of Polystyrene Randomly Labeled with Pyrene. *Can. J. Chem.* **2010**, *88*, 217-227.
25. Yip, J.; Duhamel, J.; Qiu, X. P.; Winnik, F. M. Long-Range Polymer Chain Dynamics of Pyrene-Labeled Poly(*N*-isopropylacrylamide)s Studied by Fluorescence. *Macromolecules* **2011**, *44*, 5363-5372.
26. Press, W. H.; Flannery, B. P.; Teukolsky, S. A.; Vetterling, W. T. *Numerical Recipes. The Art of Scientific Computing (Fortran Version)*; Cambridge University Press: Cambridge, **1992**.
27. Ingratta, M.; Duhamel, J. Effect of Time on the Rate of Long Range Polymer Segmental Intramolecular Encounters. *J. Phys. Chem. B* **2009**, *113*, 2284-2292.
28. Ingratta, M.; Duhamel, J. Effect of Viscosity on Long Range Polymer Chain Dynamics in Solution Studied with a Fluorescence Blob Model. *Macromolecules* **2009**, *42*, 1244-1251.
29. Kanagalingam, S.; Spartalis, J.; Cao, T.-C.; Duhamel, J. Scaling Relations Related to the Kinetics of Excimer Formation between Pyrene Groups Attached onto Poly(*N,N*-dimethylacrylamide)s. *Macromolecules* **2002**, *35*, 8571-8577.
30. Farhangi, S.; Duhamel, J. Probing Side Chain Dynamics of Branched Macromolecules by Pyrene Excimer Fluorescence. *Macromolecules* **2016**, *49*, 353-361.

31. De Gennes, P. G. *Scaling Concepts in Polymer Physics*. Cornell University Press, Ithaca, **1979**.
32. Flory, P. J. *Principles of Polymer Chemistry*, Cornell University Press, Ithaca, **1953**.

Chapter 4

1. Beers, K. L.; Gaynor, S. G.; Matyjaszewski, K.; Sheiko, S. S.; Möller, M. The Synthesis of Densely Grafted Copolymers by Atom Transfer Radical Polymerization. *Macromolecules* **1998**, *31*, 9413-9415.
2. Lee, H.-I.; Pietrasik, J.; Sheiko, S. S.; Matyjaszewski, K. Stimuli-Responsive Molecular Brushes. *Prog. Polym. Sci.* **2010**, *35*, 24-44.
3. Stals, P. J. M.; Li, Y.; Burdyska, J.; Nicolÿ, R.; Nese, A.; Palmans, A. R. A.; Meijer, E. W.; Matyjaszewski, K.; Sheiko, S. S. How Far Can We Push Polymer Architecture? *J. Am. Chem. Soc.* **2013**, *135*, 11421-11424.
4. He, Y.-M.; Feng, Y.; Fan, Q.-H. Asymmetric Hydrogenation in the Core of Dendrimers. *Acc. Chem. Res.* **2014**, *47*, 2894-2906.
5. Caminade, A.-M.; Turrin, C.-O. Dendrimers for Drug Delivery. *J. Mater. Chem. B* **2014**, *2*, 4055-4066.

6. Hadjichristidis, N.; Pitsikalis, M.; Iatrou, H.; Pispas, S. The Strength of the Macromonomer Strategy for Complex Macromolecular Architecture: Molecular Characterization, Properties, and Applications of Polymacromonomers. *Macromol. Rapid Comm.* **2003**, *24*, 979-1013.
7. Gauthier, M. Arborescent Polymers and Other Dendigraft Polymers: A Journey into Structural Diversity. *J. Polym. Sci. A: Polym. Chem.* **2007**, *45*, 3803-3810.
8. Seog, J.; Dean, D.; Plaas, A. H. K.; Wong-Palms, S.; Grodzinsky, A. J.; Ortiz, C. Direct Measurement of Glycosaminoglycan Intermolecular Interactions via High Resolution Force Spectroscopy. *Macromolecules* **2002**, *35*, 5601-5615.
9. McNelles, S. A.; Knight, S. D.; Janzen, N.; Valliant, J. F.; Adronov, A. Synthesis, Radiolabeling, and In Vivo Imaging of PEGylated High Generation Polyester Dendrimers. *Biomacromolecules* **2015**, *16*, 3033-3041.
10. Olesen, K. R.; Bassett, D. R.; Wilkerson, C. L. Surfactant Co-Thickening in Model Associative Polymers. *Prog. Org. Coatings* **1998**, *35*, 161-170.
11. Wang, X.; Guerrand, L.; Wu, B.; Li, X.; Boldon, L.; Chen, W.-R.; Liu, L. Characterizations of Polyamidoamine Dendrimers with Scattering Techniques. *Polymers* **2012**, *4*, 600-616.

12. Caminade, A.-M.; Laurent, R.; Majoral, J.-P. Characterization of Dendrimers. *Adv. Drug Delivery Rev.* **2005**, *57*, 2130-2146.
13. Sheiko, S. S.; Möller, M. Visualization of Macromolecules – A First Step to Manipulation and Controlled Response. *Chem. Rev.* **2001**, *101*, 4099-4123.
14. Mathew, A.; Siu, H.; Duhamel, J. A *Blob* Model to Study Chain Folding by Fluorescence. *Macromolecules* **1999**, *32*, 7100-7108.
15. Duhamel, J. Polymer Chain Dynamics in Solution Probed with a Fluorescence Blob Model *Acc. Chem. Res.* **2006**, *39*, 953-960.
16. Duhamel, J. New Insights in the Study of Pyrene Excimer Fluorescence to Characterize Macromolecules and their Supramolecular Assemblies in Solution. *Langmuir* **2012**, *28*, 6527-6538.
17. Duhamel, J. Global Analysis of Fluorescence Decays to Probe the Internal Dynamics of Fluorescently Labeled Macromolecules. *Langmuir* **2014**, *30*, 2307-2324.
18. Winnik, M. A.; Redpath, T.; Richards, D. H. The Dynamics of End-to-End Cyclization in Polystyrene Probed by Pyrene Excimer Formation. *Macromolecules* **1980**, *13*, 328-335.
19. Winnik, M. A. End-to-End Cyclization of Polymer Chains. *Acc. Chem. Res.* **1985**, *18*, 73-79.

20. Farhangi, S.; Duhamel, J. A Pyrenyl Derivative with a Four Atom-Linker that Can Probe the Local Polarity of Pyrene-Labeled Macromolecules. *J. Phys. Chem. B.* **2016**, *120*, 834-842.
21. Farhangi, S.; Weiss, H.; Duhamel, J. Effect of Side-Chain Length on the Polymer Chain Dynamics of Poly (Alkyl Methacrylate)s in Solution. *Macromolecules* **2013**, *46*, 9738-9747.
22. Zaragoza-Galán, G.; Fowler, M.; Duhamel, J.; Rein, R.; Solladié, N.; Rivera, E. Synthesis and Characterization of Novel Pyrene-Dendronized Porphyrins Exhibiting Efficient Fluorescence Resonance Energy Transfer (FRET): Optical and Photophysical Properties. *Langmuir* **2012**, *28*, 11195-11205.
23. Flory, P. J.; Principles of Polymer Chemistry, Cornell University Press, **1953**.
24. De Gennes, P.-G. Scaling Concepts in Polymer Physics, Cornell University Press, **1979**.
25. Kanagalingam, S.; Spartalis, J.; Cao, T.-C.; Duhamel, J. Scaling Relations Related to the Kinetics of Excimer Formation between Pyrene Groups Attached onto Poly(*N,N*-dimethylacrylamide)s. *Macromolecules* **2002**, *35*, 8571-8577.
26. Irondi, K.; Zhang, M.; Duhamel, J. Study of the Semidilute Solutions of Poly(*N,N*-dimethylacrylamide) by Fluorescence and its Implications to the kinetics of Coil-to-Globule Transitions. *J. Phys. Chem. B*, **2006**, *110*, 2628-2637.

Chapter 5

1. Duhamel, J. New Insights in the Study of Pyrene Excimer Fluorescence to Characterize Macromolecules and their Supramolecular Assemblies in Solution. *Langmuir* **2012**, *28*, 6527-6538.
2. Duhamel, J. Global Analysis of Fluorescence Decays to Probe the Internal Dynamics of Fluorescently Labeled Macromolecules. *Langmuir* **2014**, *30*, 2307-2324.
3. Dais, P.; Spyros, A. ¹³C Nuclear Magnetic Relaxation and Local Dynamics of Synthetic Polymers in Dilute Solution and in the Bulk State. *Prog. Nucl. Magn. Res. Spectrosc.* **1995**, *27*, 555-633.
4. Li, J.; Ngai, T.; Wu, C. The Slow Relaxation Mode: From Solutions to Gel Networks. *Polym. J.* **2010**, *42*, 609-625.
5. Viovy, J. L.; Monerie, L. Fluorescence Anisotropy Technique Using Synchrotron Radiation as a Powerful Means for Studying the Orientation Correlation Function of Polymer Chains. *Adv. Polym. Sci.* **1985**, *67*, 99-122.
6. Duhamel, J.; Winnik, M. A.; Baros, F.; André, J.-C.; Martinho, J. M. G. Diffusion Effects on Pyrene Excimer Kinetics : Determination of the Excimer Formation Rate Coefficient Time Dependence. *J. Phys. Chem.* **1992**, *96*, 9805-10.
7. Winnik, M. A. End-to-End Cyclization of Polymer Chains. *Acc. Chem. Res.* **1985**, *18*, 73-79.

8. Duhamel, J. Internal Dynamics of Dendritic Molecules Probed by Pyrene Excimer Formation. *Polymers* **2012**, *4*, 211-239.
9. Duhamel, J. Polymer Chain Dynamics in Solution Probed with a Fluorescence Blob Model. *Acc. Chem. Res.* **2006**, *39*, 953-960.
10. Bains, G. K.; Kim, S. H.; Sorin, E. J.; Narayanaswami, V. The Extent of Pyrene Excimer Fluorescence Emission is a Reflector of Distance and Flexibility: Analysis of the Segment Linking the LDL Receptor-Binding and Tetramerization Domains of Apolipoprotein E3. *Biochemistry* **2012**, *51*, 6207-6219.
11. Mizuguchi, C.; Hata, M.; Dhanasekaran, P.; Nickel, M.; Phillips, M. C.; Lund-Katz, S.; Saito, H. Fluorescence Analysis of the Lipid Binding-Induced Conformational Change of Apolipoprotein E4. *Biochemistry* **2012**, *51*, 5580-5588.
12. Lee, S.; Winnik, M. A. Cyclization Rates for Two Points in the Interior of a Polymer Chain. *Macromolecules* **1997**, *30*, 2633– 2641.
13. Wilken, R.; Adams, J. End-Group Dynamics of Fluorescently Labeled Dendrimers. *Macromol. Rapid Commun.* **1997**, *18*, 659-665.
14. Zachariasse, K. A.; Busse, R.; Duvencek, G.; Kühnle, W. Intramolecular Monomer and Excimer Fluorescence with Dipyranylpropanes: Double-Exponential *versus* Triple-Exponential Decays. *J. Photochem.* **1985**, *28*, 237-253.
15. Siu, H.; Duhamel, J. Comparison of the Association Level of a Hydrophobically Modified Associative Polymer Obtained from an Analysis Based on Two Different Models. *J. Phys. Chem. B* **2005**, *109*, 1770-1780.

16. Fowler, M. A.; Duhamel, J.; Bahun, G. J.; Adronov, A.; Zaragoza-Galán, G.; Rivera, E. Studying Pyrene-Labeled Macromolecules with the Model Free Analysis. *J. Phys. Chem. B* **2012**, *116*, 14689-14699.
17. Yip, J.; Duhamel, J.; Bahun, G.; Adronov, A. A Study of the Branch Ends of a Series of Pyrene-Labeled Dendrimers Based on Pyrene Excimer Formation. *J. Phys. Chem. B* **2010**, *114*, 10254-10265.
18. Farhangi, S.; Weiss, H.; Duhamel, J. Effect of Side-Chain Length on the Polymer Chain Dynamics of Poly(alkyl methacrylate)s in Solution. *Macromolecules* **2013**, *46*, 9738-9747.
19. Ingratta, M.; Mathew, M.; Duhamel, J. How Switching the Substituent of a Pyrene Derivative from a Methyl to a Butyl Affects the Fluorescence Response of Polystyrene Randomly Labeled with Pyrene. *Can. J. Chem.* **2010**, *88*, 217-227.
20. Lu, L.; Duhamel, J. Conformation of Amylose in DMSO Probed by Pyrene Excimer Fluorescence. *In preparation*.
21. Chen, S.; Duhamel, J.; Winnik, M. A. Probing End-to-End Cyclization Beyond Willemski and Fixmann. *J. Phys. Chem. B* **2011**, *115*, 3289-3302.
22. Fowler, M.; Hisko, V.; Henderson, J.; Casier, R.; Li, L.; Thoma, J.; Duhamel, J. DiPyMe in SDS Micelles – Artefacts and their Implications on Micellar Properties. *Langmuir* **2015**, *31*, 11971-11981.
23. Farhangi, S.; Duhamel, J. Probing Side Chain Dynamics of Branched Macromolecules by Pyrene Excimer Fluorescence. *Macromolecules* **2016**, *49*, 353-361.

24. Seixas de Melo, J.; Costa, T.; da G.Miguel, M. ; Lindman, B. ; Schillen, K. Time-Resolved and Steady-State Fluorescence Studies of Hydrophobically Modified Water-Soluble Polymers. *J. Phys. Chem. B* **2003**, *107*, 12605-12621.
25. Birks, J. B. *Photophysics of Aromatic Molecules*; Wiley: New York, **1970**; p 301.

Chapter 6

1. Winnik, F. M.; Photophysics of Preassociated Pyrenes in Aqueous Polymer Solutions and in other Organized Media, *Chem.Rev.* **1993**, *93*, 587-614.
2. Lakowicz, J. R. *Principles of Fluorescence Spectroscopy*; Plenum Press: New York, **1983**.
3. Duhamel, J.; New Insights in the Study of Pyrene Excimer Fluorescence to Characterize Macromolecules and their Supramolecular Assemblies in Solution. *Langmuir* **2012**, *28*, 6527-6538.
4. Farhangi, S., Duhamel, J. A Pyrenyl Derivative with a Four Atom-Linker that Can Probe the Local Polarity of Pyrene-Labeled Macromolecules. *J. Phys. Chem. B.* **2016**, *120*, 834–842.
5. Ingratta, M.; Mathew, M.; Duhamel, J. How Switching the Substituent of a Pyrene Derivative from a Methyl to a Butyl Affects the Fluorescence Response of Polystyrene Randomly Labeled with Pyrene. *Can. J. Chem.* **2010**, *88*, 217-227.
6. Chen, S.; Duhamel, J.; Winnik, M. A. Probing End-to-End Cyclization Beyond Willemski and Fixmann. *J. Phys. Chem. B.* **2011**, *115*, 3289-3302.

7. Farhangi, S.; Duhamel, J. Probing Side Chain Dynamics of Branched Macromolecules by Pyrene Excimer Fluorescence. *Macromolecules* **2016**, *49*, 353–361.
8. Duhamel, J. Polymer Chain Dynamics in Solution Probed with a Fluorescence Blob Model *Acc. Chem. Res.* **2006**, *39*, 953-960.
9. Farhangi, S.; Weiss, H.; Duhamel, J. Effect of Side-Chain Length on the Polymer Chain Dynamics of Poly (alkyl methacrylate) s in Solution. *Macromolecules* **2013**, *46*, 9738-9747.
10. Fowler, M. A., Duhamel, J., Bahun, G. J., Adronov, A., Zaragoza-Galán, G., & Rivera, E. Studying Pyrene-Labeled Macromolecules with the Model-Free Analysis. *J. Phy. Chem. B.* **2012**, *116*, 4689-14699.
11. Chen, S.; Duhamel, J.; Bahun, G.; Adronov, A. Effect of Fluorescent Impurities in the Study of Pyrene-Labeled Macromolecules by Fluorescence. *J. Phys. Chem. B.* **2011**, *115*, 9921–9929.
12. Zaragoza-Galán, G., Fowler, M., Rein, R., Solladié, N., Duhamel, J., & Rivera, E. Fluorescence Resonance Energy Transfer in Partially and Fully Labeled Pyrene Dendronized Porphyrins Studied with Model Free Aanalysis. *J. Phys. Chem. C.* **2014**, *118*, 8280-8294.

Appendix SI3

1. Lakowicz, J. R. *Principles of Fluorescence Spectroscopy*; 2nd Ed. Kluwer Academic/Plenum Publishers NY, **1999**.

Appendix SI4

1. Duhamel, J. Polymer Chain Dynamics in Solution Probed with a Fluorescence Blob Model *Acc. Chem. Res.*, **2006**, *39*, 953-960.
2. Duhamel, J. New Insights in the Study of Pyrene Excimer Fluorescence to Characterize Macromolecules and their Supramolecular Assemblies in Solution. *Langmuir* **2012**, *28*, 6527-6538.
3. Duhamel, J. Global Analysis of Fluorescence Decays to Probe the Internal Dynamics of Fluorescently Labeled Macromolecules. *Langmuir* **2014**, *30*, 2307-2324.
4. Farhangi, S.; Duhamel, J. A Pyrenyl Derivative with a Four Atom-Linker that Can Probe the Local Polarity of Pyrene-Labeled Macromolecules. *J. Phys. Chem. B* **2016**, *120*, 834-842.
5. Farhangi, S.; Weiss, H.; Duhamel, J. Effect of Side-Chain Length on the Polymer Chain Dynamics of Poly(Alkyl Methacrylate)s in Solution. *Macromolecules* **2013**, *46*, 9738-9747.

Appendix SI5

1. Siu, H.; Duhamel, J. Comparison of the Association Level of a Hydrophobically Modified Associative Polymer Obtained from an Analysis Based on Two Different Models. *J. Phys. Chem. B* **2005**, *109*, 1770-1780.
2. Yip, J.; Duhamel, J.; Bahun, G.; Adronov, A. A Study of the Branch Ends of a Series of Pyrene-Labeled Dendrimers Based on Pyrene Excimer Formation. *J. Phys. Chem. B* **2010**, *114*, 10254-10265.

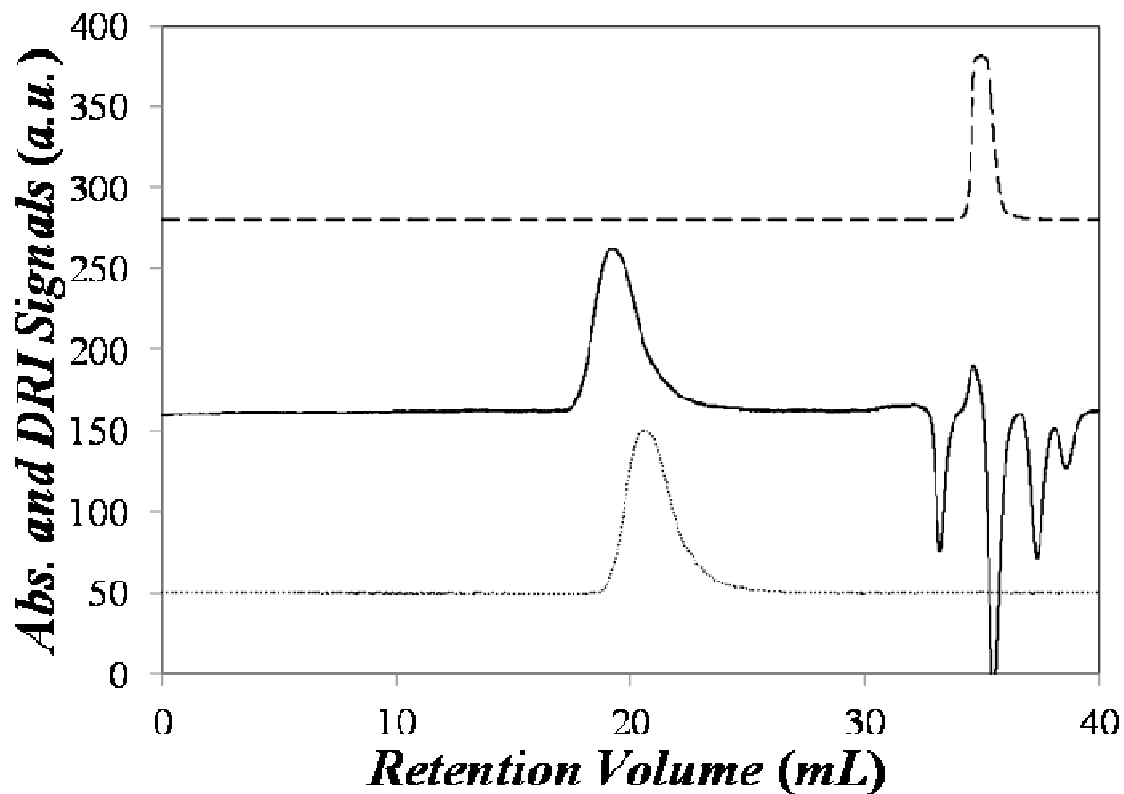
3. Duhamel, J. Internal Dynamics of Dendritic Molecules Probed by Pyrene Excimer Formation. *Polymers* **2012**, *4*, 211-239.
4. Duhamel, J. New Insights in the Study of Pyrene Excimer Fluorescence to Characterize Macromolecules and their Supramolecular Assemblies in Solution. *Langmuir* **2012**, *28*, 6527-6538.

Appendices

Appendix SI2- Supporting Information for Chapter 2: Effect of Side-Chain Length on the Polymer Chain Dynamics of Poly(alkyl methacrylate)s in Solution.

Molecular weight determination: The molecular weight and polydispersity index (PDI) of the polymer samples were determined by gel permeation chromatography (GPC) with a Viscotek instrument equipped with a differential refractive index (DRI), viscosity, light scattering, and UV-Vis absorption detector. Samples concentrations were kept below 0.5 mg/mL and reagent-grade tetrahydrofuran (THF from Aldrich) was used as solvent. The GPC sample was filtered through a filter having 0.2 μm pore size from Membrane Solutions. The GPC instrument ran at room temperature with THF solvent as the eluent with a flow rate of 1mL/min. Typical gel permeation chromatograms are shown in Figure SI2.1. The top trace in Figure SI2.1 describes the elution of 1-pyrenebutylmethacrylate probed by the UV-Vis absorption detector. Under the operating condition of the GPC used to collect the traces in Figure SI2.1, the fluorescent monomer elutes at 35 mL. The middle trace represents the elution of the sample of poly(*n*-butyl methacrylate) randomly labeled with 5.3 mol% pyrene (Py(5.3)-PC4MA) as it passes through the DRI detector. The main peaks eluting a 20 mL corresponds to the polymer while the solution signal at 35 mL represents the solvent peak where small molecules elute. The bottom trace shows the elution of the Py(5.3)-PC4MA sample through the UV-Vis absorption detector. The polymer elutes at 21 mL, 1 mL later than for the DRI detector to account for the delay between the two

detectors mounted in series. No signal around 35 mL where 1-pyrenebutylmethacrylate elutes could be detected in the bottom trace demonstrating the absence of the polymerized fluorescently labeled monomer in the Py(5.3)-PC4MA sample.



Figure

SI2.1: GPC analysis (Top) 1-pyrenebutylmethacrylate with a UV-Vis absorption detector; Py (5.3)-PC4MA with (Middle) DRI detector and (bottom) UV-Vis absorption detector. THF was used as elution solvent.

The absolute molecular weight of the samples was calculated by the software provided with the GPC instrument. Figures SI2.2 show the DRI and UV-Vis absorption detector signal for a representative sample of each series of the pyrene-labeled poly(alkyl methacrylate)s and poly(methyl acrylate) prepared in this study. From sample to sample, differences in the position of the solvent peak in the DRI trace can be observed. These changes in position are due to changes of the GPC columns that needed to be replaced over the two years that this study was conducted.

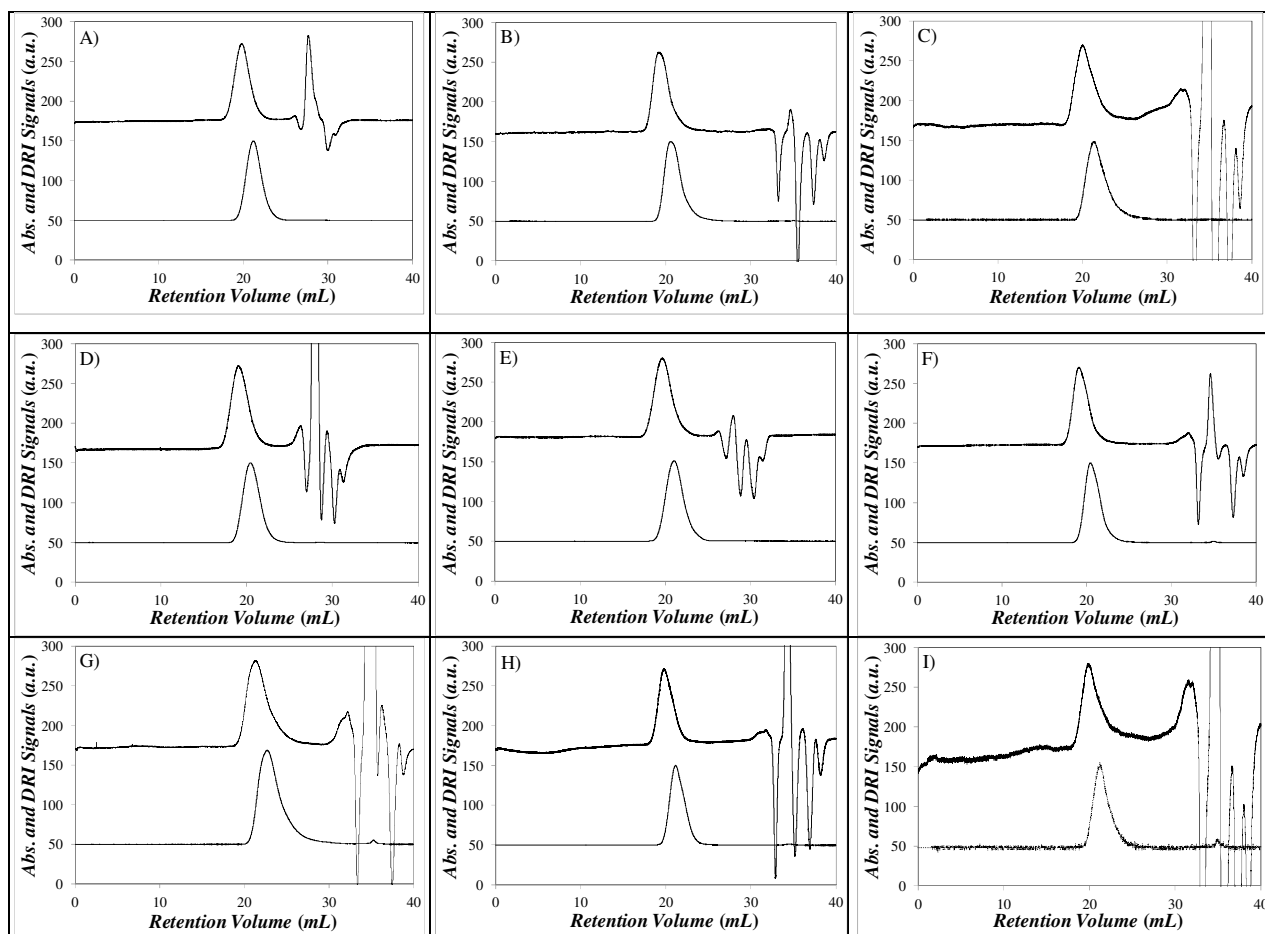


Figure SI2.2: GPC analysis conducted with DRI (top) and UV-Vis absorption (bottom) detector for (A) Py(4.0)-PC1MA, (B) Py(5.3)-PC4MA, (C) Py(6.6)-PC6MA, (D) Py(7.3)-PC8MA, (E) Py(5.6)-PC12MA, (F) Py(6.7)-PC18MA, (G) Py(5.0)-PC1A, (H) Py(3.6)-PC4TMA, and (I) Py(6.2)-PC6CyMA. Mn and PDIs of all pyrene-labeled samples are listed in Table 2.1.

¹HNMR characterization of the copolymers: To lessen the composition drift caused by a possible difference in the reactivity ratios, the copolymerization was conducted up to maximum conversion of 0.2. ¹HNMR was used to determine the degree of conversion. A small sample was taken from the reaction mixture at different time intervals for ¹HNMR analysis in order to monitor the reduction of the monomer signal being paralleled by an increase of the signal corresponding to the copolymer. The NMR tube contained the reaction mixture in toluene to which CDCl₃ was added. This explains why the alignment of the NMR signals is not perfect between the middle spectrum of the reaction mixtures and the top and bottom spectra obtained in pure CDCl₃. Examples of conversion calculation and representative ¹HNMR spectra for each copolymer series are shown in Table SI2.1 and Figure SI2.3-11 respectively.

Table SI2.1: Calculation example of monomer conversions from ^1H NMR spectra shown in Figures SI2.3-11.

Polymer Type	Eq. 1 used to determine Conv%	Eq. 2 used to determine Conv%	^1H NMR Spectrum	Conv% (Eq. 1)	Conv% (Eq. 2)
Py-PC1MA	$\%Conv = \frac{\frac{B}{3}}{\frac{B}{3} + a} \times 100$	$\%Conv = \frac{C}{C + c} \times 100$	Fig.SI.3	13.3	15.0
Py-PC4MA	$\%Conv = \frac{\frac{E+e}{2} - a}{\frac{E+e}{2}} \times 100$	$\%Conv = \frac{C}{C + c} \times 100$	Fig.SI2.4	14.4	14.4
Py-PC6MA	$\%Conv = \frac{\frac{E+e}{6} - a}{\frac{E+e}{6}} \times 100$	$\%Conv = \frac{C}{C + c} \times 100$	Fig.SI2.5	18.2	15.8
Py-PC8MA	$\%Conv = \frac{\frac{E+e}{10} - a}{\frac{E+e}{10}} \times 100$	$\%Conv = \frac{C}{C + c} \times 100$	Fig.SI2.6	18.0	12.7
Py-PC12MA	$\%Conv = \frac{\frac{E+e}{18} - a}{\frac{E+e}{18}} \times 100$	$\%Conv = \frac{C}{C + c} \times 100$	Fig.SI2.7	18.0	15.1
Py-PC18MA	$\%Conv = \frac{\frac{E+e}{30} - a}{\frac{E+e}{30}} \times 100$	$\%Conv = \frac{C}{C + c} \times 100$	Fig.SI2.8	18.6	17.1
Py-PC1A	$\%Conv = \frac{\frac{A}{2}}{\frac{A}{2} + \frac{c}{3}} \times 100$	$\%Conv = \frac{C}{C + c} \times 100$	Fig.SI2.9	13.3	19.0

Py-PC4TMA	$\%Conv = \frac{\frac{B}{3}}{\frac{B}{3} + a} \times 100$	$\%Conv = \frac{\frac{C+c}{9} - a}{\frac{C+c}{9}} \times 100$	Fig.SI2.10	13.3	15.7
Py-PCy6MA	$\%Conv = \frac{\frac{B}{3}}{\frac{B}{3} + a} \times 100$	$\%Conv = \frac{C}{C+c} \times 100$	Fig.SI2.11	12.2	15.3

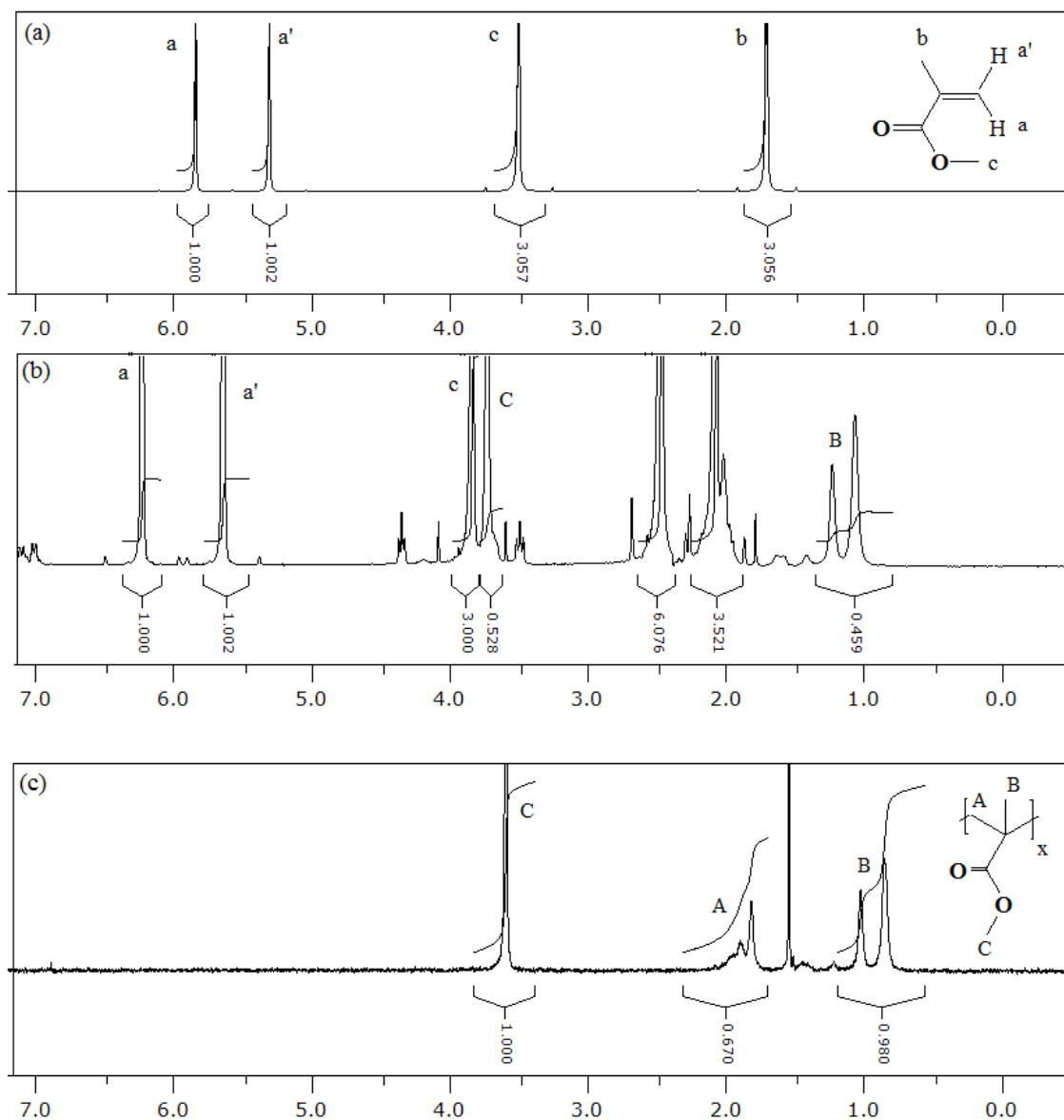


Figure SI2.3: ^1H NMR spectra of (a) the methylmethacrylate monomer, (b) the reaction mixture after polymerization in toluene from which conversion was calculated, and (c) the unlabeled PC1MA polymer. Solvent: CDCl_3

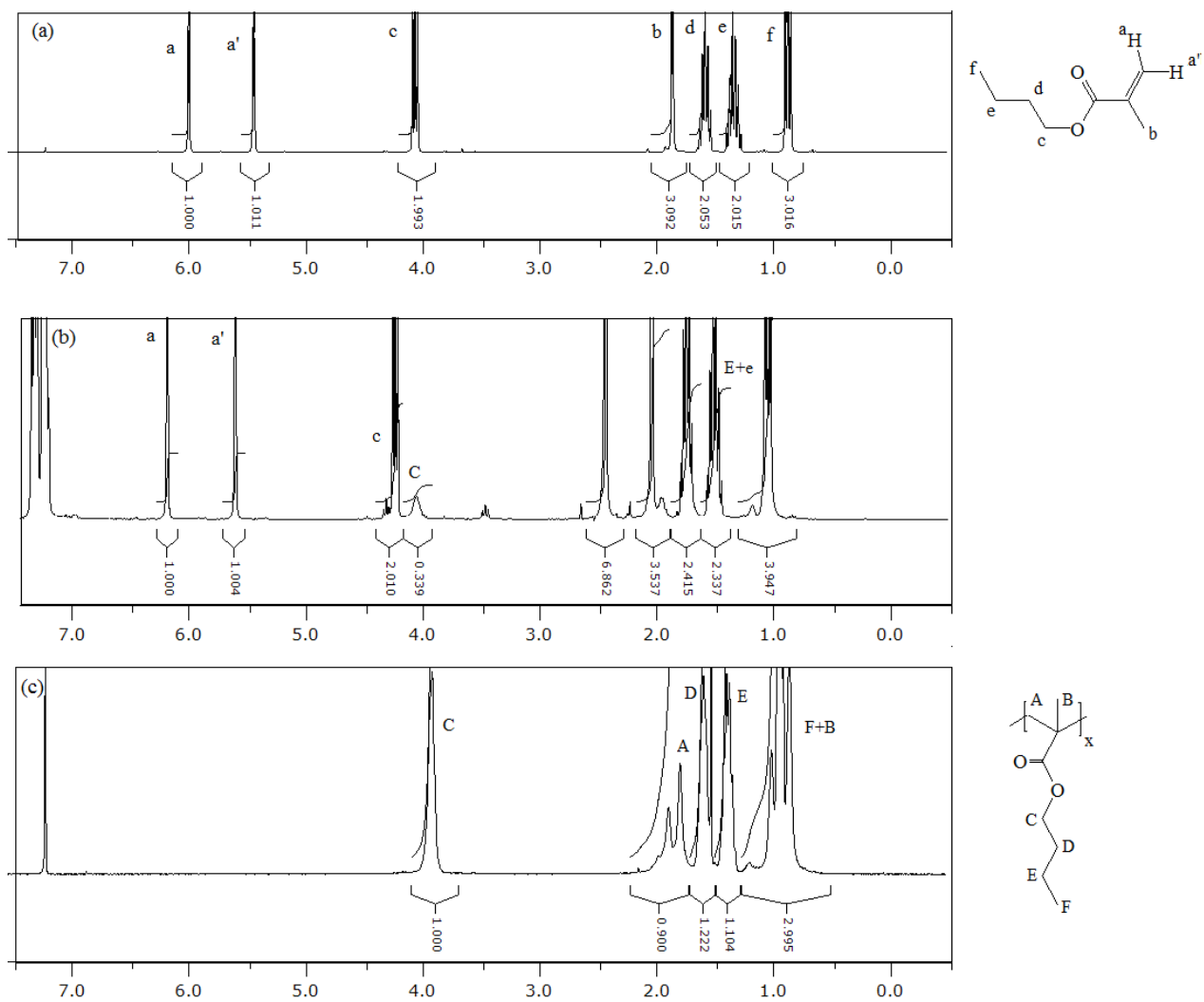


Figure S12.4: ^1H NMR spectra of (a) the butylmethacrylate monomer, (b) the reaction mixture after polymerization in toluene from which conversion was calculated, and (c) the unlabeled PC4MA polymer. Solvent: CDCl_3

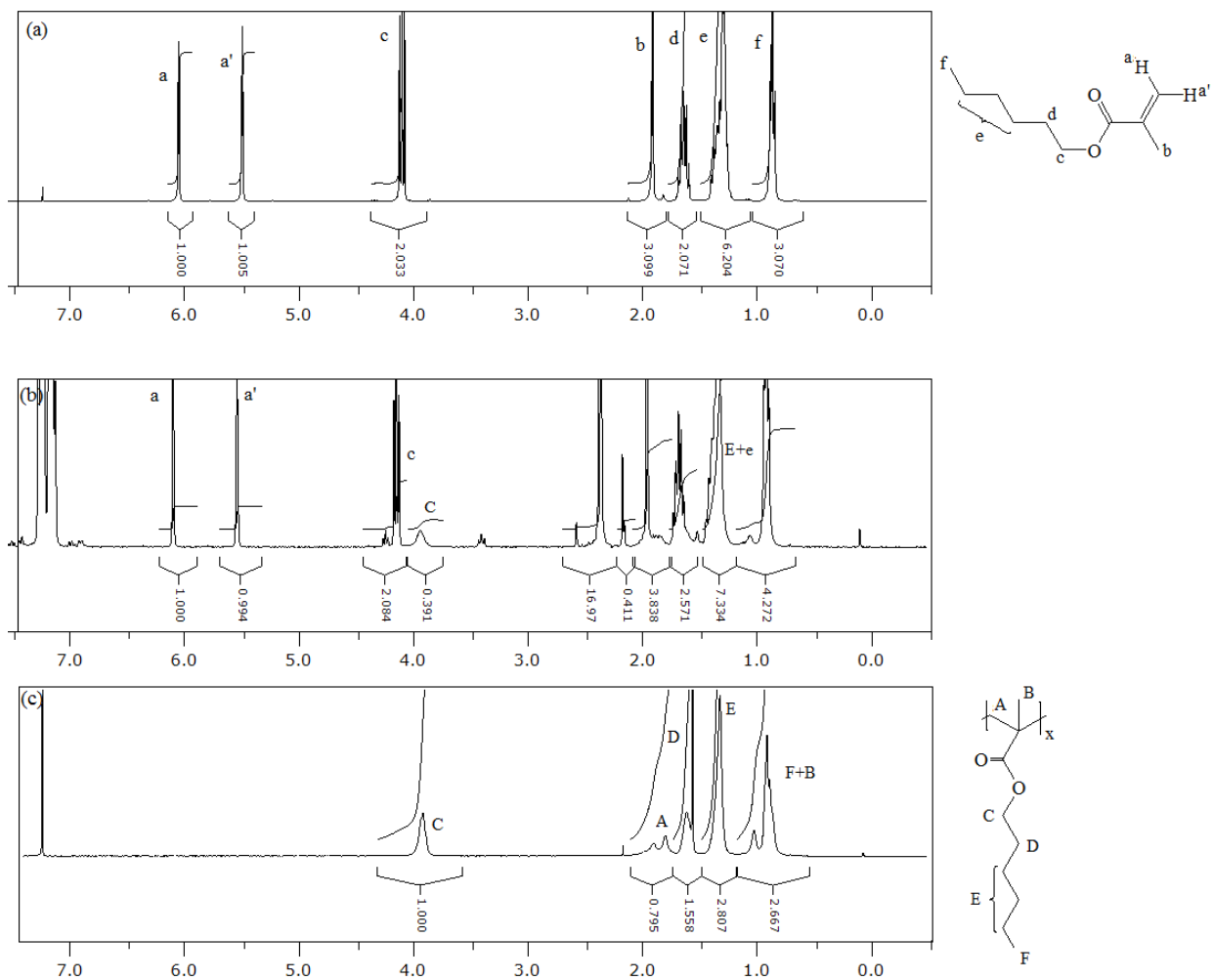


Figure SI2.5: ^1H NMR spectra of (a) the hexylmethacrylate monomer, (b) the reaction mixture after polymerization in toluene from which conversion was calculated, and (c) the unlabeled PC6MA polymer. Solvent: CDCl_3

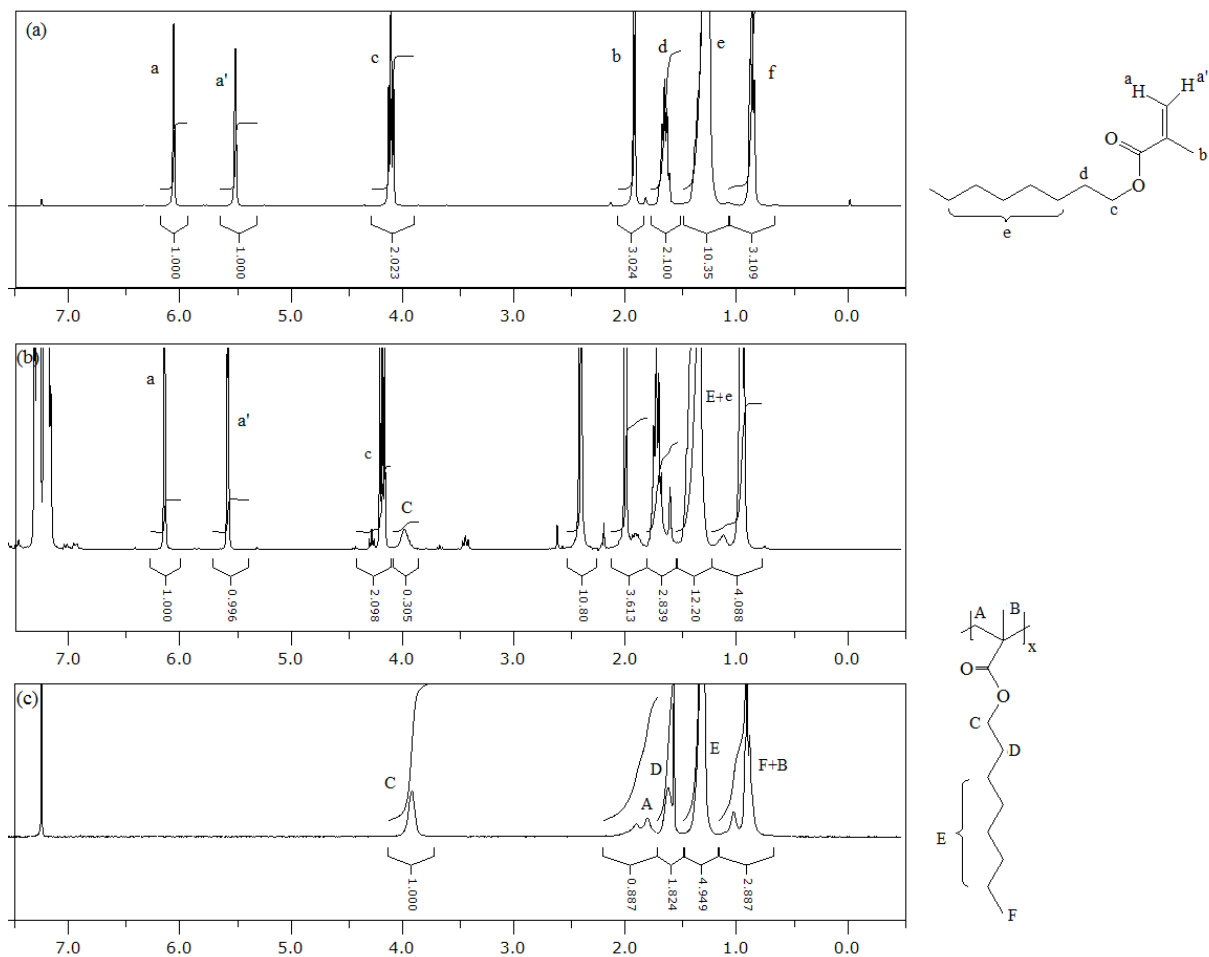


Figure S12.6: ^1H NMR spectra of (a) the octylmethacrylate monomer, (b) the reaction mixture after polymerization in toluene from which conversion was calculated, and (c) the unlabeled PC8MA polymer. Solvent: CDCl_3

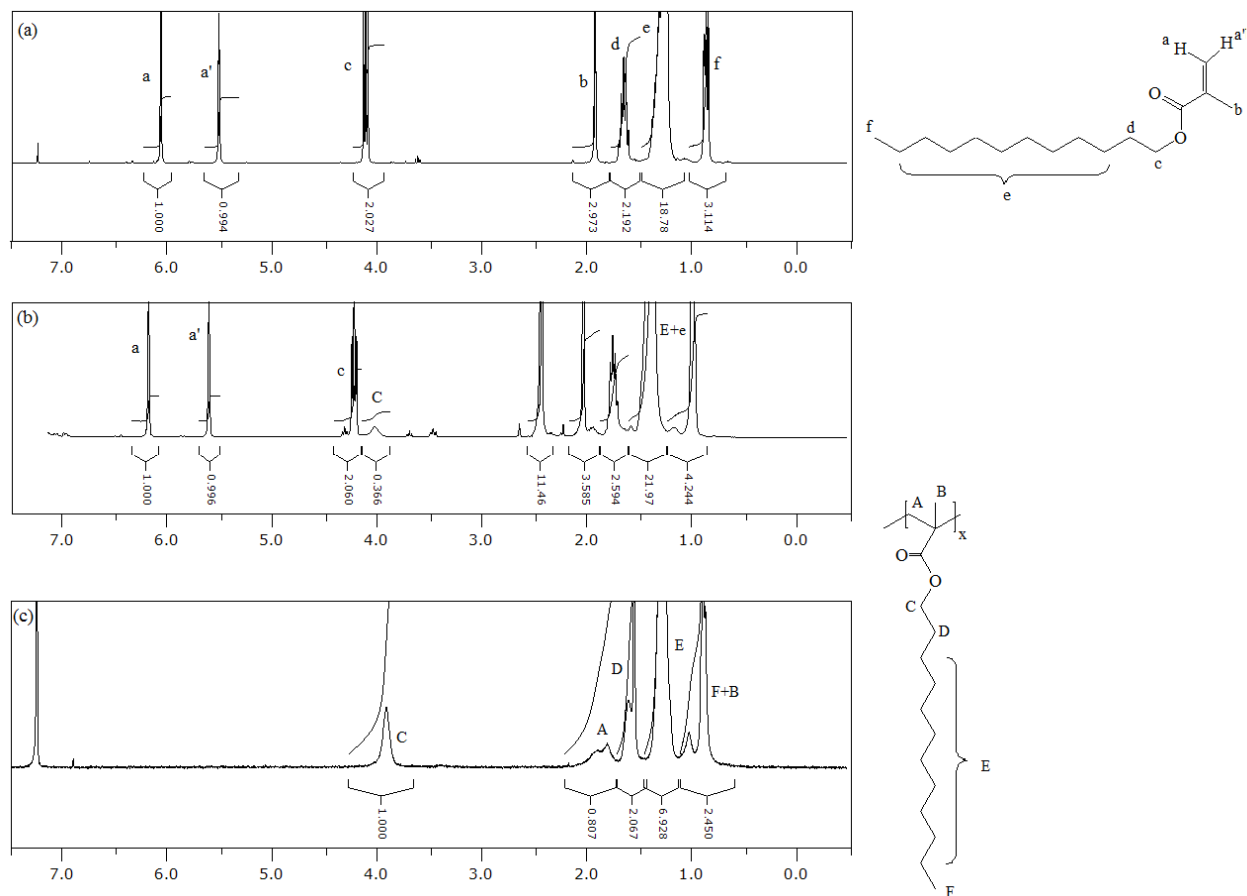


Figure SI2.7: ^1H NMR spectra of (a) the laurylmethacrylate monomer, (b) the reaction mixture after polymerization in toluene from which conversion was calculated, and (c) the unlabeled PC12MA polymer. Solvent: CDCl_3

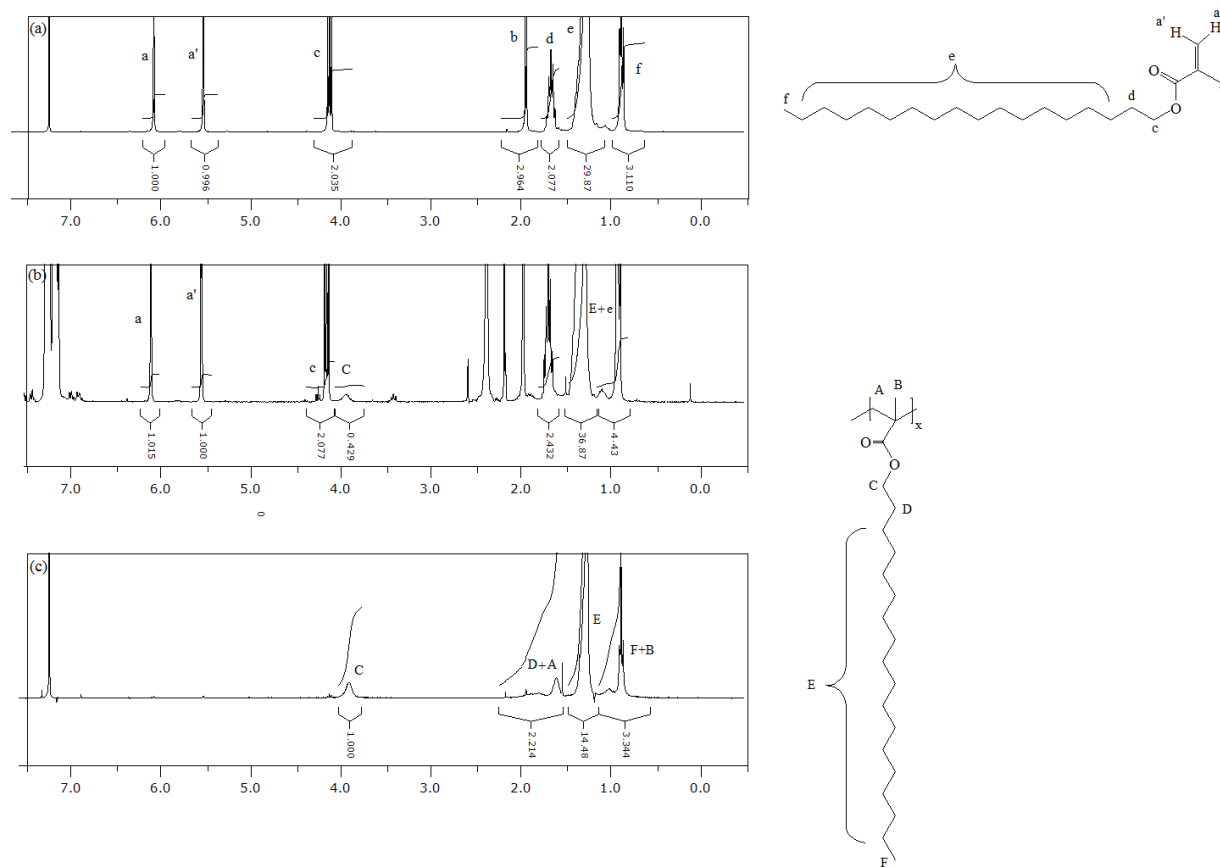


Figure SI2.8: ^1H NMR spectra of (a) the stearylmethacrylate monomer, (b) the reaction mixture after polymerization in toluene from which conversion was calculated, and (c) the unlabeled PC18MA polymer. Solvent: CDCl_3

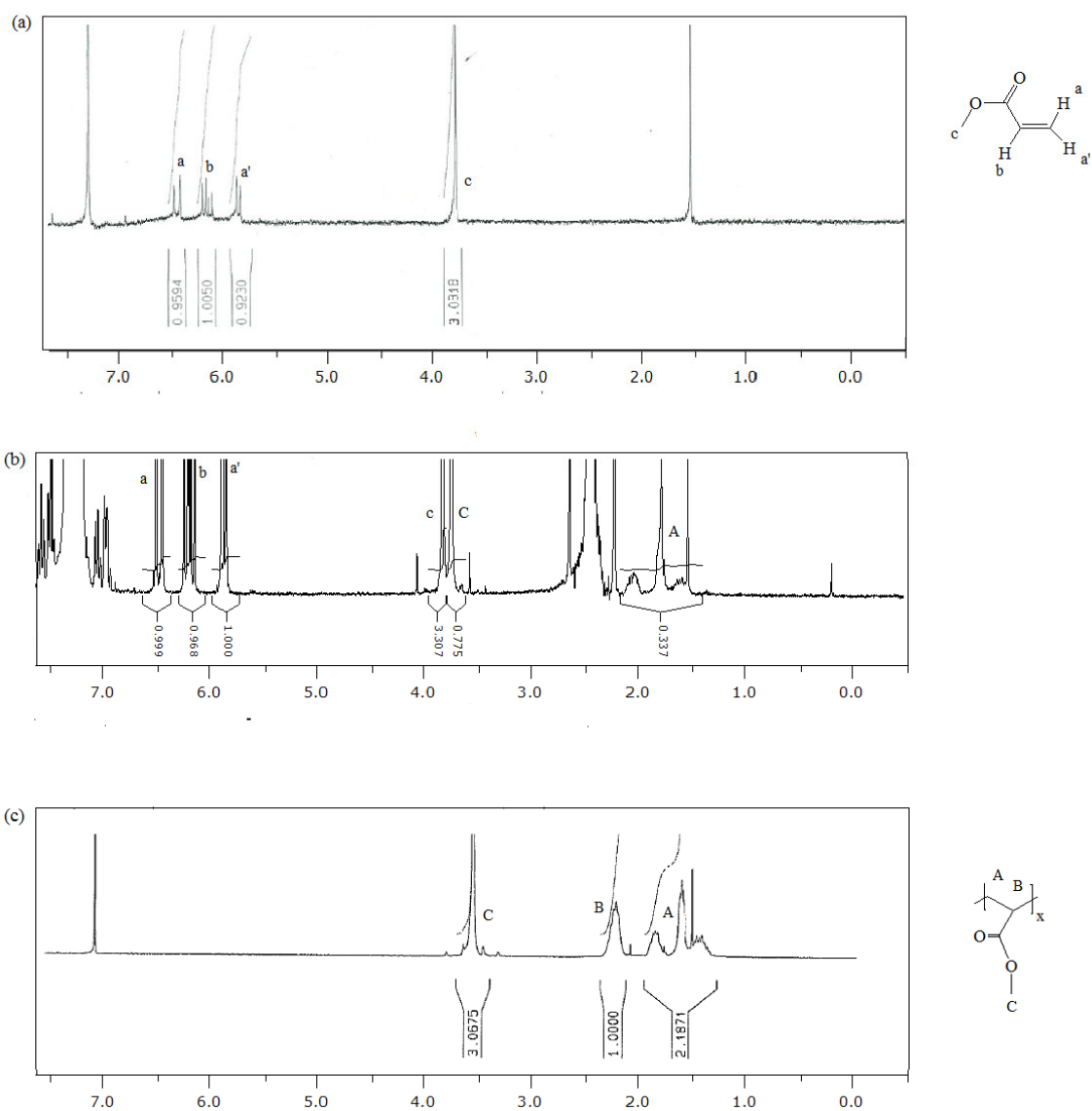


Figure SI2.9: ^1H NMR spectra of (a) the methylacrylate monomer, (b) the reaction mixture after polymerization in toluene from which conversion was calculated, and (c) the unlabeled PC1A polymer. Solvent: CDCl_3

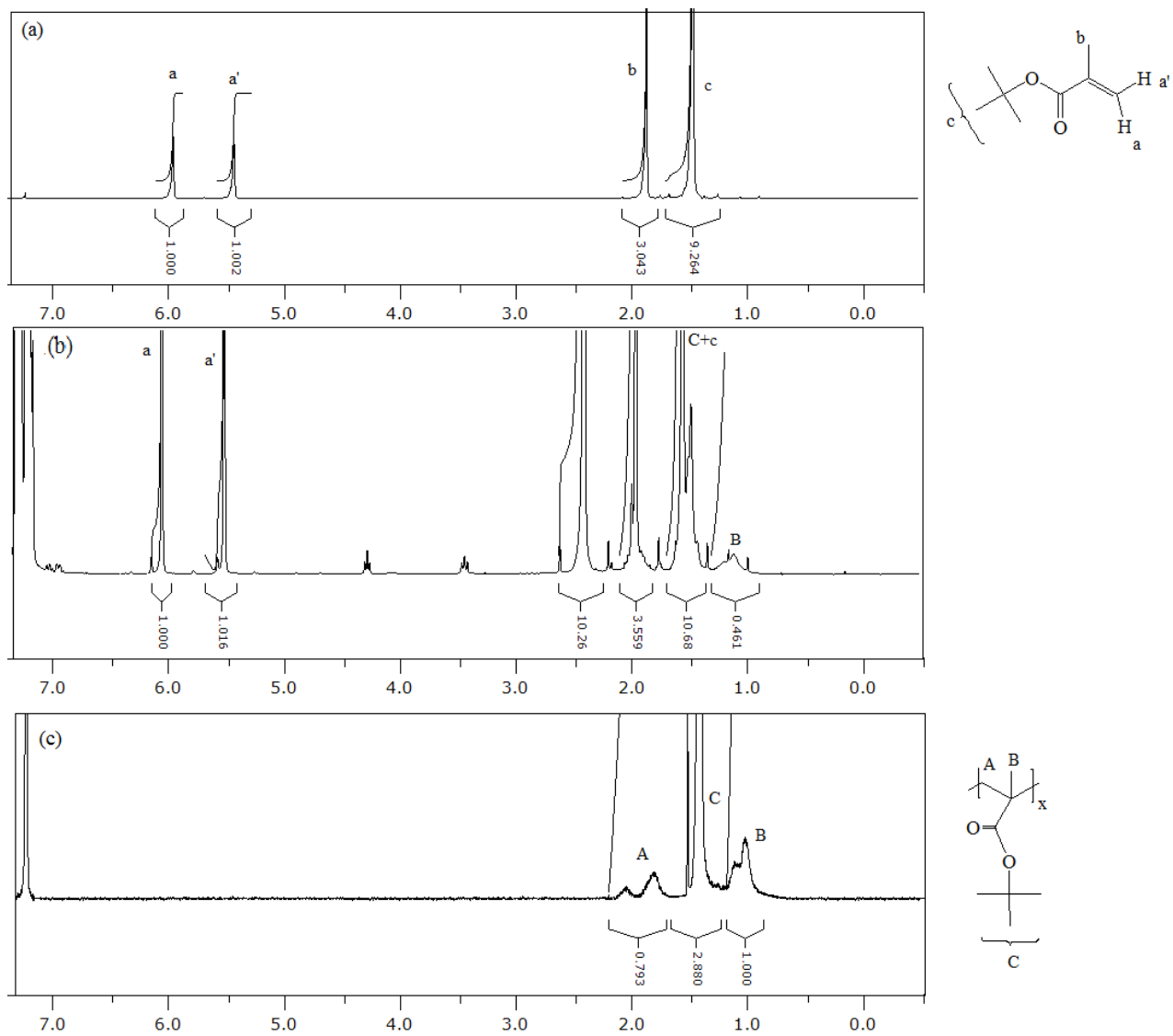


Figure S12.10: ^1H NMR spectra of (a) the tert-butyl methacrylate monomer, (b) the reaction mixture after polymerization in toluene from which conversion was calculated, and (c) the unlabeled PC4TMA polymer. Solvent: CDCl_3

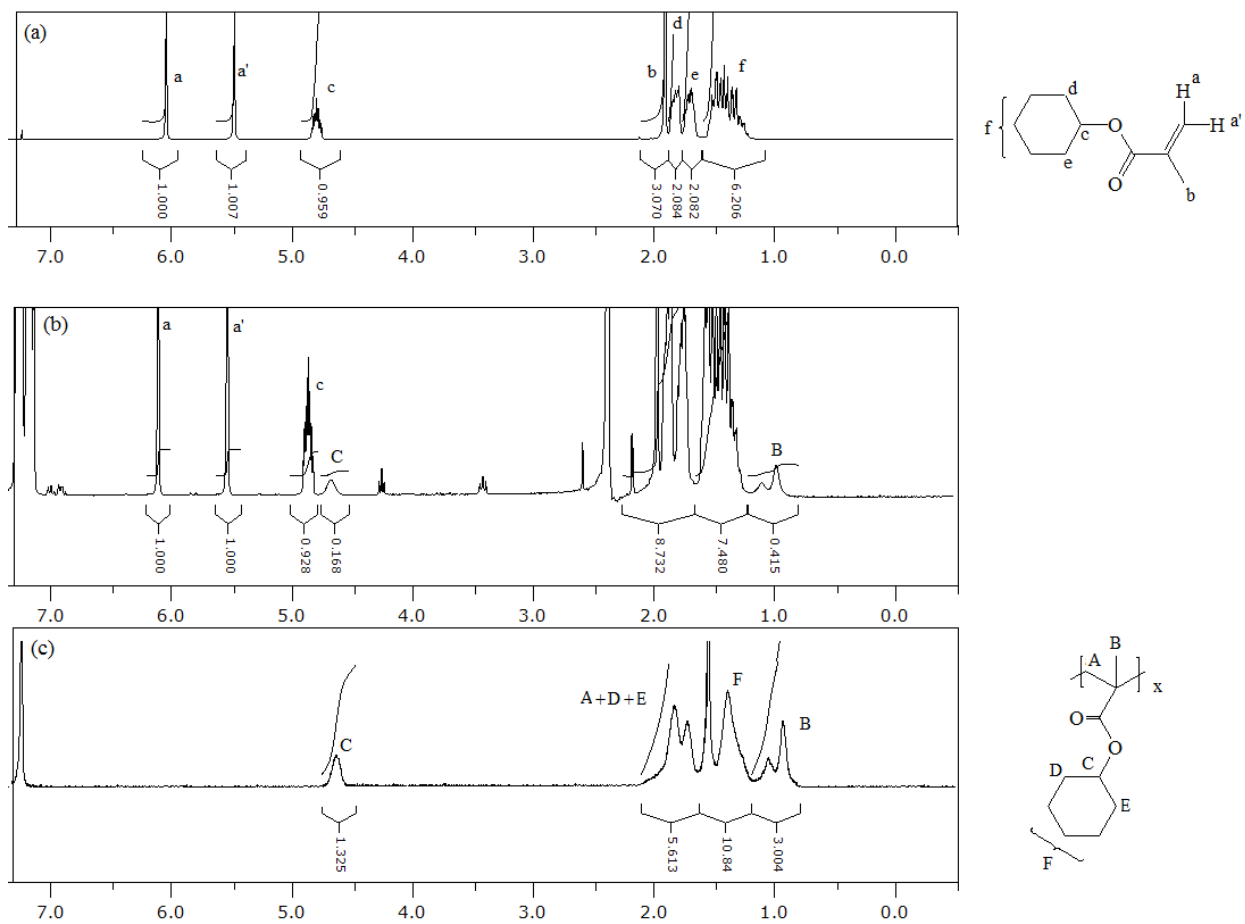


Figure SI2.11: ^1H NMR spectra of (a) the cyclohexyl methacrylate monomer, (b) the reaction mixture after polymerization in toluene from which conversion was calculated, and (c) the unlabeled PC6CyMA polymer. Solvent: CDCl_3

Table SI2.2: Parameters retrieved from the FBM analysis of the monomer decays of the randomly labeled poly(alkyl methacrylate)s and poly(methyl acrylate)s in THF.

Sample	Mol%	k_{blob} (10^7s^{-1})	$\langle n \rangle$	$k_e[\text{blob}]$ (10^7s^{-1})	f_{Mdiff}	k_2 (ns^{-1})	f_{k_2}	τ_{M} (ns)	f_{Mfree}	χ^2
Py-PC1MA	1.2	0.68 (± 0.04)	0.90 (± 0.03)	0.50 (± 0.04)	0.73 (± 0.01)	0.13	0.08 (± 0.01)	195	0.20 (± 0.01)	1.1
	2.6	0.70 (± 0.03)	1.64 (± 0.05)	0.47 (± 0.02)	0.79 (± 0.01)	0.13	0.18 (± 0.00)	195	0.02 (± 0.00)	1.0
	4.0	0.75 (± 0.02)	2.3 (± 0.1)	0.52 (± 0.01)	0.75 (± 0.00)	0.13	0.23 (± 0.00)	195	0.02 (± 0.00)	1.0
	5.2	0.78 (± 0.02)	2.8 (± 0.1)	0.44 (± 0.02)	0.68 (± 0.01)	0.13	0.30 (± 0.00)	195	0.01 (± 0.00)	1.1
	5.3	0.65 (± 0.02)	3.6 (± 0.0)	0.41 (± 0.03)	0.65 (± 0.01)	0.13	0.33 (± 0.00)	195	0.01 (± 0.00)	1.1
	5.6	0.62 (± 0.01)	3.6 (± 0.1)	0.35 (± 0.03)	0.65 (± 0.01)	0.13	0.34 (± 0.00)	195	0.00 (± 0.00)	1.0
	7.2	0.64 (± 0.02)	4.4 (± 0.1)	0.26 (± 0.03)	0.56 (± 0.00)	0.13	0.41 (± 0.00)	195	0.03 (± 0.00)	1.1
Py-PC4MA	1.1	0.66 (± 0.09)	0.78 (± 0.08)	0.63 (± 0.04)	0.50 (± 0.01)	0.12	0.06 (± 0.01)	195	0.44 (± 0.01)	1.1
	2.2	0.64 (± 0.03)	1.0 (± 0.0)	0.51 (± 0.02)	0.73 (± 0.01)	0.12	0.12 (± 0.00)	195	0.15 (± 0.01)	1.1
	3.0	0.64 (± 0.03)	1.5 (± 0.0)	0.61 (± 0.02)	0.72 (± 0.01)	0.12	0.12 (± 0.04)	195	0.11 (± 0.01)	0.9
	3.6	0.63 (± 0.03)	2.0 (± 0.1)	0.46 (± 0.04)	0.70 (± 0.01)	0.12	0.23 (± 0.00)	195	0.07 (± 0.00)	1.0
	5.3	0.64 (± 0.03)	2.2 (± 0.1)	0.47 (± 0.02)	0.72 (± 0.01)	0.12	0.26 (± 0.00)	195	0.01 (± 0.00)	1.1
	7.2	0.66 (± 0.02)	3.2 (± 0.1)	0.54 (± 0.03)	0.60 (± 0.01)	0.12	0.38 (± 0.00)	195	0.01 (± 0.00)	1.1
Py-PC6MA	2.0	0.70 (± 0.05)	0.9 (± 0.0)	0.49 (± 0.01)	0.69 (± 0.04)	0.13	0.12 (± 0.01)	204	0.18 (± 0.06)	1.0
	3.3	0.71 (± 0.04)	1.0 (± 0.04)	0.52 (± 0.01)	0.76 (± 0.01)	0.13	0.15 (± 0.00)	204	0.08 (± 0.00)	1.0
	4.7	0.69 (± 0.04)	1.4 (± 0.1)	0.50 (± 0.03)	0.74 (± 0.01)	0.13	0.18 (± 0.00)	204	0.07 (± 0.00)	1.1
	5.8	0.75 (± 0.04)	1.7 (± 0.1)	0.60 (± 0.01)	0.70 (± 0.00)	0.13	0.23 (± 0.00)	204	0.07 (± 0.00)	1.2

	6.6	0.77 (±0.00)	2.0 (±0.1)	0.65 (±0.03)	0.67 (±0.00)	0.13	0.28 (±0.00)	204	0.05 (±0.00)	1.1
	8.1	0.79 (±0.02)	2.3 (±0.04)	0.63 (±0.01)	0.66 (±0.00)	0.13	0.33 (±0.00)	204	0.00 (±0.00)	1.1
Py-PC8MA	1.8	0.60 (±0.01)	0.86 (±0.20)	0.46 (±0.05)	0.57 (±0.01)	0.10	0.1 (±0.01)	200	0.31 (±0.01)	1.0
	2.7	0.51 (±0.06)	1.0 (±0.1)	0.48 (±0.07)	0.69 (±0.01)	0.10	0.13 (±0.00)	200	0.18 (±0.01)	1.1
	4.3	0.71 (±0.05)	1.1 (±0.1)	0.50 (±0.03)	0.66 (±0.00)	0.10	0.19 (±0.00)	200	0.15 (±0.00)	1.0
	5.1	0.55 (±0.07)	1.5 (±0.1)	0.51 (±0.06)	0.73 (±0.00)	0.10	0.22 (±0.01)	200	0.05 (±0.00)	1.0
	6.1	0.81 (±0.00)	1.4 (±0.06)	0.71 (±0.00)	0.71 (±0.00)	0.10	0.25 (±0.00)	200	0.03 (±0.00)	1.0
	7.3	0.56 (±0.02)	2.4 (±0.1)	0.34 (±0.02)	0.65 (±0.00)	0.10	0.34 (±0.00)	200	0.01 (±0.00)	1.1
Py-PC12MA	1.4	0.88 (±0.14)	0.60 (±0.07)	0.6 (±0.04)	0.33 (±0.01)	0.09	0.08 (±0.05)	200	0.60 (±0.01)	1.0
	3.5	0.55 (±0.07)	0.99 (±0.06)	0.47 (±0.06)	0.66 (±0.01)	0.09	0.14 (±0.00)	200	0.19 (±0.00)	1.1
	5.6	0.53 (±0.03)	1.4 (±0.1)	0.38 (±0.05)	0.72 (±0.01)	0.09	0.22 (±0.00)	200	0.05 (±0.02)	1.0
	6.0	0.54 (±0.03)	1.6 (±0.1)	0.44 (±0.03)	0.70 (±0.02)	0.09	0.26 (±0.01)	200	0.02 (±0.00)	1.0
	7.7	0.59 (±0.03)	1.7 (±0.0)	0.39 (±0.02)	0.66 (±0.06)	0.09	0.29 (±0.00)	200	0.03 (±0.00)	1.0
	10.2	0.49 (±0.02)	2.9 (±0.0)	0.28 (±0.03)	0.58 (±0.00)	0.09	0.41 (±0.00)	200	0.01 (±0.00)	1.1
Py-PC18MA	1.4	1.0 (±0.08)	0.57 (±0.07)	0.75 (±0.02)	0.32 (±0.00)	0.12	0.07 (±0.01)	206	0.61 (±0.01)	1.0
	4.5	0.77 (±0.05)	0.88 (±0.03)	0.52 (±0.01)	0.66 (±0.01)	0.12	0.16 (±0.01)	206	0.18 (±0.00)	1.1
	5.8	0.92 (±0.05)	1.0 (±0.0)	0.56 (±0.00)	0.64 (±0.01)	0.12	0.23 (±0.00)	206	0.12 (±0.01)	1.1
	6.7	0.88 (±0.02)	1.1 (±0.0)	0.54 (±0.01)	0.69 (±0.00)	0.12	0.25 (±0.00)	206	0.06 (±0.00)	1.0
	6.8	0.82 (±0.00)	1.2 (±0.0)	0.51 (±0.00)	0.68 (±0.00)	0.12	0.24 (±0.00)	206	0.07 (±0.00)	1.0
	14.1	0.78 (±0.02)	2.7 (±0.1)	0.39 (±0.02)	0.50 (±0.00)	0.12	0.48 (±0.00)	206	0.02 (±0.00)	1.2

Py-PC1A	1.7	1.30 (±0.04)	1.1 (±0.1)	0.58 (±0.02)	0.75 (±0.01)	0.17	0.18 (±0.00)	190	0.06 (±0.00)	1.1
	2.6	1.10 (±0.03)	2.0 (±0.03)	0.41 (±0.02)	0.63 (±0.02)	0.17	0.31 (±0.00)	190	0.05 (±0.00)	1.1
	2.6	1.30 (±0.02)	1.7 (±0.0)	0.57 (±0.01)	0.68 (±0.00)	0.17	0.29 (±0.00)	190	0.02 (±0.00)	1.2
	3.0	1.40 (±0.03)	1.7 (±0.0)	0.65 (±0.02)	0.64 (±0.01)	0.17	0.27 (±0.00)	190	0.08 (±0.00)	1.1
	5.0	1.50 (±0.03)	3.0 (±0.1)	0.51 (±0.03)	0.47 (±0.03)	0.17	0.51 (±0.01)	190	0.01 (±0.00)	0.9
	6.2	1.50 (±0.04)	3.0 (±0.1)	0.56 (±0.04)	0.45 (±0.00)	0.17	0.51 (±0.00)	190	0.03 (±0.00)	1.2
	6.6	1.40 (±0.05)	3.6 (±0.1)	0.34 (±0.05)	0.35 (±0.00)	0.17	0.63 (±0.01)	190	0.01 (±0.00)	0.9
Py-PC4TMA	2.0	0.80 (±0.07)	0.58 (±0.04)	0.71 (±0.04)	0.72 (±0.01)	0.12	0.10 (±0.00)	207	0.18 (±0.01)	1.1
	3.6	0.66 (±0.03)	0.90 (±0.03)	0.55 (±0.03)	0.76 (±0.01)	0.12	0.15 (±0.00)	207	0.08 (±0.00)	1.0
	3.8	0.73 (±0.04)	1.0 (±0.05)	0.62 (±0.03)	0.76 (±0.00)	0.12	0.18 (±0.00)	207	0.05 (±0.00)	1.2
	4.7	0.71 (±0.02)	1.4 (±0.02)	0.55 (±0.03)	0.74 (±0.00)	0.12	0.24 (±0.00)	207	0.02 (±0.00)	1.0
	5.6	0.66 (±0.06)	1.8 (±0.1)	0.60 (±0.04)	0.67 (±0.00)	0.12	0.31 (±0.00)	207	0.01 (±0.00)	1.1
	7.6	0.88 (±0.03)	2.0 (±0.05)	0.65 (±0.00)	0.64 (±0.00)	0.12	0.35 (±0.00)	207	0.01 (±0.00)	1.0
Py-PCy6MA	2.0	0.64 (±0.07)	0.79 (±0.06)	0.53 (±0.05)	0.56 (±0.01)	0.12	0.95 (±0.02)	205	0.35 (±0.01)	1.1
	3.0	0.80 (±0.02)	0.74 (±0.01)	0.71 (±0.00)	0.76 (±0.00)	0.12	0.12 (±0.01)	205	0.11 (±0.00)	1.1
	3.8	0.74 (±0.05)	1.0 (±0.04)	0.66 (±0.03)	0.77 (±0.00)	0.12	0.16 (±0.00)	205	0.06 (±0.00)	1.0
	5.1	0.80 (±0.04)	1.2 (±0.05)	0.751 (±0.03)	0.73 (±0.01)	0.12	0.22 (±0.00)	205	0.04 (±0.00)	1.1
	6.2	0.72 (±0.04)	1.5 (±0.1)	0.68 (±0.01)	0.71 (±0.01)	0.12	0.26 (±0.00)	205	0.02 (±0.00)	1.1
	7.0	0.81 (±0.04)	1.9 (±0.1)	0.71 (±0.04)	0.65 (±0.05)	0.12	0.33 (±0.03)	205	0.12 (±0.01)	1.2

Table SI2.3: Parameters retrieved from the FBM analysis of the excimer decays of the randomly labeled poly(alkyl methacrylate)s and poly(methyl acrylate)s in THF.

Sample	Mol%	f_{Ediff}	τ_{E0} (ns)	f_{EE0}	τ_{EL} (ns)	f_{EEL}	k_2 (ns ⁻¹)	f_{E}	χ^2
Py-PC1MA	1.2	0.88 (±0.00)	55 (±2)	0.00 (±0.02)	135 (±40)	0.03 (±0.02)	0.13	0.09 (±0.02)	1.1
	2.6	0.80 (±0.00)	53 (±1)	0.00 (±0.01)	117 (±40)	0.02 (±0.01)	0.13	0.18 (±0.00)	1.0
	4.0	0.73 (±0.00)	52 (±1)	0.00 (±0.01)	91 (±10)	0.04 (±0.01)	0.13	0.22 (±0.01)	1.0
	5.2	0.64 (±0.00)	51 (±0)	0.01 (±0.02)	88 (±7)	0.06 (±0.02)	0.13	0.28 (±0.03)	1.1
	5.3	0.63 (±0.00)	51 (±0)	0.00 (±0.02)	84 (±16)	0.04 (±0.02)	0.13	0.32 (±0.01)	1.1
	5.6	0.62 (±0.00)	52 (±1)	0.00 (±0.02)	85 (±22)	0.05 (±0.02)	0.13	0.32 (±0.02)	1.0
	7.2	0.52 (±0.00)	51 (±0)	0.00 (±0.02)	74 (±4)	0.09 (±0.02)	0.13	0.38 (±0.03)	1.1
Py-PC4MA	1.1	0.87 (±0.00)	55 (±3)	0.00 (±0.01)	181 (±26)	0.02 (±0.01)	0.12	0.10 (±0.04)	1.1
	2.2	0.84 (±0.01)	55 (±1)	0.02 (±0.00)	178 (±18)	0.01 (±0.00)	0.12	0.13 (±0.02)	1.1
	3.0	0.76 (±0.04)	54 (±2)	0.03 (±0.01)	156 (±22)	0.01 (±0.02)	0.12	0.17 (±0.01)	0.9
	3.6	0.71 (±0.00)	51 (±1)	0.00 (±0.02)	100 (±27)	0.05 (±0.02)	0.12	0.23 (±0.01)	1.0
	5.3	0.69 (±0.00)	52 (±1)	0.00 (±0.01)	95 (±15)	0.05 (±0.02)	0.12	0.25 (±0.01)	1.1
	7.2	0.57 (±0.01)	50 (±0)	0.00 (±0.02)	83 (±12)	0.07 (±0.02)	0.12	0.36 (±0.02)	1.1
Py-PC6MA	2.0	0.82 (±0.00)	58 (±2)	0.01 (±0.01)	150 (±9)	0.02 (±0.01)	0.13	0.13 (±0.02)	1.0

	3.3	0.80 (±0.00)	57 (±1)	0.00 (±0.01)	112 (±18)	0.04 (±0.01)	0.13	0.16 (±0.01)	1.0
	4.7	0.76 (±0.01)	54 (±2)	0.00 (±0.02)	107 (±35)	0.04 (±0.02)	0.13	0.19 (±0.01)	1.1
	5.8	0.72 (±0.00)	54 (±1)	0.00 (±0.00)	110 (±5)	0.04 (±0.01)	0.13	0.23 (±0.00)	1.2
	6.6	0.67 (±0.00)	54 (±1)	0.00 (±0.01)	102 (±20)	0.04 (±0.01)	0.13	0.28 (±0.00)	1.1
	8.1	0.63 (±0.00)	54 (±0.4)	0.01 (±0.00)	100 (±2)	0.04 (±0.01)	0.13	0.32 (±0.01)	1.1
Py-PC8MA	1.8	0.81 (±0.01)	54 (±2)	0.00 (±0.01)	167 (±30)	0.02 (±0.01)	0.10	0.16 (±0.06)	1.0
	2.7	0.82 (±0.00)	53 (±3)	0.00 (±0.01)	147 (±71)	0.02 (±0.01)	0.10	0.15 (±0.02)	1.1
	4.3	0.748 (±0.02)	54 (±1.5)	0.01 (±0.00)	118 (±14)	0.04 (±0.02)	0.10	0.21 (±0.01)	1.0
	5.1	0.74 (±0.00)	51 (±2)	0.0 (±0.02)	113 (±26)	0.04 (±0.02)	0.10	0.2 (±0.01)	1.0
	6.1	0.67 (±0.01)	56 (±1)	0.06 (±0.04)	107 (±18)	0.01 (±0.05)	0.10	0.24 (±0.02)	1.0
	7.3	0.57 (±0.00)	52 (±1)	0.00 (±0.01)	89 (±2)	0.13 (±0.01)	0.10	0.30 (±0.04)	1.1
Py-PC12MA	1.4	0.77 (±0.01)	65 (±5)	0.00 (±0.01)	184 (±16)	0.04 (±0.02)	0.09	0.17 (±0.05)	1.0
	3.5	0.79 (±0.05)	54 (±2)	0.03 (±0.01)	157 (±40)	0.02 (±0.01)	0.09	0.16 (±0.02)	1.1
	5.6	0.72 (±0.00)	51 (±1.4)	0.00 (±0.01)	120 (±24)	0.05 (±0.01)	0.09	0.22 (±0.00)	1.0
	6.0	0.68 (±0.01)	50 (±0)	0.00 (±0.01)	94 (±8)	0.05 (±0.01)	0.09	0.26 (±0.01)	1.0
	7.7	0.62 (±0.01)	51 (±1)	0.00 (±0.00)	96 (±1)	0.09 (±0.01)	0.09	0.28 (±0.01)	1.0
	10.2	0.52 (±0.00)	50 (±1)	0.00 (±0.02)	89 (±5)	0.10 (±0.02)	0.09	0.37 (±0.04)	1.1
Py-PC18MA	1.4	0.80 (±0.01)	58 (±5)	0.01 (±0.00)	241 (±10)	0.01 (±0.00)	0.12	0.18 (±0.08)	1.0

	4.5	0.78 (±0.03)	52 (±2)	0.00 (±0.01)	122 (±8)	0.18 (±0.02)	0.12	0.19 (±0.02)	1.1
	5.8	0.71 (±0.02)	53 (±1)	0.02 (±0.00)	132 (±20)	0.00 (±0.04)	0.12	0.25 (±0.03)	1.1
	6.7	0.71 (±0.00)	55 (±1)	0.01 (±0.01)	112 (±31)	0.01 (±0.01)	0.12	0.26 (±0.01)	1.0
	6.8	0.72 (±0.00)	53 (±0.9)	0.01 (±0.01)	113 (±36)	0.01 (±0.07)	0.12	0.26 (±0.02)	1.0
	14.1	0.46 (±0.00)	50 (±1)	0.00 (±0.01)	84 (±3)	0.09 (±0.02)	0.12	0.43 (±0.04)	1.2
Py-PC1A	1.7	0.78 (±0.00)	55 (±1)	0.03 (±0.01)	277 (±11)	0.00 (±0.01)	0.17	0.18 (±0.00)	1.1
	2.6	0.66 (±0.01)	51 (±1)	0.00 (±0.01)	124 (±26)	0.00 (±0.01)	0.17	0.3 (±0.00)	1.1
	2.6	0.67 (±0.02)	52 (±0)	0.00 (±0.00)	144 (±37)	0.00 (±0.01)	0.17	0.29 (±0.00)	1.2
	3.0	0.67 (±0.00)	50 (±0)	0.00 (±0.00)	86 (±4)	0.04 (±0.01)	0.17	0.28 (±0.01)	1.1
	5.0	0.43 (±0.00)	50 (±0)	0.00 (±0.01)	67 (±3)	0.10 (±0.01)	0.17	0.46 (±0.05)	0.9
	6.2	0.43 (±0.01)	51 (±0.20)	0.02 (±0.01)	67 (±1)	0.07 (±0.02)	0.17	0.48 (±0.04)	1.2
	6.6	0.32 (±0.00)	50 (±0)	0.00 (±0.01)	60 (±5)	0.08 (±0.02)	0.17	0.59 (±0.04)	1.0
Py-PC4TMA	2.0	0.08 (±0.03)	60 (±2)	0.03 (±0.00)	248 (±24)	0.00 (±0.02)	0.12	0.12 (±0.02)	1.1
	3.6	0.80 (±0.00)	53 (±1)	0.00 (±0.01)	138 (±15)	0.04 (±0.01)	0.12	0.16 (±0.01)	1.0
	3.8	0.76 (±0.04)	53 (±2)	0.00 (±0.02)	111 (±18)	0.05 (±0.02)	0.12	0.18 (±0.00)	1.2
	4.7	0.70 (±0.01)	53 (±1)	0.00 (±0.01)	106 (±1)	0.67 (±0.02)	0.12	0.23 (±0.04)	1.0
	5.6	0.64 (±0.00)	52 (±2)	0.00 (±0.03)	102 (±20)	0.06 (±0.03)	0.12	0.29 (±0.00)	1.1
	7.6	0.56 (±0.00)	51 (±1)	0.00 (±0.01)	82 (±2)	0.13 (±0.01)	0.12	0.31 (±0.05)	1.0
Py-PCy6MA	2.0	0.82 (±0.01)	54 (±3)	0.00 (±0.01)	153 (±30)	0.03 (±0.01)	0.12	0.14 (±0.04)	1.1

	3.0	0.82 (±0.00)	57 (±2)	0.03 (±0.02)	202 (±30)	0.00 (±0.02)	0.12	0.14 (±0.02)	1.1
	3.8	0.79 (±0.01)	54 (±1)	0.00 (±0.01)	125 (±20)	0.03 (±0.01)	0.12	0.17 (±0.00)	1.0
	5.1	0.74 (±0.04)	54 (±1)	0.00 (±0.01)	116 (±23)	0.03 (±0.01)	0.12	0.22 (±0.00)	1.1
	6.2	0.70 (±0.00)	54 (±1)	0.00 (±0.01)	108 (±7)	0.03 (±0.00)	0.12	0.26 (±0.00)	1.1
	7.0	0.62 (±0.00)	54 (±1)	0.00 (±0.03)	88 (±11)	0.06 (±0.03)	0.12	0.31 (±0.01)	1.2

Table SI2.4: Overall fractions of pyrene species obtained from the FBM analysis of the monomer and excimer decays for the randomly labeled poly(alkyl methacrylate)s and poly(methyl acrylate)s in THF.

Sample	Mol%	f_{k2}	f_{free}	f_{E0}	f_{diff}	f_{EI}
Py-PC1MA	1.2	0.07 (± 0.00)	0.19 (± 0.00)	0.00 (± 0.02)	0.71 (± 0.01)	0.02 (± 0.01)
	2.6	0.17 (± 0.01)	0.02 (± 0.01)	0.01 (± 0.01)	0.78 (± 0.00)	0.02 (± 0.01)
	4.0	0.22 (± 0.00)	0.02 (± 0.00)	0.00 (± 0.02)	0.72 (± 0.00)	0.03 (± 0.01)
	5.2	0.28 (± 0.00)	0.01 (± 0.00)	0.01 (± 0.01)	0.64 (± 0.01)	0.05 (± 0.03)
	5.3	0.32 (± 0.00)	0.01 (± 0.00)	0.00 (± 0.02)	0.62 (± 0.01)	0.04 (± 0.02)
	5.6	0.32 (± 0.00)	0.00 (± 0.00)	0.00 (± 0.03)	0.62 (± 0.00)	0.05 (± 0.04)
	7.2	0.37 (± 0.01)	0.03 (± 0.00)	0.00 (± 0.05)	0.51 (± 0.04)	0.09 (± 0.01)
Py-PC4MA	1.1	0.06 (± 0.00)	0.43 (± 0.01)	0.00 (± 0.00)	0.50 (± 0.01)	0.01 (± 0.00)
	2.2	0.11 (± 0.00)	0.15 (± 0.01)	0.01 (± 0.01)	0.71 (± 0.01)	0.01 (± 0.00)
	3.0	0.16 (± 0.01)	0.10 (± 0.01)	0.03 (± 0.02)	0.68 (± 0.02)	0.01 (± 0.02)
	3.6	0.21 (± 0.01)	0.06 (± 0.01)	0.00 (± 0.02)	0.66 (± 0.00)	0.05 (± 0.02)
	5.3	0.25 (± 0.01)	0.01 (± 0.00)	0.00 (± 0.01)	0.68 (± 0.01)	0.05 (± 0.00)
	7.2	0.36 (± 0.01)	0.01 (± 0.00)	0.00 (± 0.03)	0.56 (± 0.00)	0.07 (± 0.02)
Py-PC6MA	2.0	0.11 (± 0.00)	0.18 (± 0.05)	0.01 (± 0.01)	0.68 (± 0.05)	0.02 (± 0.00)
	3.3	0.15 (± 0.00)	0.08 (± 0.00)	0.00 (± 0.01)	0.73 (± 0.00)	0.03 (± 0.01)
	4.7	0.18 (± 0.01)	0.07 (± 0.00)	0.00 (± 0.02)	0.71 (± 0.01)	0.04 (± 0.02)
	5.8	0.22 (± 0.00)	0.07 (± 0.00)	0.00 (± 0.00)	0.67 (± 0.00)	0.04 (± 0.00)

	6.6	0.27 (±0.00)	0.04 (±0.01)	0.00 (±0.01)	0.64 (±0.00)	0.04 (±0.01)
	8.1	0.31 (±0.00)	0.01 (±0.00)	0.01 (±0.00)	0.62 (±0.00)	0.04 (±0.01)
Py-PC8MA	1.8	0.10 (±0.00)	0.34 (±0.02)	0.00 (±0.00)	0.62 (±0.02)	0.02 (±0.01)
	2.7	0.13 (±0.00)	0.17 (±0.01)	0.00 (±0.01)	0.67 (±0.01)	0.02 (±0.06)
	4.3	0.19 (±0.01)	0.14 (±0.00)	0.00 (±0.01)	0.63 (±0.00)	0.03 (±0.01)
	5.1	0.21 (±0.00)	0.04 (±0.00)	0.00 (±0.02)	0.71 (±0.00)	0.04 (±0.02)
	6.1	0.23 (±0.01)	0.03 (±0.00)	0.06 (±0.04)	0.66 (±0.00)	0.01 (±0.05)
	7.3	0.30 (±0.00)	0.01 (±0.00)	0.00 (±0.01)	0.56 (±0.00)	0.13 (±0.01)
Py-PC12MA	1.4	0.07 (±0.00)	0.57 (±0.01)	0.00 (±0.01)	0.33 (±0.01)	0.02 (±0.01)
	3.5	0.13 (±0.00)	0.19 (±0.01)	0.02 (±0.01)	0.64 (±0.01)	0.01 (±0.01)
	5.6	0.21 (±0.00)	0.05 (±0.00)	0.00 (±0.01)	0.68 (±0.01)	0.04 (±0.01)
	6.0	0.25 (±0.00)	0.02 (±0.00)	0.00 (±0.01)	0.66 (±0.01)	0.05 (±0.01)
	7.7	0.27 (±0.01)	0.03 (±0.00)	0.00 (±0.00)	0.60 (±0.01)	0.09 (±0.01)
	10.2	0.37 (±0.01)	0.01 (±0.00)	0.00 (±0.01)	0.52 (±0.01)	0.10 (±0.02)
Py-PC18MA	1.4	0.07 (±0.01)	0.60 (±0.02)	0.00 (±0.01)	0.32 (±0.00)	0.00 (±0.00)
	4.5	0.14 (±0.01)	0.15 (±0.01)	0.00 (±0.02)	0.57 (±0.02)	0.13 (±0.01)
	5.8	0.23 (±0.01)	0.12 (±0.01)	0.02 (±0.00)	0.62 (±0.01)	0.00 (±0.04)
	6.7	0.24 (±0.01)	0.07 (±0.01)	0.00 (±0.01)	0.67 (±0.01)	0.01 (±0.01)
	6.8	0.25 (±0.01)	0.06 (±0.01)	0.01 (±0.01)	0.67 (±0.00)	0.01 (±0.01)

	14.1	0.43 (±0.00)	0.02 (±0.00)	0.00 (±0.02)	0.45 (±0.00)	0.09 (±0.01)
Py-PC1A	1.7	0.17 (±0.00)	0.06 (±0.00)	0.02 (±0.01)	0.73 (±0.01)	0.00 (±0.01)
	2.6	0.31 (±0.02)	0.05 (±0.00)	0.00 (±0.02)	0.63 (±0.00)	0.00 (±0.01)
	2.6	0.29 (±0.00)	0.02 (±0.00)	0.00 (±0.00)	0.68 (±0.00)	0.00 (±0.01)
	3.0	0.26 (±0.00)	0.08 (±0.02)	0.00 (±0.00)	0.62 (±0.00)	0.04 (±0.00)
	5.0	0.46 (±0.00)	0.01 (±0.01)	0.00 (±0.01)	0.43 (±0.01)	0.10 (±0.01)
	6.2	0.47 (±0.00)	0.03 (±0.00)	0.018 (±0.02)	0.41 (±0.00)	0.06 (±0.02)
	6.6	0.59 (±0.00)	0.01 (±0.00)	0.00 (±0.00)	0.32 (±0.00)	0.08 (±0.00)
	Py- PC4TMA	2.0	0.08 (±0.02)	0.13 (±0.04)	0.22 (±0.00)	0.55 (±0.01)
3.6		0.14 (±0.01)	0.08 (±0.00)	0.00 (±0.01)	0.73 (±0.00)	0.03 (±0.01)
3.8		0.17 (±0.02)	0.05 (±0.00)	0.00 (±0.02)	0.72 (±0.01)	0.05 (±0.02)
4.7		0.14 (±0.00)	0.01 (±0.00)	0.00 (±0.01)	0.43 (±0.01)	0.04 (±0.02)
5.6		0.29 (±0.00)	0.01 (±0.00)	0.00 (±0.03)	0.63 (±0.00)	0.06 (±0.02)
7.6		0.30 (±0.00)	0.01 (±0.00)	0.00 (±0.01)	0.55 (±0.00)	0.13 (±0.01)
Py-PCy6MA	2.0	0.09 (±0.00)	0.34 (±0.01)	0.00 (±0.01)	0.54 (±0.01)	0.02 (±0.01)
	3.0	0.12 (±0.00)	0.10 (±0.00)	0.03 (±0.00)	0.74 (±0.00)	0.00 (±0.00)
	3.8	0.16 (±0.00)	0.06 (±0.00)	0.00 (±0.01)	0.74 (±0.01)	0.03 (±0.01)
	5.1	0.22 (±0.01)	0.04 (±0.00)	0.00 (±0.02)	0.71 (±0.00)	0.03 (±0.01)
	6.2	0.26 (±0.00)	0.02 (±0.00)	0.00 (±0.00)	0.68 (±0.01)	0.04 (±0.00)
	7.0	0.28 (±0.00)	0.11 (±0.01)	0.00 (±0.01)	0.55 (±0.01)	0.05 (±0.02)

Appendix SI3- Supporting Information for Chapter 3: Pyrenyl Derivative with a Four Atom-Linker That Can Probe the Local Polarity of Pyrene-Labeled Macromolecules

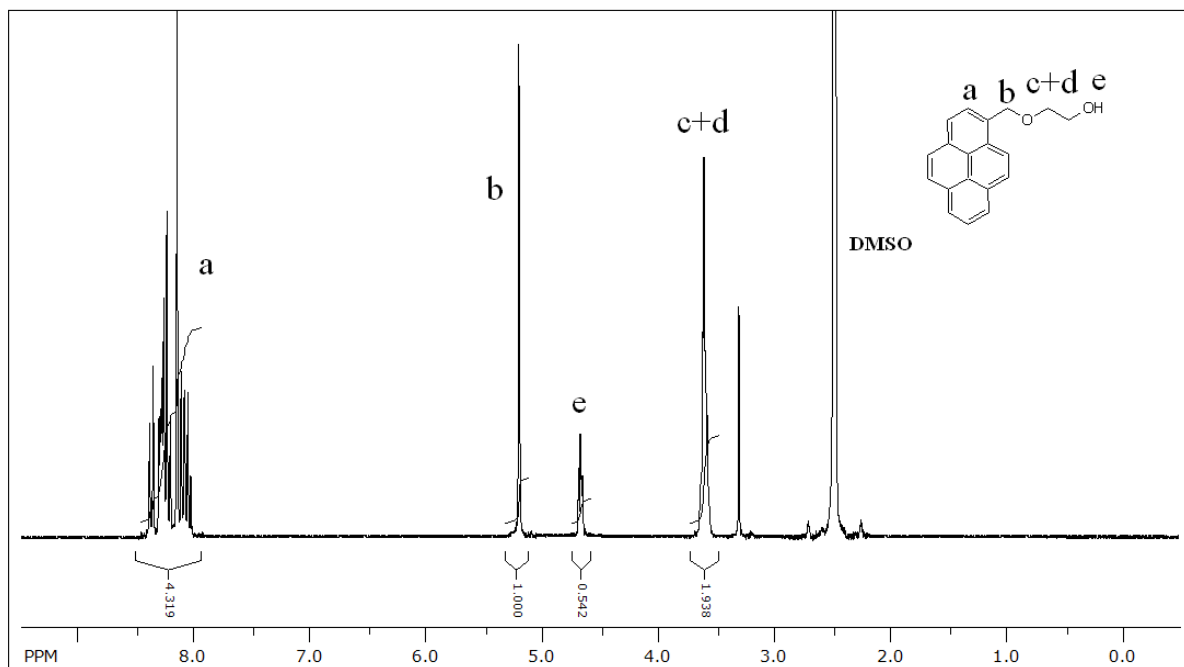


Figure SI3.1: ^1H NMR spectrum of PyMeEGOH in DMSO-d_6 .

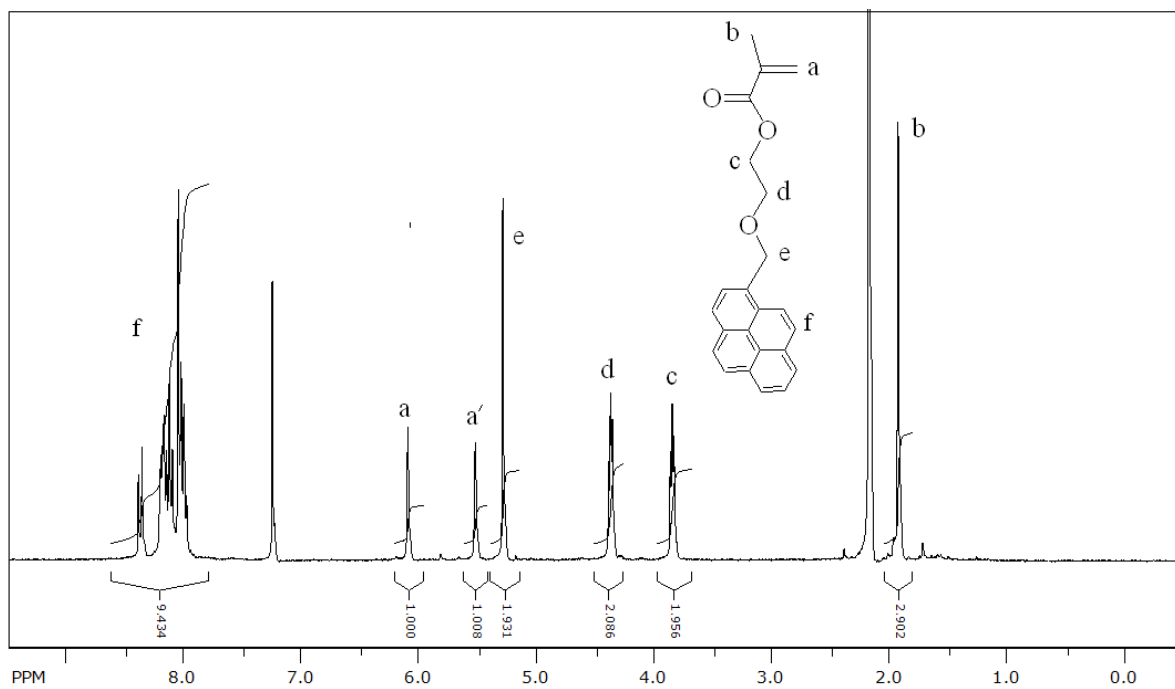


Figure SI3.2: ^1H NMR spectrum of PyMeEG-MA in CDCl_3 .

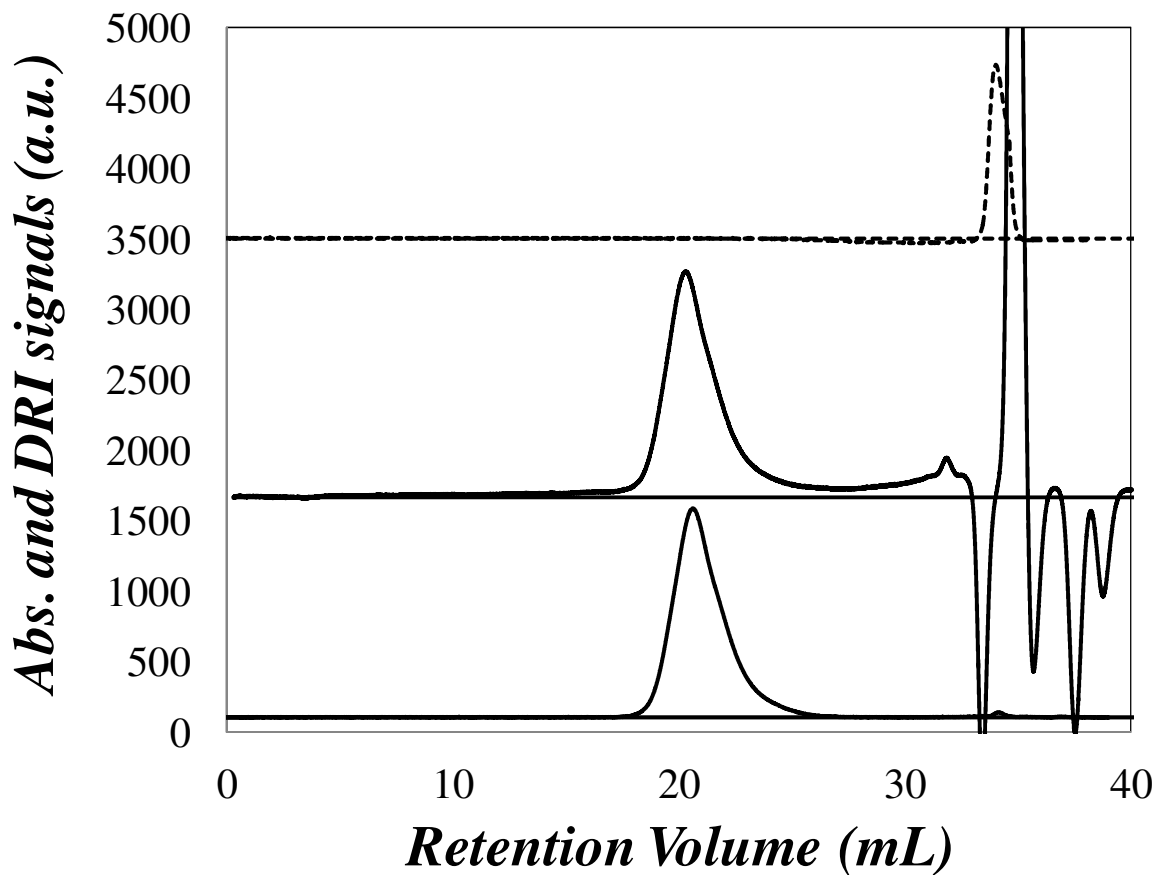
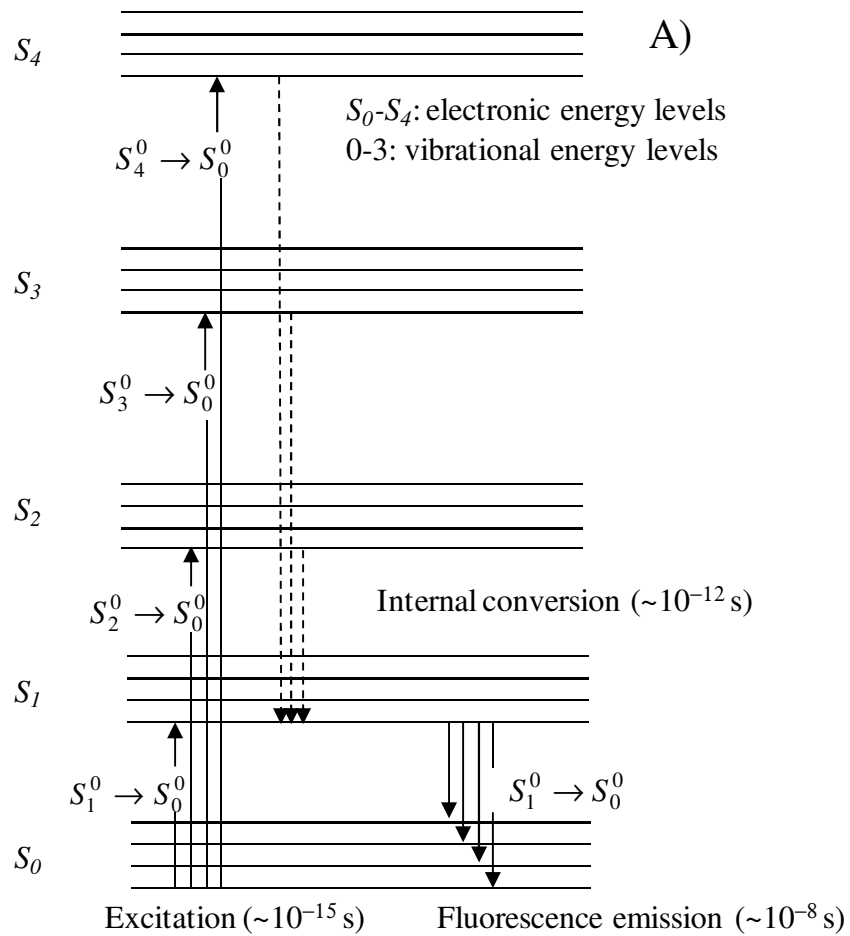


Figure SI3.3: GPC traces of (top) 2-(1-pyrenemethoxy ethyl) methacrylate acquired with a UV-Vis absorption detector and PyMeEG(3.8)-PBMA acquired with (middle) a DRI detector and (bottom) a UV-Vis absorption detector set at $\lambda=344$ nm. Elution solvent: THF

Photophysical properties of PyButOH and PyMeEGOH

The absorption spectra of PyButOH and PyMeEGOH in THF along with their fluorescence spectra are shown in Figures SI3.4B and S4C. Figure SI3.4A shows the Jablonski diagram depicting the different transitions observed in the absorption and fluorescence spectra. As can be seen in Figures SI3.4B and SI3.4C, the symmetry forbidden 0-0 transition of the pyrene labels is strongly reduced in the absorption and emission spectra of the PyMeEGOH samples. The molar absorption coefficient (ϵ) of 1-PyButOH and 1-PyMeEGOH at 344 nm were found to equal 42,000 and 45,000 $\text{M}^{-1}\cdot\text{cm}^{-1}$ in THF, respectively.



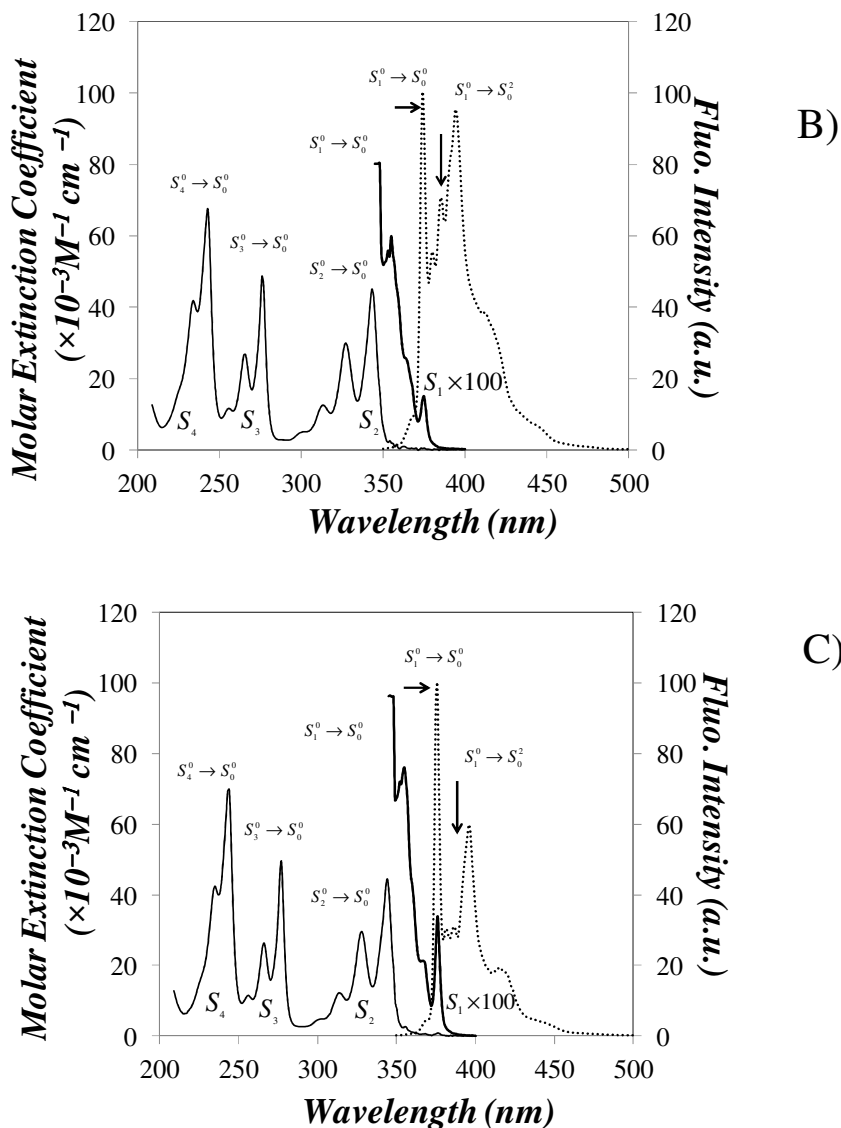


Figure SI3.4: A) Jablonsky diagram and the corresponding transitions of a chromophore. Absorption (solid line) and fluorescence emission (dashed line) spectra of B) PyMeEGOH and C) PyButOH in THF respectively. $[Py] = 2.5 \times 10^{-6} M$ and $\lambda_{ex} = 334$ nm for the emission spectra. The ϵ_{375} value of 1-PyButOH and 1-PyMeEGOH at 375 nm for the 0-0 transition equaled 263 and $151 M^{-1} \cdot cm^{-1}$. The much larger ϵ_{375} value obtained for PyButOH suggests that the 0-0

transition is more allowed than for PyMeEGOH, a consequence of the oxygen atom in the position β to pyrene which restores the wavefunction of pyrene.

Fluorescence Blob Model (FBM) and its parameters

The monomer and excimer fluorescence decays of the randomly labeled PBMA samples of PyBut-PBMA and PyMeEG-PBMA were fitted globally according to Equations SI3.1 and SI3.2 derived for the FBM. The different parameters that are used in the FBM have been listed in Table SI3.1.

Table SI3.1: List of parameters used for the FBM analysis of fluorescence decays.

Type of pyrene species	
Py_{diff}^*	Pyrene labels attached onto the structural units of the polymer that diffuse toward each other in solution.
Py_{free}^*	Pyrenes that are isolated and do not form excimer.
$Py_{k_2}^*$	Pyrenes that have been brought in close proximity by diffusive backbone motions and form excimer rapidly with a rate constant k_2 .
$E0^*$	Pyrene excimer resulting from well-stacked pyrenes.
EL^*	Long-lived excited pyrene dimers resulting from poorly stacked pyrenes.
Lifetime of pyrene species	
τ_{E0}	Fluorescence lifetime of pyrene excimer.
τ_{EL}	Fluorescence lifetime of the long-lived dimers.
τ_M	Fluorescence lifetime of excited pyrene monomer.
Molar Fraction of pyrene species contributing to the monomer decays	
f_{Mdiff}	Molar fraction of the Py_{diff}^* species.
f_{Mk_2}	Molar fraction of the $Py_{k_2}^*$ species.
f_{Mfree}	Molar fraction of the Py_{free}^* species.

Molar Fraction of pyrene species contributing to the excimer decays	
f_{Ediff}	Molar fraction of the Py_{diff}^* species.
f_{EK2}	Molar fraction of the Py_{k2}^* species.
f_{EE0}	Molar fraction of the $E0^*$ species.
f_{EEL}	Molar fraction of the EL^* species.
Overall molar fraction of the pyrene species	
f_{diff}	Molar fraction of the Py_{diff}^* species in the solution.
f_{k2}	Molar fraction of the Py_{k2}^* species in the solution.
f_{free}	Molar fraction of the Py_{free}^* species in the solution.
f_{E0}	Molar fraction of the $E0^*$ species excimer in the solution.
f_{EL}	Molar fraction of the EL^* species in the solution.
Fluorescence Blob Model parameters	
k_{blob}	Rate constant describing the encounters between one excited Py_{diff}^* monomer and one ground-state pyrene monomer located in the same <i>blob</i> as they diffuse toward each other to form a species Py_{k2}^* .
$k_e \times [blob]$	Rate constant of pyrene exchange between <i>blobs</i> times the local concentration of <i>blobs</i> inside the polymer coil.
N_{blob}	Average number of structural units per <i>blob</i> whose expression is given in Eq. S4.
$\langle n \rangle$	Average number of pyrenes per <i>blob</i> .
k_2	Rate constant for the rapid rearrangement of the pyrene labels to form an excimer.

Based on the kinetic scheme shown in Figure SI3.5, pyrene excimer formation occurs in a sequential manner. First the structural units bearing a pyrene label Py_{diff}^* diffuse toward each other with a rate constant k_{blob} . Upon contact, the structural units Py_{diff}^* turn into the Py_{k2}^* species. The pyrene labels rearrange on a fast time scale with a rate constant k_2 to form an excimer. Excimers can be the result of two well-stacked pyrenes ($E0^*$) or two improperly stacked pyrenes (EL^*) that emit with a lifetime τ_{EL} which is larger than that of the excimer τ_{E0} . The excimer species $E0^*$ and EL^* can be generated by diffusive encounters between an excited and a ground-state-pyrene or direct excitation of a pyrene aggregate. Pyrene labels that cannot form excimer are referred to as Py_{free}^* and they emit with the monomer natural lifetime τ_M .

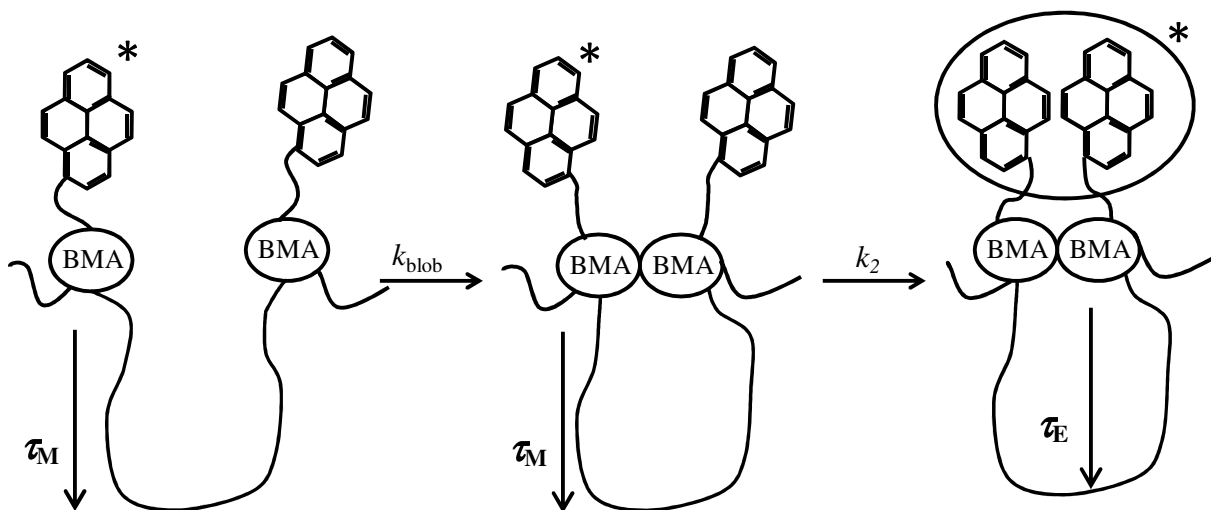


Figure SI3.5: Scheme representing the kinetics of excimer formation for the pyrene-labeled PBMA.

The diffusive motion of the pyrene-labeled structural units in the polymer coil can be described by the FBM parameters $\langle n \rangle$, k_{blob} , and $k_e \times [\text{blob}]$. By fitting the monomer decays, the molar fractions f_{Mdiff} , f_{Mk2} , and f_{Mfree} representing the pyrene species Py_{diff}^* , Py_{k2}^* , and Py_{free}^* that contribute to the monomer decays can be calculated. In a similar manner, the excimer decay analysis yields the fractions f_{Ediff} , f_{Ek2} , f_{EE0} , and f_{EEL} which represent the molar fractions of the respective pyrene species Py_{diff}^* , Py_{k2}^* , $E0^*$, and EL^* that contribute to the excimer decay. The fractions f_{Mdiff} , f_{Mk2} , f_{Mfree} , f_{Ediff} , f_{Ek2} , f_{EE0} , and f_{EEL} can then be combined to determine the overall molar fractions f_{diff} , f_{k2} , f_{free} , f_{E0} , and f_{EL} of each pyrene species present in solution. Equations SI3.1 and SI3.2 employ the parameters described above and in Table SI3.1 to fit the monomer and excimer decays globally.

$$\begin{aligned}
[Py^*]_{(t)} &= [Py_{\text{diff}}^*]_{(t)} + [Py_{k2}^*]_{(t)} + [Py_{\text{free}}^*]_{(t)} = [Py_{\text{diff}}^*]_o \exp\left(-\left(A_2 + \frac{1}{\tau_M}\right)t - A_3(1 - \exp(-A_4 t))\right) \\
&+ \left([Py_{k2}^*]_o + [Py_{\text{diff}}^*]_o e^{-A_3} \sum_{i=0}^{\infty} \frac{A_3^i}{i!} \frac{A_2 + iA_4}{A_2 + iA_4 - k_2} \right) \exp\left(-\left(k_2 + \frac{1}{\tau_M}\right)t\right) \\
&- [Py_{\text{diff}}^*]_o e^{-A_3} \sum_{i=0}^{\infty} \frac{A_3^i}{i!} \frac{A_2 + iA_4}{A_2 + iA_4 - k_2} \exp\left(-\left(A_2 + iA_4 + \frac{1}{\tau_M}\right)t\right)
\end{aligned}$$

$$+[Py_{free}^*]_o \exp\left(-\frac{t}{\tau_M}\right) \quad (SI3.1)$$

$$\begin{aligned}
[E^*]_{(t)} = [E0^*]_{(t)} + [EL^*]_{(t)} = k_2 & \left(\left([Py_{k_2}^*]_o + [Py_{diff}^*]_o e^{-A_3} \sum_{i=0}^{\infty} \frac{A_3^i}{i!} \frac{A_2 + iA_4}{A_2 + iA_4 - k_2} \right) \right. \\
& \times \frac{\exp\left(-\frac{t}{\tau_{E0}}\right) - \exp\left(-\left(k_2 + \frac{1}{\tau_M}\right)t\right)}{k_2 + \frac{1}{\tau_M} - \frac{1}{\tau_{E0}}} \\
& \left. + [Py_{diff}^*]_o e^{-A_3} \sum_{i=0}^{\infty} \frac{A_3^i}{i!} \frac{A_2 + iA_4}{A_2 + iA_4 - k_2} \frac{\exp\left(-\left(A_2 + iA_4 + \frac{1}{\tau_M}\right)t\right) - \exp\left(-\frac{t}{\tau_{E0}}\right)}{A_2 + iA_4 + \frac{1}{\tau_M} - \frac{1}{\tau_{E0}}} \right) \\
& + [E0^*]_o \times \exp\left(-\frac{t}{\tau_{E0}}\right) + [EL^*]_o \times \exp\left(-\frac{t}{\tau_{EL}}\right) \quad (SI3.2)
\end{aligned}$$

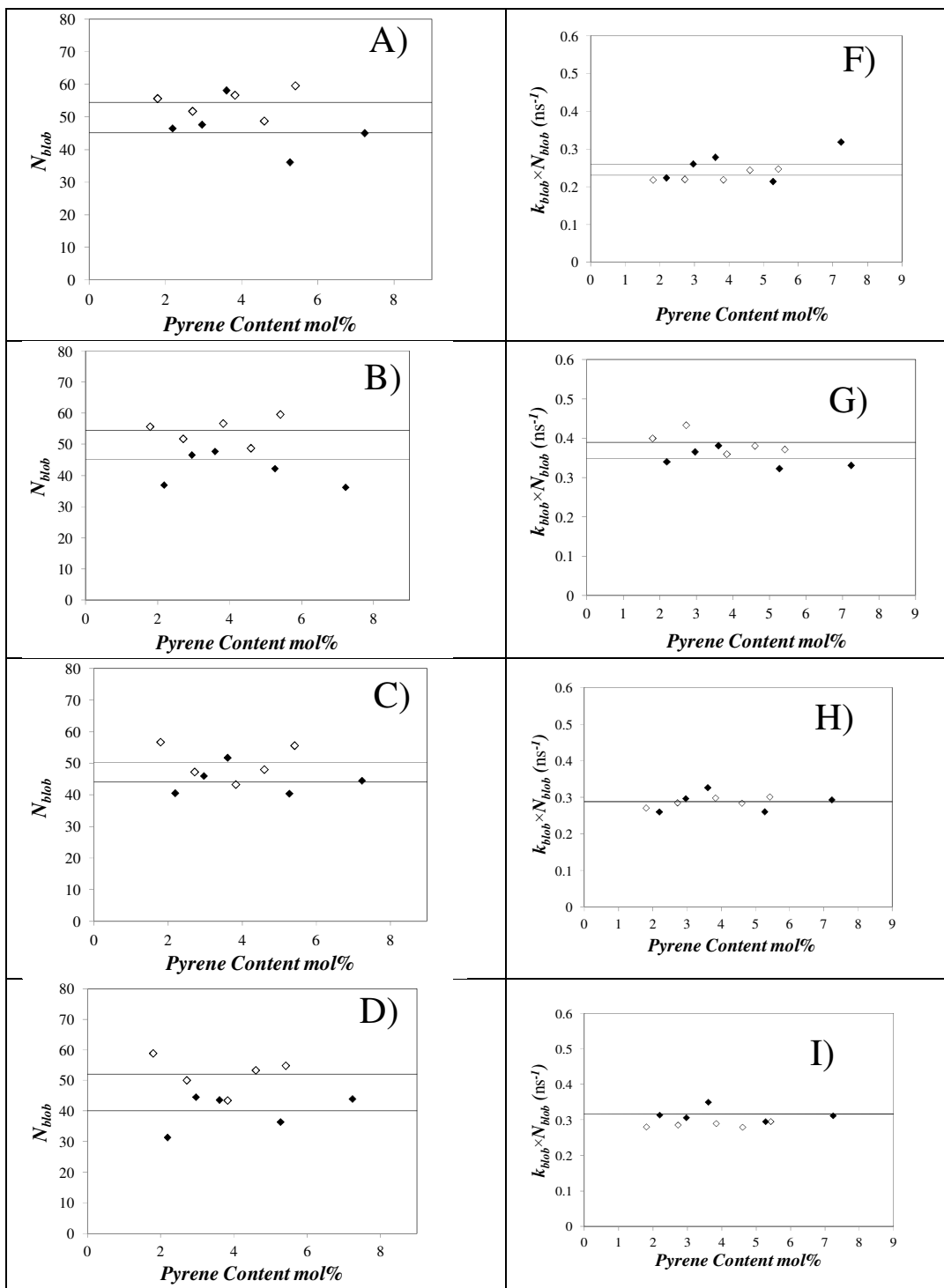
The expression of the parameters A_2 , A_3 , and A_4 used in Equations SI3.1 and SI3.2 have been provided in Equation SI3.3 as a function of $\langle n \rangle$, k_{blob} , and $k_c \times [blob]$ which have been already discussed in Table SI3.1.

$$A_2 = \langle n \rangle \frac{k_{blob} k_e [blob]}{k_{blob} + k_e [blob]} \quad A_3 = \langle n \rangle \left(\frac{k_{blob}}{k_{blob} + k_e [blob]} \right)^2 \quad A_4 = k_{blob} + k_e [blob] \quad (\text{SI3.3})$$

The parameters f_{Mfree} and $\langle n \rangle$ obtained from the FBM decay analysis and the pyrene content λ_{py} can be combined into Equation SI3.4 to yield N_{blob} , the number of structural units found in a *blob*.

$$N_{blob} = \frac{1 - f_{Mfree}}{\lambda_{py}} \frac{\langle n \rangle}{[M_{py}(x) + M_{BMA}(1-x)]} \quad (\text{SI3.4})$$

In Equation SI3.4, M_{BMA} is the molar mass of the BMA monomer ($M_{BMA}=142\text{g/mol}$) and M_{py} is the molar mass of the pyrene labeled monomer, M_{py} being equal to 344 g/mol or 342 g/mol for PyMeEGMA or PyButMA, respectively. Plots of N_{blob} and $k_{blob} \times N_{blob}$ are presented as a function of pyrene content in Figures SI3.6A-E and F-J, respectively.



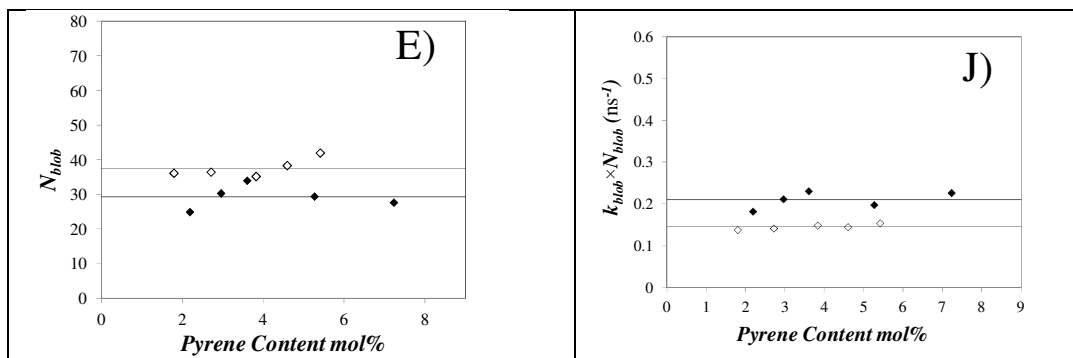


Figure SI3.6: Plots of N_{blob} (A-E) and $k_{blob} \times N_{blob}$ (F-J) as a function of pyrene content for (\diamond) PyMeEG-PBMA and (\blacklozenge) PyBut-PBMA in different solvents: A and F) DMF, B and G) DCM, C and H) THF, D and I) toluene, and E and F) cyclohexane. $[Py] = 2.5 \times 10^{-6}$ M, $\lambda_{ex} = 344$ nm.

Adjusting the lifetime of the PyMeEG-PBMA samples by fluorescence dynamic quenching

In order to investigate the effect that the lifetime (τ_M) of PyMeEG-OH used to prepare the PyMeEG-PBMA samples has on N_{blob} and the product $k_{\text{blob}} \times N_{\text{blob}}$, τ_M was adjusted by adding nitromethane, an efficient quencher of pyrene to a dilute solution of PyMeEG(0.3)-PBMA in THF. This sample had a very low pyrene content of 15.8 $\mu\text{mol/g}$ equivalent to 0.3 mol% pyrene-labeled monomer. A Stern Volmer (SV) plot was built where the fluorescence decays of PyMeEG(0.3)-PBMA were fitted with a sum of exponentials after the solution had been spiked with a known amount of nitromethane. The exponential with the longest decay time had a pre-exponential weight of 80% and this decay time was attributed to τ_M since most pyrene labels were unable to form an excimer and decayed with their natural lifetime. τ_M decreased with each addition of nitromethane and a linear SV plot was obtained in Figure SI3.4 where the ratio τ_M^0/τ_M was plotted as a function of nitromethane concentration. The intercept of the plot equaled unity and the slope equaled the product $k_q \times \tau_M^0$ where k_q is the quenching rate constant and τ_M^0 is the lifetime of the pyrene label in the absence of quencher. Since τ_M^0 in THF equaled 270 ns for PyMeEG(0.3)-PBMA, k_q took a value of $1.12 \times 10^9 \text{ M}^{-1} \cdot \text{s}^{-1}$. The value of k_q and τ_M^0 were then applied to determine the amount of nitromethane that needed to be added to a solution of PyMeEG-PBMA solution in THF to achieve a given τ_M value.

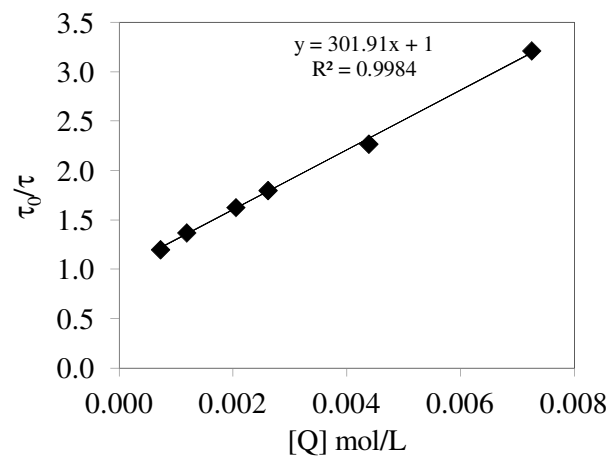


Figure SI3.7: Plot of τ_M^0/τ_M versus nitromethane concentration $[Q]$ for a PyMeEG(0.2)-PBMA solution in THF.

Table SI3.2: Intrinsic viscosities of poly(butyl methacrylate) ($M_n = 337,000$, PDI = 1.48) in different organic solvents.

Solvent	Intrinsic viscosity (mL.g⁻¹)	Error
THF	50.12	±0.93
Toluene	50.93	±0.85
DCM	56.50	±1.15
DMF	25.90	±0.44
Cyclohexane	20.44	±0.34

Table SI3.3: Parameters retrieved from the FBM analysis of the monomer decays of the PyMeEG-PBMA samples.

Sample	Mol%	k_{blob} (10^7s^{-1})	$\langle n \rangle$	$k_e[\text{blob}]$ (10^7s^{-1})	f_{Mdiff}	k_2 (ns^{-1})	f_{k_2}	τ_{M} (ns)	f_{Mfree}	χ^2
Py-PEGMA (THF)	1.8	0.48	1.2	0.19	0.75	0.1	0.12	270	0.12	1.1
	2.7	0.60	1.4	0.31	0.75	0.1	0.19	270	0.06	1.1
	3.8	0.65	1.7	0.34	0.71	0.1	0.25	270	0.04	1.0
	4.6	0.59	2.2	0.37	0.67	0.1	0.31	270	0.02	1.1
	5.4	0.54	3.0	0.25	0.62	0.1	0.38	270	0.00	1.1
Py-PEGMA (DMF)	1.8	0.39	1.2	0.31	0.73	0.08	0.13	228	0.14	1.2
	2.7	0.43	1.4	0.28	0.81	0.08	0.17	228	0.03	1.1
	3.8	0.39	2.2	0.35	0.70	0.08	0.28	228	0.02	1.1
	4.6	0.50	2.3	0.48	0.69	0.08	0.29	228	0.01	1.3
	5.4	0.42	3.3	0.40	0.64	0.08	0.35	228	0.01	1.1
Py-PEGMA (CycloHexane)	1.8	0.38	0.7	0.19	0.8	0.06	0.10	288	0.07	1.3
	2.7	0.39	1.1	0.28	0.7	0.06	0.17	288	0.10	1.2
	3.8	0.42	1.4	0.24	0.7	0.06	0.26	288	0.03	1.0
	4.6	0.38	1.8	0.23	0.7	0.06	0.30	288	0.00	1.0
	5.4	0.37	2.3	0.19	0.6	0.06	0.37	288	0.01	1.0
Py-PEGMA (Toluene)	1.8	0.48	1.2	0.22	0.75	0.1	0.12	246	0.13	1.3
	2.7	0.57	1.5	0.37	0.74	0.1	0.18	246	0.08	1.2
	3.8	0.67	1.7	0.42	0.69	0.1	0.27	246	0.04	1.1
	4.6	0.53	2.5	0.24	0.66	0.1	0.31	246	0.03	1.1
	5.4	0.54	3.0	0.23	0.62	0.1	0.37	246	0.00	1.1
Py-PEGMA (DCM)	1.8	0.87	0.9	0.39	0.74	0.12	0.14	155	0.12	1.0
	2.7	0.89	1.4	0.50	0.71	0.12	0.21	155	0.08	1.1
	3.8	0.69	2.0	0.29	0.72	0.12	0.26	155	0.02	1.0
	4.6	0.75	2.4	0.45	0.68	0.12	0.30	155	0.01	1.1
	5.4	0.66	3.1	0.30	0.61	0.12	0.38	155	0.01	1.0

Table SI3.4: Parameters retrieved from the FBM analysis of the excimer decays of the PyMeEG-PBMA samples.

Sample	Mol %	f_{Ediff}	τ_{E0} (ns)	f_{EE0}	τ_{EL} (ns)	f_{EEL}	k_2 (ns^{-1})	f_{E}	χ^2
Py-PEGMA (THF)	1.8	0.79	47	0.03	157	0.05	0.1	0.13	1.1
	2.7	0.73	53	0.05	146	0.03	0.1	0.19	1.1
	3.8	0.66	53	0.08	121	0.02	0.1	0.24	1.0
	4.6	0.59	52	0.11	108	0.02	0.1	0.28	1.1
	5.4	0.53	48	0.00	82	0.15	0.1	0.32	1.1
Py-PEGMA (DMF)	1.8	0.78	47	0.02	144	0.06	0.08	0.14	1.2
	2.7	0.76	46	0.02	126	0.06	0.08	0.16	1.1
	3.8	0.64	53	0.09	148	0.01	0.08	0.26	1.1
	4.6	0.60	51	0.12	106	0.02	0.08	0.25	1.3
	5.4	0.55	48	0.13	119	0.02	0.08	0.30	1.1
Py-PEGMA (Cyclohexane)	1.8	0.82	46	0.06	194	0.02	0.06	0.10	1.3
	2.7	0.70	52	0.12	177	0.02	0.06	0.16	1.2
	3.8	0.58	52	0.14	143	0.06	0.06	0.22	1.0
	4.6	0.54	51	0.16	121	0.07	0.06	0.23	1.0
	5.4	0.49	53	0.20	119	0.06	0.08	0.24	1.0
Py-PEGMA (Toluene)	1.8	0.80	41	0.02	132	0.06	0.1	0.13	1.3
	2.7	0.73	48	0.08	142	0.01	0.1	0.18	1.2
	3.8	0.63	50	0.11	108	0.01	0.1	0.25	1.1
	4.6	0.58	45	0.07	90	0.08	0.1	0.27	1.1
	5.4	0.52	45	0.04	78	0.14	0.1	0.31	1.1
Py-PEGMA (DCM)	1.8	0.76	53	0.02	100	0.08	0.12	0.14	1.0
	2.7	0.69	53	0.10	146	0.01	0.12	0.20	1.1
	3.8	0.64	46	0.07	89	0.05	0.12	0.23	1.0
	4.6	0.57	45	0.01	70	0.16	0.12	0.25	1.1
	5.4	0.50	46	0.00	67	0.18	0.12	0.31	1.0

Table SI3.5: Overall molar fractions of pyrene species obtained from the FBM analysis of the monomer and excimer decays for the PyMeEG-PBMA samples.

Sample	Mol	fk_2	F_{free}	f_{E0}	f_{diff}	f_{E1}
Py-PEGMA (THF)	1.8	0.12	0.11	0.03	0.70	0.04
	2.7	0.18	0.06	0.05	0.69	0.03
	3.8	0.23	0.04	0.07	0.64	0.02
	4.6	0.28	0.01	0.10	0.59	0.02
	5.4	0.32	0.00	0.00	0.52	0.15
Py-PEGMA (DMF)	1.8	0.12	0.13	0.02	0.68	0.05
	2.7	0.15	0.03	0.02	0.74	0.06
	3.8	0.26	0.02	0.09	0.63	0.01
	4.6	0.25	0.01	0.12	0.60	0.02
	5.4	0.30	0.01	0.13	0.55	0.02
Py-PEGMA (Cyclohexane)	1.8	0.09	0.07	0.09	0.77	0.02
	2.7	0.15	0.09	0.15	0.64	0.02
	3.8	0.21	0.02	0.21	0.57	0.06
	4.6	0.23	0.00	0.23	0.54	0.07
	5.4	0.28	0.01	0.28	0.47	0.06
Py-PEGMA (Toluene)	1.8	0.11	0.12	0.02	0.70	0.05
	2.7	0.17	0.07	0.08	0.68	0.01
	3.8	0.24	0.04	0.11	0.61	0.01
	4.6	0.26	0.03	0.07	0.56	0.08
	5.4	0.31	0.00	0.04	0.51	0.14
Py-PEGMA (DCM)	1.8	0.13	0.11	0.01	0.68	0.07
	2.7	0.19	0.07	0.09	0.64	0.01
	3.8	0.23	0.02	0.07	0.63	0.05
	4.6	0.25	0.01	0.01	0.57	0.16
	5.4	0.31	0.00	0.00	0.50	0.18

Table SI3.6: Parameters retrieved from the FBM analysis of the monomer decays of the PyBut-PBMA samples.

Sample	Mol%	k_{blob} ($10^7 s^{-1}$)	$\langle n \rangle$	$k_e[blob]$ ($10^7 s^{-1}$)	f_{Mdiff}	k_2 (ns^{-1})	f_{k2}	τ_M (ns)	f_{Mfree}	χ^2
Py-PC4MA (THF)	2.2	0.67	0.8	0.63	0.50	0.12	0.06	195	0.44	1.1
	2.9	0.64	1.0	0.51	0.73	0.12	0.12	195	0.15	1.2
	3.6	0.65	1.5	0.61	0.72	0.12	0.17	195	0.11	1.0
	5.2	0.63	2.0	0.46	0.70	0.12	0.23	195	0.07	1.1
	7.2	0.65	2.2	0.47	0.72	0.12	0.27	195	0.01	1.1
Py-PC4MA (DMF)	2.2	0.55	1.0	0.77	0.67	0.09	0.11	160	0.23	1.2
	2.9	0.56	1.5	0.52	0.74	0.09	0.19	160	0.07	1.2
	3.6	0.58	2.1	1.24	0.62	0.09	0.21	160	0.17	1.2
	5.2	0.55	2.3	0.66	0.68	0.09	0.24	160	0.03	1.0
	7.2	0.88	2.4	0.98	0.70	0.09	0.38	160	0.01	1.2
Py-PC4MA (Cyclohexane)	2.2	0.73	0.63	0.57	0.77	0.12	0.10	224	0.13	1.0
	2.9	0.70	0.96	0.53	0.80	0.12	0.14	224	0.06	1.1
	3.6	0.68	1.35	0.54	0.72	0.12	0.19	224	0.09	1.2
	5.2	0.67	1.56	0.46	0.77	0.12	0.22	224	0.01	1.3
	7.2	0.82	2.05	0.59	0.71	0.12	0.27	224	0.03	1.3
Py-PC4MA (Toluene)	2.2	1.00	0.9	0.68	0.68	0.12	0.12	180	0.20	1.1
	2.9	0.69	1.5	0.70	0.72	0.12	0.19	180	0.09	1.2
	3.6	0.82	1.7	0.68	0.70	0.12	0.22	180	0.08	1.2
	5.2	0.81	2.0	0.60	0.76	0.12	0.22	180	0.02	1.2
	7.2	0.71	3.2	0.44	0.60	0.12	0.39	180	0.01	1.1
Py-PC4MA (DCM)	2.2	0.80	1.1	0.65	0.68	0.12	0.13	110	0.18	1.1
	2.9	0.72	1.6	0.43	0.74	0.12	0.21	110	0.05	1.0
	3.6	0.60	2.4	0.22	0.66	0.12	0.29	110	0.06	1.0
	5.2	0.66	2.6	0.24	0.68	0.12	0.32	110	0.00	1.1
	7.2	0.53	4.6	0.17	0.52	0.12	0.47	110	0.01	1.3

Table SI3.7: Parameters retrieved from the FBM analysis of the excimer decays of the PyBut-PBMA samples.

Sample	Mol %	f_{Ediff}	τ_{E0} (ns)	f_{EE0}	τ_{EL} (ns)	f_{EEL}	k_2 (ns^{-1})	f_{E}	χ^2
Py-PC4MA (THF)	2.2	0.84	56	0.02	178.9	0.01	0.12	0.13	1.2
	2.9	0.77	54	0.04	156.5	0.02	0.12	0.18	1.0
	3.6	0.71	52	0.00	100.3	0.06	0.12	0.23	1.1
	5.2	0.69	53	0.00	95.7	0.05	0.12	0.26	1.1
	7.2	0.57	51	0.00	83.8	0.07	0.12	0.36	1.1
Py-PC4MA (DMF)	2.2	0.83	53	0.00	139	0.04	0.09	0.13	1.2
	2.9	0.74	54	0.00	103	0.07	0.09	0.19	1.2
	3.6	0.69	50	0.00	106	0.07	0.09	0.24	1.2
	5.2	0.66	52	0.09	91	0.07	0.09	0.23	1.0
	7.2	0.53	56	0.09	98	0.05	0.09	0.33	1.2
Py-PC4MA (Cyclohexane)	2.2	0.84	53	0.00	140	0.05	0.12	0.10	1.0
	2.9	0.78	55	0.02	121	0.06	0.12	0.14	1.1
	3.6	0.71	53	0.00	110	0.10	0.12	0.19	1.2
	5.2	0.68	53	0.02	104	0.11	0.12	0.19	1.3
	7.2	0.57	50	0.00	91	0.22	0.12	0.21	1.3
Py-PC4MA (Toluene)	2.2	0.79	60	0.07	284	0.00	0.12	0.14	1.1
	2.9	0.74	53	0.06	185	0.01	0.12	0.19	1.2
	3.6	0.69	53	0.08	197	0.00	0.12	0.22	1.2
	5.2	0.66	52	0.13	78	0.02	0.12	0.19	1.2
	7.2	0.52	49	0.00	72	0.14	0.12	0.34	1.0
Py-PC4MA (DCM)	2.2	0.80	52	0.0	93	0.05	0.12	0.16	1.1
	2.9	0.73	52	0.1	94	0.01	0.12	0.20	1.0
	3.6	0.65	51	0.0	78	0.06	0.12	0.29	1.0
	5.2	0.62	49	0.0	77	0.09	0.12	0.29	1.1
	7.2	0.46	50	0.0	70	0.13	0.12	0.42	1.3

Table SI3.8: Overall molar fractions of pyrene species obtained from the FBM analysis of the monomer and excimer decays for the PyBut-PBMA samples

Sample	Mol%	f_{k2}	f_{free}	f_{E0}	f_{diff}	f_{E1}
Py-PC4MA (THF)	2.2	0.11	0.15	0.02	0.71	0.01
	2.9	0.16	0.11	0.03	0.68	0.02
	3.6	0.22	0.06	0.00	0.67	0.05
	5.2	0.25	0.01	0.00	0.68	0.05
	7.2	0.36	0.01	0.00	0.56	0.07
Py-PC4MA (DMF)	2.2	0.10	0.22	0.00	0.65	0.03
	2.9	0.18	0.06	0.00	0.70	0.06
	3.6	0.20	0.16	0.00	0.58	0.06
	5.2	0.27	0.02	0.02	0.63	0.05
	7.2	0.30	0.01	0.09	0.55	0.05
Py-PC4MA (Cyclohexane)	2.2	0.09	0.13	0.00	0.74	0.05
	2.9	0.13	0.05	0.02	0.74	0.06
	3.6	0.17	0.08	0.00	0.65	0.09
	5.2	0.19	0.01	0.02	0.68	0.11
	7.2	0.21	0.02	0.00	0.56	0.21
Py-PC4MA (Toluene)	2.2	0.11	0.19	0.05	0.65	0.00
	2.9	0.18	0.08	0.05	0.68	0.00
	3.6	0.21	0.07	0.07	0.64	0.00
	5.2	0.18	0.02	0.13	0.65	0.02
	7.2	0.34	0.01	0.00	0.52	0.14
Py-PC4MA (DCM)	2.2	0.13	0.18	0.00	0.66	0.04
	2.9	0.19	0.05	0.05	0.70	0.01
	3.6	0.27	0.05	0.00	0.62	0.06
	5.2	0.29	0.00	0.00	0.62	0.09
	7.2	0.41	0.01	0.00	0.45	0.13

Table SI3.9: Parameters retrieved from the FBM analysis of the monomer decays of the PyMeEG-PBMA samples when the lifetime was adjusted using nitromethane as quencher in THF.

Sample	Mol%	k_{blob} (10^7s^{-1})	$\langle n \rangle$	$k_e[\text{blob}]$ (10^7s^{-1})	f_{Mdiff}	k_2 (ns^{-1})	f_{k_2}	τ_{M} (ns)	f_{Mfree}	χ^2
Py-PEGMA (THF) $\tau=270$	1.8	0.48	1.2	0.19	0.75	0.1	0.12	270	0.12	1.1
	2.7	0.60	1.4	0.31	0.75	0.1	0.19	270	0.06	1.1
	3.8	0.65	1.7	0.34	0.71	0.1	0.25	270	0.04	1.0
	4.6	0.59	2.2	0.37	0.67	0.1	0.31	270	0.02	1.1
	5.4	0.54	3.0	0.25	0.62	0.1	0.38	270	0.00	1.1
Py-PEGMA (THF) $\tau=200$	1.8	0.48	1.2	0.32	0.77	0.085	0.14	200	0.09	1.0
	2.7	0.58	1.4	0.40	0.74	0.085	0.20	200	0.05	1.1
	3.8	0.50	2.0	0.29	0.71	0.085	0.26	200	0.02	1.2
	4.6	0.44	2.7	0.14	0.69	0.085	0.31	200	0.00	1.1
	5.4	0.45	3.2	0.20	0.64	0.085	0.36	200	0.01	1.1
Py-PEGMA (THF) $\tau=150$	1.8	0.51	1.2	0.45	0.75	0.085	0.15	150	0.10	1.2
	2.7	0.63	1.3	0.41	0.74	0.085	0.20	150	0.05	1.1
	3.8	0.57	1.9	0.41	0.72	0.085	0.24	150	0.04	1.1
	4.6	0.46	2.7	0.28	0.67	0.085	0.32	150	0.01	1.2
	5.4	0.57	2.7	0.38	0.66	0.085	0.33	150	0.01	0.9
Py-PEGMA (THF) $\tau=100$	1.8	0.66	0.9	0.36	0.76	0.085	0.15	100	0.09	1.1
	2.7	0.52	1.5	0.26	0.70	0.085	0.19	100	0.11	1.1
	3.8	0.64	1.9	0.79	0.70	0.085	0.26	100	0.03	1.1
	4.6	0.72	1.8	0.40	0.68	0.085	0.31	100	0.02	1.1
	5.4	0.62	2.4	0.36	0.64	0.085	0.34	100	0.02	1.0
Py-PEGMA (THF) $\tau=50$	1.8	0.8	1.3	0.1	0.74	0.15	0.11	50	0.43	1.2
	2.7	1.2	1.0	1.0	0.74	0.15	0.14	50	0.18	1.5
	3.8	1.3	1.0	0.4	0.74	0.15	0.20	50	0.00	1.2
	4.6	0.9	2.1	0.5	0.63	0.15	0.29	50	0.05	1.1
	5.4	1.2	1.8	1.0	0.62	0.15	0.29	50	0.04	1.2

Table SI3.10: Parameters retrieved from the FBM analysis of the excimer decays of the PyMeEG-PBMA samples when the lifetime was adjusted using nitromethane as quencher in THF.

Sample	Mol%	f_{Ediff}	τ_{E0} (ns)	f_{EE0}	τ_{EL} (ns)	f_{EEL}	k_2 (ns ⁻¹)	f_E	χ^2
Py-PEGMA (THF) $\tau=270$	1.8	0.79	47	0.03	157	0.05	0.1	0.13	1.1
	2.7	0.73	53	0.05	146	0.03	0.1	0.19	1.1
	3.8	0.66	53	0.08	121	0.02	0.1	0.24	1.0
	4.6	0.59	52	0.11	108	0.02	0.1	0.28	1.1
	5.4	0.53	48	0.00	82	0.15	0.1	0.32	1.1
Py-PEGMA (THF) $\tau=200$	1.8	0.77	44	0.0	100	0.09	0.09	0.1	1.0
	2.7	0.72	48	0.0	96	0.09	0.09	0.2	1.1
	3.8	0.65	50	0.1	100	0.05	0.09	0.2	1.2
	4.6	0.58	47	0.0	84	0.15	0.09	0.3	1.1
	5.4	0.51	49	0.1	83	0.13	0.09	0.3	1.1
Py-PEGMA (THF) $\tau=150$	1.8	0.75	47	0.0	76	0.10	0.09	0.2	1.2
	2.7	0.72	50	0.0	84	0.06	0.09	0.2	1.1
	3.8	0.65	49	0.1	89	0.08	0.09	0.2	1.1
	4.6	0.58	48	0.1	81	0.09	0.09	0.3	1.2
	5.4	0.53	46	0.0	76	0.21	0.09	0.3	0.9
Py-PEGMA (THF) $\tau=100$	1.8	0.75	47	0.0	74	0.08	0.09	0.2	1.1
	2.7	0.72	47	0.0	83	0.08	0.09	0.2	1.1
	3.8	0.61	47	0.2	187	0.00	0.09	0.2	1.1
	4.6	0.59	52	0.0	71	0.09	0.09	0.3	1.1
	5.4	0.53	48	0.0	70	0.19	0.09	0.3	1.0
Py-PEGMA (THF) $\tau=50$	1.8	0.74	52	0.01		0.08	0.15	0.2	1.2
	2.7	0.74	48	0.00		0.08	0.15	0.2	1.3
	3.8	0.74	47	0.01		0.06	0.15	0.2	1.2
	4.6	0.63	46	0.09		0.01	0.15	0.3	1.1
	5.4	0.62	44	0.01		0.11	0.15	0.3	1.2

Table SI3.4: Overall fractions of pyrene species obtained from the FBM analysis of the monomer and excimer decays for the PyMeEG-PBMA samples when the lifetime was adjusted using nitromethane as quencher in THF.

Sample	Mol%	f_{k2}	f_{free}	f_{E0}	f_{diff}	f_{E1}
Py-PEGMA (THF) $\tau=270$	1.8	0.12	0.11	0.03	0.70	0.04
	2.7	0.18	0.06	0.05	0.69	0.03
	3.8	0.23	0.04	0.07	0.64	0.02
	4.6	0.28	0.01	0.10	0.59	0.02
	5.4	0.32	0.00	0.00	0.52	0.15
Py-PEGMA (THF) $\tau=200$	1.8	0.12	0.09	0.00	0.71	0.08
	2.7	0.18	0.05	0.00	0.68	0.08
	3.8	0.24	0.02	0.05	0.64	0.05
	4.6	0.26	0.00	0.00	0.58	0.15
	5.4	0.29	0.01	0.07	0.51	0.13
Py-PEGMA (THF) $\tau=150$	1.8	0.14	0.09	0.00	0.68	0.09
	2.7	0.18	0.05	0.03	0.68	0.06
	3.8	0.21	0.03	0.06	0.63	0.07
	4.6	0.27	0.01	0.06	0.57	0.09
	5.4	0.26	0.01	0.00	0.53	0.20
Py-PEGMA (THF) $\tau=100$	1.8	0.14	0.08	0.02	0.69	0.07
	2.7	0.18	0.10	0.00	0.65	0.07
	3.8	0.22	0.03	0.15	0.60	0.00
	4.6	0.27	0.01	0.04	0.59	0.09
	5.4	0.27	0.02	0.00	0.52	0.19
100Py-PEGMA (THF) $\tau=50$	1.8	0.10	0.40	0.01	0.44	0.05
	2.7	0.13	0.16	0.00	0.64	0.07
	3.8	0.19	0.00	0.01	0.74	0.06
	4.6	0.26	0.05	0.09	0.60	0.01
	5.4	0.26	0.04	0.01	0.60	0.10

Appendix SI4-Supporting Information for Chapter 4: Probing Side Chain Dynamics of Branched Macromolecules by Pyrene Excimer Fluorescence

Fluorescence Blob Model (FBM) analysis of the fluorescence decays

The derivation of the FBM and its application to fit the fluorescence decays of macromolecules randomly labeled with pyrene have been described in several papers.¹⁻⁵ In short, an excited pyrene covalently attached onto a polymer is assumed to probe a finite volume referred to as a *blob* while it remains excited. The *blob* can be viewed as a unit volume that can be used to divide the polymer coil into a cluster of *blobs*. If the pyrene labels are randomly attached onto the polymer, they distribute themselves among the *blobs* according to a Poisson distribution with an average number of pyrenes per *blob* given by $\langle n \rangle$. One excited pyrene and a ground-state pyrene located in a same *blob* diffuse toward each other with a rate constant k_{blob} . These pyrenes are referred to as $P_{y\text{diff}}$. The ground-state pyrenes can diffuse in and out of the *blobs* with a rate of $k_e \times [\text{blob}]$. When two monomers bearing the two pyrene labels are in contact, the pyrene-labels in close vicinity referred to as $P_{y_{k_2}}$ rearrange themselves with a large rate constant k_2 to form an excimer. Some pyrenes are located in pyrene-poor domains of the polymer coil where they are unable to form an excimer and emit as if they were free in solution ($P_{y\text{free}}$) with their natural lifetime τ_M . Well-stacked excimers ($E0^*$) are formed by diffusion or by direct excitation of a pyrene dimers and they emit with a lifetime τ_{E0} . Poorly stacked ground-state pyrene dimers can be excited directly to form long-lived excited dimer (EL^*) that emits with a

lifetime τ_{EL} . Based on the FBM, the monomer and excimer decays are fitted according to Equations SI4.1 and SI4.2 whose expression is given hereafter.

$$\begin{aligned}
[Py^*]_{(t)} = & [Py_{diff}^*]_{(t)} + [Py_{k_2}^*]_{(t)} + [Py_{free}^*]_{(t)} = [Py_{diff}^*]_o \exp\left(-\left(A_2 + \frac{1}{\tau_M}\right)t - A_3(1 - \exp(-A_4 t))\right) \\
& + \left([Py_{k_2}^*]_o + [Py_{diff}^*]_o e^{-A_3} \sum_{i=0}^{\infty} \frac{A_3^i}{i!} \frac{A_2 + iA_4}{A_2 + iA_4 - k_2}\right) \exp\left(-\left(k_2 + \frac{1}{\tau_M}\right)t\right) \\
& - [Py_{diff}^*]_o e^{-A_3} \sum_{i=0}^{\infty} \frac{A_3^i}{i!} \frac{A_2 + iA_4}{A_2 + iA_4 - k_2} \exp\left(-\left(A_2 + iA_4 + \frac{1}{\tau_M}\right)t\right) \\
& + [Py_{free}^*]_o \exp\left(-\frac{t}{\tau_M}\right) \quad (SI4.1)
\end{aligned}$$

$$\begin{aligned}
[E^*]_{(t)} = & [E0^*]_{(t)} + [EL^*]_{(t)} = k_2 \left(\left([Py_{k_2}^*]_o + [Py_{diff}^*]_o e^{-A_3} \sum_{i=0}^{\infty} \frac{A_3^i}{i!} \frac{A_2 + iA_4}{A_2 + iA_4 - k_2} \right) \right. \\
& \times \frac{\exp\left(-\frac{t}{\tau_{E0}}\right) - \exp\left(-\left(k_2 + \frac{1}{\tau_M}\right)t\right)}{k_2 + \frac{1}{\tau_M} - \frac{1}{\tau_{E0}}}
\end{aligned}$$

$$\begin{aligned}
& + [Py_{diff}^*]_o e^{-A_3} \sum_{i=0}^{\infty} \frac{A_3^i}{i!} \frac{A_2 + iA_4}{A_2 + iA_4 - k_2} \frac{\exp\left(-\left(A_2 + iA_4 + \frac{1}{\tau_M}\right)t\right) - \exp\left(-\frac{t}{\tau_{E0}}\right)}{A_2 + iA_4 + \frac{1}{\tau_M} - \frac{1}{\tau_{E0}}} \Bigg) \\
& + [E0^*]_o \times \exp\left(-\frac{t}{\tau_{E0}}\right) + [EL^*]_o \times \exp\left(-\frac{t}{\tau_{EL}}\right) \quad (SI4.2)
\end{aligned}$$

The expression of the parameters A_2 , A_3 , and A_4 used in Equations SI4.1 and SI4.2 have been provided in Equation SI4.3 as a function of $\langle n \rangle$, k_{blob} , and $k_e \times [blob]$.

$$A_2 = \langle n \rangle \frac{k_{blob} k_e [blob]}{k_{blob} + k_e [blob]} \quad A_3 = \langle n \rangle \left(\frac{k_{blob}}{k_{blob} + k_e [blob]} \right)^2 \quad A_4 = k_{blob} + k_e [blob] \quad (S4.3)$$

The parameters retrieved from the global FBM analysis of the fluorescence decays have been listed in Tables SI4.3-SI4.5.

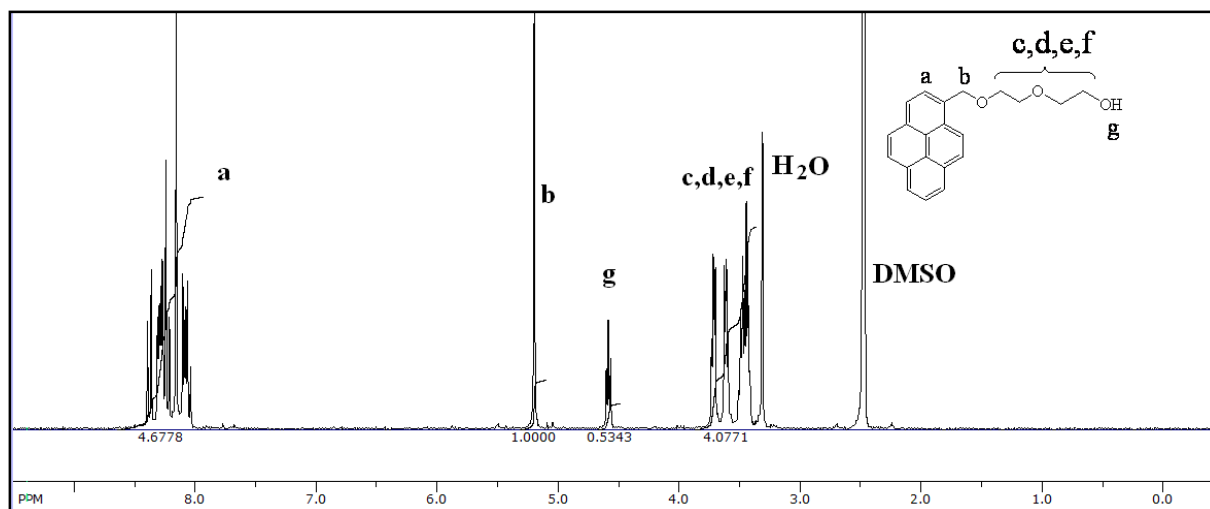


Figure SI4.1: ^1H NMR spectrum of PyEG₂-OH in DMSO-d₆ solvent.

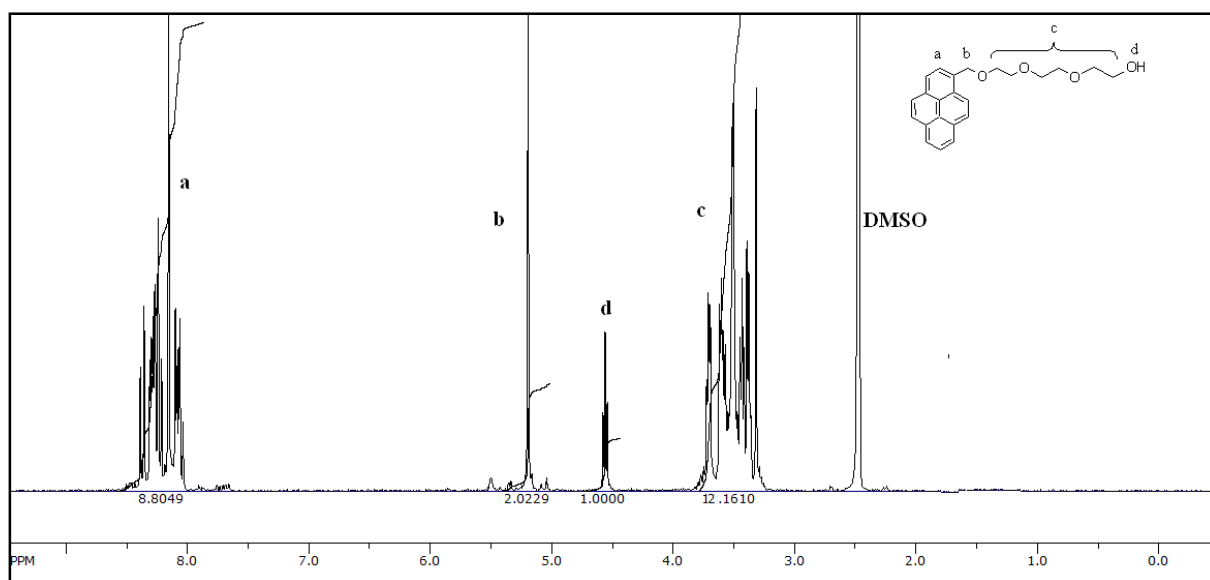


Figure SI4.2: ^1H NMR spectrum of PyEG₃-OH in DMSO-d₆ solvent.

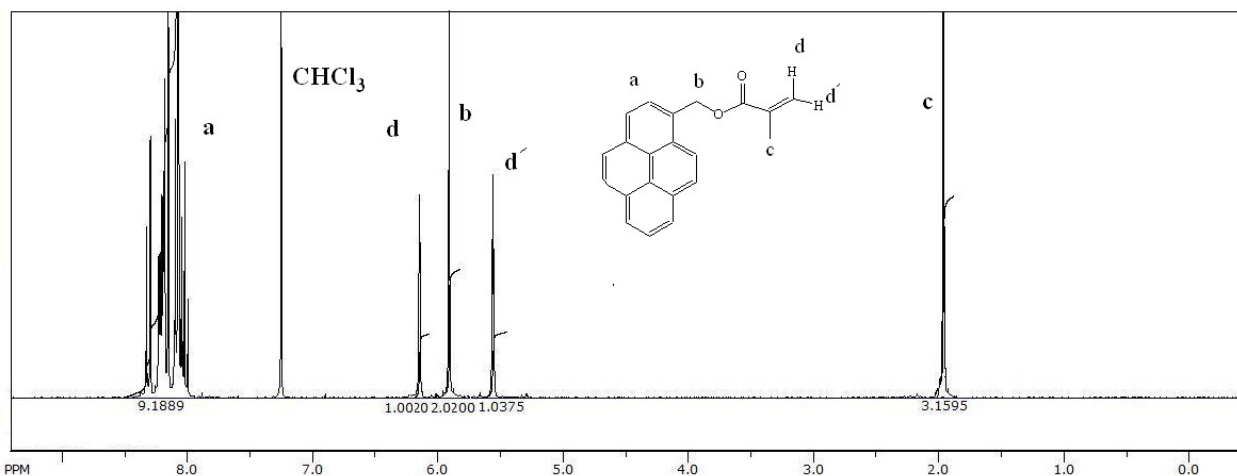


Figure SI4.3: ^1H NMR spectrum of PyEG₀-MA in (CDCl_3).

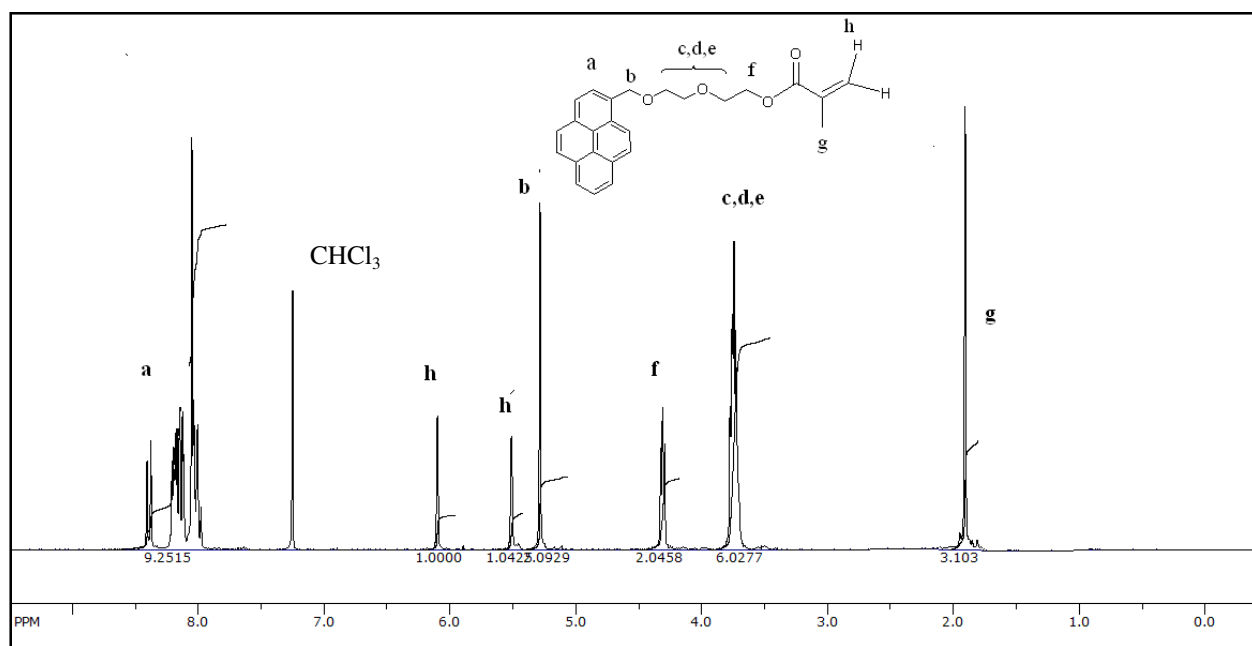


Figure SI4.4: ^1H NMR spectrum of PyEG₂-MA in (CDCl_3).

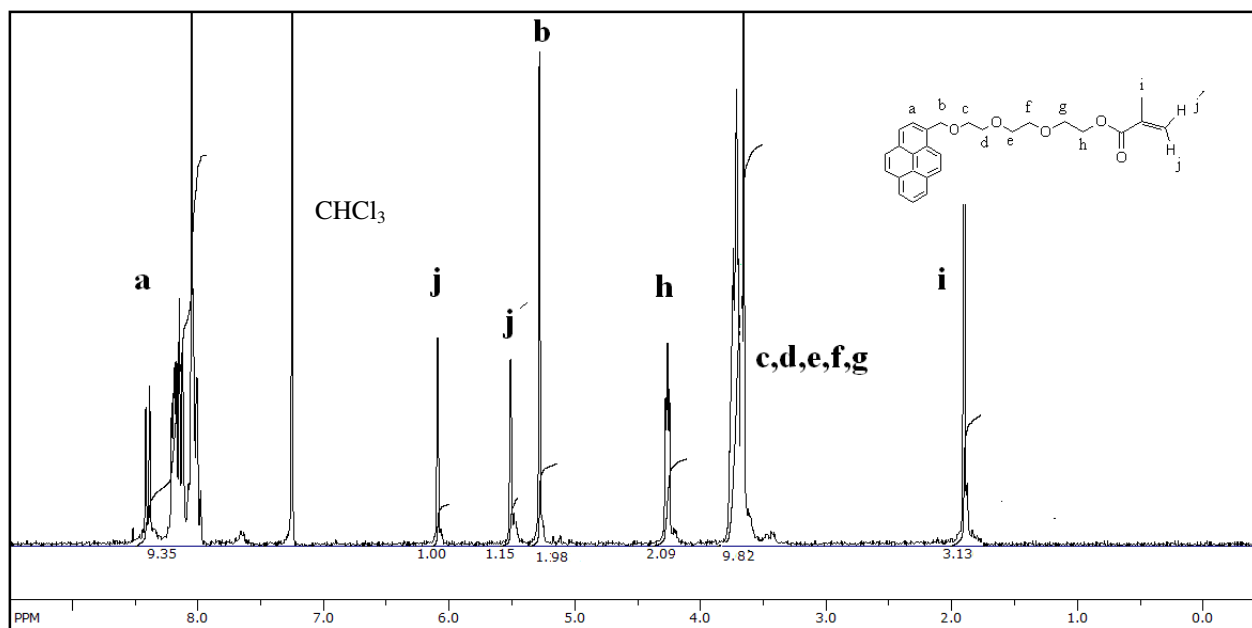


Figure SI4.5: ^1H NMR spectrum of PyEG₃-MA in (CDCl_3).

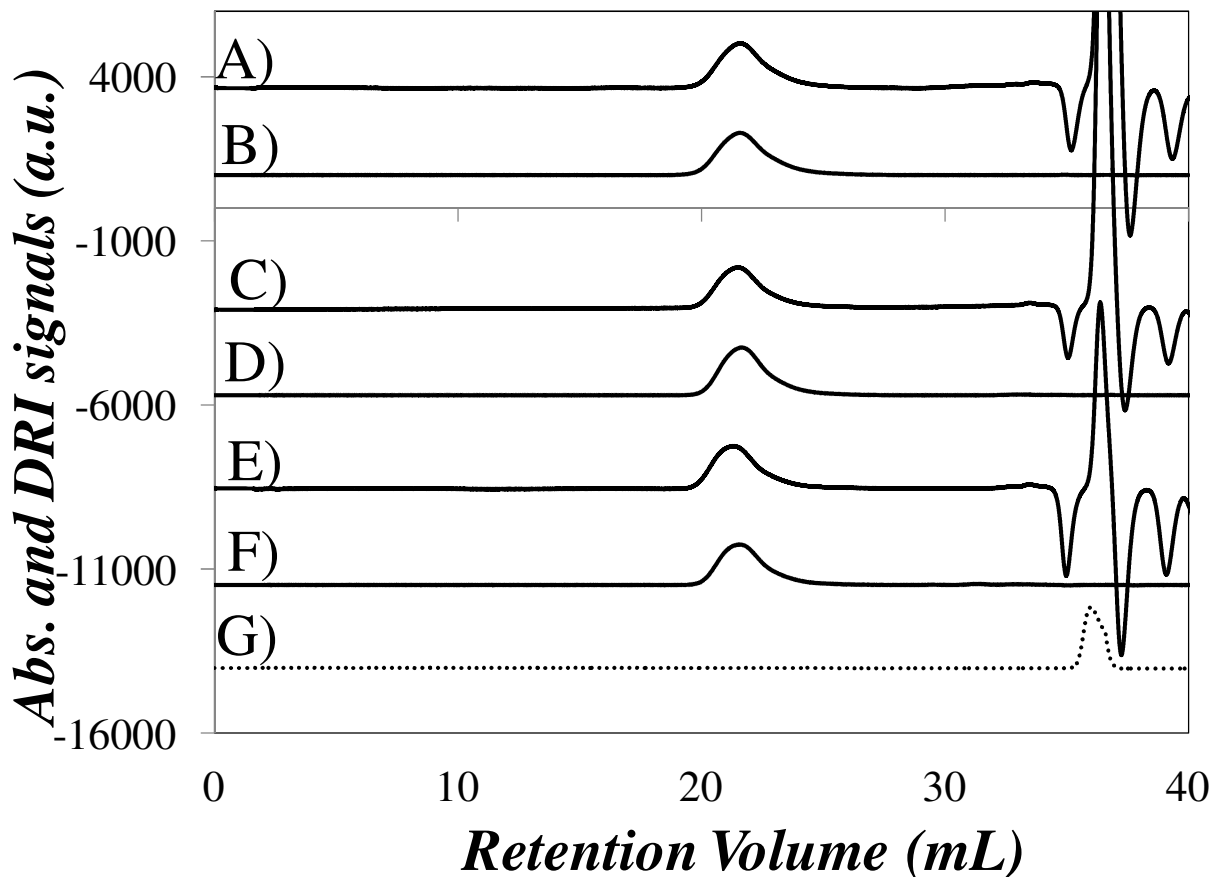


Figure SI4.6: GPC traces for (A,B) PyEG₀(4.0)-PBMA, (C,D) PyMeEG₂(2.3)-PBMA, (E,F) PyMeEG₃(2.8)-PBMA, and (G) PyEG₁-MA acquired with (A, C, and E) a DRI and (B, D, F, and G) UV-Vis absorption detector with excitation wavelength set at 344 nm where the 1-pyrenemethoxide label absorbs. Elution solvent: THF

Figure SI4.6 shows that the UV-Vis absorption and DRI traces of the PyEG_x-PBMA samples overlapped demonstrating that the polymers were labeled with pyrene. The absorption traces of the polymers showed no signal corresponding to low molecular species demonstrating that the

pyrene-labeled monomers used to prepare the PyEG_x-PBMA samples had been effectively removed (compare with trace G) for PyEG₁-MA).

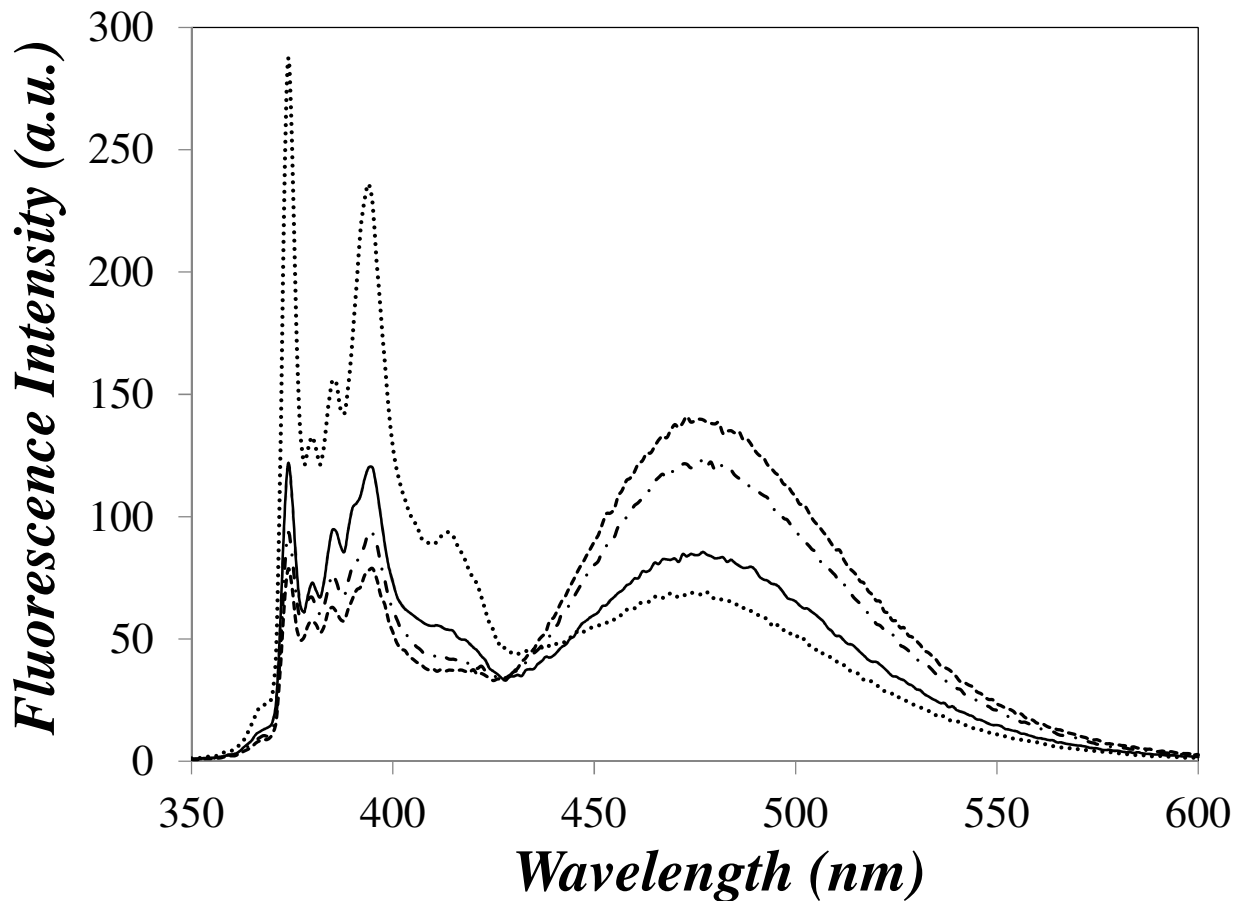


Figure SI4.7: Unnormalized steady-state fluorescence spectra of (....., $\phi_F = 0.38$) Py(4.0)EG₀-PBMA, (—, $\phi_F = 0.27$) Py(3.8)EG₁-PBMA, (-.-, $\phi_F = 0.32$) Py(3.9)EG₂-PBMA, and (-.-.-, $\phi_F = 0.28$) Py(4.2)EG₃-PBMA in THF. $[Py] = 2.5 \times 10^{-6}$ M, $\lambda_{ex} = 344$ nm.

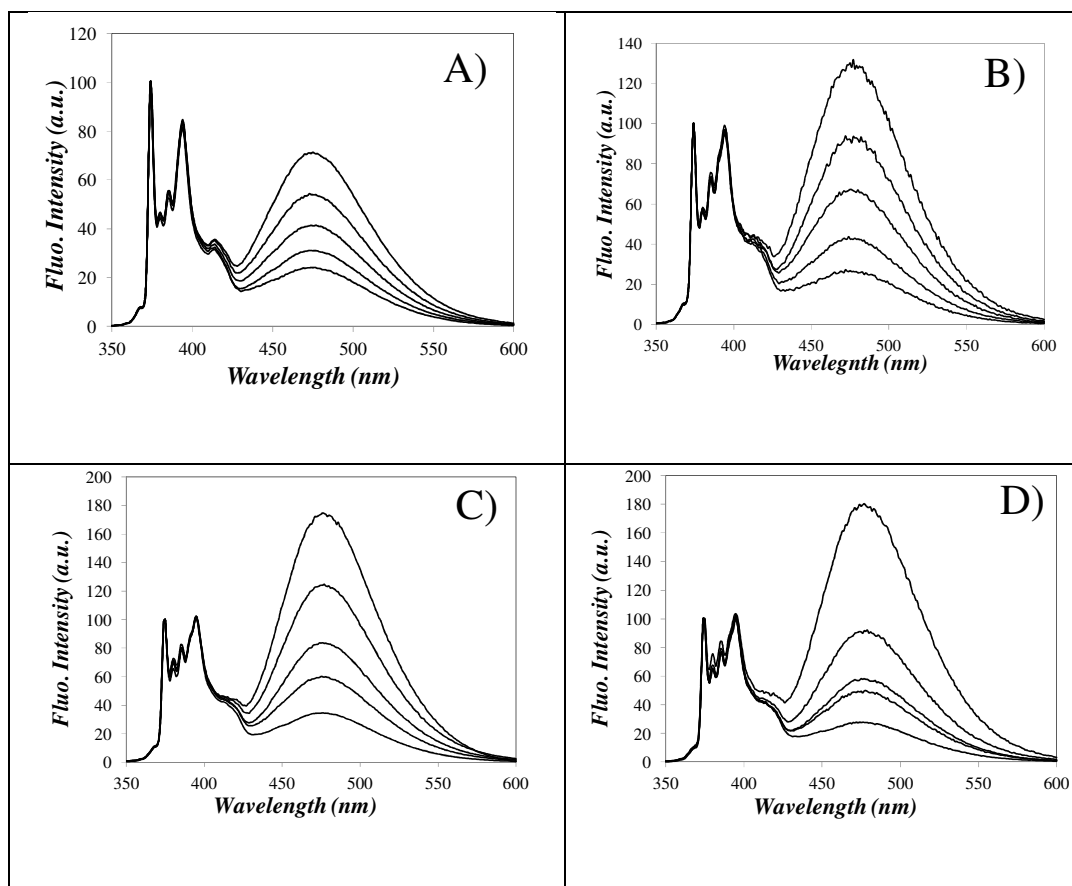


Figure SI4.8: Steady-state fluorescence spectra of A) PyEG₀-PBMA labeled with 4.0, 5.3, 6.3, 7.1, and 8.1 mol% pyrene (from bottom to top), B) PyEG₁-PBMA labeled with 1.8, 2.7, 3.8, 4.6 and 5.4 mol% pyrene (from bottom to top), C) PyEG₂-PBMA with 1.8, 2.3, 3.2, 3.9, and 5.3 mol% pyrene (from bottom to top), and D) PyEG₃-PBMA labeled with 1.0, 1.8, 2.1, 2.7, and 4.3 mol% pyrene (from bottom to top) in THF. $[Py] = 2.5 \times 10^{-6}$ M, $\lambda_{ex} = 344$ nm.

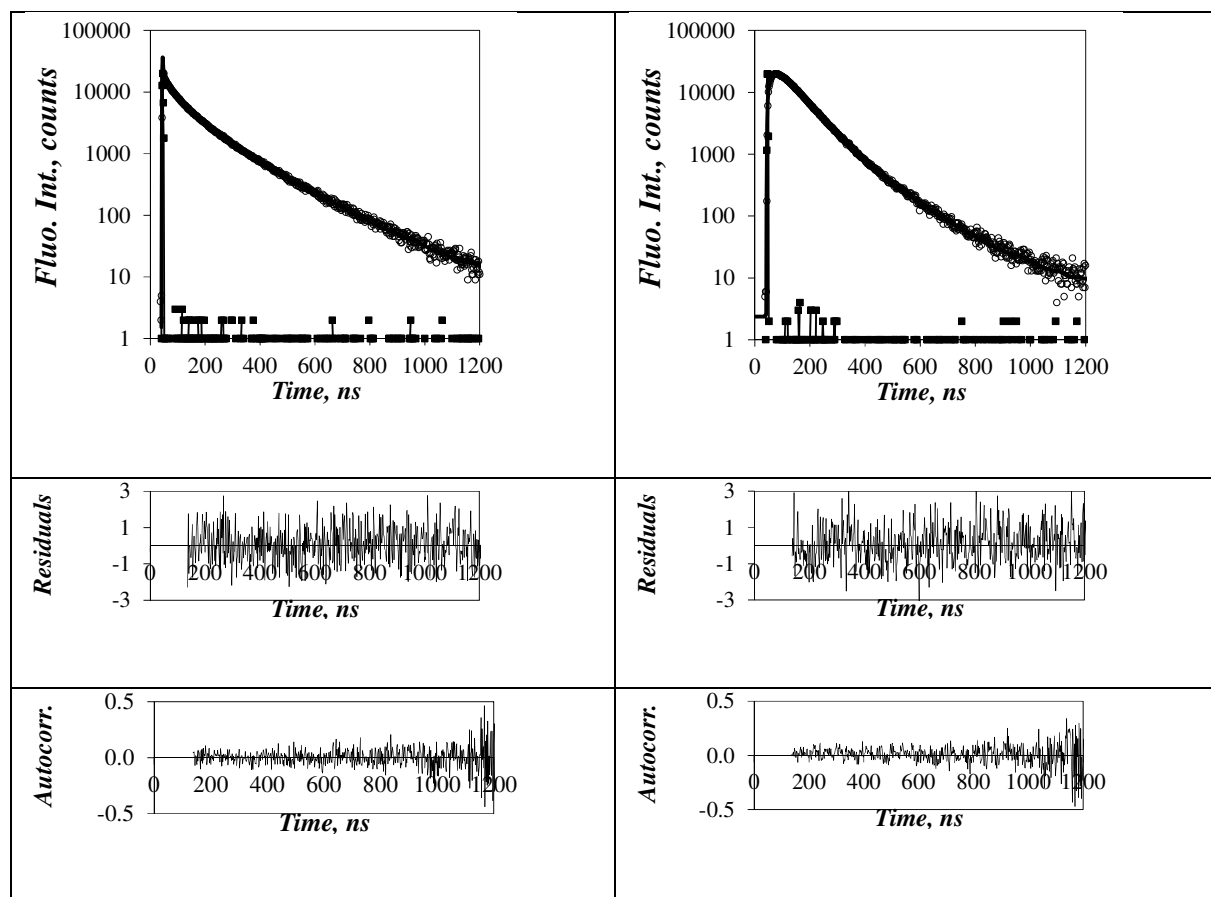


Figure SI4.9: Fit of the monomer (left; $\lambda_{\text{ex}} = 344 \text{ nm}$, $\lambda_{\text{em}} = 375 \text{ nm}$) and excimer (right; $\lambda_{\text{ex}} = 344 \text{ nm}$, $\lambda_{\text{em}} = 510 \text{ nm}$) fluorescence decays of Py(2.3)EG₂-PBMA in THF with Equations S1 and S2, respectively. Residuals and autocorrelation function are randomly distributed around zero. $\chi^2 = 1.05$.

Table SI4.1: Intrinsic viscosities of poly(n-butyl methacrylate) standards in THF at 25 °C.

M_n (g.mol ⁻¹)	PDI	Intrinsic Viscosity mL.g ⁻¹	Error
2800	1.10	1.15	±0.21
7000	1.60	6.08	±0.53
13000	1.12	8.49	±0.23
24000	1.25	15.19	±0.51
38000	1.15	24.79	±0.84

A log-log plot of $[\eta]$ vs M_n for the series of PBMA standards listed in Table SI4.1 yields a straight line in Figure SI4.8. The slope and intercept were obtained to determine the Mark-Houwink-Sakurada parameters K and a found to equal $2.8 (\pm 0.6) \times 10^{-4}$ mL/g and 1.09 ± 0.03 , respectively.

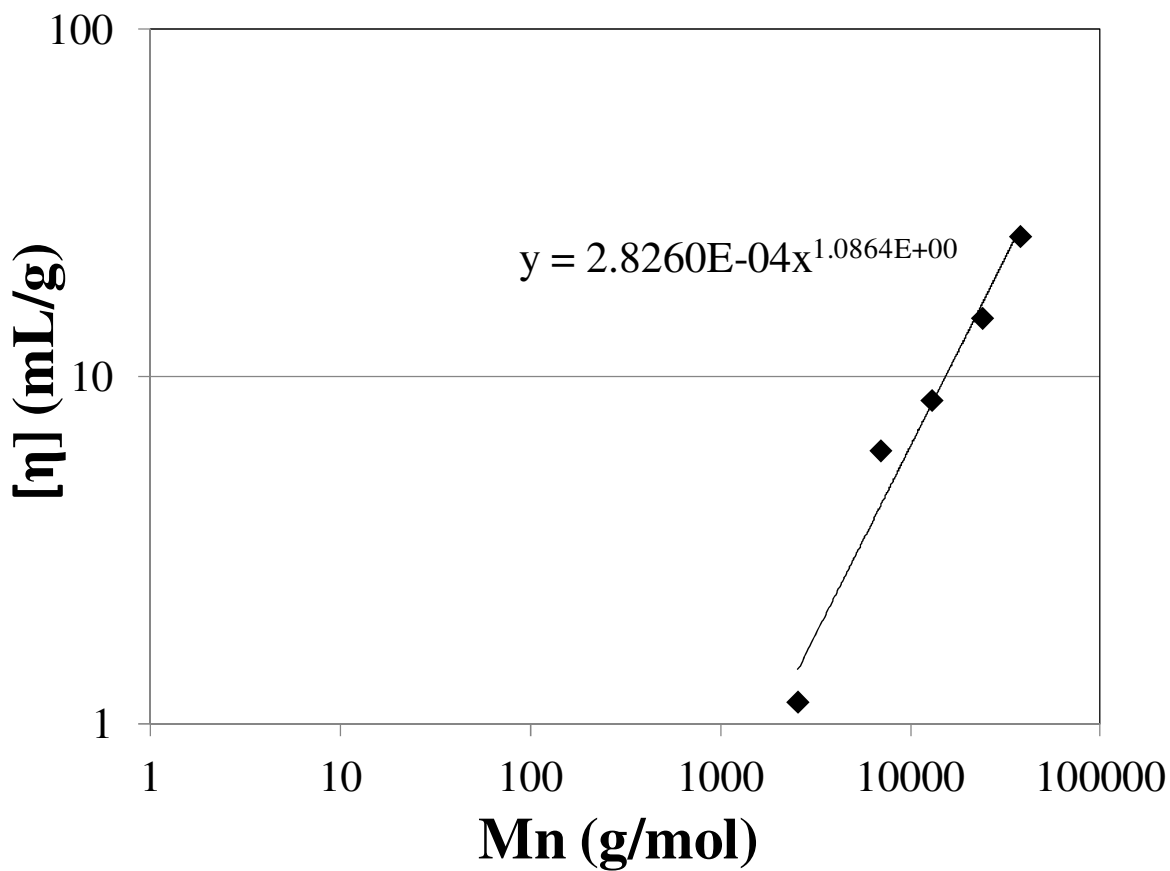


Figure SI4.10: Plot of intrinsic viscosity versus M_n for PBMA standards listed in Table SI4.1.

Table SI4.2: Chemical structure and distance (d) between the center of the pyrene label to the carbon atom bearing the ester function in the corresponding methacrylate monomer.

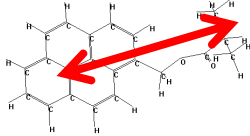
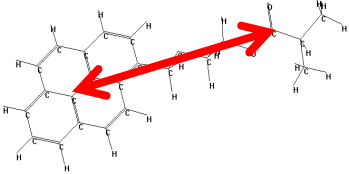
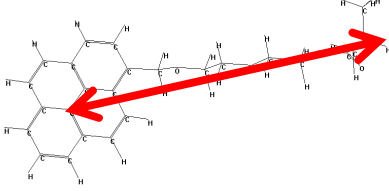
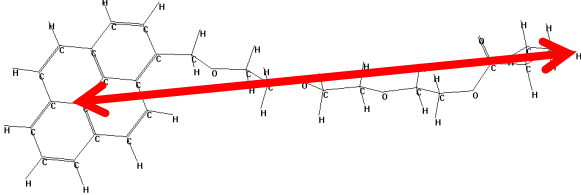
Sample	Structure	Distance (nm)
PyEG ₀ -PBMA		0.73
PyEG ₁ -PBMA		1.08
PyEG ₂ -PBMA		1.44
PyEG ₃ -PBMA		1.87

Table SI4.3: Parameters retrieved from the FBM analysis of the monomer decays of the randomly labeled poly(butymethacrylate)s.

Sample	Mol %	k_{blob} ($10^7 s^{-1}$)	$\langle n \rangle$	$k_e[blob]$ ($10^7 s^{-1}$)	f_{Mdiff}	k_2 (ns^{-1})	f_{k2}	τ_M (ns)	f_{Mfree}	χ^2
PyEG ₀ PBMA (THF) $\tau_M=260$ nm	4.0	0.35	1.8	0.31	0.8	0.09	0.1	260	0.06	1.1
	5.3	0.33	2.4	0.20	0.8	0.09	0.1	260	0.02	1.1
	6.3	0.36	2.7	0.32	0.7	0.09	0.2	260	0.03	1.0
	7.1	0.41	2.8	0.50	0.7	0.09	0.2	260	0.02	1.3
	8.1	0.45	3.1	0.54	0.7	0.09	0.2	260	0.01	1.3
PyEG ₁ PBMA (THF) $\tau_M=270$ nm	1.8	0.48	1.2	0.19	0.7	0.1	0.1	270	0.12	1.1
	2.7	0.60	1.4	0.31	0.7	0.1	0.1	270	0.06	1.1
	3.8	0.65	1.7	0.34	0.7	0.1	0.2	270	0.04	1.0
	4.6	0.59	2.2	0.37	0.6	0.1	0.3	270	0.02	1.1
	5.4	0.54	3.0	0.25	0.6	0.1	0.3	270	0.00	1.1
PyEG ₂ PBMA (THF) $\tau_M=270$ nm	1.8	0.62	1.3	0.15	0.7	0.1	0.1	270	0.04	1.0
	2.3	0.63	1.7	0.22	0.7	0.1	0.2	270	0.03	1.1
	3.2	0.67	2.1	0.31	0.6	0.1	0.3	270	0.01	1.0
	3.9	0.61	2.7	0.21	0.6	0.1	0.3	270	0.00	1.0
	5.3	0.60	3.5	0.35	0.5	0.1	0.4	270	0.00	1.0
PyEG ₃ PBMA (THF) $\tau_M=275$ nm	1.0	0.59	1.0	0.17	0.7	0.07	0.1	275	0.08	1.1
	1.9	0.58	1.5	0.20	0.7	0.07	0.2	275	0.03	1.0
	2.8	0.53	1.8	0.17	0.7	0.07	0.2	275	0.03	1.0
	2.1	0.59	2.2	0.25	0.6	0.07	0.3	275	0.01	1.1
	4.2	0.47	3.6	0.19	0.4	0.07	0.5	275	0.00	1.0

Table SI4.4: Parameters retrieved from the FBM analysis of the excimer decays of the randomly labeled poly(butymethacrylate)s.

Sample	Mol %	f_{Ediff}	τ_{E0} (ns)	f_{EE0}	τ_{EL} (ns)	f_{EEL}	k_2 (ns ⁻¹)	f_{Ek2}	χ^2
PyEG ₀ PBMA (THF)	4.0	0.81	51	0.01	144	0.060	0.09	0.12	1.1
	5.3	0.77	51	0.00	124	0.064	0.09	0.17	1.1
	6.3	0.72	51	0.01	114	0.071	0.09	0.20	1.0
	7.1	0.66	56	0.09	177	0.004	0.09	0.24	1.3
	8.1	0.60	55	0.17	185	0.005	0.09	0.22	1.3
PyEG ₁ PBMA (THF)	1.8	0.79	47	0.03	157	0.05	0.1	0.13	1.1
	2.7	0.73	53	0.05	146	0.03	0.1	0.19	1.1
	3.8	0.66	53	0.08	121	0.02	0.1	0.24	1.0
	4.6	0.59	52	0.11	108	0.02	0.1	0.28	1.1
	5.4	0.53	48	0.00	82	0.15	0.1	0.32	1.1
PyEG ₂ PBMA (THF)	1.8	0.70	48	0.03	155	0.05	0.1	0.22	1.0
	2.3	0.67	49	0.05	137	0.04	0.1	0.23	1.1
	3.2	0.59	52	0.12	187	0.01	0.1	0.29	1.0
	3.9	0.54	47	0.00	84	0.12	0.1	0.34	1.0
	5.3	0.47	46	0.00	76	0.15	0.1	0.38	1.0
PyEG ₃ PBMA (THF)	1.0	0.78	45	0.00	154	0.04	0.07	0.18	1.1
	1.9	0.68	50	0.04	139	0.03	0.07	0.25	1.0
	2.8	0.63	51	0.09	152	0.02	0.07	0.26	1.0
	2.1	0.65	48	0.05	125	0.05	0.07	0.25	1.1
	4.2	0.40	50	0.13	103	0.02	0.07	0.45	1.0

Table SI4.5: Overall fractions of pyrene species obtained from the FBM analysis of the monomer and excimer decays for the randomly labeled poly(butymethacrylate)s.

Sample	Mol%	f_{k2}	f_{diff}	f_{free}	f_{E0}	f_{EL}
PyEG ₀ PBMA (THF)	4.0	0.11	0.77	0.05	0.01	0.06
	5.3	0.16	0.76	0.02	0.00	0.06
	6.3	0.20	0.70	0.02	0.01	0.07
	7.1	0.24	0.65	0.02	0.09	0.00
	8.1	0.22	0.59	0.01	0.17	0.01
PyEG ₁ PBMA (THF)	1.8	0.12	0.70	0.11	0.03	0.04
	2.7	0.18	0.69	0.06	0.05	0.03
	3.8	0.23	0.64	0.04	0.07	0.02
	4.6	0.28	0.59	0.01	0.10	0.02
	5.4	0.32	0.52	0.00	0.00	0.15
PyEG ₂ PBMA (THF)	1.8	0.12	0.70	0.11	0.03	0.04
	2.3	0.18	0.69	0.06	0.05	0.03
	3.2	0.23	0.64	0.04	0.07	0.02
	3.9	0.28	0.59	0.01	0.10	0.02
	5.3	0.32	0.52	0.00	0.00	0.15
PyEG ₃ PBMA (THF)	1.0	0.17	0.72	0.08	0.00	0.04
	1.9	0.24	0.66	0.03	0.04	0.03
	2.8	0.24	0.63	0.02	0.09	0.02
	2.1	0.32	0.58	0.01	0.05	0.05
	4.2	0.45	0.40	0.00	0.13	0.02

Appendix SI5-Supporting Information for Chapter 5: Characterization of the Long Range Internal Dynamics of Pyrene-Labeled Macromolecules by Pyrene Excimer.

MODEL FREE ANALYSIS (MFA)

The derivation of the equations used to fit the monomer and excimer decays has been described succinctly in the main text of this report and in more details in earlier publications.¹⁻⁴ The expressions used for the global MFA of the monomer and excimer decays are given in Equations S5I.1 and SI5.2, respectively.

$$[Py^*]_{(t)}/[Py^*]_o = (f_{diff}^{E0} + f_{diff}^D) \times \sum_{i=1}^n a_i \times \exp(-t/\tau_i) + f_{free} \times \exp(-t/\tau_M) \quad (SI5.1)$$

$$[E^*]/[Py^*]_o = -f_{diff}^{E0} \times \sum_{i=1}^n a_i \frac{\frac{1}{\tau_i} - \frac{1}{\tau_M}}{\frac{1}{\tau_i} - \frac{1}{\tau_{E0}}} \exp(-t/\tau_i) + \left(f_{E0} + f_{diff}^{E0} \times \sum_{i=1}^n a_i \frac{\frac{1}{\tau_i} - \frac{1}{\tau_M}}{\frac{1}{\tau_i} - \frac{1}{\tau_{E0}}} \right) \times \exp(-t/\tau_{E0}) - f_{diff}^D \times \sum_{i=1}^n a_i \frac{\frac{1}{\tau_i} - \frac{1}{\tau_M}}{\frac{1}{\tau_i} - \frac{1}{\tau_D}} \exp(-t/\tau_i)$$

$$+ \left(f_D + f_{diff}^D \times \sum_{i=1}^n a_i \frac{\frac{1}{\tau_i} - \frac{1}{\tau_M}}{\frac{1}{\tau_i} - \frac{1}{\tau_D}} \right) \times \exp(-t / \tau_D) \quad (\text{SI5.2})$$

The parameters used in Equations SI5.1 and SI5.2 have been described in the main text. There are five types of excited pyrenes, namely the pyrenes that do not form excimer (Py_{free}^*), those that form an excimer by diffusive encounters with a ground-state pyrene to give either an excimer $E0^*$ (Py_{diff}^{E0}) or D^* (Py_{diff}^D), and those that are involved in a pyrene aggregate and form an excimer $E0^*$ or D^* upon direct absorption. The molar fractions representing the five species Py_{free}^* , Py_{diff}^{E0} , Py_{diff}^D , $E0^*$, and D^* are referred to as f_{free} , f_{diff}^{E0} , f_{diff}^D , f_{E0} , and f_D , respectively. Since the pyrene monomer only reports on Py_{free}^* , Py_{diff}^{E0} , and Py_{diff}^D , the fit of the monomer decay yields the respective molar fractions f_{Mfree} and f_{Mdiff} ($= f_{Mdiff}^{E0} + f_{Mdiff}^D$). Similarly, the excimer decay reports only on the species Py_{diff}^{E0} , Py_{diff}^D , $E0^*$, and D^* and its fit yields the corresponding molar fractions f_{Ediff}^{E0} , f_{Ediff}^D , f_{EE0} , and f_{ED} , respectively. The expression of the molar fractions f_{Mfree} , f_{Mdiff} , f_{Ediff}^{E0} , f_{Ediff}^D , f_{EE0} , and f_{ED} are listed in Equations SI5.3-SI5.9.

$$f_{Mdiff} = \frac{[Py_{diff}^{E0}]_o + [Py_{diff}^D]_o}{[Py_{diff}^{E0}]_o + [Py_{diff}^D]_o + [Py_{free}^*]_o} \quad (\text{SI5.3})$$

$$f_{Mfree} = \frac{[Py_{free}^*]_o}{[Py_{diff}^{E0*}]_o + [Py_{diff}^D*]_o + [Py_{free}^*]_o} \quad (SI5.4)$$

$$f_{Ediff}^{E0} = \frac{[Py_{diff}^{E0*}]_o}{[Py_{diff}^{E0*}]_o + [Py_{diff}^D*]_o + [E0^*]_o + [D^*]_o} \quad (SI5.5)$$

$$f_{Ediff}^D = \frac{[Py_{diff}^D*]_o}{[Py_{diff}^{E0*}]_o + [Py_{diff}^D*]_o + [E0^*]_o + [D^*]_o} \quad (SI5.6)$$

$$f_{EE0} = \frac{[E0^*]_o}{[Py_{diff}^{E0*}]_o + [Py_{diff}^D*]_o + [E0^*]_o + [D^*]_o} \quad (SI5.7)$$

$$f_{ED} = \frac{[D^*]_o}{[Py_{diff}^{E0*}]_o + [Py_{diff}^D*]_o + [E0^*]_o + [D^*]_o} \quad (SI5.8)$$

The fractions obtained from the global analysis of the monomer and excimer fluorescence decay analysis can be used to calculate the overall molar fraction of f_{diff} , f_{free} , f_{E0} , f_D , and f_{agg} according to Equations SI5.9 – SI5.13.

$$f_{diff}^{E0} = \frac{[Py_{diff}^{E0*}]_o}{[Py_{diff}^{E0*}]_o + [Py_{diff}^D*]_o + [Py_{free}^*]_o + [E0^*]_o + [D^*]_o} = \left(1 + \frac{f_{Mfree}}{f_{Mdiff}} + \frac{f_{Ediff}^D}{f_{Ediff}^{E0}} + \frac{f_{EE0}}{f_{Ediff}^{E0}} + \frac{f_{ED}}{f_{Ediff}^{E0}} \right)^{-1}$$

(SI5.9)

$$f_{diff}^D = \frac{[Py_{diff}^D *]_o}{[Py_{diff}^{E0} *]_o + [Py_{diff}^D *]_o + [Py_{diff} *]_o + [E0*]_o + [D*]_o} = f_{diff}^{E0} \times \frac{f_{Ediff}^D}{f_{Ediff}^{E0}}$$

(SI5.10)

$$f_{free} = \frac{[Py_{free} *]_o}{[Py_{diff}^{E0} *]_o + [Py_{diff}^D *]_o + [Py_{free} *]_o + [E0*]_o + [D*]_o} = f_{diff}^{E0} \times \frac{f_{Mfree}}{f_{Mdiff}} \quad (SI5.11)$$

$$f_{E0} = \frac{[E0*]_o}{[Py_{diff}^{E0} *]_o + [Py_{diff}^D *]_o + [Py_{free} *]_o + [E0*]_o + [D*]_o} = f_{diff}^{E0} \times \frac{f_{EE0}}{f_{Ediff}^{E0}} \quad (SI5.12)$$

$$f_{E0} = \frac{[D*]_o}{[Py_{diff}^{E0} *]_o + [Py_{diff}^D *]_o + [Py_{free} *]_o + [E0*]_o + [D*]_o} = f_{diff}^{E0} \times \frac{f_{ED}}{f_{Ediff}^{E0}} \quad (SI5.13)$$

The molar fraction of pyrene labels that form excimer by diffusion or upon direct excitation of a pyrene aggregate are referred to as f_{diff} ($= f_{diff}^{E0} + f_{diff}^D$) and f_{agg} ($= f_{E0} + f_D$).

The monomer and excimers $E0^*$ and D^* have a natural lifetime τ_M , τ_{E0} , and τ_D , respectively. The pre-exponential factor a_i in Equation S5I.1 are normalized to unity

($\sum_{i=1}^n a_i = 1$). All parameters retrieved from the MFA of the decays according to Equations SI5.1

and SI5.2 have been listed in Tables SI5.1-12.

Table SI5.1: Parameters retrieved from the MFA of the monomer decays of the pyrene labeled constructs in THF.

Sample	Mol %	τ_1 (ns)	a_1	τ_2 (ns)	a_2	τ_3 (ns)	a_3	τ_M (ns)	f_{Mfree}	χ^2
Py-C1A $\tau_M = 190$ ns	2.6	34	0.41	9.7	0.30	85	0.28	190	0.02	1.2
	2.6	78	0.26	30.7	0.38	9	0.30	190	0.06	1.0
	5.0	58	0.10	21.1	0.39	7	0.49	190	0.01	1.0
	6.7	54	0.07	17.0	0.41	5	0.51	190	0.01	1.2
Py-C1MA $\tau_M = 200$ ns	2.6	46	0.41	11.1	0.14	106	0.43	200	0.02	1.2
	4.1	38	0.46	10.4	0.18	84	0.34	200	0.02	1.1
	5.3	29	0.50	7.1	0.22	65	0.27	200	0.01	1.2
	5.2	32	0.50	9.2	0.22	75	0.27	200	0.01	1.0
	5.6	32	0.53	8.0	0.24	70	0.23	200	0.00	1.2
	7.3	25	0.53	6.3	0.24	58	0.19	200	0.03	1.2
Py-C4MA $\tau_M = 195$ ns	2.2	64	0.30	12.0	0.09	134	0.48	195	0.13	1.2
	3.0	38	0.26	8.0	0.10	99	0.52	195	0.12	1.0
	3.6	44	0.37	10.7	0.20	99	0.37	195	0.06	1.1
	5.3	44	0.43	10.7	0.22	96	0.34	195	0.01	1.1
	7.2	26	0.44	6.7	0.21	63	0.33	195	0.01	1.1
Py-C4TMA $\tau_M = 207$ ns	3.6	58	0.22	11.6	0.12	138	0.58	207	0.07	1.0
	3.8	49	0.24	11.1	0.14	123	0.57	207	0.05	1.2
	4.7	45	0.30	9.0	0.19	111	0.49	207	0.02	1.2
	5.6	37	0.30	8.7	0.23	95	0.46	207	0.01	1.0
	7.6	30	0.36	8.4	0.25	80	0.37	207	0.01	1.2
Py-C6MA $\tau_M = 204$ ns	2.0	64	0.24	15.1	0.09	140	0.49	204	0.17	1.0
	3.3	41	0.24	5.8	0.13	121	0.55	204	0.09	1.1
	4.8	55	0.33	14.9	0.17	114	0.43	204	0.07	1.1
	5.8	49	0.33	16.9	0.18	102	0.42	204	0.07	1.2
	6.7	38	0.39	10.3	0.20	90	0.36	204	0.04	1.1
	8.1	37	0.42	10.5	0.25	81	0.33	204	0.01	1.1

Py-C6CyMA $\tau_M = 205$ ns	2.1	47	0.14	9.1	0.08	142	0.44	205	0.33	1.2
	3.0	64	0.23	12.8	0.10	142	0.59	205	0.07	1.2
	3.8	52	0.23	11.7	0.14	123	0.58	205	0.05	1.0
	5.1	39	0.26	8.1	0.15	107	0.55	205	0.04	1.1
	6.2	51	0.36	11.3	0.24	108	0.39	205	0.01	1.1
	7.0	29	0.34	6.6	0.22	79	0.43	205	0.02	1.1
Py-C8MA $\tau_M = 200$ ns	4.3	46	0.24	10.7	0.14	118	0.46	200	0.15	1.1
	5.1	43	0.27	8.9	0.15	106	0.53	200	0.05	1.1
	2.7	61	0.22	11.4	0.09	132	0.50	200	0.19	1.0
	6.1	43	0.27	12.6	0.20	98	0.49	200	0.03	1.1
	7.3	34	0.35	10.0	0.22	85	0.40	200	0.02	1.1
Py-C12MA $\tau_M = 200$ ns	3.5	53	0.19	11.6	0.11	137	0.53	200	0.17	1.1
	5.6	51	0.27	11.4	0.18	120	0.49	200	0.07	1.0
	6.0	44	0.30	8.9	0.18	108	0.48	200	0.03	1.2
	7.7	43	0.32	10.4	0.22	104	0.42	200	0.04	1.1
	10.	34	0.37	8.6	0.27	86	0.34	200	0.01	1.1
Py-C18MA $\tau_M = 206$ ns	4.5	45	0.19	9.1	0.13	130	0.50	206	0.18	1.1
	5.9	52	0.28	11.1	0.21	126	0.39	206	0.12	1.1
	6.8	44	0.28	9.0	0.18	117	0.46	206	0.08	1.1
	6.7	47	0.30	9.1	0.21	122	0.43	206	0.05	1.0
	14.	27	0.38	6.9	0.36	73	0.23	206	0.12	1.2
CoBuE-PS-BuPy $\tau_M = 200$ ns	2.1	52	0.31	17.7	0.15	122	0.47	200	0.07	1.1
	3.1	39.	0.40	12.5	0.18	102	0.39	200	0.03	1.0
	4.5	27.	0.48	7.6	0.17	74	0.34	200	0.01	1.2
	5.4	27.	0.40	10.3	0.27	63	0.32	200	0.01	1.1
	6.0	28.	0.47	9.9	0.31	67	0.22	200	0.00	1.1
PEO(3.4K)-Py ₂	-	48	0.10	123	0.81	-	-	258	0.09	1.1
PEO(5K)-Py ₂	-	51	0.10	153	0.73	-	-	258	0.17	1.0
PEO(6K)-Py ₂	-	47	0.11	187	0.80	-	-	258	0.09	1.2
PP-G2-BuPy4	-	2.5	0.80	5.0	0.18	39	0.02	200	0.01	1.1

PP-G3-BuPy8	-	1.5	0.67	2.6	0.32	40	0.01	200	0.00	1.0
PP-G4-BuPy16	-	1.2	0.82	2.3	0.15	32	0.01	200	0.03	1.0
DiPy	-	2.8	0.25	5	0.69	32	0.04	241	0.03	1.1
Poly(PyEG ₃ MA)	-	1.1	0.93	4	0.06	43	0.01	200	0.00	1.1
Poly(PyBuMA)	-	1.7	0.85	20	0.07	54	0.07	280	0.00	1.1

Table SI5.2: Parameters retrieved from the MFA of the monomer decays of the pyrene labeled constructs in Toluene.

Sample	Mol %	τ_1 (ns)	a_1	τ_2 (ns)	a_2	τ_3 (ns)	a_3	τ_M (ns)	f_{Mfree}	χ^2
Py-C1MA $\tau_M = 176$ ns	2.6	115	0.21	25	0.31	70	0.46	176	0.23	1.1
	4.1	11	0.20	37	0.48	78	0.31	176	0.01	1.1
	5.3	12	0.30	30	0.41	57	0.28	176	0.01	1.0
	5.2	30	0.37	63	0.33	12	0.29	176	0.02	1.2
	5.6	10	0.14	43	0.36	87	0.44	176	0.06	1.2
	7.3	24	0.50	50	0.22	9	0.27	176	0.00	1.1
Py-C4MA $\tau_M = 180$ ns	2.2	13	0.08	49	0.21	110	0.50	180	0.21	1.0
	3.0	14	0.14	52	0.36	106	0.43	180	0.07	1.1
	3.6	10	0.17	40	0.37	89	0.39	180	0.08	1.2
	5.3	13	0.20	77	0.47	35	0.30	180	0.02	1.1
	7.2	10	0.30	29	0.40	63	0.28	180	0.01	1.1
CoBuE-PS-BuPy $\tau_M = 184$ ns	2.1	16	0.16	50	0.3	113	0.43	184	0.08	1.1
	3.1	18	0.30	52	0.4	103	0.29	184	0.03	1.1
	4.5	13	0.32	34	0.4	72	0.25	184	0.02	1.2
	5.4	30	0.43	67	0.2	12	0.37	184	0.01	1.2
	6.0	10	0.35	65	0.2	29	0.47	184	0.00	1.1
PEO(3.4K)-Py ₂	-	50	0.10	105	0.84	-	-	232	0.06	1.1
PEO(5K)-Py ₂	-	50	0.11	130	0.77	-	-	232	0.12	1.0
PEO(6K)-Py ₂	-	47	0.05	162	0.88	-	-	232	0.07	1.1
PP-G2-BuPy ₄	-	2.0	0.79	4.1	0.19	36	0.01	179	0.01	1.1
PP-G3-BuPy ₈	-	1.4	0.89	4.3	0.09	28	0.01	179	0.02	1.1
PP-G4-BuPy ₁₆	-	0.9	0.84	2.0	0.13	31	0.01	179	0.02	1.0
DiPy	-	3.0	0.95	5.8	0.04	38	0.00	226	0.00	1.1
Poly(PyEG ₃ MA)	-	1.0	0.91	3.7	0.10	40	0.01	179	0.00	1.0
Poly(PyBuMA)	-	1.8	0.73	18.4	0.10	49	0.12	246	0.00	1.0

Table SI5.3: Parameters retrieved from the MFA of the monomer decays of the pyrene labeled constructs in DMF.

Sample	Mol %	τ_1 (ns)	a_1	τ_2 (ns)	a_2	τ_3 (ns)	a_3	τ_M (ns)	f_{Mfree}	χ^2
Py-C1A $\tau_M = 165$ ns	1.7	13	0.19	42	0.30	110	0.46	165	0.06	1.1
	2.6	10	0.21	35	0.40	88	0.37	165	0.03	1.1
	2.6	9	0.19	30	0.42	81	0.37	165	0.02	1.0
	5.0	20	0.48	52	0.20	7	0.31	165	0.01	1.1
	6.7	15	0.48	43	0.22	6	0.28	165	0.01	1.1
Py-C1MA $\tau_M = 164$ ns	2.6	12	0.13	50	0.36	105	0.47	164	0.03	1.1
	4.1	10	0.11	99	0.54	40	0.31	164	0.04	1.1
	5.2	35	0.35	79	0.47	9	0.16	164	0.02	1.2
	5.3	37	0.52	11	0.27	76	0.21	164	0.01	0.9
	7.3	9	0.20	32	0.43	73	0.35	164	0.01	1.1
Py-C4MA $\tau_M = 160$ ns	2.2	13	0.07	46	0.15	107	0.57	160	0.21	1.1
	3.0	11	0.11	43	0.28	97	0.54	160	0.07	1.1
	3.6	16	0.29	53	0.29	79	0.33	160	0.16	1.0
	5.3	15	0.19	44	0.36	80	0.42	160	0.03	1.1
	7.2	11	0.26	30	0.38	59	0.35	160	0.01	1.1
CoBuE-PS-BuPy $\tau_M = 168$ ns	2.1	21	0.13	59	0.33	114	0.48	168	0.06	1.0
	3.1	22	0.25	51	0.35	99	0.37	168	0.04	1.1
	4.5	19	0.34	46	0.36	76	0.28	168	0.01	1.1
	5.4	9	0.15	28	0.50	64	0.33	168	0.01	1.0
	6.0	59	0.16	27	0.52	59	0.31	168	0.01	1.1
Amylopectin $\tau_M = 161$ ns	4.1	4	0.22	30	0.35	91	0.39	161	0.04	1.0
	5.7	3	0.25	24	0.36	79	0.34	161	0.05	1.0
	8.7	3	0.30	17	0.43	48	0.25	161	0.01	1.0
	9.6	3	0.31	18	0.43	47	0.25	161	0.00	1.0
	12.0	3	0.33	16	0.47	42	0.20	161	0.00	1.0

Amylose $\tau_M = 161$ ns	5.1	57	0.27	22	0.20	118	0.48	161	0.05	1.0
	5.6	20	0.18	58	0.30	116	0.45	161	0.07	1.0
	5.6	16	0.28	45	0.26	104	0.36	161	0.11	1.0
	7.5	4	0.23	27	0.34	84	0.39	161	0.05	1.0
	10.1	21	0.39	3	0.30	69	0.28	161	0.02	1.0
PEO(3.4K)-Py ₂	-	55	0.05	141	0.85	-	-	220	0.10	1.1
PEO(5K)-Py ₂	-	52	0.06	162	0.77	-	-	220	0.17	1.1
PEO(6K)-Py ₂	-	46	0.06	185	0.81	-	-	220	0.13	1.0
PP-G2-BuPy4	-	2.9	0.66	5	0.32	39	0.02	163	0.01	1.1
PP-G3-BuPy8	-	2.2	0.85	4	0.14	42	0.01	163	0.00	1.2
PP-G4-BuPy16	-	1.5	0.74	3	0.20	71	0.03	163	0.03	1.1
DiPy	-	3.9	0.17	5.5	0.81	35	0.02	202	0.00	1.1
Poly(PyBuMA)	-	1.1	0.84	3	0.13	23	0.01	163	0.01	1.1
Poly(PyEG ₃ MA)	-	2.1	0.89	14	0.09	44	0.02	234	0.00	1.1

Table SI5.4: Parameters retrieved from the MFA of the monomer decays of the pyrene labeled constructs in DMSO.

Sample	Mol%	τ_1 (ns)	a_1	τ_2 (ns)	a_2	τ_3 (ns)	a_3	τ_M (ns)	f_{Mfree}	χ^2
Py-C1A $\tau_M = 86$ ns	1.7	64	0.55	25	0.24	7	0.06	86	0.15	1.1
	2.6	58	0.54	24	0.31	6	0.08	86	0.06	1.1
	2.6	58	0.50	25	0.37	7	0.10	86	0.03	1.0
	5.0	48	0.25	21	0.54	6	0.21	86	0.00	1.1
	6.7	38	0.32	15	0.52	3	0.15	86	0.01	1.1
Amylose $\tau_M = 90$ ns	5.1	18	0.23	0.52	0.37	80	0.26	90	0.13	1.0
	5.6	6	0.11	64	0.21	72	0.56	90	0.12	1.0
	5.6	17	0.23	25	0.26	78	0.46	90	0.05	1.0
	7.5	7	0.15	54	0.29	69	0.55	90	0.00	1.0
	10.1	9	0.23	29	0.38	68	0.38	90	0.00	1.0
	14.9	4	0.18	31	0.38	48	0.41	90	0.02	1.0
Amylopectin $\tau_M = 92$ ns	4.1	23	0.24	64	0.64	4	0.08	92	0.03	1.0
	5.7	21	0.29	59	0.56	3	0.11	92	0.04	1.0
	8.7	19	0.36	45	0.44	3	0.19	92	0.01	1.0
	9.6	19	0.39	45	0.41	3	0.20	92	0.00	1.0
	12.0	15	0.36	39	0.38	2	0.25	92	0.00	1.0
PEO(3.4K)-Py ₂	-	35	0.04	82	0.88	-	-	96	0.08	1.1
PEO(5K)-Py ₂	-	35	0.06	88	0.73	-	-	96	0.21	1.1
PEO(6K)-Py ₂	-	34	0.05	93	0.69	-	-	96	0.26	1.2
PP-G2-BuPy4	-	2.6	0.31	6.1	0.67	39	0.02	130	0.00	1.1
PP-G3-BuPy8	-	1.9	0.34	4.2	0.65	42	0.01	130	0.00	1.1
PP-G4-BuPy16	-	1.6	0.42	3.1	0.52	66	0.06	130	0.00	1.1
DiPy	-	5	0.52	7	0.46	29	0.01	88	0.00	1.0
Poly(PyBuMA)	-	1.5	0.61	4.6	0.36	38	0.02	130	0.00	1.1
Poly(PyEG ₃ MA)	-	1.8	0.72	5.2	0.26	22	0.02	193	0.00	1.2

Table SI5.5: Parameters retrieved from the MFA of the excimer decays of of the pyrene labeled constructs in THF.

Sample	Mol %	f_{Ediff}^{E0}	f_{Ediff}^D	τ_{E0} (ns)	τ_D (ns)	τ_S (ns)	f_{EE0}	f_{ED}	f_{ES}^*	χ^2
Py-C1A $\tau_M = 190$ ns	2.6	0.97	-	52	183	-	0.03	0.00	-	1.2
	2.6	0.97	-	51	86	-	0.00	0.03	-	1.0
	5.0	0.94	-	50	141	-	0.06	0.00	-	1.0
	6.7	0.90	-	51	141	-	0.10	0.00	-	1.2
Py-C1MA $\tau_M = 200$ ns	2.6	0.98	-	53	116	-	0.00	0.02	-	1.2
	4.1	0.96	-	53	115	-	0.03	0.01	-	1.1
	5.3	0.98	-	52	110	-	0.01	0.01	-	1.2
	5.2	0.93	-	51	89	-	0.00	0.07	-	1.0
	5.6	0.96	-	52	94	-	0.00	0.04	-	1.2
	7.3	0.92	-	51	91	-	0.03	0.05	-	1.2
Py-C4MA $\tau_M = 195$ ns	2.2	0.97	-	52	153	-	0.01	0.02	-	1.2
	3.0	0.94	-	55	171	-	0.04	0.01	-	1.0
	3.6	0.94	-	55	86	-	0.04	0.03	-	1.1
	5.3	0.94	-	54	85	-	0.01	0.05	-	1.1
	7.2	0.93	-	52	79	-	0.00	0.07	-	1.1
Py-C4TMA $\tau_M = 207$ ns	3.6	0.94	-	51	136	-	0.00	0.06	-	1.0
	3.8	0.94	-	53	115	-	0.00	0.06	-	1.2
	4.7	0.93	-	54	117	-	0.02	0.05	-	1.2
	5.6	0.91	-	53	88	-	0.00	0.08	-	1.0
	7.6	0.88	-	55	53	-	0.11	0.01	-	1.2
Py-C6MA $\tau_M = 204$ ns	2.0	0.94	-	57	159	-	0.03	0.02	-	1.0
	3.3	1.00	-	60	151	-	0.00	0.00	-	1.1
	4.8	0.92	-	57	150	-	0.07	0.01	-	1.1
	5.8	0.88	-	56	157	-	0.12	0.00	-	1.2
	6.7	0.91	-	57	145	-	0.08	0.00	-	1.1

	8.1	0.90	-	55	148	-	0.10	0.00	-	1.1
Py-C6CyMA $\tau_M = 205$ ns	2.1	0.95	-	60	148	-	0.00	0.05	-	1.2
	3.0	0.95	-	50	143	-	0.00	0.05	-	1.2
	3.8	0.94	-	52	120	-	0.00	0.06	-	1.0
	5.1	0.96	-	54	119	-	0.00	0.04	-	1.1
	6.2	0.95	-	52	116	-	0.00	0.05	-	1.1
	7.0	0.96	-	54	118	-	0.03	0.02	-	1.1
Py-C8MA $\tau_M = 200$ ns	4.3	0.95	-	56	169	-	0.02	0.01	-	1.1
	5.1	0.96	-	53	157	-	0.00	0.01	-	1.1
	2.7	0.97	-	50	159	-	0.05	0.03	-	1.0
	6.1	0.94	-	54	108	-	0.13	0.01	-	1.1
	7.3	0.86	-	57	108	-	0.04	0.02	-	1.1
Py-C12MA $\tau_M = 200$ ns	3.5	0.95	-	56	136	-	0.03	0.02	-	1.1
	5.6	0.95	-	53	134	-	0.02	0.03	-	1.0
	6.0	0.96	-	51	136	-	0.04	0.01	-	1.2
	7.7	0.91	-	54	134	-	0.08	0.02	-	1.1
	10.3	0.90	-	55	115	-	0.09	0.01	-	1.1
Py-C18MA $\tau_M = 206$ ns	4.5	0.98	-	54	163	-	0.02	0.00	-	1.1
	5.9	0.95	-	50	121	-	0.01	0.03	-	1.1
	6.8	0.97	-	51	119	-	0.00	0.03	-	1.1
	6.7	0.97	-	53	123	-	0.01	0.02	-	1.0
	14.1	0.95	-	52	106	-	0.02	0.03	-	1.2
CoBuE-PS-BuPy $\tau_M = 200$ ns	2.1	0.95	-	53	93	-	0.00	0.05	-	1.1
	3.1	0.96	-	54	99	-	0.00	0.04	-	1.0
	4.5	0.96	-	53	78	-	0.00	0.04	-	1.2
	5.4	0.94	-	52	82	-	0.00	0.06	-	1.1
	6.0	0.94	-	53	95	-	0.04	0.02	-	1.1
PEO(3.4K)-Py ₂	-	0.99	-	54	-	-	0.1	-	-	1.1
PEO(5K)-Py ₂	-	0.99	-	61.3	-	-	0.01	-	-	1.0
PEO(6K)-Py ₂	-	0.99	-	83.3	-	-	0.01	-	-	1.2

PP-G2-BuPy4	-	0.9	-	54.3	-	4	0.03	-	-	1.1
PP-G3-BuPy8	-	1	-	54.5	-	4	0	-	-	1.0
PP-G4-BuPy16	-	0.89	-	55.1	-	4	0.06	-	-	1.0
DiPy	-	0.45	0.5	59	32.1	-	0.02	0.02	-	1.1
Poly(PyEG ₃ MA)	-	0.21	0.5	67	49.2	-	0.2	0.02	-	1.1
Poly(PyBuMA)	-	0.52	0.0	50	32	-	0.3	0.32	-	1.1

Table SI5.6: Parameters retrieved from the MFA of the excimer decays of of the pyrene labeled constructs in Toluene.

Sample	Mol%	f_{Ediff}^{E0}	f_{Ediff}^D	τ_{E0} (ns)	τ_D (ns)	τ_S (ns)	f_{EE0}	f_{ED}	f_{ES}^*	χ^2
Py-C1MA $\tau_M = 176$ ns	2.6	0.71	-	55	114	-	0.08	0.02	-	1.1
	4.1	0.90	-	52	107	-	0.07	0.02	-	1.1
	5.3	0.85	-	52	104	-	0.12	0.01	-	1.0
	5.2	0.86	-	52	112	-	0.11	0.02	-	1.2
	5.6	0.84	-	48	104	-	0.02	0.10	-	1.2
	7.3	0.84	-	49	78	-	0.05	0.10	-	1.1
Py-C4MA $\tau_M = 180$ ns	2.2	0.74	-	53	162	-	0.06	0.02	-	1.0
	3.0	0.84	-	49	112	-	0.04	0.06	-	1.1
	3.6	0.85	-	52	130	-	0.08	0.01	-	1.2
	5.3	0.83	-	53	152	-	0.16	0.00	-	1.1
	7.2	0.85	-	51	137	-	0.13	0.01	-	1.1
CoBuE-PS-BuPy $\tau_M = 184$ ns	2.1	0.88	-	50	111	-	0.01	0.04	-	1.1
	3.1	0.90	-	53	152	-	0.07	0.00	-	1.1
	4.5	0.89	-	52	163	-	0.09	0.00	-	1.2
	5.4	0.88	-	51	91	-	0.08	0.04	-	1.2
	6.0	0.89	-	51	94	-	0.09	0.02	-	1.1
PEO(3.4K)-Py ₂	-	0.99	-	49.7	-	-	0.01	-	-	1.1
PEO(5K)-Py ₂	-	0.99	-	53.1	-	-	0.01	-	-	1.0
PEO(6K)-Py ₂	-	0.99	-	55.9	-	-	0.01	-	-	1.1
PP-G2-BuPy ₄	-	0.86	-	50.3	-	4.0	0.13	-	0.01	1.1
PP-G3-BuPy ₈	-	1.00	-	50.8	-	4.0	0.00	-	0.00	1.1
PP-G4-BuPy ₁₆	-	0.80	-	50.9	-	4.0	0.16	-	0.04	1.0
DiPy	-	0.63	0.3	52.5	29.0	-	0.00	0.02	-	1.1
Poly(PyEG ₃ MA)	-	0.49	0.1	45.0	16.2	-	0.33	0.08	-	1.0
Poly(PyBuMA)	-	0.21	0.4	58.4	42.6	-	0.31	0.05	-	1.0

Table SI5.7: Parameters retrieved from the MFA of the excimer decays of of the pyrene labeled constructs in DMF.

Sample	Mol%	$f_{E_{diff}}^{E0}$	$f_{E_{diff}}^D$	τ_{E0} (ns)	τ_D (ns)	τ_S (ns)	f_{EE0}	f_{ED}	f_{ES}^*	χ^2
Py-C1A $\tau_M = 165$ ns	1.7	0.96	0.00	55	58	-	0.03	0.01	0.00	1.1
	2.6	0.98	0.00	51	79	-	0.00	0.02	0.00	1.1
	2.6	0.97	0.00	52	36	-	0.00	0.03	0.00	1.0
	5.0	0.96	0.00	50	67	-	0.00	0.04	0.00	1.1
	6.7	0.91	0.00	49	68	-	0.00	0.09	0.00	1.1
Py-C1MA $\tau_M = 164$ ns	2.6	0.96	0.00	53	109	-	0.00	0.04	0.00	1.1
	4.1	0.96	0.00	56	47	-	0.00	0.04	0.00	1.1
	5.2	0.95	0.00	52	95	-	0.00	0.05	0.00	1.2
	5.3	0.93	0.00	51	83	-	0.00	0.07	0.00	0.9
	7.3	0.94	0.00	52	86	-	0.00	0.06	0.00	1.1
Py-C4MA $\tau_M = 160$ ns	2.2	0.96	0.00	54	128	-	0.00	0.04	0.00	1.1
	3.0	0.93	0.00	55	98	-	0.01	0.05	0.00	1.1
	3.6	0.92	0.00	55	112	-	0.06	0.03	0.00	1.0
	5.3	0.88	0.00	53	106	-	0.08	0.04	0.00	1.1
	7.2	0.87	0.00	55	123	-	0.12	0.01	0.00	1.1
CoBuE-PS-BuPy $\tau_M = 168$ ns	2.1	0.98	0.00	53	140	-	0.01	0.01	-	1.0
	3.1	0.96	0.00	57	131	-	0.04	0.01	-	1.1
	4.5	0.94	0.00	54	78	-	0.06	0.04	-	1.1
	5.4	0.97	0.00	52	100	-	0.03	0.01	-	1.0
	6.0	0.97	0.00	52	111	-	0.01	0.01	-	1.1
Amylose $\tau_M = 161$ ns	5.1	0.33	0.34	46	72	3.5	0.11	0.07	0.15	1.1
	5.6	0.12	0.56	85	53	3.5	0.00	0.16	0.16	1.0
	5.6	0.08	0.49	90	55	3.5	0.03	0.25	0.15	1.0

	7.5	0.31	0.36	67	47	3.5	0.00	0.09	0.25	1.0
	10.1	0.24	0.38	63	51	3.5	0.00	0.12	0.26	1.0
	14.9	0.52	0.09	50	65	3.5	0.11	0.12	0.16	1.0
Amylopectin	4.1	0.22	0.45	72	47	3.5	0.03	0.23	0.23	1.0
$\tau_M = 161$ ns	5.7	0.00	0.65	99	53	3.5	0.07	0.22	0.22	1.0
Amylose	8.7	0.37	0.34	52	55	3.5	0.10	0.19	0.19	1.0
$\tau_M = 257$ ns	9.6	0.32	0.39	47	57	3.5	0.05	0.19	0.19	1.0
	12.0	0.46	0.21	50	58	3.5	0.03	0.16	0.16	1.0
PEO(3.4K)-Py ₂	-	0.99	-	50.	-	-	0.01	-	-	1.1
PEO(5K)-Py ₂	-	0.99	-	57.	-	-	0.01	-	-	1.0
PEO(6K)-Py ₂	-	0.99	-	79.	-	-	0.01	-	-	1.1
PP-G2-BuPy4	-	0.79	-	51.	-	4.0	0.17	-	0.02	1.2
PP-G3-BuPy8	-	0.92	-	51.	-	4.0	0.06	-	0.02	1.1
PP-G4-BuPy16	-	0.90	-	50.	-	4.0	0.00	-	0.09	1.1
DiPy	-	0.42	0.54	55.	30.	-	0.03	0.01	-	1.1
Poly(PyEG ₃ MA)	-	0.60	0.00	48.	21.	-	0.23	0.17	-	1.1
Poly(PyBuMA)	-	0.18	0.61	72.	50.	-	0.13	0.09	-	1.1

Table SI5.8: Parameters retrieved from the MFA of the excimer decays of of the pyrene labeled constructs in DMSO.

Sample	Mol%	f_{Ediff}^{E0}	f_{Ediff}^D	τ_{E0} (ns)	τ_D (ns)	τ_S (ns)	f_{EE0}	f_{ED}	f_{ES}^*	χ^2
Py-C1A $\tau_M = 86$ ns	1.7	0.98	0.00	44	1.0	3.5	0.02	0.0	0.00	1.1
	2.6	0.98	0.00	41	1.0	3.5	0.02	0.0	0.00	1.1
	2.6	0.98	0.00	41	1.0	3.5	0.02	0.0	0.00	1.0
	5.0	0.96	0.00	40	1.0	3.5	0.04	0.0	0.00	1.1
	6.7	0.95	0.00	40	1.0	3.5	0.05	0.0	0.00	1.1
Amylose $\tau_M = 90$ ns	5.1	0.65	0.00	51	1.0	3.5	0.15	0.0	0.20	1.0
	5.6	0.63	0.00	51	1.0	3.5	0.10	0.0	0.27	1.0
	5.6	0.66	0.00	52	1.0	3.5	0.18	0.0	0.16	1.0
	7.5	0.75	0.00	47	1.0	3.5	0.13	0.0	0.23	1.0
	10.1	0.61	0.00	47	1.0	3.5	0.19	0.0	0.20	1.0
	14.9	0.68	0.00	44	1.0	3.5	0.19	0.0	0.14	1.0
Amylopectin $\tau_M = 92$ ns	4.1	0.71	0.00	48	1.0	3.5	0.11	0.0	0.18	1.0
	5.7	0.70	0.00	46	1.0	3.5	0.11	0.0	0.19	1.0
	8.7	0.70	0.00	44	1.0	3.5	0.12	0.0	0.19	1.0
	9.6	0.69	0.00	45	1.0	3.5	0.13	0.0	0.18	1.0
	12.0	0.70	0.00	44	1.0	3.5	0.10	0.0	0.20	1.0
PEO(3.4K)-Py ₂	0.99	-	41.9	-	-	0.01	-	-	0.99	1.1
PEO(5K)-Py ₂	0.99	-	54.5	-	-	0.01	-	-	0.99	1.1
PEO(6K)-Py ₂	0.99	-	71.6	-	-	0.01	-	-	0.99	1.2
PP-G2-BuPy ₄	0.90	-	38.7	-	4.00	0.00	-	0.1	0.90	1.1
PP-G3-BuPy ₈	0.91	-	39.8	-	4.00	0.00	-	0.0	0.91	1.1
PP-G4-BuPy ₁₆	0.89	-	39.7	-	4.00	0.00	-	0.1	0.89	1.1
DiPy	0.39	0.48	41.1	25.8	-	0.00	0.13	-	0.39	1.0
Poly(PyBuMA)	0.01	0.63	64.2	39.4	-	0.20	0.16	-	0.01	1.1
Poly(PyEG ₃ MA)	0.50	0.22	40.8	22.7	-	0.26	0.02	-	0.50	1.2

Table SI5.9: Overall fractions of pyrene species obtained from the MFA of the monomer and excimer decays for the pyrene labeled constructs in THF.

Sample	Mol%	f_{free}	f_{diff}^{E0}	f_{diff}^D	f_{diff}	f_{E0}	f_D	f_{agg}
Sample Py-C1A $\tau_M = 257$ ns	2.2	0.02	0.96	0.00	0.96	0.03	0.00	0.03
	2.6	0.06	0.91	0.00	0.91	0.00	0.03	0.03
	2.6	0.01	0.93	0.00	0.93	0.06	0.00	0.06
	5.0	0.01	0.89	0.00	0.89	0.10	0.00	0.10
Py-C1MA $\tau_M = 253$ ns	2.6	0.02	0.95	0.00	0.95	0.00	0.02	0.02
	4.1	0.02	0.95	0.00	0.95	0.03	0.01	0.04
	5.3	0.01	0.96	0.00	0.96	0.01	0.01	0.02
	5.2	0.01	0.92	0.00	0.92	0.00	0.07	0.07
	5.6	0.00	0.95	0.00	0.95	0.00	0.04	0.04
	7.3	0.03	0.90	0.00	0.90	0.03	0.05	0.08
Py-C4MA $\tau_M = 257$ ns	2.2	0.13	0.85	0.00	0.85	0.01	0.02	0.03
	3.0	0.11	0.84	0.00	0.84	0.04	0.01	0.05
	3.6	0.06	0.88	0.00	0.88	0.03	0.03	0.06
	5.3	0.01	0.93	0.00	0.93	0.01	0.05	0.06
	7.2	0.01	0.92	0.00	0.92	0.00	0.07	0.07
Py-C4TMA $\tau_M = 257$ ns	3.6	0.07	0.88	0.00	0.88	0.00	0.05	0.05
	3.8	0.05	0.90	0.00	0.90	0.00	0.06	0.06
	4.7	0.02	0.91	0.00	0.91	0.02	0.05	0.07
	5.6	0.01	0.90	0.00	0.90	0.00	0.08	0.08
	7.6	0.01	0.87	0.00	0.87	0.11	0.01	0.12
Py-C6MA $\tau_M = 190$ ns	2.0	0.16	0.79	0.00	0.79	0.03	0.02	0.05
	3.3	0.09	0.91	0.00	0.91	0.00	0.00	0.00
	4.8	0.07	0.86	0.00	0.86	0.07	0.01	0.08
	5.8	0.06	0.83	0.00	0.83	0.11	0.00	0.11
	6.7	0.04	0.88	0.00	0.88	0.08	0.00	0.09

	8.1	0.01	0.89	0.00	0.89	0.10	0.00	0.10
Py-C6CyMA $\tau_M = 258$ ns	2.1	0.32	0.64	0.00	0.64	0.00	0.03	0.03
	3.0	0.07	0.89	0.00	0.89	0.00	0.04	0.04
	3.8	0.05	0.90	0.00	0.90	0.00	0.05	0.05
	5.1	0.04	0.92	0.00	0.92	0.00	0.03	0.04
	6.2	0.01	0.94	0.00	0.94	0.00	0.05	0.05
	7.0	0.02	0.94	0.00	0.94	0.03	0.02	0.05
Py-C8MA $\tau_M = 200$ ns	4.3	0.15	0.81	0.00	0.81	0.04	0.01	0.04
	5.1	0.05	0.92	0.00	0.92	0.02	0.01	0.03
	2.7	0.18	0.79	0.00	0.79	0.00	0.02	0.02
	6.1	0.03	0.91	0.00	0.91	0.05	0.01	0.06
	7.3	0.02	0.84	0.00	0.84	0.12	0.02	0.14
Py-C12MA $\tau_M = 258$ ns	3.5	0.02	0.79	0.00	0.79	0.02	0.02	0.04
	5.6	0.06	0.89	0.00	0.89	0.02	0.02	0.04
	6.0	0.03	0.93	0.00	0.93	0.03	0.01	0.04
	7.7	0.04	0.87	0.00	0.87	0.07	0.02	0.09
	10.3	0.01	0.88	0.00	0.88	0.09	0.01	0.10
Py-C18MA $\tau_M = 190$ ns	4.5	0.18	0.80	0.00	0.80	0.02	0.00	0.02
	5.9	0.11	0.85	0.00	0.85	0.01	0.03	0.04
	6.8	0.08	0.89	0.00	0.89	0.00	0.03	0.03
	6.7	0.05	0.92	0.00	0.92	0.00	0.02	0.03
	14.1	0.11	0.84	0.00	0.84	0.02	0.03	0.04
CoBuE-PS-BuPy $\tau_M = 200$ ns	2.1	0.07	0.89	0.00	0.89	0.00	0.05	0.05
	3.1	0.03	0.93	0.00	0.93	0.00	0.04	0.04
	4.5	0.01	0.95	0.00	0.95	0.00	0.04	0.04
	5.4	0.01	0.93	0.00	0.93	0.00	0.06	0.06
	6.0	0.00	0.94	0.00	0.94	0.04	0.02	0.06
PEO(3.4K)-Py ₂	-	0.09	0.90	-	0.90	0.01	-	0.01
PEO(5K)-Py ₂	-	0.17	0.83	-	0.83	0.00	-	0.00

PEO(6K)-Py ₂	-	0.09	0.90	-	0.90	0.00	-	0.00
PP-G2-BuPy4	-	0.01	0.92	-	0.92	0.07	-	0.07
PP-G3-BuPy8	-	0.00	1.00	-	1.00	0.00	-	0.00
PP-G4-BuPy16	-	0.03	0.92	-	0.92	0.05	-	0.05
DiPy	-	0.03	0.44	0.49	0.93	0.02	0.02	0.04
Poly(PyEG ₃ MA)	-	0.00	0.52	0.00	0.52	0.31	0.17	0.48
Poly(PyBuMA)	-	0.00	0.21	0.57	0.78	0.20	0.02	0.22

Table SI5.10: Overall fractions of pyrene species obtained from the MFA of the monomer and excimer decays for the pyrene labeled constructs in Toluene.

Sample	Mol%	f_{free}	f_{diff}^{E0}	f_{diff}^D	f_{diff}	f_{E0}	f_D	f_{agg}
Py-C1MA $\tau_M = 257$ ns	2.6	0.21	0.71	0.00	0.71	0.06	0.02	0.08
	4.1	0.01	0.90	0.00	0.90	0.07	0.02	0.09
	5.3	0.01	0.85	0.00	0.85	0.12	0.01	0.13
	5.2	0.02	0.86	0.00	0.86	0.10	0.02	0.12
	5.6	0.05	0.84	0.00	0.84	0.02	0.09	0.11
	7.3	0.00	0.84	0.00	0.84	0.05	0.10	0.15
Py-C4MA $\tau_M = 253$ ns	2.2	0.20	0.74	0.00	0.74	0.04	0.01	0.06
	3.0	0.07	0.84	0.00	0.84	0.04	0.05	0.09
	3.6	0.07	0.85	0.00	0.85	0.07	0.01	0.08
	5.3	0.02	0.83	0.00	0.83	0.15	0.00	0.15
	7.2	0.01	0.85	0.00	0.85	0.13	0.01	0.14
CoBuE-PS-BuPy $\tau_M = 200$ ns	2.1	0.08	0.88	0.00	0.88	0.01	0.04	0.05
	3.1	0.03	0.90	0.00	0.90	0.07	0.00	0.08
	4.5	0.02	0.89	0.00	0.89	0.09	0.00	0.09
	5.4	0.01	0.88	0.00	0.88	0.08	0.04	0.11
	6.0	0.00	0.89	0.00	0.89	0.09	0.02	0.11
PEO(3.4K)-Py ₂	-	0.06	0.93	-	0.93	0.01	-	0.01
PEO(5K)-Py ₂	-	0.12	0.87	-	0.87	0.00	-	0.00
PEO(6K)-Py ₂	-	0.07	0.92	-	0.92	0.00	-	0.00
PP-G2-BuPy ₄	-	0.01	0.86	-	0.86	0.13	-	0.13
PP-G3-BuPy ₈	-	0.01	0.98	-	0.98	0.00	-	0.00
PP-G4-BuPy ₁₆	-	0.02	0.82	-	0.82	0.16	-	0.16
DiPy	-	0.00	0.63	0.35	0.98	0.00	0.02	0.02
Poly(PyEG ₃ MA)	-	0.00	0.49	0.10	0.59	0.33	0.08	0.41
Poly(PyBuMA)	-	0.00	0.21	0.42	0.64	0.31	0.05	0.36

Table SI5.11: Overall fractions of pyrene species obtained from the MFA of the monomer and excimer decays for the pyrene labeled constructs in DMF.

Sample	Mol%	f_{free}	f_{diff}^{E0}	f_{diff}^D	f_{diff}	f_{E0}	f_D	f_{agg}
Py-C1A $\tau_M = 257$ ns	1.7	0.06	0.91	0.00	0.91	0.03	0.01	0.03
	2.6	0.03	0.96	0.00	0.96	0.00	0.02	0.02
	2.6	0.02	0.95	0.00	0.95	0.00	0.03	0.03
	5.0	0.01	0.95	0.00	0.95	0.00	0.04	0.04
	6.7	0.01	0.90	0.00	0.90	0.00	0.09	0.09
Py-C1MA $\tau_M = 257$ ns	2.6	0.03	0.93	0.00	0.93	0.00	0.04	0.04
	4.1	0.04	0.93	0.00	0.93	0.00	0.03	0.04
	5.2	0.02	0.93	0.00	0.93	0.00	0.05	0.05
	5.3	0.01	0.92	0.00	0.92	0.00	0.07	0.07
	7.3	0.01	0.93	0.00	0.93	0.00	0.06	0.06
Py-C4MA $\tau_M = 253$ ns	2.2	0.21	0.76	0.00	0.76	0.00	0.04	0.04
	3.0	0.06	0.88	0.00	0.88	0.01	0.04	0.06
	3.6	0.15	0.78	0.00	0.78	0.05	0.02	0.07
	5.3	0.03	0.86	0.00	0.86	0.08	0.04	0.12
	7.2	0.01	0.87	0.00	0.87	0.12	0.01	0.12
CoBuE-PS-BuPy $\tau_M = 200$ ns	2.1	0.06	0.92	0.00	0.92	0.01	0.01	0.02
	3.1	0.04	0.92	0.00	0.92	0.04	0.01	0.04
	4.5	0.01	0.89	0.00	0.89	0.06	0.04	0.10
	5.4	0.01	0.95	0.00	0.95	0.03	0.01	0.04
	6.0	0.01	0.96	0.00	0.96	0.01	0.01	0.03
Amylose $\tau_M = 257$ ns	5.1	0.04	0.12	0.08	0.75	0.12	0.08	0.20
	5.6	0.06	0.00	0.18	0.76	0.00	0.18	0.18
	5.6	0.08	0.04	0.27	0.62	0.04	0.27	0.30
	7.5	0.04	0.00	0.11	0.84	0.00	0.11	0.11
	10.1	0.02	0.00	0.16	0.82	0.00	0.16	0.16

	14.9	0.02	0.13	0.14	0.72	0.13	0.14	0.26
Amylopectin $\tau_M = 190$ ns	4.1	0.04	0.28	0.57	0.85	0.08	0.04	0.11
	5.7	0.04	0.00	0.80	0.80	0.07	0.09	0.16
	8.7	0.01	0.45	0.41	0.86	0.00	0.13	0.13
	9.6	0.00	0.39	0.48	0.87	0.06	0.06	0.12
	12.0	0.00	0.54	0.25	0.79	0.17	0.03	0.21
PEO(3.4K)-Py ₂	-	0.10	0.89	-	0.89	0.01	-	0.01
PEO(5K)-Py ₂	-	0.17	0.82	-	0.82	0.00	-	0.00
PEO(6K)-Py ₂	-	0.13	0.86	-	0.86	0.00	-	0.00
PP-G2-BuPy4	-	0.01	0.82	-	0.82	0.17	-	0.17
PP-G3-BuPy8	-	0.00	0.94	-	0.94	0.06	-	0.06
PP-G4-BuPy16	-	0.03	0.96	-	0.96	0.01	-	0.01
DiPy	-	0.00	0.42	0.54	0.96	0.03	0.01	0.04
Poly(PyEG ₃ MA)	-	0.00	0.60	0.00	0.60	0.23	0.17	0.40
Poly(PyBuMA)	-	0.01	0.18	0.60	0.78	0.13	0.09	0.21

Table SI5.12: Overall fractions of pyrene species obtained from the MFA of the monomer and excimer decays for the pyrene labeled constructs in DMSO.

Sample	Mol%	f_{free}	f_{diff}^{EO}	f_{diff}^D	f_{diff}	f_{EO}	f_D	f_{agg}
Py-C1A $\tau_M = 257$ ns	1.7	0.00	0.84	0.00	0.84	0.02	0.00	0.02
	2.6	0.00	0.92	0.00	0.92	0.02	0.00	0.02
	2.6	0.00	0.96	0.00	0.96	0.02	0.00	0.02
	5.0	0.00	0.96	0.00	0.96	0.04	0.00	0.04
	6.7	0.00	0.95	0.00	0.95	0.05	0.00	0.05
Amylose $\tau_M = 190$ ns	5.1	0.00	0.72	0.00	0.72	0.17	0.00	0.17
	5.6	0.00	0.76	0.00	0.76	0.13	0.00	0.13
	5.6	0.00	0.76	0.00	0.76	0.20	0.00	0.20
	7.5	0.00	0.86	0.00	0.86	0.14	0.00	0.14
	10.1	0.00	0.76	0.00	0.76	0.24	0.00	0.24
	14.9	0.00	0.85	0.00	0.85	0.13	0.00	0.13
Amylopectin $\tau_M = 190$ ns	4.1	0.00	0.84	0.00	0.84	0.13	0.00	0.13
	5.7	0.00	0.85	0.00	0.85	0.15	0.00	0.15
	8.7	0.00	0.84	0.00	0.84	0.16	0.00	0.16
	9.6	0.00	0.87	0.00	0.87	0.13	0.00	0.13
	12.0	0.00	0.72	0.00	0.72	0.17	0.00	0.17
PEO(3.4K)-Py ₂	-	0.08	0.91	-	0.91	0.01	-	0.01
PEO(5K)-Py ₂	-	0.21	0.78	-	0.78	0.00	-	0.00
PEO(6K)-Py ₂	-	0.25	0.74	-	0.74	0.00	-	0.00
PP-G2-BuPy ₄	-	0.00	1.00	-	1.00	0.00	-	0.00
PP-G3-BuPy ₈	-	0.00	1.00	-	1.00	0.00	-	0.00
PP-G4-BuPy ₁₆	-	0.01	0.99	-	0.99	0.00	-	0.00
DiPy	-	0.00	0.39	0.48	0.87	0.00	0.13	0.13
Poly(PyEG ₃ MA)	-	0.00	0.50	0.22	0.72	0.26	0.02	0.28
Poly(PyBuMA)	-	0.00	0.01	0.63	0.64	0.20	0.16	0.36